SYNTHESIS OF CHIRAL THIOUREA LIGANDS AND THEIR TRANSITION METAL COMPLEXES

by

HAILE GHEBREGZIABIHER BERHE

Thesis presented in fulfilment of the requirements for the degree of **Masters of Science** in **Chemistry** at the **University of Stellenbosch**

Study leaders:

Professor Klaus R. Koch
University of Stellenbosch
&
Dr. M. W. Bredenkamp
University of Stellenbosch

Dec. 2003

DECLARATION

I, the undersigned, hereby declare the work contained in this thesis is my own original work and has not previously in it's entirely or partly thereof been submitted at any university for a degree.

Haile G. Berhe

Dedicated to my mother, Abrahazion

Abstract

Modification of chitosan with benzoylisothiocyanate was attempted, however due to solvent problem the study was left incomplete till appropriate solvent is designed.

N,N-diethyl-*N´*-camphanoylthiourea (HL^8), *N*-piperidyl-*N´*-camphanoylthiourea (HL^9), *N*-pyrrolidyl-*N´*-camphanoylthiourea (HL^{10}) and *N,N*-diethyl-*N´*-adamantylcarbonyl thiourea (HL^{11}) have been synthesised and characterised for the first time. Two of these ligands HL^8 and HL^{11}, were used to form a number of transition metal complexes, namely $H_3O^+\{fac\text{-}[Co(L^8\text{-}S,O)_3]^-\}$, *cis*-$[Ni(L^8\text{-}S,O)_2]$, *trans*-$[Cu(L^8\text{-}S,O)_2]$, *trans/cis*-$[Zn(L^8\text{-}S,O)_2]$, *trans/cis*-$[Pt(L^8\text{-}S,O)_2]$, $Ag_2[(HL^8\text{-}S)(L\text{-}\mu\text{-}S,O)]_2$, *trans/cis*-$[Ni(L^{11}\text{-}S,O)_2]$ and *trans/cis*-$[Cu(L^{11}\text{-}S,O)_2]$. The new products are fully characterised by means of MS, IR spectroscopy, NMR spectroscopy, elemental (C, H, N and S) analysis and melting point determinations. The $H_3O^+\{fac\text{-}[Co(L^8\text{-}S,O)_3]^-\}$, *cis*-$[Ni(L^8\text{-}S,O)_2]$, *trans*-$[Cu(L^8\text{-}S,O)_2]$ and $Ag_2[(HL^8\text{-}S)(L\text{-}\mu\text{-}S,O)]_2$ are also characterised by X-ray diffraction analysis.

The structure of the new chiral *N,N*-dialkyl-*N´*-camphanoylthiourea ligand (HL^8) has a significant effect on its coordination chemistry with transition metal ions. This ligand forms H_3O^+ $\{fac\text{-}[Co(L^8\text{-}S,O)_3]^-\}$, *cis*-$[Ni(L^8\text{-}S,O)_2]$, *trans*-$[Cu(L\text{-}S,O)_2]$ and $Ag_2[(HL^8\text{-}S)(L^8\text{-}\mu\text{-}S,O)]_2$ complexes with the Co(II), Ni(II), Cu(II) and Ag(I) metal ions respectively. The spectroscopic and X-ray diffraction results of these complexes indicate a bidentate mode of coordination of the ligand (with its *S* and *O* donor atoms) to the Co(II), Ni(II) and Cu(II) metal ions. The reaction of this ligand with silver(I) however affords the formation of a binuclear silver(I) complex exhibiting monodentate and bidentate modes of coordination within the same complex. The exclusive formation of *trans*-$[Cu(L^8\text{-}S,O)_2]$ is a new phenomenon for the HL type thiourea ligands with *S* and *O* donor atoms. Up to this point a maximum of 15 % *trans*-isomer has been reported in literature.[29]

All the transition metal complexes made with HL^8 and HL^{11} are air stable in both the liquid and solid states except the $H_3O^+\{fac\text{-}[Co(L^8\text{-}S,O)_3]^-\}$. Interestingly the deep green *fac*- $H_3O^+\{fac\text{-}[Co(L^8\text{-}S,O)_3]^-\}$ complex is air sensitive and the Co(II) oxidizes to Co(III) in the complex by atmospheric O_2. The oxidation of Co(II) to Co(III) in the complex is confirmed by ^1H and ^{13}C NMR spectra as well as by UV-Visible spectra of

the complex. The NMR spectra of the complexes indicated the presence of one isomer in each complex except for the NMR spectra of the platinum complex of the HL^8 ligand. The presence of the minor *trans*-[Pt(L^8-*S,O*)$_2$] isomer in combination with the major *cis*-[Pt(L^8-*S,O*)$_2$] isomer in the platinum complex was indicated by the ^{1}H, ^{13}C and ^{195}Pt NMR spectra of the complex.

Opsomming

Pogings om chitosan met benzoylisothiocyanate te modifiseer is onvoltooid gelaat weens die gebrek aan'n geskikte oplosmiddel.

N,N-diethyl-*N´*-camphanoylthiourea (HL^8), *N*-piperidyl-*N´*-camphanoylthiourea (HL^9), *N*-pyrrolidyl-*N´*-camphanoylthiourea (HL^{10}) en *N,N*-diethyl-*N´*-adamantylcarbonyl thiourea (HL^{11}) is vir die eerste keer gesintetiseer en gekarakteriseer. Twee van die ligande, HL^8 en HL^{11}, is gebruik om verskeie oorgangsmetaalkomplekse te berei, nl. $H_3O^+\{$*fac*-$[Co(L^8\text{-}S,O)_3]^-\}$, *cis*-$[Ni(L^8\text{-}S,O)_2]$, *trans*-$[Cu(L^8\text{-}S,O)_2]$, *trans/cis*-$[Zn(L^8\text{-}S,O)_2]$, *trans/cis*-$[Pt(L^8\text{-}S,O)_2]$, $Ag_2[(HL^8\text{-}S)(L\text{-}\mu\text{-}S,O)]_2$, *trans/cis*-$[Ni(L^{11}\text{-}S,O)_2]$ en *trans/cis*-$[Cu(L^{11}\text{-}S,O)_2]$. Die nuwe produkte is volledig gekarakteriseer deur middel van MS, IR spektroskopie, KMR spektrometrie, elemente (C, H, N en S) analise en smeltpuntbepaling. Die komplekse $H_3O^+\{$*fac*-$[Co(L^8\text{-}S,O)_3]^-\}$, *cis*-$[Ni(L^8\text{-}S,O)_2]$, *trans*-$[Cu(L^8\text{-}S,O)_2]$ en $Ag_2[(HL^8\text{-}S)(L\text{-}\mu\text{-}S,O)]_2$ is ook deur middel van X-straaldiffraksie-analise gekarakteriseer.

Die struktuur van die nuwe chirale *N,N*-dialkyl-*N´*-camphanoylthiourea ligand (HL^8) het 'n beduidende invloed op die koordinasie van hierdie ligand met oorgangsmetaalione. Die ligand vorm $H_3O^+\{$*fac*-$[Co(L^8\text{-}S,O)_3]^-\}$, *cis*-$[Ni(L^8\text{-}S,O)_2]$, *trans*-$[Cu(L\text{-}S,O)_2]$ en $Ag_2[(HL^8\text{-}S)(L^8\text{-}\mu\text{-}S,O)]_2$ komplekse met Co(II)-, Ni(II)-, Cu(II)- en Ag(I)-ione respektiewelik. Spektroskopiese en X-straaldiffraksie-analise van die komplekse toon dat die ligande op 'n bidentate wyse d.m.v. die *S*- en *O*-donoratome met Co(II), Ni(II) en Cu(II) koordineer. Die reaksie van hierdie ligand met Ag(I)-ione lei egter tot die vorming van 'n dikernige silwer(I)-kompleks waarin die ligande monodentaat (*S*) en bidentaat (*S* en *O*) aan die metaal gebind is. Die vorming van uitsluitlik die *trans*-$[Cu(L^8\text{-}S,O)_2]$ in die reaksie van HL^8 met Cu(II) is 'n besondere fenomeen in die chemie van hierdie tipe ligande; in die literatuur word melding gemaak van slegs een ander *trans*-kompleks met hierdie ligande, en dan wel met 'n maksimum opbrengs van 15%.[29]

Alle oorgangsmetaalkomplekse met HL^8 en HL^{11} is stabiel indien blootgestel aan lug, ongeag of die verbindings opgelos word of in die vastetoestand verkeer, behalwe $H_3O^+\{$*fac*-$[Co(L^8\text{-}S,O)_3]^-\}$. Die diep-groen gekleurde $H_3O^+\{$*fac*-$[Co(L^8\text{-}S,O)_3]^-\}$

kompleks is lugsensitief; Co(II) word deur lugsuurstof na Co(III) ge-oksideer. Die oksidasie in die kompleks kan deur middel van ^{1}H en ^{13}C KMR spektrometrie sowel as UV-sigbare spektrofotometrie bevestig word. Die KMR spektra van alle komplekse dui op die teenwoordigheid van slegs een isomeer in oplossing, behalwe in die geval van die platinum(II) kompleks met HL^{8}. Die teenwoordigheid van lae konsentrasies *trans*-[Pt(L^{8}-*S*,*O*)$_2$] isomeer tesame met veel hoër konsentrasies van die *cis*-[Pt(L^{8}-*S*,*O*)$_2$] isomeer word deur ^{1}H, ^{13}C en ^{195}Pt KMR spektroskopie aangedui.

ACKNOWLEDGEMENTS

I sincerely thank the following persons and government for their financial help, guidance and support in my study:

Prof. K. R. Koch & Dr. M.W. Bredenkamp: For their unlimited guidance, assistance and encouragement during this project

Jean McKenzie, Sibusiso Mtongana and Arian Westra: For always showing interest in my work, willingness to give advice when needed and assistance in acquiring and interpreting the NMR data.

My family: for moral support to complete this project.

Government of Eritrea, NRF and the University of Stellenbosch: for financial support and use of facilities.

TABLE OF CONTENTS

LIST OF ABBREVIATIONS

PGMs	Platinum group metals (Pt, Pd, Os, Ru, Ir and Rh)
H_2L^0	*N*-(2-hydroxyethyl)-*N*′-benzoylthiourea
H_2L^1	*N*-propyl-*N*′-benzoylthiourea
H_2L^2	*N*-butyl-*N*′-benzoylthiourea
H_2L^3	*N*-propyl-*N*-propanoylthiourea
HL^4	*N*-pyrrolidyl-*N*′-(2,2-diethlpropanoyl)thiourea
HL^5	*N,N*-di(2-hydroxyethyl)-*N*′-benzoylthiourea
HL^6	*N,N*-dibutyl-*N*′-benzoylthiourea
HL^7	*N,N*-dibuthyl-*N*′-naphthoylthiourea
HL^8	*N,N* –diethyl-*N*′-camphanoylthiourea
HL^9	*N*-pyrolidyl-*N*′-camphanoylthiourea
HL^{10}	*N*-pyrrrolidyl-*N*′-camphanoylthiourea
HL^{11}	*N,N*-diethyl-*N*′-adamantylcarbonylthiourea
DMF	Dimethyl formamide
DMSO	Dimethyl sulphoxide
HMPA	Hexamethylphosphoric triamide
IR	Infrared spectroscopy
MS	Mass spectroscopy
NMR	Nuclear magnetic resonance
COSY	H-H Correlation Spectroscopy
GHSQC	Gradient Heteronuclear (C-H) Single Quantum Coherence
$CDCl_3$	Deuterated chloroform
Å	Angstrom; 10^{-10} metres
${}^nJ_{X,Y}$	Coupling constant between X and Y protons in hertz (Hz)
δ	NMR chemical shift in parts per million (ppm)
TLC	Thin layer chromatography
R_f	Peak position (mm) divided by solvent front (mm)
2874w	w stands for weak
1806vs	vs stands for very strong (s alone if present stands for strong)
3407m	m stands for medium

CHAPTER ONE

ATTEMPTED FUNCTIONALISATION OF CHITOSAN

1.1. SOURCE OF CHITOSAN

Chitosan, a chiral polymer is prepared from chitin, which is the most abundant natural polysaccharide after cellulose.[1] Chitin itself is found in the protective shells of crustaceans such as crabs and shrimp. To obtain pure chitin, the crustacean shells are first ground and then the proteins removed by treatment with sodium hydroxide. This is followed by the removal of minerals such as calcium carbonate and calcium phosphate with hydrochloric acid.[1] After washing the residue several times with acid, the chitin is obtained as a flaked material. The chitosan is then prepared by treating the chitin with very strong NaOH (see **reaction scheme 1.1**) to hydrolyse the *N*-acetyl linkage. The remaining material is washed, the pH adjusted and the resulting chitosan is desiccated. By grinding the chitosan a powder is obtained. It has been demonstrated that alkaline treatment of chitosan also decreases the average chain length (*i.e.* the average number of sugar units).[1] Further purification of the product can be carried out by dissolving the chitosan in an acid, such as acetic acid, followed by filtration to remove extraneous materials.

Chitosan is commercially available in the form of powder, film, fibre, shaped objects, gel, beads, paste or solution.[1]

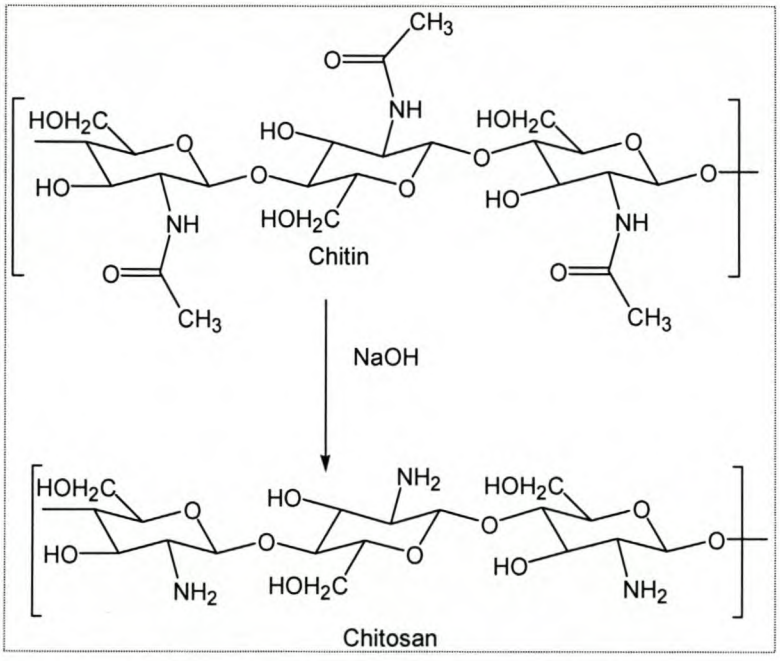

Reaction scheme 1.1. Preparation of chitosan from chitin.[1]

1.2. THE USEFULNESS OF CHITOSAN AND ITS CHEMISTRY

1.2.1. Properties of chitosan

Chitosan has many useful properties: it is biologically renewable, biodegradable, biocompatible both with animal and plant tissues, almost non-toxic, biologically functional, can be manufactured into different forms, and has hydroxyl and amino moieties, which can be chemically modified into different functional groups.[1,2,3] Chitosan is also able to form complexes with many metal ions.[1,2,3] It is therefore useful in removing metals such as Pd, Zn, Ag, U and Hg from sewage effluents. Chitosan also has the ability to clot blood and selectively bind acidic lipids. These properties combined with its biocompatibility and non-toxicity have led it to being evaluated for a number of medical applications such as wound dressing, hemostatic agents, drug delivery systems and as a hypocholesterolemic agent.[1] Moreover chitosan has been used for agricultural purposes such as coating seeds (wheat, rice and peas) and in the manufacturing of cosmetics.[1]

1.2.2. Modification of chitosan with carbon disulfide

As mentioned earlier, the amine groups of chitosan are reactive and suitable for modification. As a result there are a number of reactions that have been reported, which replace the amine moiety with various functional groups.[1,2,3,4]

O,O'-decanoyl dithiocarbamate chitosan was prepared by Kathryn *et al*[2] according to the method proposed by Nishimura *et al.*[4] for selective extraction and preconcentration of targeted transition metal ions. In the first step of the reaction the primary amine group was protected with phthalic acid anhydride. It was then possible to acylate the hydroxyl moiety of the chitosan with decanoyl chloride after which the amine group was deprotected using hydrazine to form *O,O'*-decanoylchitosan. In the second step the *O,O'*-decanoyl dithiocarbamate chitosan was prepared on addition of carbon disulfide and ammonium hydroxide to the *O,O'*-decanoylchitosan solution (**Reaction scheme 1.2**).[2]

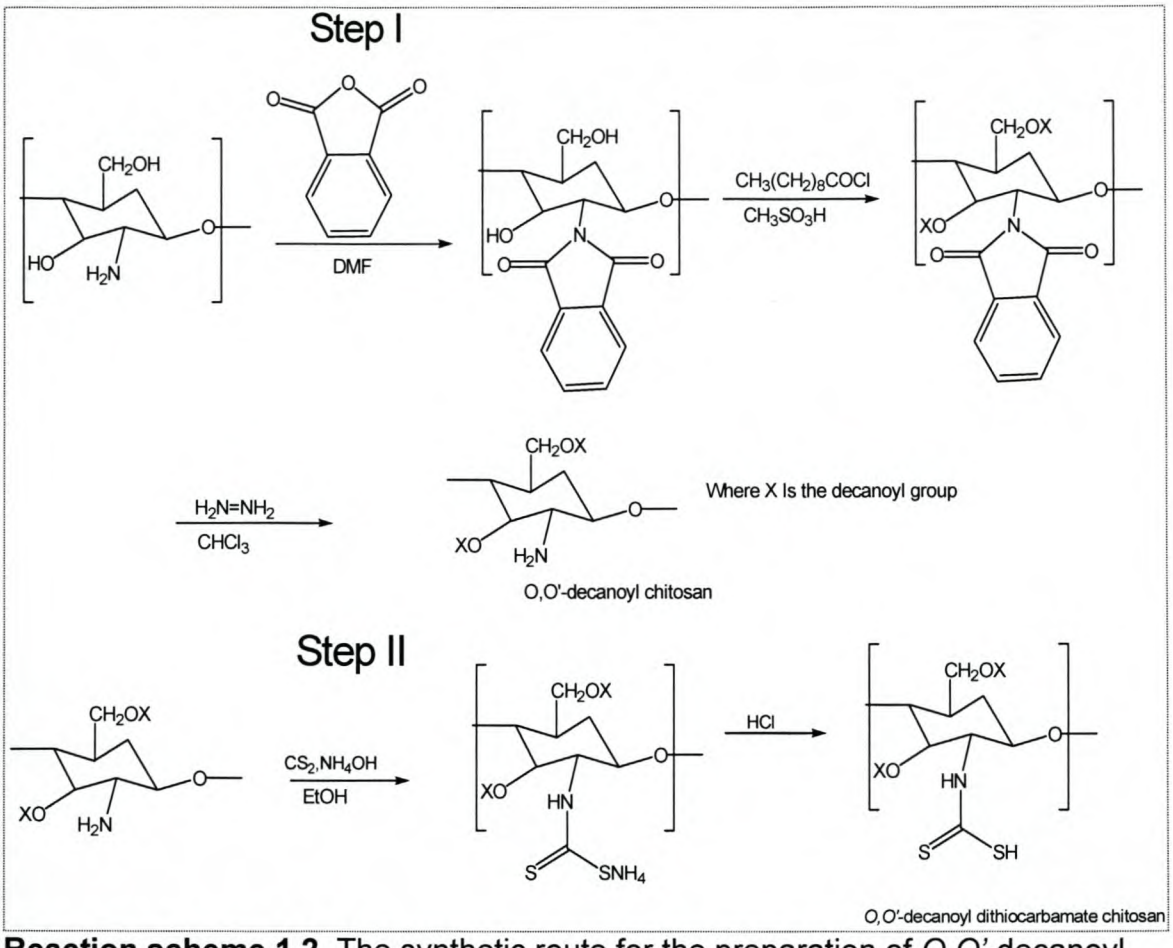

Reaction scheme 1.2. The synthetic route for the preparation of *O,O'*-decanoyl dithiocarbamate chitosan.[2]

1.2.3. Solubility properties of chitosan

Though the solubility properties of chitosan differ slightly from one form to another in the eight different commercially available forms indicated earlier, generally chitosan has specific solubility properties.[1] Chitosan in free amine form is not soluble in water, though is soluble in acidic solution (pH <6.5). In acidic water solution the free amine groups ($-NH_2$) become protonated to form cationic amine groups ($-NH_3^+$). Generally chitosan is insoluble in H_2SO_4, has limited solubility in H_3PO_4 and is insoluble in most organic solvents.[1] Chitosan is most soluble in dilute acetic acid.[1] The limited solubility of chitosan has placed a constraint on the modification of the amine and hydroxyl groups of chitosan.[1]

1.2.4. Aim of the research

The first part of this project was devoted to immobilising the benzoylisothiocyanate, which has two potential donor atoms (*S* and *O*), on the amine group of chitosan. The

second part was to involve the preparation of transition metal complexes using the modified chitosan. New products were supposed to be characterised by means of NMR spectroscopy, IR spectroscopy, MS and elemental (C, H, N and S) and X-ray diffraction analysis.

1.3. MODIFICATION OF CHITOSAN WITH BENZOYLISO THIOCYANATE

1.3.1. Proposed reaction procedure

Based on the modification of chitosan shown in **reaction scheme 1.2.**, the modification of the amine groups of chitosan with benzoylisothiocyanate was proposed as follows:

Preparation of benzoylisothiocyanate: The required amount of KSCN solution is added to the benzoyl acid chloride solution (one to one mole ratio) dropwise while stirring with a magnetic stirrer. After the addition of KSCN is completed the reaction mixture is refluxed for one hour while the whole system is under an inert atmosphere (see **reaction scheme 1.3**). At this stage the benzoylisothiocyanate is ready. Anhydrous acetone can be used as a solvent for both reagents.

Preparation of the modified chitosan: A known amount of chitosan is dissolved in DMF or any other polar aprotic solvent and its hydroxyl groups are acylated with hexanoyl chloride, but before this, the primary amine group is protected with phthalic acid anhydride against the attack by the hexanoyl chloride. The amine group is deprotected after the acylation using hydrazine and is then ready for modification. The modified chitosan in a solution form would be added dropwise while stirring to the benzoylisothiocyanate solution keeping the whole system under an inert atmosphere. After the reaction mixture is refluxed for a few hours solvents are removed under vacuum and then products are desiccated and analysed by means of IR spectroscopy, NMR spectroscopy, MS as well as elemental (C, H. N and S) and X-ray diffraction analysis. **Reaction scheme 1.4** shows the proposed synthetic route for the modification of chitosan with benzoylisothiocyanate.

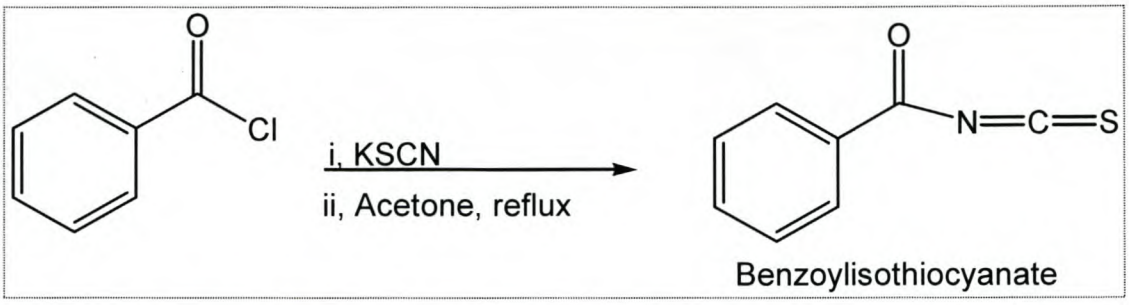

Reaction scheme 1.3. The synthetic route for the preparation of benzoylisothiocyanate.

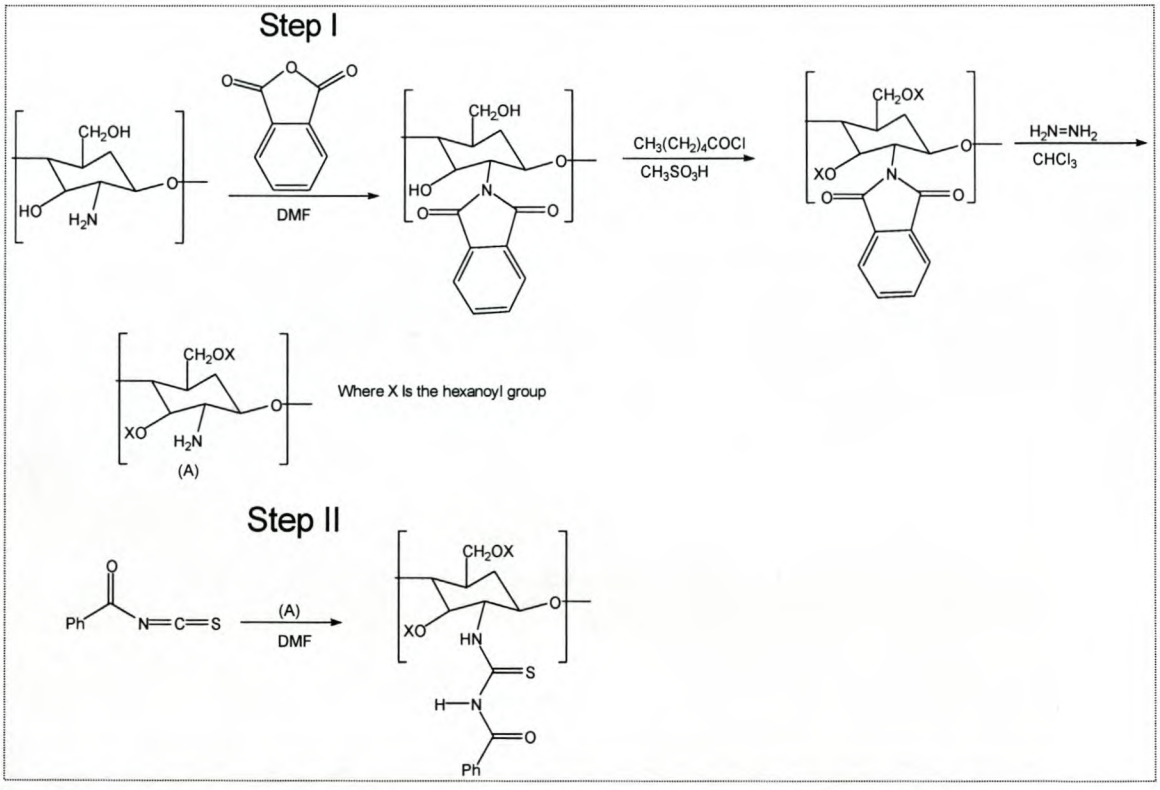

Reaction scheme 1.4. The intended synthetic route for the modification of chitosan with benzoylisothiocyanate.

1.3.2. Attempted procedure

2 g of chitosan (obtained from Aldrich Chemical Company, Inc.) was added to a 200 ml round bottom flask containing 100 ml dilute acetic acid. The mixture was then stirred with a magnetic stirrer for 48 hours at 70 °C. The dissolved chitosan was separated from the extraneous materials by filtration. The solvent was then removed and the pure chitosan was dried at 100 °C in a vacuum oven. Unfortunately the chitosan in its pure amine form is insoluble not only in all the polar aprotic solvents like CH_3CN, DMF, DMSO and HMPA, but also in most organic solvents. It is only

soluble in low molecular weight organic acids and alcohols like dilute acetic acid and acidified methanol in which the free amine groups ($-NH_2$) become protonated to form cationic amine groups ($-NH_3^+$). As discussed in **section 1.2.3,** chitosan is soluble in solvents that have low pH values. However acidic solvents cause the benzoylisothiocyanate, which is moisture sensitive, to decompose. Moisture can easily convert the benzoylisothiocyanate to benzoic acid. Hence it must be treated with well-dried reagents dissolved in anhydrous solvents under an inert atmosphere. Methanol is not a good solvent for the proposed synthesis indicated in **reaction scheme 1.4** because it can act as a nucleophile to the benzoylisothiocyanate.

1.3.3. Conclusion

The final conclusion of this research is that, chitosan, which is soluble only in solvents with pH < 6, can not be modified by benzoylisothiocyanate directly as was planned in **reaction scheme 1.4**. Thus simply because of solvent problems the modification of chitosan with benzoylisothiocyanate is left incomplete till an appropriate solvent is designed. This research was immediately replaced by another project, which is presented in the following chapters.

CHAPTER TWO

AN INTRODUCTION TO THIOUREA LIGANDS

CHAPTER TWO

2.1. GENERAL BACKGROUD ABOUT SOFT/ HARD DONOR ATOMS AND METAL IONS

A transition metal complex is an aggregate of a Lewis acid (the metal) and Lewis bases (the ligands). The ligands may contain more than one donor atom (ligand denticity) and more than one type of donor atom (so there is the possibility of binding in different ways to different metals). The binding affinity of a specific donor atom for metal ions differs from one metal ion to another depending on the softness or hardness of the metal ion and the donor atom. The Hard Soft Acid Base (HSAB) principle, which may be succinctly expressed as "Hard acids prefer hard bases; soft acids prefer soft bases", is often used to rationalise ligand preference for different metal ions.[5,6] A hard compound (acid or base) is one that has a very low polarisability. A soft compound (acid or base) is one that is more readily polarisable.[6] From the literature it is known that metal ions, including those of alkali metals, alkaline earth metals and higher transition metals in higher oxidation states such as Ti^{4+}, Cr^{3+} and Co^{3+}, are hard acids.[5] Metal ions including those of the heavier transition metals and those in lower oxidation states such as Cu^{+}, Ag^{+}, Hg^{2+}, Pd^{2+} and Pt^{2+}, are soft acids. Metal ions such as Fe^{2+}, Co^{2+}, Ni^{2+}, Cu^{2+}, Zn^{2+}, Rh^{3+}, Ir^{3+}, Ru^{2+} and Os^{2+}, are in between hard and soft acids. The softer metal ions preferentially bind with donor atoms of ligands in the order of S >N >O. The harder metal ions preferentially bind in the order of O >N >S.

The hardness or softness of an acidic or basic site is not an inherent property of the particular atom at that site, but can be influenced by the neighbouring atoms.[6] For instance addition of a soft, polarisable neighbouring atom (such as a S atom next to an O donor atom), can soften a harder site. The presence of electron-withdrawing or electron-releasing neighbouring atoms can reduce or increase the softness of a donor atom respectively. Therefore ligands have been designed with the desired softness/hardness of donor atoms by selecting suitable donor and neighbouring atoms so as to make the ligand selective for specific metal ions.[7]

Of particular interest to us are the platinum group metals, PGMs (Pt, Pd, Ru, Os, Ir, Rh), which tend to be on the border between hard and soft metals. Ligands that are especially suited for these metals are those that contain hard and soft donor atoms

such as a sulfur-oxygen bidentate ligand. A family of ligands that have this property are the *N*-acyl/aroylthioureas, in which deprotonation conjugates the carbonyl group with the thiocarbonyl group. These bidentate ligands have a preference for ligating the PGMs.

2.2. DESIGN OF THIOUREA LIGANDS AND THEIR IMPORTANCE

Before the synthesis of thiourea ligands, the trace analysis of the PGMs in severely interfering matrices such as rock samples, other materials of geological origin, catalyst residue in process solutions, and biological materials, posed serious problems, both as a result of inadequate determination limits of analytical methods and of the complexity of matrix influences. Hence in many cases selective sample preparation was required to ensure the enrichment of an individual element of interest, especially at the trace amount level. As a solution to this problem chemists designed thiourea ligands (see **Table 2.1**), which have two potential donor sites, namely the sulfur atom of the thiocarbonyl (CS) moiety and the oxygen atom of the carbonyl (RCO) moiety (where R can be an alkyl or aryl group). According to the literature,[7,8,9,10,11] the selective preconcentration of softer metals such as Cu(II), Hg(II) and Pd(II) with thiourea ligands allowed these metals to be separated from other transition metals by means of chromatographic separation techniques. Koch *et al.* also reported that using these ligands, trace amounts of PGMs could be preconcentrated and then detected by means of high-performance thin layer chromatography (HPTLC).[7] In addition, thiourea ligands such as *N,N*-di(2-hydroxylethyl)-*N'*-benzoylthiourea were used to preconcentrate trace amounts of Pt(II), Pd(II) and Rh(II) *in situ* and their concentrations determined by means of Laser-ablation inductively coupled plasma mass spectroscopy (LA-ICP-MS). This method showed remarkably linear concentration curves with >99% recovery of the PGMs.[7] Moreover these ligands were found to be very effective for on-line preconcentration of the above-mentioned target precious metals at ultra trace level with electrothermal atomic absorption spectroscopy being used for determination of the PGMs.[7] Koch *et al.* also reported that with increasing acidity, these ligands were found to be selective in the coordination of the PGMs over other transition metal ions.[12,13]

2.2.1. Historical development of thiourea ligands

Chemists initially started to synthesise unsubstituted thiourea ligands such as $CH_3C(O)NHC(S)NH_2$, which was first prepared by Neucki.[14] The platinum complex of this ligand has been known for more than a century. After some years the monoalkyl substituted thiourea ligands and dialkyl substituted thiourea ligands began to be synthesised. **Table 2.1** shows some examples of the monoalkyl substituted thiourea ligands (H_2L) and dialkyl substituted thiourea ligands (HL) synthesised by Koch and co-workers.[7] Interestingly the coordination chemistry of these monoalkyl and dialkyl substituted thiourea ligands with PGMs was found to differ not only from the unsubstituted thiourea ligands but also from one ligand to another.[7,8,12]

Table 2.1. Examples of monoalkyl and dialkyl substituted thiourea ligands.

Monoalkyl substituted thiourea ligands (H_2L)	Dialkyl substituted thiourea ligands (HL)
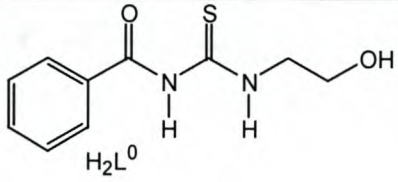 H_2L^0	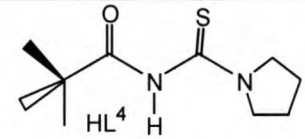 HL^4
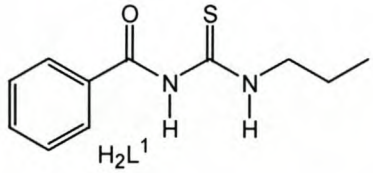 H_2L^1	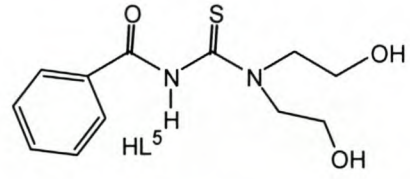 HL^5
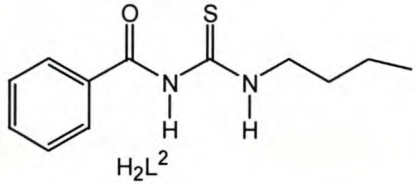 H_2L^2	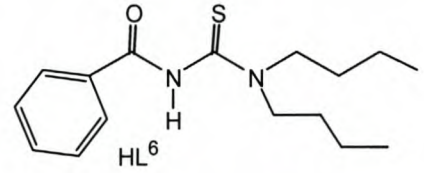 HL^6
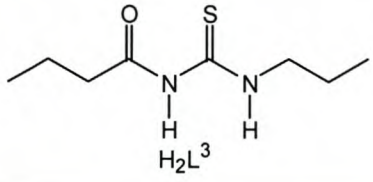 H_2L^3	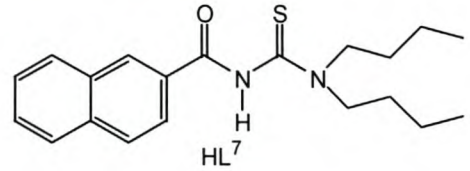 HL^7

2.2.2. Synthesis of thiourea ligands and related problems

Thiourea ligands have long been recognised as compounds that can be synthesised easily in two steps of a one pot process from readily available starting materials following the procedures employed by Douglas and Dains.[15,17,18] Following this procedure, to 0.1 mol NH_4SCN in 4 ml. of hot acetone, 0.1 mol of acyl/aroyl chloride is added dropwise. After the initial reaction is completed, the mixture is heated for five minutes and then a hot solution of amine (0.1 mol) in acetone (4 ml.) is added slowly while stirring. Upon pouring into five times its volume of distilled water, the thiourea precipitates.[15]

The general synthetic route of the preparation of thiourea ligands is shown in **reaction scheme 2.1.**

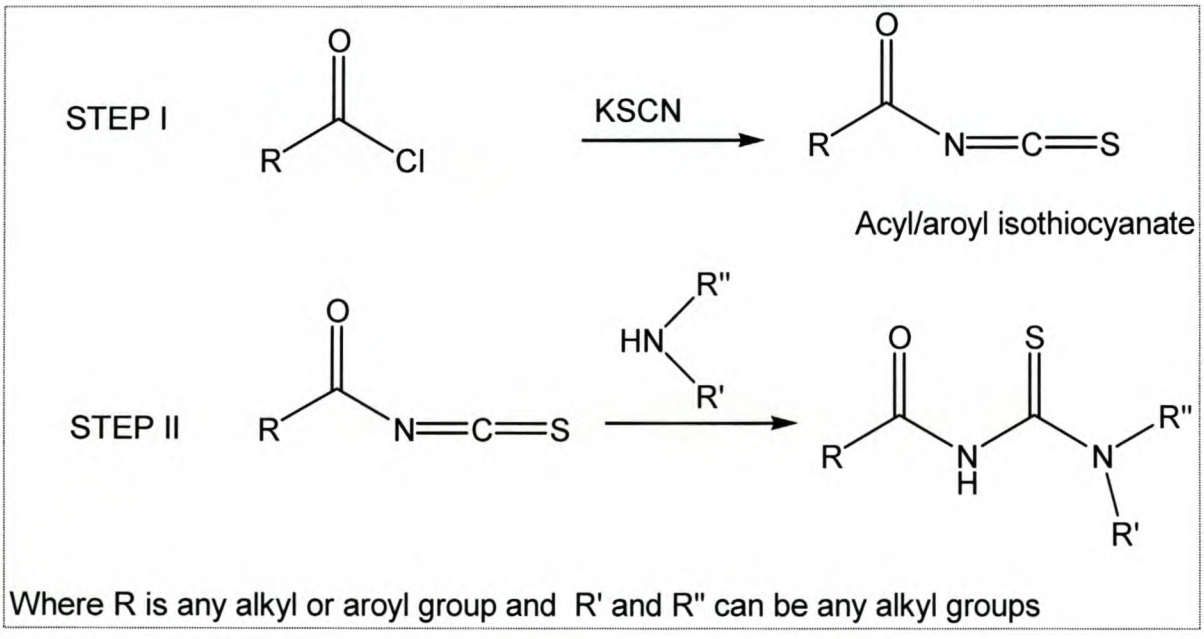

Reaction scheme 2.1. The general synthetic route for the preparation of thiourea ligands.

Though the synthesis of these ligands is easy and cost effective, unavoidable side reactions may occur. According to the literature,[19] when the thiocyanate ion and acyl/aroyl halide are combined in a reaction mixture, *S*-acylation is a common side reaction, forming the isocyanate product in the first step of the reaction (**reaction scheme 2.2**). In most cases however exclusive *N*-acylation [**reaction scheme 2.2 (b)**] is favoured.[19]

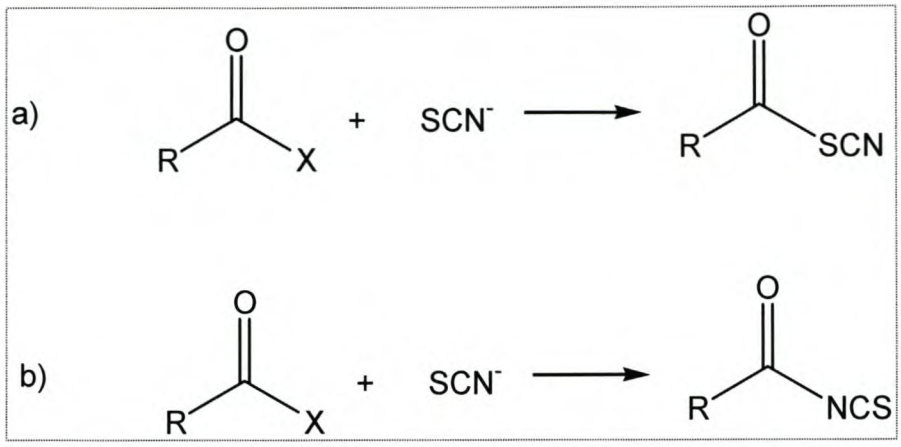

Reaction scheme 2.2. The two possible nucleophilic attacks by SCN^- on acyl/aroyl chlorides.

A common side reaction that can take place in the second step of the synthesis of these types of thiourea ligands is the nucleophilic attack by the amine group at the carbonyl (RCO) position, instead of at the electrophilic centre of the thiocarbonyl group [**reaction scheme 2.3**]. The electrophilicity of the carbon in the carbonyl group is dependent on the type of R group. The electrophilicity of this carbon decreases when R is an electron-releasing group and increases when R is an electron-withdrawing group.

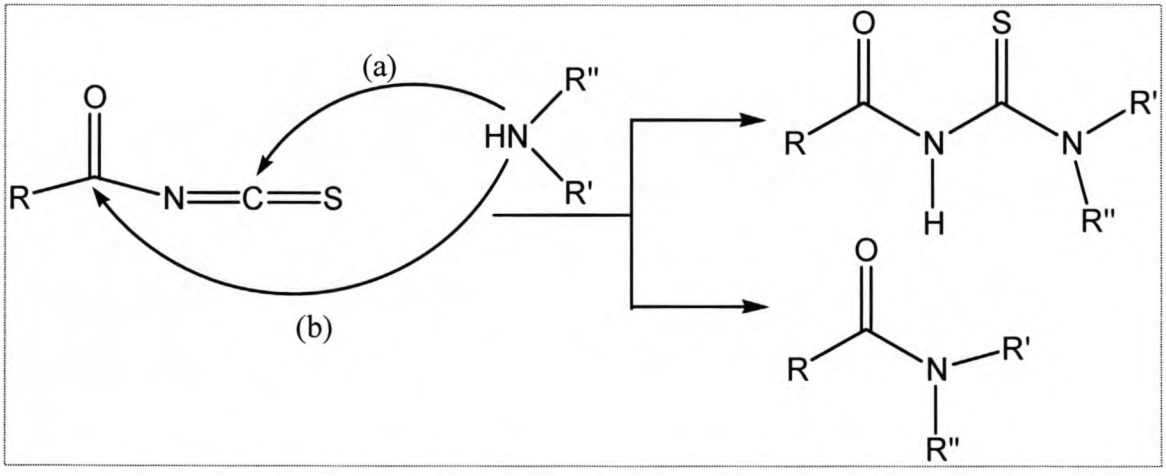

Reaction scheme 2.3. The two possible nucleophilic attacks in the second step of the preparation of thiourea ligands. (a) Desired nucleophilic attack on the carbon of the thiocarbonyl group. (b) Undesired nucleophilic attack on the carbon of the carbonyl group.

A bulky alkyl/aryl (R) group is expected to hinder the nucleophilic attack at the carbonyl position and cause the nucleophile to be directed towards the thiocarbonyl site. In other words route **(a)** in **reaction scheme 2.3** is favoured.

2.2.3. Acidity and the possible resonance structures of acyl/aroylthiourea ligands.

As is seen from the structures of the HL and H_2L types of thiourea ligands in **Table 2.1,** the NH proton of these types of ligands is flanked by carbonyl and thiocarbonyl groups making the proton acidic. The acid dissociation constant [$pK_{a(N-H)}$] for this proton in different acyl and aroyl thiourea ligands was found to range from 7.5 to 10.9 in a water/dioxane mixture.[7] The acidic proton is easily removed by a weak base such as sodium acetate or sodium bicarbonate, to form an enolate ion ligand (L^-). This ionic ligand is expected to stabilise its charge by a resonance effect in the conjugated structure of the –C(O)NC(S)- moiety. The deprotonation of the NH proton and the expected resonance structures of the resulting enolate ion are shown in **Figure 2.1**.

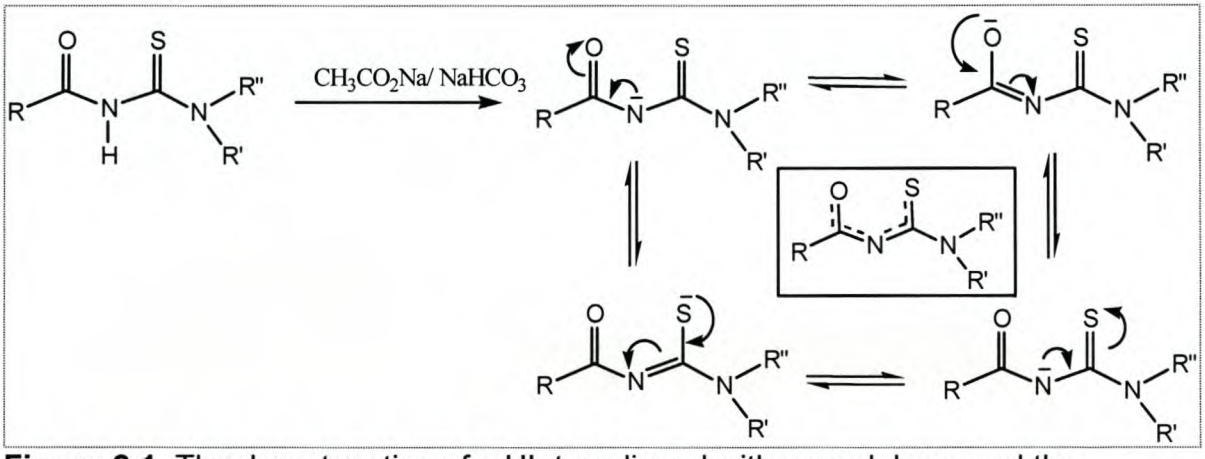

Figure 2.1. The deprotonation of a HL type ligand with a weak base and the resonance structures of its enolate ion.

2.2.4. Relative stability and complex formation potential of acyl/aroylthiourea ligands

It is realistic that the rearrangement of the formal charges on the oxygen and sulphur atoms, as shown in **Figure 2.1**, would greatly enhance the affinity of the enolate ion for metal complex formation. Schuster, reported that the high pK_s value of the enolate ion and the ability to increase the charge on the sulphur donor atom by means of resonance effects leads to very selective complex formation behaviour.[9] This indicates that the resonance in the -(O)CNC(S)- moiety increases the stability of metal complexes that can be synthesised with such types of ligands. Any factor that hinders the freedom of this resonance will decrease the effectiveness of the

complexing ability of the enolate ion with transition metal ions.[9] The acylthiourea ligands are therefore expected to form more stable transition metal complexes compared to the aroylthiourea ligands. As a result of the presence of the aromatic ring attached to the -C(O)N group in the aroyl thiourea ligands the resonance route is expected to be extended toward the benzene ring. This is outside the -(O)CNC(S)- moiety and thus reduces the resonance effect of the enolate ions in the -(O)CNC(S)- moiety. This in turn decreases the stability of the transition metal complexes of these ligands compared to the stability of the complexes of acylthiourea ligands.

2.2.5. Structures of the dialkyl and monoalkyl substituted thiourea ligands

Although both the monoalkyl and dialkyl substituted thiourea ligands (HL and H_2L) have acidic NH protons that can be deprotonated to give enolate ion ligands with two donor atoms, the proton in the –C(S)NHR moiety of the H_2L type ligands forms an intramolecular hydrogen bond with the oxygen atom of the amidic group, –C(O)NH, and this locks the -(O)NHC(S)NHR unit into a planar six membered ring structure.[7,8,12] Therefore these ligands are found to be restricted to unidentate *S* coordination to the transition metal ions.[6,11] This is similar to the mode of coordination of the simple unsubstituted thiourea ligands to PGM ions.[7] **Figure 2.2** shows the structure of *N*-propyl-*N*´-benzoylthiourea (H_2L^3) and indicates the presence of an intramolecular H-bond.

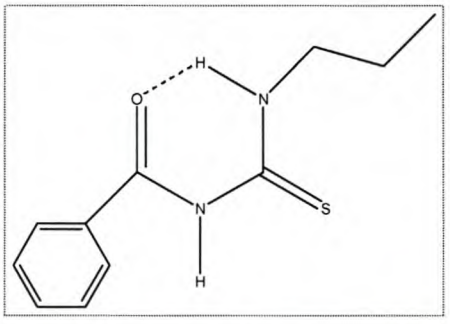

Figure 2.2. The structure of *N*-propyl-*N*´-benzoylthiourea (H_2L^3) showing the intramolecular H-bond.[11]

The corresponding HL type ligands are found to exist in a twisted conformation in the solid state with the sulphur and oxygen donor atoms pointing in approximately opposite directions.[7] The coordination chemistry of the HL type ligands with the PGMs is found to be remarkably different from that of the H_2L thiourea ligands.[7,8,12,18]

The dialkyl substituted thiourea ligands coordinate in a bidentate fashion with their *S* and *O* donor atoms to Pd(II), Pt(II) and Rh(III).[7,20,21,22,23,24] Detailed information about the coordination chemistry of both the HL and H_2L types of thiourea ligands will be given in **section 2.3**.

An interesting observation was made from the X-ray diffraction results of the HL and H_2L types of ligands. The average C-N bond distances of (O)C-NH, N'H-C(S) and (S)C-N(R/H) were 1.374±0.011 Å, 1.409±0.016 Å and 1.327±0.006 Å respectively.[7,8,12] These bonds were found to be shorter than a normal C-N single bond, which indicates the presence of partial double bond character.[7,8,12] It is also reported that upon coordination with metal ions the C=S and C=O bonds of such ligands become longer while the C-N bonds become shorter than their corresponding bonds in the free ligand.[25,26,27] In addition, Koch *et al.* reported that restricted rotation about the (S)C-N$(CH_2R)_2$ bond caused by the resonance interaction between the lone pair electron of the nitrogen atom and π-bond of the thiocarbonyl (S=C) group made the two methylene protons of the (S)CN$(CH_2R)_2$ moiety of the HL type ligand lie at different chemical shifts in the proton NMR spectrum.[7] For the unsymmetrical *N,N*-dialkyl substituted HL ligands, the restricted rotation about this bond helps to distinguish *E/Z* isomers in solution form.[7,12]

2.2.6. Identification of the ^{13}C NMR signals of the carbonyl and thiocarbonyl groups in the free HL ligand and its metal complexes

An interesting study has been carried out on the ^{13}C NMR peak positions of the carbonyl and thiocarbonyl groups of the HL type ligands, comparing the shifts when the ligand is uncoordinated and when it is coordinated. The positions of the ^{13}C NMR peaks of the two carbons in the free ligand and complex forms were studied using a special thiourea ligand of *N,N*-diethyl-*N'*-benzoylthiourea and its platinum complex [Pt(L-*S,O*)$_2$]. This ligand was prepared with 45 % ^{13}C isotopically enriched potassium thiocyanate salt.[28] This makes the ^{13}C peak of the thiocarbonyl (S=C) more intense than the ^{13}C peak of the carbonyl (O=C), both in the ^{13}C NMR spectra of the free ligand as well as in the metal complex and this allows identification of the positions of the peaks of both carbons in the free ligand and in their metal complex. The ^{13}C NMR peak of the thiocarbonyl was found further downfield than the ^{13}C NMR peak of the

carbonyl in the free ligand, whereas in its metal complex, the ^{13}C peak of the carbonyl was further downfield than the ^{13}C NMR peak of the thiocarbonyl.[28]

2.3. THE COORDINATION CHEMISTRY OF THIOUREA LIGANDS

Chemists have found that the different aryl or alkyl groups attached to the -(O)CNHC(S)- moiety cause different modes of coordination of the thiourea ligands to the PGMs.[7,8,18,21,29] These properties have prompted chemists to explore the variety of coordination properties of these types of ligands by changing the functionality of the ligands on both sides of the -(O)CNHC(S)- moiety.[10]

2.3.1. The coordination chemistry of the monodentate (H_2L-*S*) type thiourea ligands with transition metal ions

As discussed in the previous section, due to the presence of intramolecular hydrogen bonds, the coordination chemistry of the monoalkyl substituted thiourea (H_2L-*S*) ligands is found to be different from the analogous dialkyl substituted ligands. The monoalkyl substituted thiourea ligands are normally found to form *cis* and *trans*–$[M(H_2L\text{-}S)_2X_2]$ (where X = Cl, Br and I and M is a transition metal ion) complexes involving unidentate coordination *via* their sulphur donor atom to the metal ion (M).[7,18,30] According to Koch *et al.*, several *cis*-$[M(H_2L)_2Cl_2]$ and *trans*-$[M(H_2L)_2Cl_2]$ complexes have been isolated and their coordination chemistry studied using X-ray diffraction and other spectroscopic methods.[8]

2.3.2. The coordination chemistry of the bidentate (HL-*S,O*) type thiourea ligands with transition metal ions

The coordination of dialkyl substituted thiourea ligands (HL) to the first and second row transition metals has been studied and it was found that the leading mode of coordination of the HL ligands is bidentate chelate formation through the *S* and *O* atoms with loss of the N-H proton.[7] The interest in the family of these types of thiourea ligands arises from their versatile complex formation potential with transition

metal ions.[27] The general synthetic route for the preparation of transition metal complexes with HL type ligands is shown in **reaction scheme 2.4**.

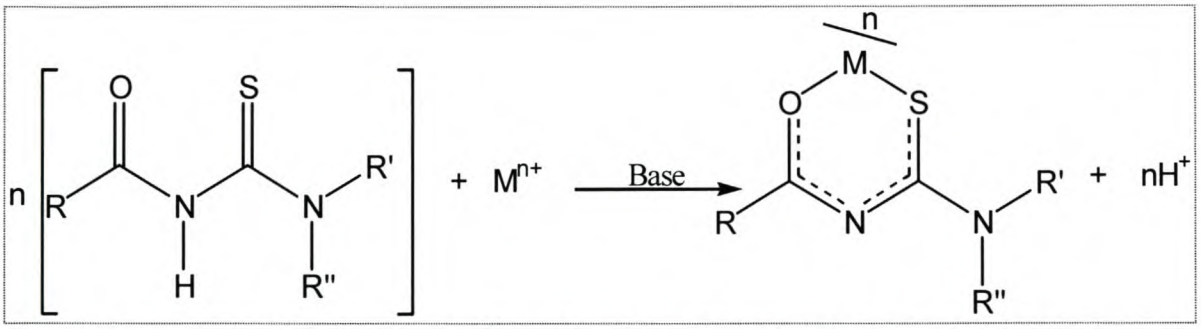

Reaction scheme 2.4. Synthetic route for the preparation of transition metal complexes with HL type ligands.

A very amazing coordinating property of this type of thiourea ligand, not completely explained yet, is the tendency to form almost exclusively *cis*-[M(L-*S,O*)$_2$] isomers with transition metal ions.[7,24,27,30,31] The formation of *trans* complexes in d^8 metal ions is very rare.[7,26] *Cis-bis*(*N,N*-diethyl-*N'*-benzoylthioureato)nickel(II)[23] and *cis-bis*(*N,N*-diethyl-*N'*-benzoylthioureato)copper(II)[27] are good examples of such complexes. Koch also indicated that the HL^4, HL^5, HL^6 ligands (see **Table 2.1**) were found to form stable hydrophilic *cis*-[M(L-*S,O*)$_2$] complexes [where M = Pt(II) and Pd(II)].[7]

It is reported that *trans* complexes of these types of ligands can only be made in the form of *trans*-[M(HL-*S*)$_2$I$_2$] in the presence of coordinating anions. The *trans* complexes can be synthesised by protonation of *cis*-complexes such as *cis*-[Pt(L-*S,O*)$_2$] with acids like HCl, HBr or HI in acetone (see **reaction scheme 2.5**).[7,30] The X-ray diffraction analysis of such complexes revealed that the potentially bidentate ligand was found to bind to the central metal ion through the sulphur donor atom only.[7]

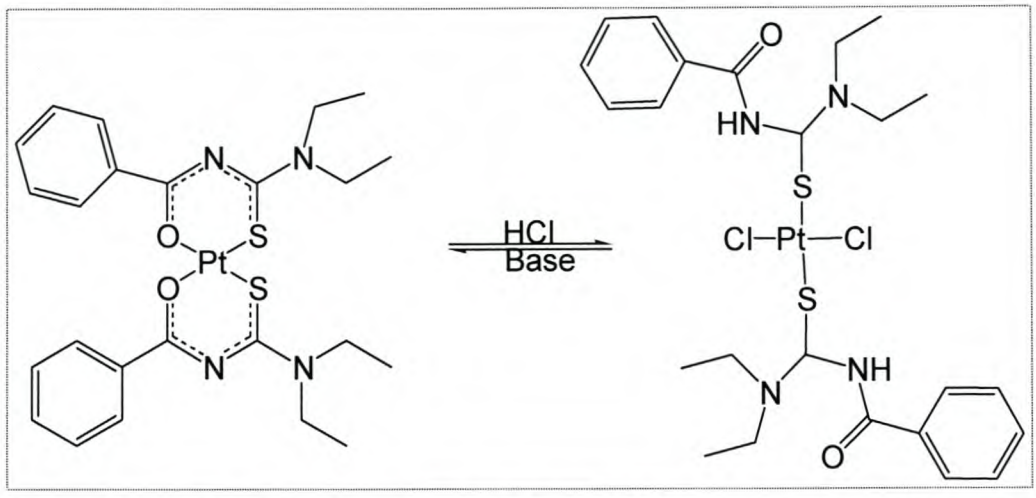

Reaction scheme 2.5. The formation of *trans*-[Pt(HL-*S*)$_2$Cl$_2$] on addition of HCl to *cis*-[Pt(L-S,O)$_2$].

The striking phenomenon of almost exclusive *cis*-[M(L-*S,O*)$_2$] complex formation of the dialkyl substituted thiourea ligands (HL) with the first and second row transition metal ions (M) has led chemists to synthesise a number of HL-type thiourea ligands, forming a basis for an extensive study of their coordination chemistry with different transition metal ions. As part of their curiosity to study the reason behind this phenomenon, Koch and co-workers prepared the potentially fluorescent *N,N*-dibutyl-*N´*-naphthoylthiourea (HL^7, **Table 2.1**) ligand and grew crystals of its Pt(II) complex.[29] Fortunately the coordination chemistry of *N,N*-dibutyl-*N´*-naphthoylthiourea with Pt(II) proved to be different from the previously synthesised dialkyl substituted thiourea ligands. Surprisingly the *N,N*-dibutyl-*N´*-naphthoylthiourea ligand was found to form the *trans*-[M(L^7-*S,O*)$_2$] isomer in combination with the dominant *cis*-[M(L^7-*S,O*)$_2$] isomer. According to Koch and co-workers this was the first ligand in the history of dialkyl substituted thiourea (HL) ligands that forms such a *trans*-[Pt(L^7-*S,O*)$_2$] isomer, which could be separated and then analysed by means of NMR spectroscopy and X-ray diffraction analysis.[29] The *trans*-[Pt(L^7-*S,O*)$_2$] complex was isolated as a minor component from a 15:85 *trans:cis* ratio solution by means of fractional crystallisation. It was suggested that the formation of the *trans*-[Pt(L^7-*S,O*)$_2$] isomer was due to steric hindrance caused by the bulky naphthoyl group. The crystal structure of the *trans*-[Pt(L^7-*S, O*)$_2$] complex showed a square-planar *O,S* coordination of ligand to metal.

Other complexes of HL-type ligands reported by Koch *et al.* which show the presence of small quantities of the *trans*-isomer in combination with the dominant *cis*-[M(L-

S,O)$_2$] isomer are Pt(II) complexes of *N,N*-dibutyl-*N´*-(3,4,5-trimethoxy)-benzoylthiourea and *N*-morpholino-*N´*-(3,4,5-trimethoxy)-benzoyl thiourea.[7] The *trans* isomers of these complexes were however found to occur in such small amounts as to make it impossible to separate them from the dominant *cis*-isomer and therefore analysis was made only by ^{195}Pt, ^{1}H and ^{13}C NMR spectroscopy. Further structural information could not be obtained from X-ray diffraction analysis.[29] From this result, it was concluded that *trans* Pt(II) complexes can only be isolated for bulky electron-rich *N*-aroylthiourea ligands, possibly because electron-releasing aroyl groups enhance the relative softness of the amidic oxygen donor atom thus stabilizing a *trans* isomer of a [M(L-*S,O*)$_2$] complex.[7]

The HL-types of ligands are also found to form *fac*-[M(L-*S,O*)$_3$] octahedral complexes with Rh(III), Ru(III) and Co(III).[7,23,24,32] According to Bench and Schuster, *N,N*-diethyl-*N´*-benzoylthiourea forms a neutral facial octahedral complex with Co(III).[24] It is reported that three *N,N*-diethyl-*N´*-benzoylthiourea molecules bidentately coordinate with their *S* and *O* donor atoms to the central Co(III) ion to form a distorted octahedral complex. The oxygen and sulphur donor atoms were found to be in a facial arrangement to form *facial*-[Co(L-*S,O*)$_3$].

Though extensive studies have been carried out on the coordination chemistry of the HL type thiourea ligands with transition metal ions, no study has been made on the coordination chemistry of chiral dialkyl substituted thiourea ligands. Therefore in this thesis attention has been given to the coordination chemistry of chiral dialkyl substituted thiourea ligands.

2.4 OUTLINE OF THE STUDY

This study has the following parts:

► The first part of the study covers the synthesis of new chiral *N,N*-dialkyl-*N´*-acylthiourea ligands and analogous achiral thiourea ligands. The new ligands were characterised by means of NMR spectroscopy, IR spectroscopy, MS, elemental (C, H, N and S) analysis and melting point determination methods.

►The second part of this study focuses on the synthesis of transition metal complexes with the new chiral acylthiourea ligands. Extensive investigation of the coordination chemistry of the new complexes was carried out using NMR spectroscopy, IR spectroscopy, MS, elemental (C, H, N and S) and X-ray diffraction analysis.

CHAPTER THREE

EXPERIMENTAL

3.1 EXPERIMENTAL DETAILS

The four new ligands shown in **Table 3.1** were prepared in high yield and were fully characterised by means of NMR spectroscopy, IR spectroscopy,MS and elemental (C, H, N and S) analysis. In addition to these ligands transition metal complexes H_3O^+{*fac*-[Co(L^8-*S,O*)$_3$]$^-$}, *cis*-[Ni(L^8-*S,O*)$_2$], *trans*-[Cu(L^8-*S,O*)$_2$], *trans/cis*-[Zn(L^8-*S,O*)$_2$], *cis/trans*-[Pt(L^8-*S,O*)$_2$], Ag_2[(HL^8-S)(L^8-μ-S,O)]$_2$ *cis/trans*-[Ni(L^{11}-*S,O*)$_2$] and trans/*cis*-[Cu(L^{11}-*S,O*)$_2$], were also prepared using the new chiral *N,N*-diethyl-*N´*-camphanoylthiourea (HL^8) and *N,N*-diethyl-*N´*-adamantylcarbonylthiourea (HL^{11}). The new complexes were fully characterised by means of NMR spectroscopy, IR spectroscopy , MS, elemental (C, H, N and S) and X-ray diffraction analysis.

3.1.1. Instruments used for characterisation of new products

Nuclear Magnetic Resonance (NMR) Spectroscopy: One-dimensional NMR spectra (^{1}H, ^{13}C and DEPT) and two-dimensional NMR spectra (COSY and GHSQC) of the new ligands and their corresponding metal complexes were measured in 5 mm NMR tubes in $CDCl_3$ solution at 25 °C. The chemical shifts (δ) were referenced to tetramethylsilane (TMS) as an internal standard. The instrument used was a Varian Unity Inova 600 spectrometer operating at 600 MHz for ^{1}H NMR spectra and 150 MHz for ^{13}C NMR spectra.

Infrared (IR) Spectroscopy: Infrared spectra were measured with a NEXUS FT-IR instrument, custom-made by Thermo Nicolet Instruments. KBr pellets were used to run the infrared spectra of the compounds in the range of 4000-400 cm^{-1} at a standard resolution of 4 cm^{-1}, representing a data point spacing of just under 2 cm^{-1}. The spectrometer was equipped with a Ge-on-KBr beamsplitter and DTGS/CsI detector. The instrument was continuously purged with high purity nitrogen gas during recording. The operating and data manipulating software is the OMNIC package.

Mass Spectrometry (MS), Polarimetry, UV-Visible spectroscopy and elemental (C, H, N and S) analysis: Mass Spectra were determined with an AMD 604 instrument. The specific rotations of the three chiral ligands in either CH_3Cl or CH_3CH_2OH were measured using an ADP 220 Polarimeter. The characterisations of

compounds by means of elemental (C, H, N and S) analysis were carried out using a Heraeus CHN rapid combustion analyser at the University of Cape Town (UCT). The UV-Vis spectrum of the oxidation of Co(II) to Co(III) in the $H_3O^+\{fac\text{-}[Co(L\text{-}S,O)_3]^-\}$ complex was collected with an Agilent 8453 instrument. Thin layer chromatography (TLC) was done for all the four new *N,N*-dialkyl-*N´*-acylthiourea ligands and all the metal complexes of HL^8 and HL^{11} ligands using silica gel plates (TLC aluminium sheets) and $CHCl_3$ as the mobile phase. Melting points were determined in open capillary tubes and are uncorrected.

Crystal diffraction analysis: The crystal structures of $H_3O^+\{fac\text{-}[Co(L^8\text{-}S,O)_3]^-\}$, *cis*-$[Ni(L^8\text{-}S,O)_2]$, *trans*-$[Cu(L^8\text{-}S,O)_2]$ and $Ag_2[(HL^8\text{-}S)(L^8\text{-}\mu\text{-}S,O)]_2$ were determined by X-ray diffraction analysis. The methods of analysis and refinement followed for the four complexes were the same. Suitable crystals of the above mentioned complexes were mounted on a thin glass fiber and coated in silicone-based oil to prevent decomposition. Data were collected at UCT on a Nonius Kappa CCD diffractometer using graphite monochromated Mo-Kα radiation (λ = 0.7107 Å) with a detector to crystal distance of 45 mm. 363 {for *trans*-$[Cu(L^8\text{-}S,O)_2]$ and *cis*-$[Ni(L^8\text{-}S,O)_2]$} and 453 {for $H_3O^+\{fac\text{-}[Co(L^8\text{-}S,O)_3]^-\}$ and $Ag_2[(HL^8\text{-}S)(L^8\text{-}\mu\text{-}S,O)]_2$} oscillation frames were recorded, each of width 1° in ϕ, followed by 251 (for *trans*-$[Cu(L^8\text{-}S,O)_2]$ and *cis*-$[Ni(L^8\text{-}S,O)_2]$ and 241 (for $H_3O^+\{fac\text{-}[Co(L^8\text{-}S,O)_3]^-\}$ and $Ag_2((HL^8\text{-}S)(L^8\text{-}\mu\text{-}S,O))_2$) frames of 1° width in ω (with $\kappa \neq 0$). Crystals were indexed from the first ten frames using the DENZO package[33] and positional data were refined along with diffractometer constants to give the final cell parameters. Integration and scaling (DENZO, Scalepack[33]) resulted in unique data sets corrected for Lorentz-polarisation effects and for the effects of crystal decay and absorption by a combination of averaging of equivalent reflections and an overall volume and scaling correction. The structures were solved using SHELXS-97[34] and developed *via* alternating least squares cycles and Fourier difference synthesis (SHELXL-97[34]) with the aid of the interface program X-SEED.[35] All non-hydrogen atoms of the complexes were modelled anisotropically. The hydrogen atoms of nickel and silver complexes were assigned an isotropic thermal parameter 1.2 times that of the parent atom (1.5 times for terminal atoms) and allowed to ride on their parent atoms whereas the hydrogen atoms of the cobalt and copper complexes were placed in calculated positions and included in the model during later stages of the refinement.

The molecular structures and crystallographic data of the four complexes are discussed in chapter four. Selected bond lengths, angles, atomic coordination and anisotropic displacement parameters including torsion angles of the three complexes, except the cobalt complex are listed in appendix B.

3.2 SYNTHESIS AND CHARACTERISATION OF LIGANDS

3.2.1. Experimental procedures related to the preparation of four new ligands

The four new ligands were prepared according to the methods employed by Douglas and Dains.[15] The major problem in the synthesis of these types of ligands (from acyl or aroyl acid chlorides) is the extreme sensitivity of the reaction to moisture.[15] It was therefore imperative to avoid moisture in the reaction procedure. Thus the reactions for the preparation of these ligands were carried out under dry argon gas using well-dried glassware and anhydrous acetone as a solvent. The general procedure followed to synthesise these ligands is as follows:

Approximately 2 g (21 mmol) of potassium thiocyanate, dried in a vacuum oven for 6 hours at 100 °C was weighed and dissolved in 50 ml of anhydrous acetone in a two-necked round bottom flask under argon. An equimolar amount of acid chloride [(*S*)-(-)-camphanic chloride or adamantane carbonyl chloride] dissolved in the same amount of anhydrous acetone was added dropwise to the potassium thiocyanate solution using a dropping funnel while stirring with a magnetic stirrer. After the addition of the acid chloride was complete the reaction mixture was refluxed for one hour at 50 °C. The reaction mixture was then cooled to room temperature. At this stage the acylisothiocyanate intermediate (camphanoylisothiocyanate or adamatylcarbonylisothiocyanate) together with a KCl precipitate were formed and the success of the reaction was monitored by means of IR spectroscopy. Removal of the KCl at this stage was unnecessary, as it has no effect on the formation of the final target ligands. After the reaction was cooled to room temperature, an equimolar amount of amine (diethyl amine, piperidine or pyrrolidine) dissolved in 50 ml of anhydrous acetone was added dropwise, while stirring. When the addition of the amine was complete the reaction mixture was refluxed for another hour. The reaction mixture was allowed to cool to room temperature and then poured into a beaker containing about 80 ml of distilled water, which was left in a fume cupboard

overnight. On evaporation of the acetone the ligands precipitated out of solution and were collected by filtration and washed three to four times with distilled water. The ligands were dried in a vacuum oven at 85 °C for two hours and then characterised by means of NMR spectroscopy, IR spectroscopy, MS, elemental (C, H, N, and S) analysis, specific rotation and melting point determinations. The new ligands formed with their respective reagents are listed in **Table 3.1**. The KCl salt dissolves in the distilled water during recrystallisation of the ligands at the end of the synthesis.

All the commercially available reagents indicated in **Table 3.1** were used without further purification. The acetone however was distilled under dry argon gas and the distillate was dried with 4Å molecular sieves prior to use.

Table 3.1. The new ligands with their respective reagents besides KSCN.

New ligands synthesised	Reagents used	
	Acid chloride	Amine
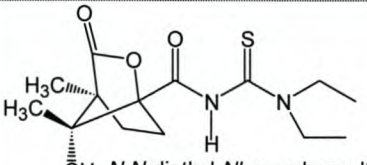 *N,N*-diethyl-*N'*-camphanoylthiourea, HL^8	(*S*)-(-)-Camphanic chloride	Diethylamine
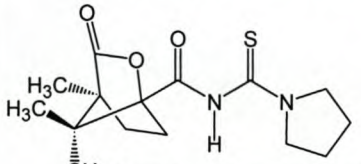 *N*-pyrrolidyl-*N'*-camphanoylthiourea, HL^{10}	(*S*)-(-)-Camphanic chloride	Pyrrolidine
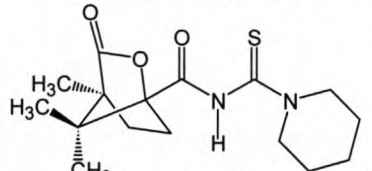 *N*-piperidyl-*N'*-camphanoylthiourea, HL^9	(*S*)-(-)-Camphanic chloride	Piperidine
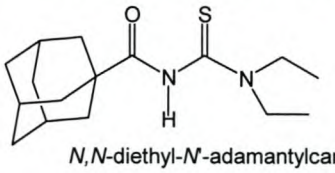 *N,N*-diethyl-*N'*-adamantylcarbonylthiourea, HL	Adamantane carbonyl chloride	Diethylamine

The synthetic routes for the preparation of ligands HL^8, HL^9, HL^{10} and HL^{11} are shown in **reaction scheme 3.1**.

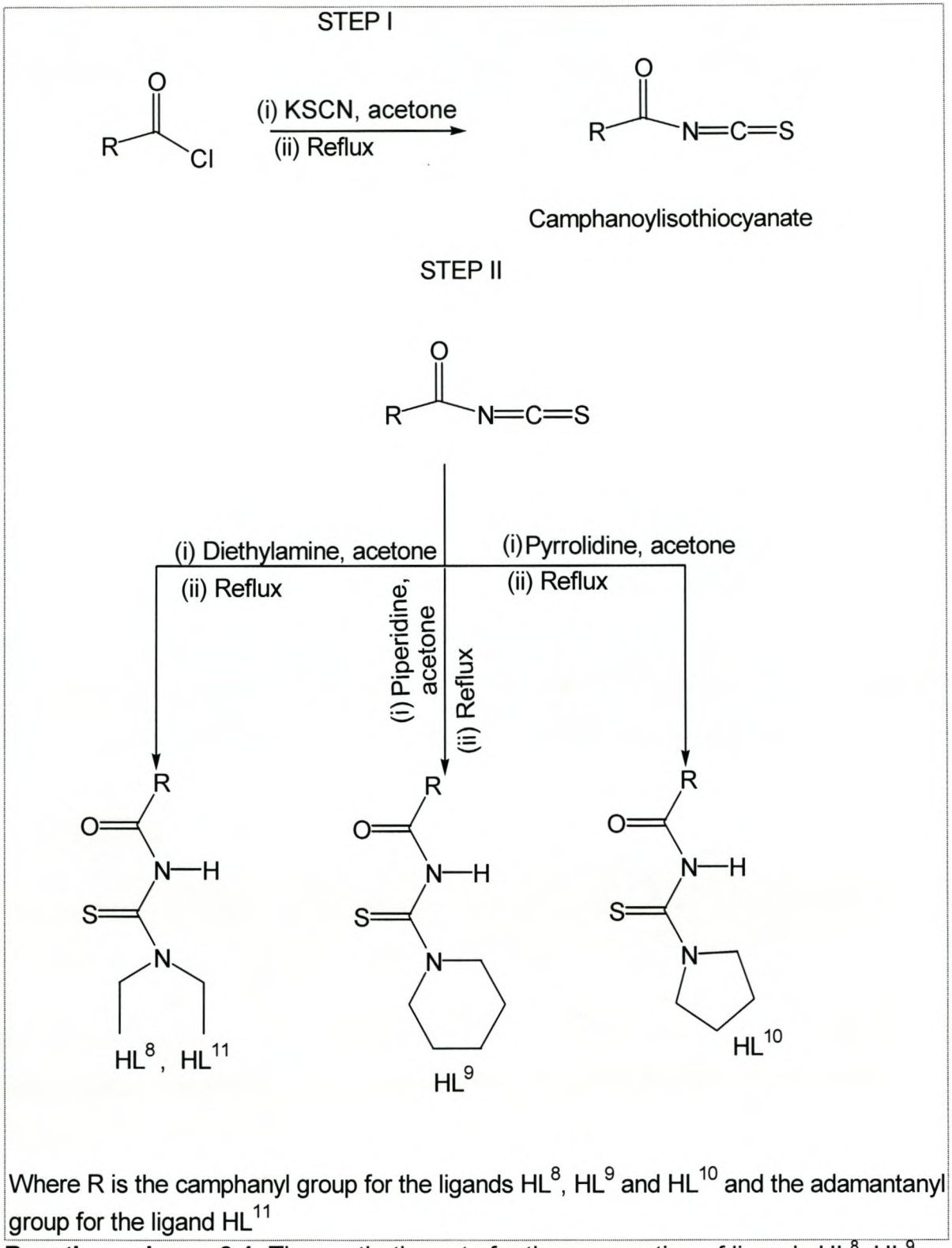

Reaction scheme 3.1. The synthetic route for the preparation of ligands HL^8, HL^9, HL^{10} and HL^{11}.

3.2.2. Characterisation of the four new ligands

The proposed structures and atomic numbering of the four new ligands are shown in **Figure 3.1**.

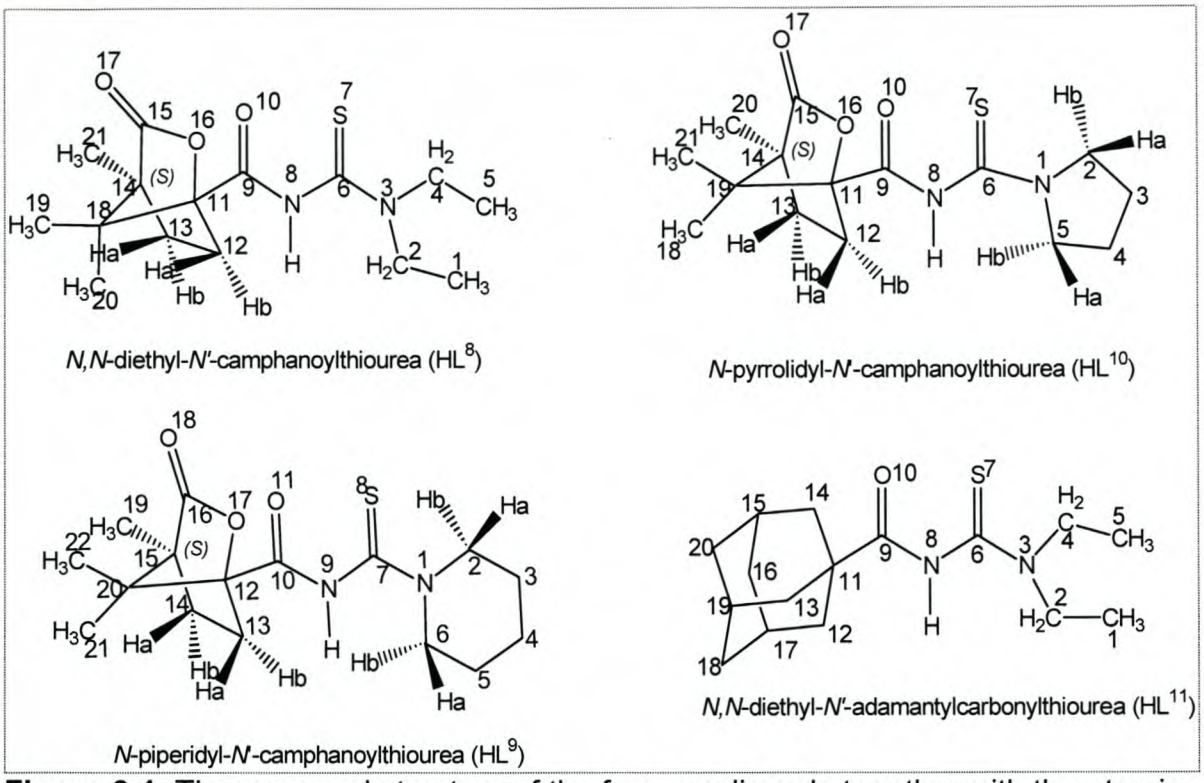

Figure 3.1. The proposed structure of the four new ligands together with the atomic numbering scheme.

3.2.2.1. *N,N*-diethyl-*N'*-camphanoylthiourea, HL^8

Recrystallised yield 87 %; m.p.142 °C; Specific rotation $[\alpha]_D^{21.4}$ = -22.39 (c 0.097 g/ml in CH_3CH_2OH); Found: C, 57.61; H, 7.72; N, 8.91; S, 9.94. $C_{15}H_{24}N_2O_3S$ requires C, 57.66; H, 7.74; N, 8.97; S, 10.26 %); *m/z* 312(M^+, 95.54 %), 283(11.78), 253(28.03), 209(7.00), 181(12.74), 159(25.48), 151(27.58) 125(23.57), 97(17.83), 83(47.13), 72(100), 44(31.85) and 29(12.61); Characteristic absorption bands: ν_{max}/cm^{-1} 3407m (N-H), 2969m (C-H), 2874w (C-H), 1806vs [C(15)=O(17)], 1707vs [C(9)=O(10)] and 1228m (S=C); δ_H (600 MHz, $CDCl_3$) 8.37(1H, s, NH), 3.96 (2H, broad s, H^2), 3.53 (2H, broad s, H^4), 2.48 (2H, ddd, $^2J_{12b,12a}$, $^3J_{12b,13b}$, $^3J_{12b,13a}$ 13.5, 10.5, 4.5 Hz, H^{12b}), 1.97 (2H, ddd, $^2J_{12a,12b}$, $^3J_{12a,13a}$, $^3J_{12a,13b}$ 13.5, 7.5, 3.3 Hz, H^{12a}), 1.92 (2H, ddd, $^2J_{13b,13a}$, $^3J_{13b,2b}$, $^3J_{13b,12a}$ 13.5, 10.5, 3.3 Hz, H^{13b}), 1.68 (2H, ddd, $^2J_{13a,13b}$, $^3J_{13a,12a}$, $^3J_{13a,12b}$ 13.5, 7.5, 4.5 Hz, H^{13a}), 1.26 (3H, t, $^3J_{1,2}$ 6.3 Hz, H^1), 1.26 (3H, t, $^3J_{5,4}$ 6.3 Hz H^5), 1.09 (3H, s, H^{21}), 1.07 (3H, s, H^{19}), 0.98 (3H, s, H^{20}); δ_c (150 MHz, $CDCl_3$) 177.6 (C^{15}), 177.5 (C^6), 164.3 (C^9), 91.9 (C^{11}), 55.38 (C^{18}), 54.9 (C^{14}), 47.9 (C^2), 47.5 (C^4), 30.2 (C^{12}), 28.8 (C^{13}), 16.5 (C^{20}), 16.4 (C^{19}), 13.1 (C^1), 13.0 (C^5), 9.4 (C^{21}).

3.2.2.2. *N*-piperidyl-*N´*-camphanoylthiourea, HL[9]

Recrystallised yield 82 %; m.p. 137 °C; Specific rotation $[\alpha]_D^{24.7}$ = -6.00 (c 0.01 g/ml in $CHCl_3$); Found: C, 59.14; H, 7.41; N, 8.58; S, 9.7. $C_{16}H_{24}N_2O_3S$ requires C, 59.23; H, 7.46; N, 8.63; S, 9.88 %; *m/z* 324(M^+, 52.53 %), 265(4.43), 181(5.70), 171(7.59), 143(9.49), 84(100) and 55(9.49); Characteristic absorption bands: ν_{max}/cm^{-1} 3397m (N-H), 2972m and 2858w (C-H), 1790vs [C(16)=O(18)], 1700vs [C(10)=O(11)] and 1249m (S=C); δ_H (600 MHz, $CDCl_3$)* 8.51 (1H, s, NH), 4.16 (1H, broad s, $H^{6a/6b}$), 4.02 (1H, broad s, $H^{6b/6a}$), 3.51 (1H, broad s, $H^{2a/2b}$), 3.36 (1H, broad s, $H^{2b/2a}$), 2.50 (1H, ddd, $^2J_{13a,13b}$, $^3J_{13a,14a}$, $^3J_{13a,14b}$ 13.2,10.2, 4.2 Hz, H^{13a}), 1.99 (1H, ddd, $^2J_{13b,13a}$, $^3J_{13b,14b}$,$^3J_{13b,14a}$ 13.2, 9, 4.2 Hz, H^{13b}), 1.94 (1H, ddd, $^2J_{14b,14a}$, $^3J_{14b,13b}$, $^3J_{14b,13a}$ 13.8,10.2, 4.2 Hz, H^{14b}), 1.69 (7H, broad m, H^3, H^4, H^5, and H^{14a}), 1.12 (3H, s, H^{22}), 1.08 (3H, s, H^{19}), 1.01 (3H, s, H^{21}); δ_c (150 MHz, $CDCl_3$) 177.1 (C^{16}), 176.3 (C^7), 163.3 (C^{10}), 91.7 (C^{12}), 55.4 (C^{20}), 55.0 (C^{15}), 53.1 (C^6), 52.6 (C^2), 30.3 (C^{13}), 28.9 (C^{14}), 26.1 (C^3), 25.1 (C^5), 23.8 (C^4), 16.8 (C^{21}), 16.6 (C^{22}), 9.6 (C^{19}).

* The H^{2a}/ H^{2b} and H^{6a}/ H^{6b} indicate the reversibility of the assignments of the two protons in each pair.

3.2.2.3. *N*-pyrrolidyl-*N´*-camphanoylthiourea, HL[10]

Recrystallised yield 74 %; m.p. 134 °C; Specific rotation $[\alpha]_D^{25.2}$ = -16 (c 0.098 g/ml in $CHCl_3$); Found: C, 57.89; H, 7.11; N, 9.12; S,10.12. $C_{15}H_{22}N_2O_3S$ requires C, 58.03; H, 7.14; N, 9.02; S, 10.33 %; *m/z* 310(M^+, 54.43 %), 251(25.95), 223(5.06), 204(13.92), 157(10.13), 125(10.76), 98(22.78), 70(100) and 55(30.38); Characteristic absorption bands: ν_{max}/cm^{-1} 3371m (N-H), 2969m and 2882w (C-H), 1776vs [C(15)=O(17)],1691vs [C(9)=O(10)], and1252m (S=C); δ_H (600 MHz, $CDCl_3$) 8.52 (1H, s, NH), 3.78 (1H, broad s, $H^{5b/5a}$), 3.71 (1H, broad s, $H^{5a/5b}$), 3.64 (1H, dt, $^2J_{2b,2a}$, $^3J_{2b,3}$ 10.2, 3.3 Hz, $H^{2b/2a}$), 3.62 (1H, dt, $^2J_{2a,2b}$, $^3J_{2a,3}$ 10.2, 3.3 Hz, $H^{2a/2b}$), 3.42 (2H, broad s, H^3), 3.41 (2H, broad s, H^4), 2.47 (H12b, ddd, $^2J_{12b,12a}$, $^3J_{12b,13b}$, $^3J_{12b,13a}$ 12.9, 6.9, 4.2 Hz, H^{12b}), 1.96 (1H, ddd, $^2J_{12a,12b}$,$^3J_{12a,13a}$, $^3J_{12a,13b}$ 12.9, 9.9, 3.3 Hz, H^{12a}), 1.88 (1H, ddd, $^2J_{13b,13a}$, $^3J_{13b,12b}$, $^3J_{13b,12a}$ 9.6, 6.9, 3.3 Hz, H^{13b}), 1.63 (1H, ddd, $^2J_{13a,13b}$, $^3J_{13a,12a}$, $^3J_{13a,12b}$ 9.6, 9.9, 4.2 Hz, H^{13a}), 1.10 (3H, s, H^{18}), 1.09 (3H, s, H^{21}), 0.97 (3H, s, H^{20}); δ_C (150 MHz, $CDCl_3$) 179.0 (C^{15}), 177.1 (C^6), 165.6 (C^9), 93.0 (C^{11}),

55.4 (C^{19}), 54.0 (C^{14}), 47.6 (C^5), 47.5 (C^2), 30.4 (C^{12}), 29.1 (C^{13}), 24.6 (C^3), 26.7 (C^4), 16.8 (C^{21}), 16.7 (C^{18}), 9.6 (C^{20}).

3.2.2.4. *N,N*-diethyl-*N´*-adamantylcarbonylthiourea, HL^{11}

Recrystallised yield 92 %; m.p. 145 °C; Found: C, 65.10; H, 9.36; N, 9.43; S, 10.77. $C_{16}H_{26}N_2OS$ requires C, 65.26; H, 8.90; N, 9.51; S, 10.89 %; *m/z* 294(M^+, 6.37 %), 158(4.78), 135(100), 107(13.38), 79(29.30) and 41(13.38); Characteristic absorption bands: ν_{max}/cm^{-1} 3283m (N-H), 2917m and 2848w (C-H), 1644vs (O=C) and 1235m (S=C); δ_H (600 MHz, $CDCl_3$) 7.63 (1H, s, NH), 3.97 (2H, broad s, H^2), 3.46 (2H, broad s, H^4), 2.01 (3H, broad m, H^{15}, H^{17}, H^{19}), 1.83 (6H, broad s, H^{12}, H^{13}, H^{14}), 1.65 (6H, broad s, H^{16}, H^{18}, H^{20}),1.24 (3H, s, H^1), 1.18 (3H, s, H^5); δ_C (150 MHz, $CDCl_3$) 179.7 (C^6), 174.1 (C^9), 48.0 (C^4), 47.5 (C^2), 43.22 (C^{11}), 38.8 (C^{15}, C^{17}, C^{19}), 36.2 (C^{12}, C^{13}, C^{14}), 27.9 (C^{16}, C^{18}, C^{20}), 13.2 (C^5), 11.5 (C^1).

3.3. SYNTHESIS AND CHARACTERISATION OF TRANSITIO N METAL COMPLEXES OF *N,N*-DIETHYL-*N´*-CAMPHANOYL THIOUREA AND *N,N*-DIETHYL-*N´*-ADAMANTYLCARBONYL THIOUREA.

As indicated in **section 2.3.2**, the HL type thiourea ligands can readily form metal complexes with the 1st and 2nd row transition metal ions upon deprotonation of the NH proton with a weak base such as CH_3CO_2Na or $NaHCO_3$. The methods of preparation for such types of metal complexes differs from one metal ion to another depending on the behaviour of the metal ion and also differs depending on the type of alkyl/aryl substituents on the ligands.

3.3.1. Experimental procedures related to the preparation of new transition metal complexes of ligands HL^8 and HL^{11}.

After the ligands were purified and fully characterised, complexes of Co(II), Ni(II), Cu(II), Zn(II), Ag(I), and Pt(II) were formed with ligands HL^8 and HL^{11}. Preparations of these complexes differ slightly from each other depending on the properties of the metal salts and behaviour of the metal ions used. The methods of preparation

including the reaction schemes will be discussed later. The metal complexes prepared are shown in **Table 3.2** with the respective reagents used. All the metal salts listed in **Table 3.2** were commercially available and were used without further purification.

Table 3.2. The metal complexes with their respective reagents.

Metal complex formed	Ligand	Metal salt	CH_3CO_2Na
$H_3O^+\{fac\text{-}[Co(L^8\text{-}S,O)_3]^-\}$	HL^8	$Co(NO_3)_2{\cdot}6H_2O$	✓
cis-$[Ni(L^8\text{-}S,O)_2]$	HL^8	$Ni(CH_3CO_2)_2{\cdot}4H_2O$	
trans-$[Cu(L^8\text{-}S,O)_2]$	HL^8	$Cu(NO_3)_2{\cdot}3H_2O$	✓
trans/cis-$[Zn(L^8\text{-}S,O)_2]$*	HL^8	$Zn(NO_3)_2{\cdot}6H_2O$	✓
trans/cis-$[Pt(L^8\text{-}S,O)_2]$*	HL^8	K_2PtCl_4	✓
$Ag_2[(HL^8\text{-}S)(L^8\text{-}\mu\text{-}S,O)]_2$	HL^8	$AgNO_3$	✓
trans/cis-$[Ni(L^{11}\text{-}S,O)_2]$*	HL^{11}	$Ni(CH_3CO_2)_2{\cdot}4H_2O$	
trans/cis-$[Cu(L^{11}\text{-}S,O)_2]$*	HL^{11}	$Cu(NO_3)_2{\cdot}3H_2O$	✓

* The *trans* or *cis*-$[M(L\text{-}S,O)_2]$ formation of these complexes has not been confirmed by X-ray diffraction analysis. The symbol ✓ indicates the use of CH_3CO_2Na in the complex formation reaction of certain complexes.

The detailed procedures followed to prepare the complexes of these metal ions are discussed in the following sections.

3.3.1.1. Preparation of hydronium *fac-tris*(*N,N*-diethyl-*N´*-camphanoyl thioureato)Co(II), $H_3O^+\{fac\text{-}[Co(L^8\text{-}S,O)_3]^-\}$

0.10 g (3.20 mmol) of *N,N*-diethyl-*N´*-camphanoylthiourea was dissolved in 4 ml of acetone in a two-necked round bottom flask. The ligand solution was warmed to 40 °C. Then 31.1 mg (0.11 mmol) of $Co(NO_3)_2{\cdot}6H_2O$ dissolved in 1 ml of distilled water was added dropwise using a dropping funnel. After the addition of the cobalt salt solution was complete, 26.30 mg (0.32 mmol) of sodium acetate dissolved in 1 ml of distilled water was added to the reaction mixture, which was then refluxed while stirring for one hour at 40 °C. The reaction mixture was cooled to room temperature and then poured into a small reaction vessel containing 1 ml of distilled water. The reaction vessel was covered with parafilm that was punctured with needle-sized holes and the vessel was then left in the fume cupboard. The evaporation of the

acetone was controlled by the needle-sized holes in the parafilm. Within 8 days needle-shaped green crystals, which were suitable for X-ray diffraction analysis, had grown and were collected by filtration and washed three times with distilled water. After drying in a vacuum oven at 100 °C for two hours, the crystals were characterised by means of IR spectroscopy, MS, NMR spectroscopy, elemental (C, H, N and S) and X-ray diffraction analysis. The reaction route of the synthesis of hydronium *fac-tris*(*N,N*-diethyl-*N'*-camphanoylthioureato)Co(II) complex is shown in **reaction scheme 3.2**.

$$3HL^8 + Co(NO_3)_2 \cdot 6H_2O \xrightarrow[\text{acetone, water, 40 °C}]{3CH_3CO_2Na} H_3O^+ [(CoL^8\text{-}S,O)_3)]^- + 3CH_3CO_2H + 2NaNO_3 + NaOH + 4H_2O$$

Reaction scheme 3.2. The synthetic route for the preparation of $H_3O^+\{fac\text{-}[Co(L^8\text{-}S,O)_3]^-\}$ in a one-pot process.

$H_3O^+\{fac\text{-}[Co(L^8\text{-}S,O)_3]^-\}$ is air sensitive with the Co(II) in the complex being readily oxidized to Co(III) by atmospheric O_2. This process was confirmed with UV-visible spectroscopy. Hence preparation of $H_3O^+\{fac\text{-}[Co(L^8\text{-}S,O)_3]^-\}$ under an inert atmosphere was imperative. For the UV-Vis spectroscopy study the ligand was dissolved in anhydrous acetone in a two-neck round bottom flask under argon gas and heated to 40 °C. The $Co(NO_3)_2 \cdot 6H_2O$ salt was dissolved in anhydrous acetone and added to the ligand solution dropwise. The CH_3CO_2Na was dissolved in moisture free methanol and added to the reaction mixture while stirring. After the addition of the sodium acetate was complete the reaction mixture was refluxed. After one hour, which is the optimum time for this complex formation reaction, the solvents were removed under vacuum and then immediately the first UV-Vis spectrum of the fresh sample was taken using 20.0 mg of the complex in 33 ml of anhydrous CH_2Cl_2. After the first spectrum was taken the complex was exposed to the atmosphere and the oxidation of Co(II) to Co(III) by atmospheric O_2 was monitored using UV-Vis spectroscopy once every 24 hours for one week (see **Figure 4.22**).

3.3.1.2. Preparation of *cis-bis*(*N,N*-diethyl-*N'*-camphanoylthioureato)Ni(II), *cis*-[Ni(L^8-*S,O*)$_2$]

85 mg (0.272 mmol) of HL^8 was dissolved in 4 ml of acetone in a two-necked round bottom flask and the ligand solution warmed to 40 °C. 33.8 mg (0.136 mmol) of

hydrous nickel acetate [$Ni(CH_3CO_2)_2{\cdot}4H_2O$] dissolved in 3 ml of distilled water was added dropwise to the warm ligand solution. After the addition of the nickel acetate solution was complete the reaction mixture was refluxed for one hour at 40 °C while stirring. Finally, pale purple crystals, which were stable in air and suitable for X-ray diffraction analysis, were grown within one week in a small reaction vessel by controlling the evaporation of the acetone. The crystals were washed three times with distilled water and collected by filtration. After the crystals were dried in a vacuum oven at 100 °C for two hours the complex was characterised by means of MS, NMR spectroscopy, IR spectroscopy, elemental (C, H, N and S) and X-ray diffraction analysis. **Reaction scheme 3.3** shows the synthetic route for the nickel complex formation.

$$2HL^8 + Ni(CH_3CO_2)_2{\cdot}4H_2O \xrightarrow[40\ °C]{\text{acetone, water}} Ni(L^8\text{-}S,O)_2 + 2CH_3CO_2H + 4H_2O$$

Reaction scheme 3.3. The synthetic route for the preparation of *cis*-[$Ni(L^8\text{-}S,O)_2$].

3.3.1.3. Preparation of *trans-bis*(*N,N*-diethyl-*N´*-camphanoylthioureato) copper(II), *trans*-[$Cu(L^8\text{-}S,O)_2$]; *trans/cis-bis*(*N,N*-diethyl-*N´*-camphanoyl thioureato)zinc(II), *trans/cis*-[$Zn(L^8\text{-}S,O)_2$]; *cis/trans-bis*(*N,N*-diethyl-*N´*-camphanoylthioureato)Platinum, *cis/trans*-[$Pt(L^8\text{-}S,O)_2$]; and *tetrakis*(*N,N*-diethyl-*N´*-camphanoylthioureato) diargentate(I), $Ag_2[(HL^8\text{-}S)(L^8\text{-}\mu\text{-}S,O)]_2$

Trans-[$Cu(L^8\text{-}S,O)_2$], *trans/cis*-[$Zn(L^8\text{-}S,O)_2$] and *cis/trans*-[$Pt(L^8\text{-}S,O)_2$] were prepared following exactly the same procedure as that used for the preparation of H_3O^+{*fac*-[$Co(L^8\text{-}S,O)_3]^-$}. Good quality crystals, which were suitable for X-ray diffraction analysis, were grown for each of the above complexes by recrystallisation of their crude products from an acetone and water mixture. After the complexes were dried in a vacuum oven at 100 °C for 2 hours they were analysed by means of MS, NMR spectroscopy, IR spectroscopy, and elemental (C, H, N and S) analysis. The stereochemistry of *trans*-[$Cu(L^8\text{-}S,O)_2$] was also analysed by X-ray diffraction analysis. **Reaction scheme 3.4** shows the reaction routes for the preparation of *trans*-[$Cu(L^8\text{-}S,O)_2$], *trans/cis*-[$Zn(L^8\text{-}S,O)_2$] and *cis/trans*-[$Pt(L^8\text{-}S,O)_2$].

$$2HL^8 + M(NO_3)_2 \cdot xH_2O \xrightarrow[\text{acetone, water, 40 °C}]{2CH_3CO_2Na} M(L^8\text{-}S,O)_2 + 2NaNO_3 + xH_2O + 2CH_3CO_2H$$

Where M is Cu^{II} or Zn^{II} and x is the number of moles of water in their respective salts

$$2HL^8 + K_2PtCl_4 \xrightarrow[\text{acetone, water, 40 °C}]{2CH_3CO_2Na} Pt(L^8\text{-}S,O)_2 + 2KCl + 2NaCl + 2CH_3CO_2H$$

Reaction scheme 3.4. The synthetic route for the preparation of *trans*-[$Cu(L^8\text{-}S,O)_2$], *trans/cis*-[$Zn(L^8\text{-}S,O)_2$] and *cis/trans*-[$Pt(L^8\text{-}S,O)_2$].

Since the ^{13}C and ^{195}Pt NMR spectra of *cis/trans*-[$Pt(L^8\text{-}S,O)_2$] (**Figure 4.13 and 4.14** respectively in chapter four) showed the presence of a *cis* and *trans*-isomer mixture, fractional crystallization was attempted using a 20:80 (v/v) ratio of CH_3Cl/CH_3CN so as to crystallise out only one isomer of the complex. From experience it is known that the solvent of crystallisation influences the coordination chemistry of platinum complexes.[29]

The synthesis of $Ag_2[(HL^8\text{-}S)(L^8\text{-}\mu\text{-}S,O)]_2$ was carried out by employing the same procedures as for the preparation of $H_3O^+\{fac\text{-}[(Co(L^8\text{-}S,O)_3]^-\}$ from a 2:1 mole ratio of ligand to Ag(I). The synthesis as well as growing of crystals were carried out in the dark to prevent the reduction of Ag(I) to Ag(0) by UV-light. Hence during and after the reaction the containers were covered with aluminium foil and kept in a dark area for 8 days during recrystallisation. By controlling the evaporation of the acetone, colourless crystals, which were suitable for crystallographic data collection, were collected by filtration and washed with distilled water in a dark area. After drying at 110 °C for two hours in a vacuum oven, the crystals were characterised by means of MS, IR spectroscopy, NMR spectroscopy, elemental (C, H, N and S) and X-ray diffraction analysis. The synthetic route for the synthesis of $Ag_2[(HL^8\text{-}S)(L^8\text{-}\mu\text{-}S,O)]_2$ complex is shown in **reaction scheme 3.5**.

$$4HL^8 + 2AgNO_3 \xrightarrow[\text{acetone, water, 40 °C}]{2CH_3CO_2Na} Ag_2[(HL^8\text{-}S)(L^8\text{-}S,O)]_2 + 2NaNO_3 + 2CH_3CO_2H$$

Reactions scheme 3.5. The synthetic route for the preparation of $Ag_2[(HL^8\text{-}S)(L^8\text{-}\mu\text{-}S,O)]_2$.

3.3.1.4. Preparation of Ni(II) and Cu(II) complexes with *N,N*-diethyl-N´-adamantylcarbonylthiourea (HL^{11})

Good quality crystals of *trans/cis-bis*(*N,N*-diethyl-*N´*-adamantylcarbonoylthioureato) Ni(II) and *trans/cis-bis*(*N,N*-diethyl-*N´*-adamantylcarbonylthioureato)Cu(II) were prepared following the same procedure as for the preparation of *cis*-[Ni(L^8-*S,O*)$_2$] and *trans*-[Cu(L^8-*S,O*)$_2$]. The reaction schemes for the formation of *trans/cis*-[Ni(L^{11}-*S,O*)$_2$] and *trans/cis*-[Cu(L^{11}-*S,O*)$_2$] are similar to the reaction routes for the preparation of *cis*-[Ni(L^8-*S,O*)$_2$] and *trans*-[Cu(L^8-*S,O*)$_2$] discussed earlier. The only difference is the use of ligand HL^{11} instead of HL^8.

3.3.2. Characterisation of the new transition metal complexes of ligands HL^8 and HL^{11}

3.3.2.1. Hydronium *fac-tris*(*N,N*-diethyl-*N´*-camphanoylthioureato)Co(II), H_3O^+{*fac*-[Co(L^8-*S,O*)$_3$]$^-$}

Recrystallised yield 91 %; m.p 228 °C; Found: C, 52.63; H, 6.80; N, 8.34; S, 9.06. [Co(L^8-S,O)$_3$]$^-$ H_3O^+ requires C, 53.45; H, 6.89; N, 8.40; S 9.51 %; *m/z* 993 (M^+, 11%), 524(13.92), 428(6.96), 371(14.24), 312(21.52), 109(35.44) and 18(100); Characteristic absorption bands: ν_{max}/cm^{-1} 3432 (O-H), 2969m and 2873w (C-H), 1782vs [C(13=O(21)], 1427vs [C(4)=O(5)] and 817w (C=S).

The characterisation of freshly prepared H_3O^+{*fac*-[Co(L^8-*S,O*)$_3$]$^-$} by ^{1}H and ^{13}C NMR spectroscopy is prevented by the paramagnetic nature of Co(II) d^7. However when the Co(II) had been oxidized to Co(III) d^6 in the complex by atmospheric O_2 good ^{1}H and ^{13}C NMR spectra of the oxidized cobalt complex were obtained. The ^{1}H NMR spectrum of the complex 18 days after it was synthesised is shown in **Figure 4.21**. The ^{1}H and ^{13}C NMR data of the oxidized cobalt complex are presented below.

δ_H (600 MHz, $CDCl_3$) 3.76 (1H, dq, $^2J_{9a,9b}$, $^3J_{9a,10}$ 13.8, 7.2 Hz, $H^{9b/9a}$), 3.72 (1H, dq, $^2J_{9b,9a}$, $^3J_{9b,10}$ 13.8, 7.2 Hz, $H^{9a/9b}$), 3.64 (1H, dq, $^2J_{7a,2b,}$ $^3J_{7a,8}$ 13.8, 7.2 Hz, $H^{7a/7b}$), 3.58 (1H, dq, $^2J_{7b,8a}$, $^3J_{7b,8}$ 13.8, 7.2 Hz, $H^{7b/7a}$), 2.40 (1H, ddd, $^2J_{16b,16a}$, $^3J_{16e,15b,}$ $^3J_{16b,15a}$ 13.2, 9, 4.2 Hz, H^{16b}), 1.89 (1H, ddd, $^2J_{16a,16b}$, $^3J_{16a,15a}$, $^3J_{16a,15b}$ 13.2, 12.6, 4.8 Hz, H^{16a}), 1.85 (1H, ddd, $^2J_{15b,15a}$, $^3J_{15b,16b}$, $^3J_{15b,16a}$ 13.8, 9, 4.8 Hz H^{15b}), 1.60 (1H,

ddd, $^{2}J_{15a,15b}$,$^{3}J_{15a,16a}$, $^{3}J_{15a,16b}$ 13.8, 12.6, 4.2 Hz, H^{15a}), 1.29, 1.28, 1.15 (3H, t, $^{3}J_{8,7}$ 7.2 Hz, H^{8}), 1.13, 1.06 (3H, t, $^{3}J_{10,}$ 7.2 Hz, H^{10}), 1.07 (3H, s, H^{18}), 1.02 (3H, s, H^{20}), 0.92 (3H, s, H^{21})*; δ_C (150 MHz, $CDCl_3$) 182.6 (C^{13}), 177.7 (C^{4}), 176.0 (C^{2}), 96.8 (C^{11}), 57.6 (C^{19}), 56.3 (C^{14}), 48.0 (C^{9}), 47.8 (C^{7}), 33.2 (C^{16}), 31.8 (C^{15}), 19.5 (C^{21}), 19.0 (C^{20}), 15.3 (C^{10}), 15.0 (C^{8}), 12.7 (C^{18}).

*The H^{7b}/ H^{7a} and H^{9b}/ H^{9a} indicate the reversibility of the assignments of the two protons in each pair.

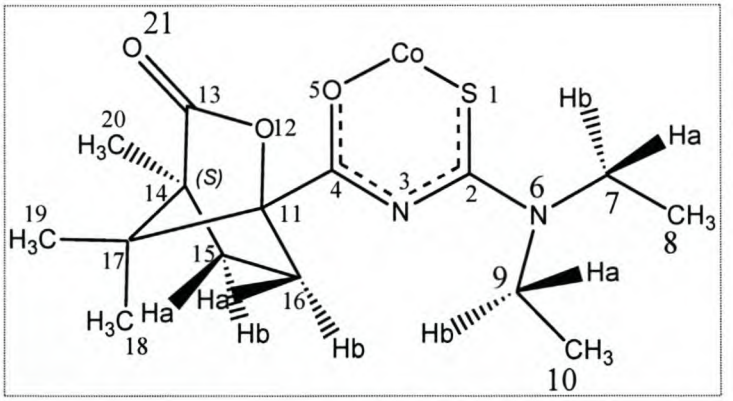

Figure 3.2. Atomic numbering scheme of H_3O^{+}{*fac*-[Co(L^{8}-*S,O*)$_3$]$^{-}$}.

3.3.2.2. *Cis-bis*(*N,N*-diethyl-*N´*-camphanoylthioureato)Ni(II), *cis*-[Ni(L^{8}-*S,O*)$_2$]

Recrystallised yield 92 %; m.p. 222 °C; Found: C, 53.22; H, 7.09; N, 8.20; S, 9.38. $(C_{15}H_{23}N_2O_3S)_2Ni$ requires C, 52.71; H, 7.08; N, 8.20; S, 9.38 %; *m/z* 681(M^{+}, 19.74 %), 648(3.18), 537(3.18), 523(2.55), 468(14.01), 442(10.82), 371(48.41), 313(13.69), 281(5.73), 189(5.73), 127(100), 72(32.48) and 55(12.74); Characterstic absorption bands: ν_{max}/cm^{-1} 2966m and 2932w (C-H), 1783vs [C(13)=O(17)], 1428vs [C(2)=O(1)] and 822w (C=S); δ_H (600 MHz, $CDCl_3$) 3.76 (1H, dq, $^{2}J_{9a,9b}$, $^{3}J_{9a,10}$ 10.2, 3.6 Hz, $H^{9a/9b}$), 3.72 (1H, dq, $^{2}J_{9a,9b}$, $^{3}J_{9a,10}$ 10.2, 3.6 Hz, $H^{9b/9a}$), 3.62 (1H, dq, $^{2}J_{7b,7a}$, $^{3}J_{7b,8}$ 9.9, 3.6 Hz, $H^{7b/7a}$), 3.58 (1H, dq, $^{2}J_{7a,7b}$, $^{3}J_{7a,8}$ 9.9, 3.6 Hz, $H^{7a/7b}$), 2.40 (1H, ddd, $^{2}J_{16b,16a}$, $^{3}J_{16b,15b}$, $^{3}J_{16b,15a}$ 13.8, 9, 4.8 Hz, H^{16b}), 1.89 (1H, ddd, $^{2}J_{16a,16b}$, $^{3}J_{16a,15a}$, $^{3}J_{16a,15b}$ 13.8, 12.6, 4.2 Hz, H^{16a}), 1.85 (1H, ddd, $^{2}J_{15b,15a}$, $^{3}J_{15b,16b}$, $^{3}J_{15b,16a}$ 13.2, 9, 4.2 Hz, H^{15b}), 1.60 (1H, ddd, $^{2}J_{15a,15b}$, $^{3}J_{15a,16a}$, $^{3}J_{15a,16b}$ 13.2, 12.6, 4.8 Hz, H^{15a}), 1.23 (3H, t, $^{3}J_{8,7}$ 3.6 Hz, H^{8}), 1.19 (3H, t, $^{3}J_{10,9}$ 3.6 Hz, H^{10}), 1.07 (3H, s, H^{18}), 1.02 (3H, s, H^{20}), 0.92 (3H, s, H^{21}); δ_C (150 MHz, $CDCl_3$), 179.4 (C^{13}), 173.5 (C^{2}), 171.9 (C^{4}), 93.7

(C^{11}), 55.2 (C^{19}), 54.2 (C14), 46.0 (C^{9}), 45.7 (C^{7}), 30.9 (C^{16}), 29.4 (C^{15}), 17.1 (C^{21}), 16.9 (C^{20}), 12.9 (C^{10}), 12.2 (C^{8}), 9.8 (C^{18}).

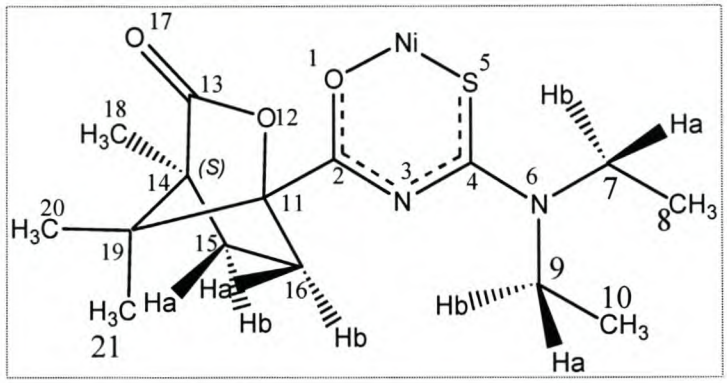

Figure 3.3. Atomic numbering scheme of *cis*-[Ni(L^{8}-*S,O*)$_2$] complex.

3.3.2.3. *Trans-bis*(*N,N*-diethyl-*N´*-camphanoylthioureato)Cu(II), *trans*-[Cu(L^{8}-S,O)$_2$]

Recrystallised yield 84 %; m.p. 176 °C; Found: C, 52.63; H, 7.02; N, 8.21; S, 9.06. ($C_{15}H_{23}N_2O_3S)_2Cu$ requires C, 52.34; H, 7.03; N, 8.14; S 9.32 %; *m/z* 682(M^+, 9.49 %), 523(5.06), 375(5.06), 312(27.85), 251(10.44), 159(10.13), 72(100) and 44(27.85); Characteristic absorption bands: ν_{max}/cm^{-1} 2968m and 2934w (C-H), 1784vs [C(13)=O(21)], 1429vs [C(4)=O(5)]* and 816w (C=S).

*The C(13)=O(21)) and C(4)=O(5) bonds are the carbonyls of the camphanic moiety and O=CN(S) moiety in the *trans*-[Cu(L^{8}-*S,O*)$_2$] complex respectively.

As for the Co(II) complex of H_3O^+{*fac*-[Co(L^{8}-*S,O*)$_3$]$^-$}, the characterisation of the *trans*-[Cu(L^{8}-*S,O*)$_2$] complex by means of NMR spectroscopy was prevented by the paramagnetic nature of Cu(II) d^9. However an extensive structural study of this complex has been made from its X-ray diffraction analysis, which is presented in chapter four.

3.3.2.4. *Trans/cis-bis*(*N,N*-diethyl-*N´*-camphanoylthioureato)Zn(II), *trans/cis*-[Zn(L^{8}-*S,O*)$_2$]

Recrystallised yield 62 %; m.p. 125 °C; Found: C, 52.38; H, 6.74; N, 8.01; S, 9.11. ($C_{15}H_{23}N_2O_3S)_2Zn$ requires C, 52.36; H, 6.74; N, 8.14; S, 9.32 %; *m/z* 687(M^+, 66.46 %), 601(24.68), 529(29.75), 447(45.57 %), 376(10.12), 313(29.11), 251(8.20), 223(11.39), 116(93.67) and 109(100); Characteristic absorption bands: ν_{max}/cm^{-1} 2969m and 2934w (C-H) 1778vs [C(15)=O(17)], 1443vs [C(4)=O(5)] and 813w

(C=S); δ_H (600 MHz, $CDCl_3$) 3.94 (1H, dq, $^2J_{9a,9b}$, $^3J_{9a,10}$ 10.2, 3.6 Hz, $H^{9a/9b}$), 3.85 (1H, dq, $^2J_{9b,9a}$, $^3J_{9b,10}$ 10.2, 3.60 Hz, $H^{9b/9a}$), 3.73 (1H, dq, $^2J_{7a,7b}$, $^3J_{7a,8}$ 9.6, 3.6 Hz, $H^{7a/7b}$), 3.51 (1H, dq, $^2J_{7b,7a}$, $^3J_{7b,8}$ 9.6, 3.6 Hz, $H^{7b/7a}$), 2.47 (1H, ddd, $^2J_{16b,16a}$, $^3J_{16b,15b}$, $^3J_{16b,15a}$ 12.9, 10.5, 4.5 Hz, H^{16b}), 1.94 (1H, ddd, $^2J_{16a,16b}$, $^3J_{16a,15a}$, $^3J_{16a,15b}$ 12.9, 10.2, 3.3 Hz, H^{16a}), 1.68 (1H, ddd, $^2J_{15b,15a}$, $^3J_{15b,16b}$, $^3J_{15b,16a}$ 13.5, 10.5, 3.3 Hz, H^{15b}), 1.65 (1H, ddd, $^2J_{15a,15b}$, $^3J_{15a,16a}$, $^3J_{15a,16b}$ 13.5, 10.2, 4.5 Hz, H^{15a}), 1.26 (3H, t, $^3J_{10,9}$ 3.6 Hz, H^{10}), 1.14 (3H, s, $^3J_{8,7}$ 3.6 Hz, H^8), 1.09 (3H, s, H^{18}), 1.09 (3H, s, H^{20}), 0.98 (3H, s, H^{21});* δ_C (150 MHz, $CDCl_3$) 177.6 (C^{13}), 172.6 (C^4), 166.4 (C^2), 91.9 (C^{11}), 55.4 (C^{19}), 54.9 (C^{14}), 47.9 (C^9), 47.5 (C^7), 30.6 (C^{16}), 28.8 (C^{15}), 16.5 (C^{21}), 16.4 (C^{20}), 12.8 (C^{10}), 12.2 (C^8), 9.4 (C^{18}).

*quoted on page 35.

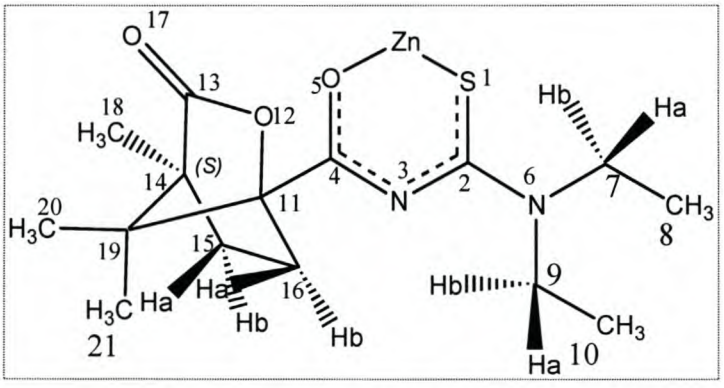

Figure 3.4. Atomic numbering scheme of *trans/cis*-[Zn(L^8-*S,O*)$_2$].

3.3.2.5. *Trans/cis-bis*(*N,N*-diethyl-*N´*-camphanoylthioureato)Pt(II), *trans/cis*-[Pt(L^8-*S,O*)$_2$]

Recrystallised yield 94 %; m.p. 224 °C; Found: C, 41.19; H, 5.34; N, 6.16; S, 6.71. $(C_{15}H_{23}N_2O_3S)_2Pt$ requires C, 41.16; H, 5.67; N, 6.14; S, 6.75 %; *m/z* 819(M^+, 5.70 %), 714(15.90), 507(6.33), 312(3.16), 181(16.46) and 83(100); Characterstic absoption bands: ν_{max}/cm^{-1} 2966m and 2872w (C-H), 1783vs [C(13)=O(17)], 1430vs [C(2)=O(1)] and 818w (C=S); δ_H (600 MHz, $CDCl_3$) 3.78 (1H, dq, $^2J_{9a,9b}$, $^3J_{9a,10}$ 13.8, 7.2 Hz, $H^{9a/9b}$), 3.71 (1H, dq, $^2J_{9b,9a}$, $^3J_{9b,10}$ 13.8, 7.2 Hz, $H^{9b/9a}$), 3.64 (1H, dq, $^2J_{7a,7b}$, $^3J_{7a,8}$ 14.4, 7.2 Hz, $H^{7a/7b}$), 3.62 (1H, dq, $^2J_{7b,7a}$, $^3J_{7b,8}$ 14.4, 7.2 Hz, $H^{7b/7a}$), 2.47 (1H, ddd, $^2J_{16b,16a}$, $^3J_{16b,15b}$, $^3J_{16b,15a}$ 13.8, 9.6, 4.8 Hz, H^{16b}), 1.96 (1H, ddd, $^2J_{16a,16b}$, $^3J_{16a,15a}$, $^3J_{16a,15b}$ 13.8, 11.4, 4.2 Hz, H^{16a}), 1.88 (1H, ddd, $^2J_{15b,15a}$, $^3J_{15b,16b}$, $^3J_{15b,16a}$ 13.2, 9.6, 4.2 Hz, H^{15b}), 1.63 (1H, ddd, $^2J_{15a,15b}$, $^3J_{15a,16a}$, $^3J_{15a,16b}$ 13.2,11.4, 4.8 Hz, H^{15a}), 1.28 (3H, t, $^3J_{10,9}$ 7.2, H^{10}), 1.15 (3H, t, $^3J_{8,7}$ 7.2 Hz, H^8), 1.09 (3H, s, H^{20}), 1.08

(3H, s, H^{18}), 0.94 (3H, s, H^{21}); δ_C (150 MHz, $CDCl_3$) 179.7 (C^{13}), 169.6 (C2), 166.4 (C^4), 94.5 (C^{11}), 55.1 (C^{19}), 54.1 (C^{14}), 46.7 (C^9), 46.0 (C^7), 30.8 (C^{16}), 29.2 (C^{15}), 16.9 (C^{21}), 16.7 (C^{20}), 12.6 (C^{10}), 11.8 (C^8), 9.6 (C^{18}).

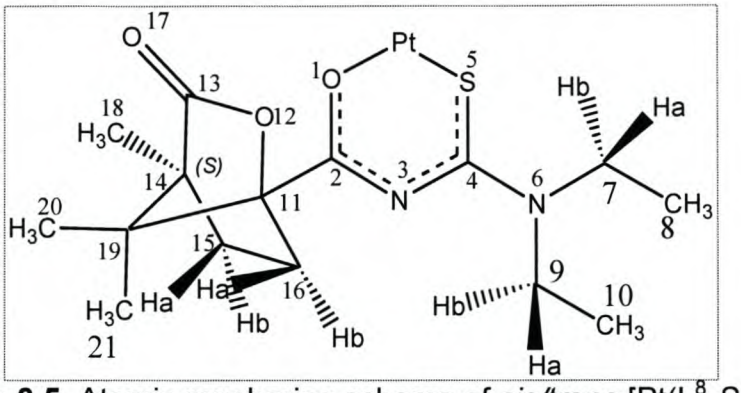

Figure 3.5. Atomic numbering scheme of *cis/trans*-[Pt(L^8-*S,O*)$_2$].

3.3.2.6. *Tetrakis*(*N,N*-diethyl-*N´*-camphanoylthioureato)diargentate(I), $Ag_2[(HL^8$-*S*)(L^8-μ-*S,O*)]$_2$.

Recrystallised yield 82 %; m.p. 178 °C; Found: C, 53.01; H, 7.12; N, 8.14; S, 9.43. $(C_{30}H_{47}N_4AgO_6S_2)_2$ requires C, 53.21; H, 6.99; N, 8.27; S, 9.47 %; *m/z* 671(M^+, 14.56 %), 639(8.23), 549(12.03), 517(13.29), 456(5.06), 355(11.34), 335(50), 254(27.84), 226(15.82), 116(34.18), and 72(100); Characteristic absorption bands: ν_{max}/cm^{-1} 3407w (N-H), 2969m and 2934w (C-H), 1777vs [C(13)=O(17)], 1701s and1435s [C(4)=O(5)], and 797w (C=S); δ_H (600 MHz, $CDCl_3$) 8.37 (1H, s, NH), 3.94 (2H, broad s, H^9), 3.60 (2H, broad s, H^7), 2.47 (1H, ddd, $^2J_{16b,16a}$, $^3J_{16b,15b}$, $^3J_{16b,15a}$ 13.8, 9.6, 4.2 Hz, H^{16b}), 2.04 (1H, ddd, $^2J_{16a,16b}$, $^3J_{16a,15a}$, $^3J_{16a,15b}$ 13.8, 10.8, 4.8 Hz, H^{16a}), 1.89 (1H, ddd, $^2J_{15b,15a}$, $^3J_{15b,16b}$, $^3J_{15b,16a}$ 13.8, 9.6, 4.8 Hz, H^{15b}), 1.64 (1H, ddd, $^2J_{15a,15b}$, $^3J_{15a,16a}$, $^3J_{15a,16b}$ 13.8,10.8, 4.2 Hz, H^{15a}), 1.32 (3H, broad s, H^{10}), 1.22 (3H, broad s, H^8), 1.22 (3H, s, H^{18}), 1.08 (3H, s, H^{20}), 1.00 (3H, s, H^{21}); δ_C (150 MHz, $CDCl_3$) 178.7 (C^{13}), 176,7/ 167.4 (C^4)*, 176.0 (C^2), 93.2 (C^{11}), 55.2 (C^{19}), 54.4 (C^{14}), 47.2 (C^9), 47.0 (C^7), 30.5 (C^{16}), 29.1 (C^{15}), 16.9 (C^{21}), 16.8 (C^{20}), 12.5 (C^{10}), 12.0 (C^8), 9.5 (C^{18}).

* 176.7 and 167.4 are assigned to the C^4 with bonded and non-bonded *O* donor atoms to the Ag(I) atoms respectively.

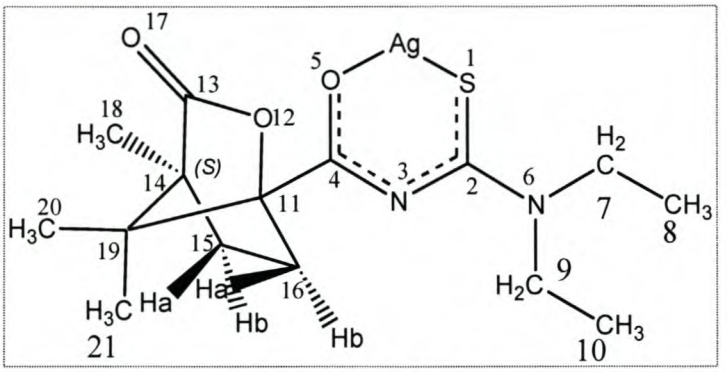

Figure 3.6. Atomic numbering scheme of $Ag_2[(HL^8\text{-}S)(L^8\text{-}\mu\text{-}S,O)]_2$. The atomic numbering of the monodentate ligands(HL) is the same as the atomic numbering of the bidentate ligands(L^-) in the complex.

3.3.2.7. *Trans/cis-bis*(*N,N*-diethyl-*N´*-adamantylcarbonylthioureato)Ni(II), *trans/cis*-[Ni(L^{11}-*S,O*)$_2$]

Recrystallised yield 88 %; m.p. 212 °C; Found: C, 59.52; H, 8.62; N, 8.70; S, 9.99. ($C_{16}H_{25}N_2OS$)Ni requires C, 59.93; H, 8.74; N, 8.68; S, 9.92 %; *m/z* 646(M^+, 59.49 %), 585(3.20), 487(20.25), 459(21.22), 353(22.11), 193(3.79), 135(1000), 79(19.62); Characteristic absorption bands: ν_{max}/cm^{-1} 2900m and 2847w (C-H), 1422vs (C=O), 804m (C=S); δ_H (600 MHz, $CDCl_3$) 3.64 (2H, q, $^2J_{9,10}$ 14.1, 7.2 Hz, H^9), 3.62 (2H, q, $^2J_{7,8}$ 14.10, 7.2 Hz, H^7), 1.92 (6H, broad s, H^{16}, H^{18}, H^{20}); 1.79 (6H, broad s, H^{12}, H^{13}, H^{14}), 1.63 (3H, broad m, H^{15}, H ^{17}, H^{19}), 1.16 (3H, t, $^3J_{10,9}$ 7.2 Hz, H^{10}), 1.09 (3H, t, $^3J_{8,7}$ 7.2 Hz, H^8), δ_C (150 MHz, $CDCl_3$) 186.5 (C^4), 172.6 (C^2), 45.0 (C^7), 45.7 (C^9), 43.0 (C^{11}), 39.9 (C^{12}, C^{13}, C^{14}), 36.8 (C^{15}, C^{17}, C^{19}), 28.4 (C^{16}, C^{18}, C^{20}) 12.7 (C^{10}), 12.3 (C^8).

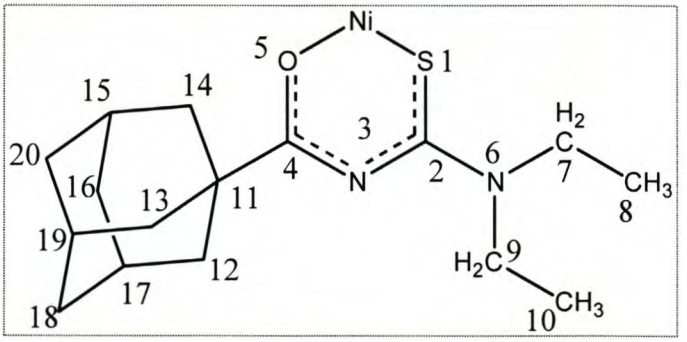

Figure 3.7. Atomic numbering scheme of *trans/cis*-[Ni(L^{11}-*S,O*)$_2$].

3.3.2.8. *Trans/cis-bis*(*N,N*-diethyl-*N´*-adamantylcarbonylthioureato)Cu(II), *trans/cis*-[Cu(L^{11}-*S,O*)$_2$]

Recrystallised yield 84 %; m.p. 179 °C; Found: C, 58.46; H, 8.43; N, 8.44; S, 9.78. $(C_{16}H_{25}N_2OS)_2Cu$ requires C, 59.09; H, 7.86; N, 8.61; S 9.86 %; *m/z* 651(M^+, 21.83 %), 294(9.49), 181(2.53), 135(100), 79(3.92); Characteristic absorption bands: ν_{max}/cm^{-1} 2902m and 2847w (C-H), 1419vs (C=O). and 795w (C=S).

Again the characterisation of *trans/cis*-[Cu(L^{11}-*S,O*)$_2$] by means of NMR spectroscopy was prevented by the paramagnetic nature of the central metal Cu(II) d^9 ion and no NMR data for the complex was obtained.

CHAPTER FOUR

RESULTS AND DISCUSSION

4.1. THE FOUR NEW *N,N*-DIETHYL-*N'*-ACYLTHIOUREA LIGANDS

4.1.1. General properties

The four crystallising colourless ligands were synthesised in good yields (87%, 82%, 74% and 92% for HL^8, HL^9, HL^{10} and HL^{11} respectively). These ligands crystallise easily from an acetone/water mixture and are air stable in both solution and in the solid state. These ligands can be stored for a long time as solids at room temperature without decomposition. Generally all these ligands are soluble in non-polar organic solvents, sparingly soluble in polar aprotic solvents and alcohols, and completely insoluble in water.

An impressive property of these ligands is their ability to selectively transport some metal ions from a source phase containing a number of metal ions to a receiving phase (see **Figure 4.1**). These ligands have been tested for the selective transport of transition metal ions. The basic principles and procedure of the process are described by Habtu.[36] It was reported that the HL^8 ligand selectively transported 81 % silver(I) from a source phase (aqueous phase) containing equimolar amounts of cobalt(II), nickel(II), copper(II), zinc(II), cadmium(II), lead(II), and silver(I), to the receiving phase (aqueous phase). This result is the highest percentage of all the *N,N*-diethyl-*N'*-acylthiourea ligands that have been tested so far in Habtu's research. **Figure 4.1** shows the cell set up for the transporting of targeted metal ions from source phase to receiving phase. The transporting results for the other three ligands are also described by Habtu.[36] The percentage of the selective transport of metal ions was quantified by measuring the amount of metal ions in the source phase and receiving phase just after the strirring process was run for some period of time by means of atomic absorption spectroscopy (AA).

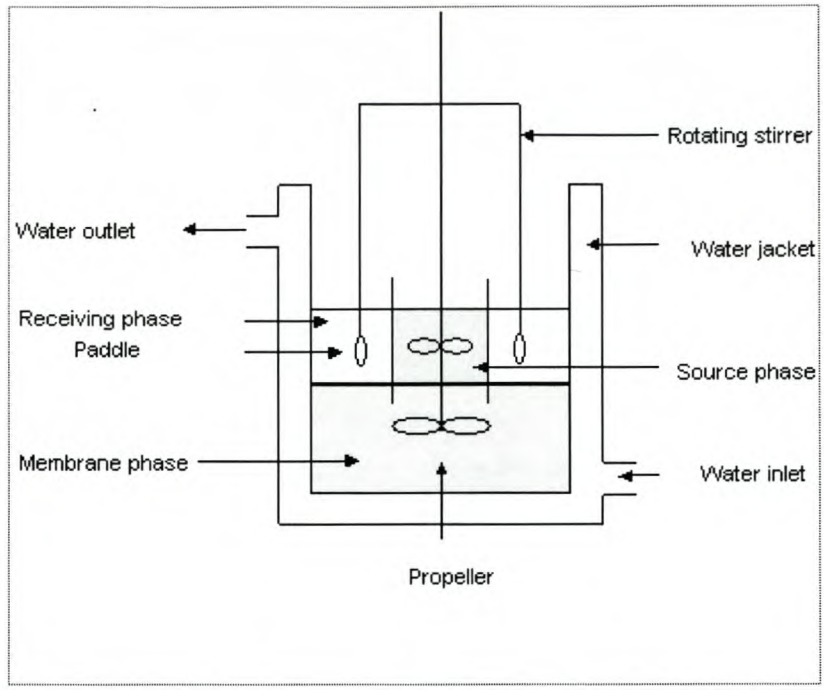

Figure 4.1. The cell set up for the selective transportation of transition metal ions. The source phase (aqueous phase) contains equimolar concentrations of cobalt(II), nickel(II), copper(II), zinc(II), cadmium(II), lead(II), and silver(I), while the membrane phase (organic phase) contains the HL^8 ligand solution.[36]

4.1.2. Synthesis of new ligands and related problems

As indicated in the experimental section, after the completion of step I in the synthesis of HL^8, HL^9, HL^{10} and HL^{11} (see **reaction scheme 4.1**) the formation of intermediate products was monitored by IR spectroscopy. The intermediates are the camphanoyl- isothiocyanate for *N,N*-diethyl-*N'*-camphanoylthiourea (HL^8), *N*-piperidyl-*N'*camphanoyl thiourea (HL^9) and *N*,-pyrrolidyl-*N'*-camphanoylthiourea (HL^{10}), and adamantylcarbonyl isothiocyanate for N,N-diethyl-N'-adamantylcarbonylthiourea (HL^{11}).

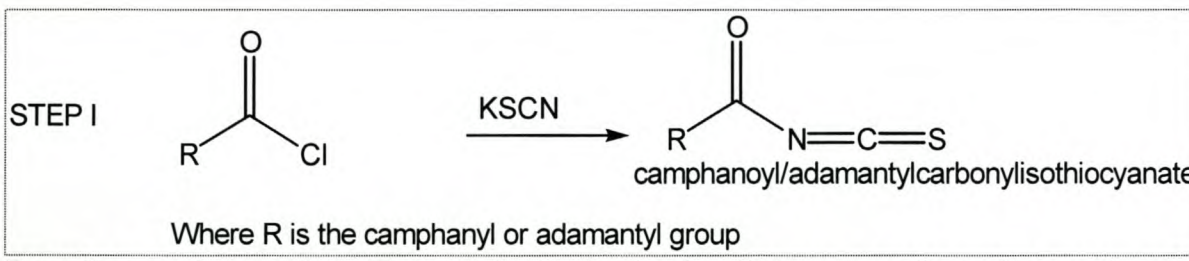

Reaction scheme 4.1. The synthetic route for the preparation of camphanoyl/ adamantyl carbonylisothiocyanate intermediate products.

The IR spectra were measured by taking about three drops of the reaction mixture after the completion of step I and diluting this with nujol. The spectra showed two

sharp, strong absorption bands at 2100 cm^{-1} and 2135 cm^{-1}. From the literature[37] it is known that the vibration of a R'-N=C=S isothiocyanate group gives one or two absorption peaks around 2125 cm^{-1}, where R' can be an alkyl, acyl, aryl or aroyl group. Hence the 2100 cm^{-1} and 2135 cm^{-1} absorption bands are assigned to the isothiocyanate vibrations of camphanoylisothiocyanate and adamantylcarbonyl isothiocyanate products respectively.

Unlike the syntheses of the HL^8, HL^9 and HL^{11} ligands, the first attempt to prepare HL^{10} showed a side reaction in step II of the synthesis of the ligand. In this case the second nucleophile (pyrrolidine) attacked at both of the electrophilic centres, *i.e.* at the amidic carbonyl and the thiocarbonyl positions in the camphanoylisothiocyanate intermediate product to give a mixture of the HL^{10} ligand and undesired *N*-pyrrolidylcamphanicamide (see **reaction scheme 4.2**). This product mixture was analysed by means of MS, IR spectroscopy and NMR spectroscopy.

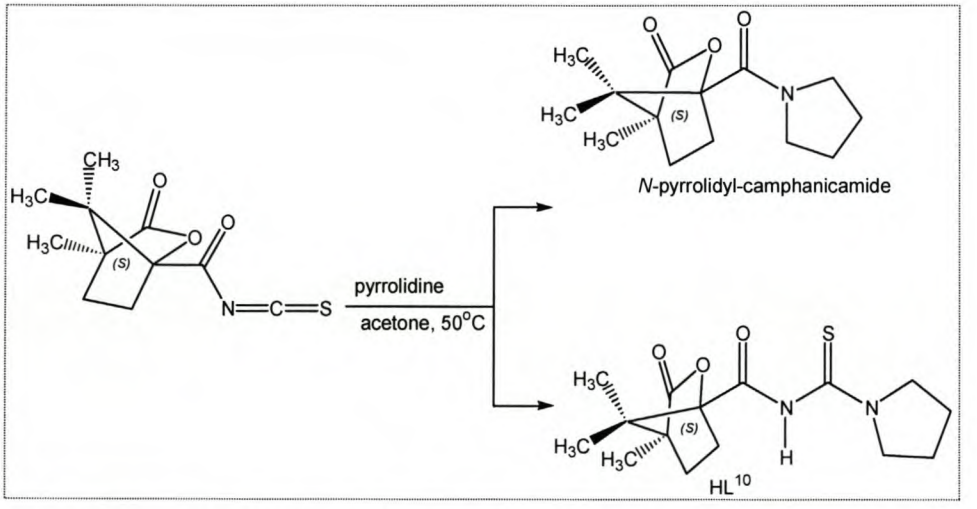

Reaction scheme 4.2. The synthetic route for the synthesis of HL^{10} and the undesired *N*-pyrrolidylcamphanicamide.

The ^1H and ^{13}C NMR spectra of the product mixture indicated the presence of a 60:40 ratio of HL^{10} to *N*-pyrrolidylcamphanicaminde. **Figure 4.2** shows the ^{13}C NMR spectrum of the product mixture.

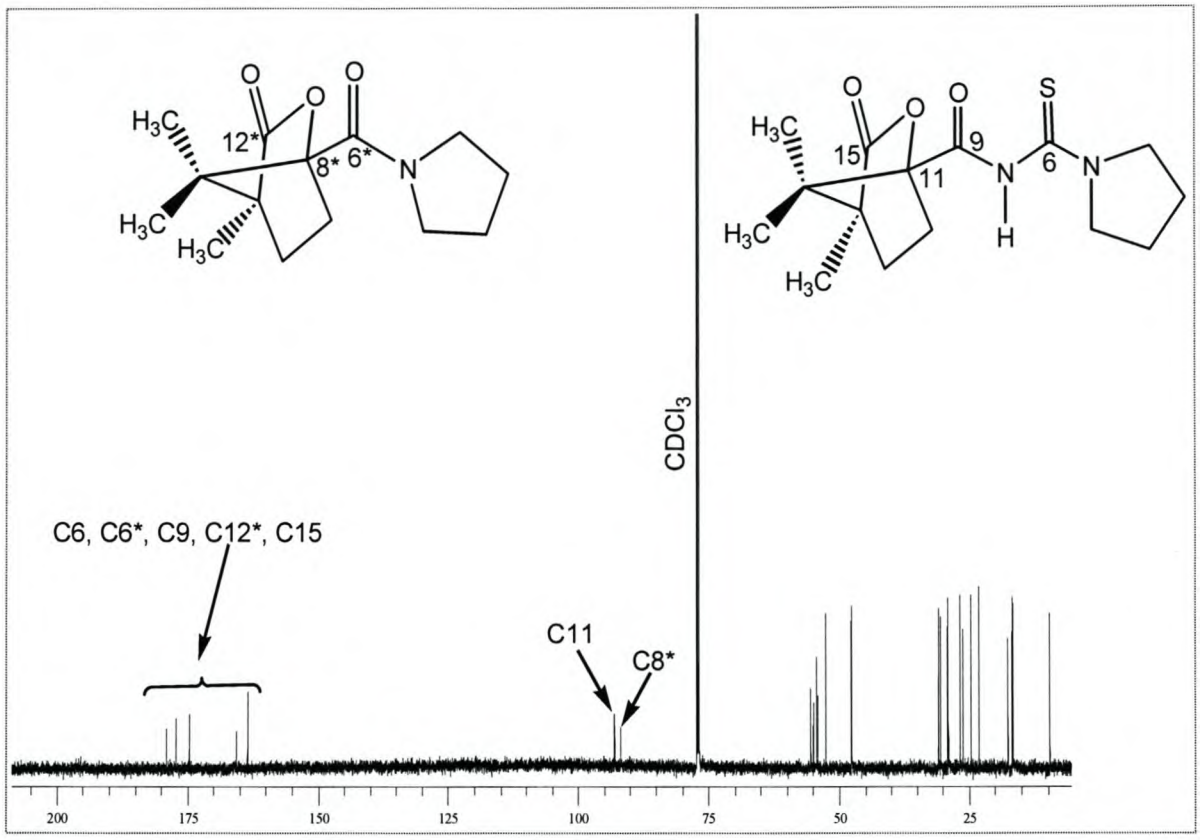

Figures 4.2. 150 MHz ^{13}C NMR spectrum of the product mixture showing the presence of the HL^{10} ligand and undesired *N*-pyrrolidylcamphanicamide.

TLC performed on the product mixture using different mobile phases showed no appreciable separation between the two components and hence no further chromatographic separation could be done to separate the two components in the mixture. Nevertheless the synthesis of pure HL^{10} ligand could be achieved using a modified synthetic procedure. This procedure involved controlling the concentration of the reacting components through dropwise addition of pyrrolidine (about one drop per five seconds) to the camphanoylisothiocyanate solution while vigorously stirring to ensure a good mixture of reactants under the condition of excess camphanoylisothiocyanate.

4.1.2. Spectroscopic characterisation of HL^8, HL^9, HL^{10} and HL^{11} ligands

4.1.2.1. The MS, IR and elemental (C, H, N and S) analysis results

As indicated in chapter three the elemental analysis results of these ligands were within 0.5% of their calculated elemental composition, which is acceptable. The mass spectra of the ligands showed intense peaks for the molecular ion (M^+) of the ligands and hence the molecular masses of the ligands were easy to confirm. This indicates

that the molecular ions of such ligands can stabilise their positive charges by delocalisation of the charge over the C(O)NHC(S) moiety.

As might be expected the IR spectra of these ligands show characteristic absorption bands in the region of 4000-400 cm^{-1}. The distinctive absorption bands for each of the four ligands are summarized in **Table 4.1**.

Table 4.1. The characteristic absorption bands for the four ligands.

Ligand	Distinctive absorption bands (cm^{-1})			
	N-H	ν(O=C) of the camphanic moiety	ν(O=C) of C(O)N	ν(S=C) of NC(S)
HL^8	3407m	1806vs	1707vs	1228m
HL^9	3397m	1790vs	1700vs	1249m
HL^{10}	3371m	1776vs	1691	1252m
HL^{11}	3283m	-	1644vs	1235m

The assignment of the two ν(C=O) vibrations in the IR spectra of HL^8, HL^9 and HL^{10} ligands was made according to the studies found in the literature.[37] It is reported that the dipole moment of a carbonyl bond is sensitive to attached atoms as a result of an electron withdrawing effect (inductive effect), as well as a resonance effect and possible hydrogen bonding caused by the attached group.[37] This indicates that the presence of the oxygen and nitrogen atoms adjacent to the two carbonyl groups of C(5)=O(6) and C(2)=O(3) respectively influence the bond strengths of both carbonyl bonds (atomic numbering is indicated in **Figure 4.3**). Since oxygen is more electronegative than nitrogen, the presence of oxygen atom O(4) in the camphanic ring is expected to withdraw electron density from C(5), this in turn should cause the withdrawal of the lone pairs of O(6) toward the C(5)=O(6) bond and thereby the C(5)=O(6) bond becomes relatively stronger than the C(2)=O(3) bond. In addition, the resonance effect of the lone pairs of the nitrogen N(1) atom in the ligand conjugated with the π-electrons of the O(2)=C(3) bond might cause an increase in single bond character of the C(2)=O(3) bond, which in turn lowers the absorption frequency of the O(2)=C(3) bond relative to the absorption frequency of the O(5)=C(6) bond. These effects hold true for the HL^8, HL^9 and HL^{10} ligands on changing the R group of the ligand in **Figure 4.3** from diethyl amine to piperidyl to

pyrrolidyl respectively. **Figure 4.3 (a)** and **(b)** show the two possible reasons that cause the two carbonyl groups in the three ligands to have different IR absorption bands.

Figure 4.3

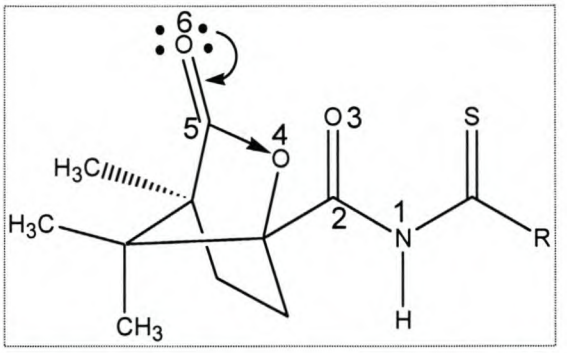

(a) Electron withdrawing effect raises the C(5)=O(6) bond frequency.

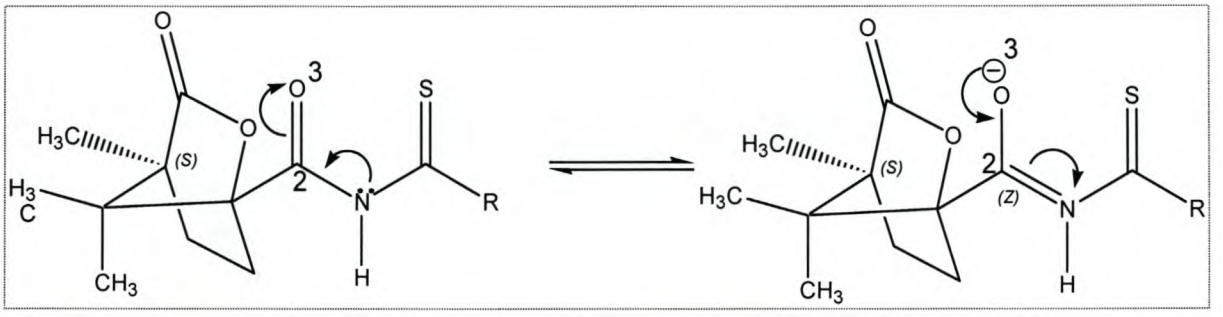

(b) Resonance effect lowers the C(2)=O(3) bond frequency.

As a result of the factors discussed earlier the carbonyl absorption bands at 1806, 1790 and 1776 cm^{-1} seen in the IR spectra of HL^8, HL^9 and HL^{10} respectively are unambiguously assigned to the ν(O=C) vibrations of the carbonyl group in the camphanic moiety. Similarly the carbonyl absorption bands at 1707, 1700, 1691 and 1644 cm^{-1} observed in the IR spectra of HL^8, HL^9, HL^{10} and HL^{11} respectively are assigned to the ν(O=C) vibrations of the amidic carbonyl group [C(O)NH moiety].

Although the exact fundamental modes of the absorption bands at about 1538 cm^{-1}, 1463 cm^{-1} and 1443 cm^{-1} in the IR spectra of the HL^8, HL^9 and HL^{10} ligands respectively are not easy to assign, a reasonable assumption has been made based on the absorption bands for similar fundamental modes given in the literature.[37] In this case these intense absorption bands are tentatively assigned to the couplings of the ν(N-C) + ν(C-O) + methyl deformation fundamental modes. The IR spectra of HL^8

and HL^9 are shown as typical examples for these types of ligands in **Figures 4.17** and **A-III** (see appendix A) respectively.

4.1.2.2. NMR spectra results of the four new ligands

NMR spectra of HL^8: The ^1H NMR spectrum of this ligand (see **Figure 4.4**) shows a broad signal at 8.37 ppm, which is assigned to the N-H proton of the ligand. This downfield chemical shift is expected of an N-H proton that is flanked by electron-withdrawing carbonyl and thiocarbonyl groups.

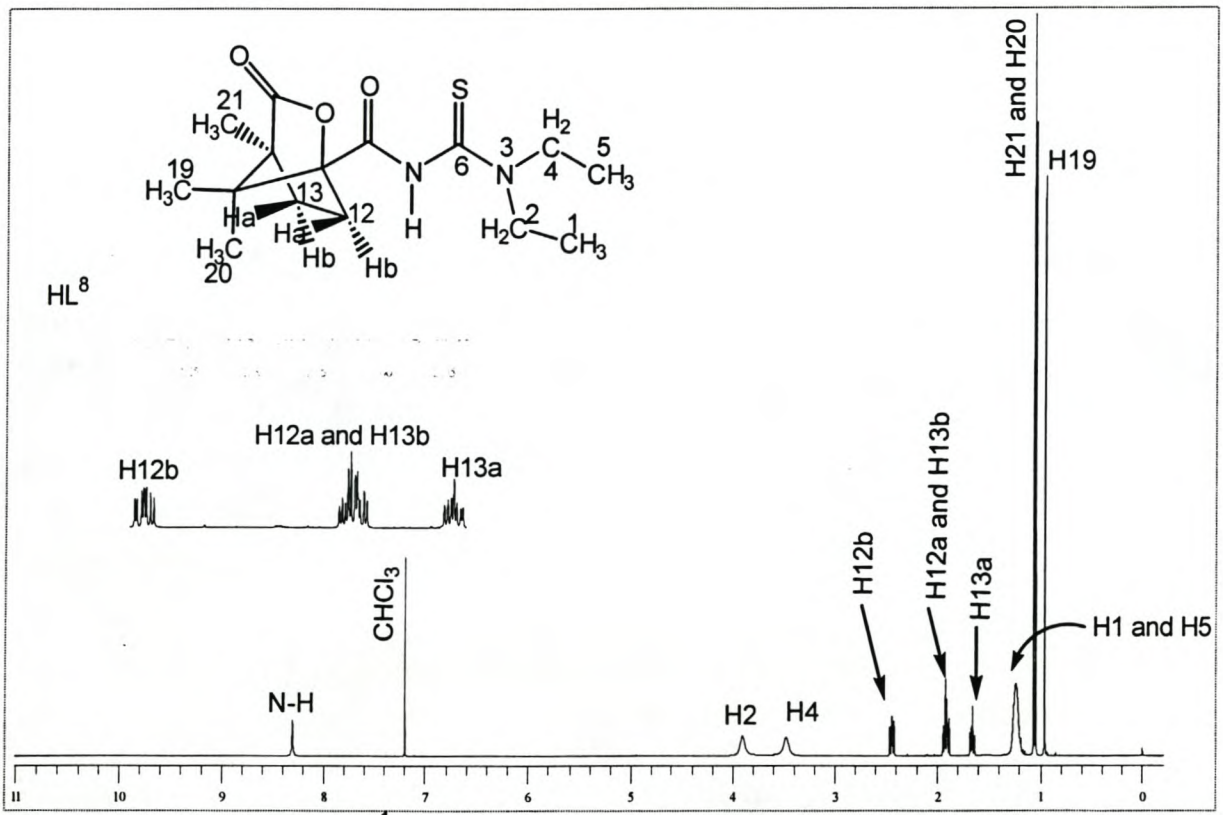

Figure 4.4. The 600 MHz ^1H NMR spectrum in $CDCl_3$ of *N,N*-diethyl-*N*-champhanoyl-thiourea (HL^8).

The selected ^1H NMR data of HL^8 is summarised in **Table 4.2**.

Table 4.2. The selected ^{1}H NMR data of HL^{8} ligand.

δ/ppm	Proton assignment	*J*/Hz (spin coupling)	Multiplicity	Coupling assignment
8.37	N-H	-	s	-
3.96	H2	-	broad	-
3.53	H4	-	broad	-
2.48	H12a	13.5, 10.5, 4.5	ddd	$^{2}J_{12a,\,2b}$, $^{3}J_{12a,13a}$, $^{3}J_{12a,13b}$
1.97	H12b	13.5, 7.5, 3.3	ddd	$^{2}J_{12b,12a}$, $^{3}J_{12b,13b,}$ $^{3}J_{12b,13a}$
1.68	H13a	13.5, 7.5, 4.5	ddd	$^{2}J_{13a,13b}$, $^{3}J_{13a,12a}$, $^{3}J_{13a,12b}$
1.92	H13b	13.5, 10.5, 3.3	ddd	$^{2}J_{13b,13a}$, $^{3}J_{13b,12b,}$ $^{3}J_{13b,12a}$
1.26	H1	6.3	t	$^{3}J_{1,2}$
1.26	H5	6.3	t	$^{3}J_{4,3}$

As a result of the restricted rotation about the C(6)-N(3) bond, which is due to the resonance effect of the π-electrons of the C=S bond and lone pair of N(3), the two methylene protons adjacent to the N(3) are in different chemical shifts. As seen in **Figure 4.4**, the ^{1}H NMR spectrum of HL^{8} has two broad peaks at 3.96 and 3.53 ppm, which are assigned to the protons in the methylene groups of carbons 2 and 4 respectively. In this particular case, the assignment is based on the reasonable assumption that the π-electrons of the C=S bond and electrons of the sulfur atom shield the nearest H(4) protons to a greater extent than the H(2) protons, and hence the chemical shift of the H(2) protons lies further downfield compared to the H(4) protons.

As a result of the rigid conformation of the bicyclic camphanic group, the two protons attached to C(12) and C(13), which are labelled as Ha and Hb protons for convenience, are in different chemical environments. In this case the H(12a) and H(13a) protons, which are relatively *cis* to C(18), C(19) and C(20) of the camphanic ring, are more shielded by the induced field of these carbon atoms compared to the corresponding Hb protons of H(12b) and H(13b). The Hb protons are relatively *trans* to C(18), C(19) and C(20) of the camphanic ring. As a result the chemical shifts of the Ha protons are further upfield compared to their corresponding Hb protons. In this case the four doublet of doublets of doublets (ddd) at 2.48, 1.97, 1.92 and 1.68 ppm are assigned to the protons of H(12b), H(12a), H(13b) and H(13a) respectively.

Similar to the ^{1}H NMR spectrum of this ligand discussed earlier, as a result of the restricted rotation about the C(6)-N(3) bond and the presence of S atom closer to C(4) than to C(2), the two methylene carbons of C(2) and C(4) and two methyl carbons of C(1) and C(5) are in different chemical environments. In this case C(4), which is more shielded by the electron density of the S atom, is further upfield compared to the C(2). Thus the two peaks at 47.9 and 47.4 ppm are assigned to C(2) and C(4) respectively. Since C(5) is closer to the S atom than to C(1) the peaks at 13.1 and 13.0 ppm are assigned to C(1) and C(5) respectively. The ^{13}C NMR signals of C(6) and C(15) are found more or less at the same chemical shifts of 177.6 and 177.5 ppm and these are tentatively assigned to the esteric carbon of C(15) and amidic carbon of C(6) respectively. The chemical shifts of the remaining carbons are shown in **section 3.2.2.1** and the ^{13}C NMR spectrum of the ligand is seen in **Figure 4.5**

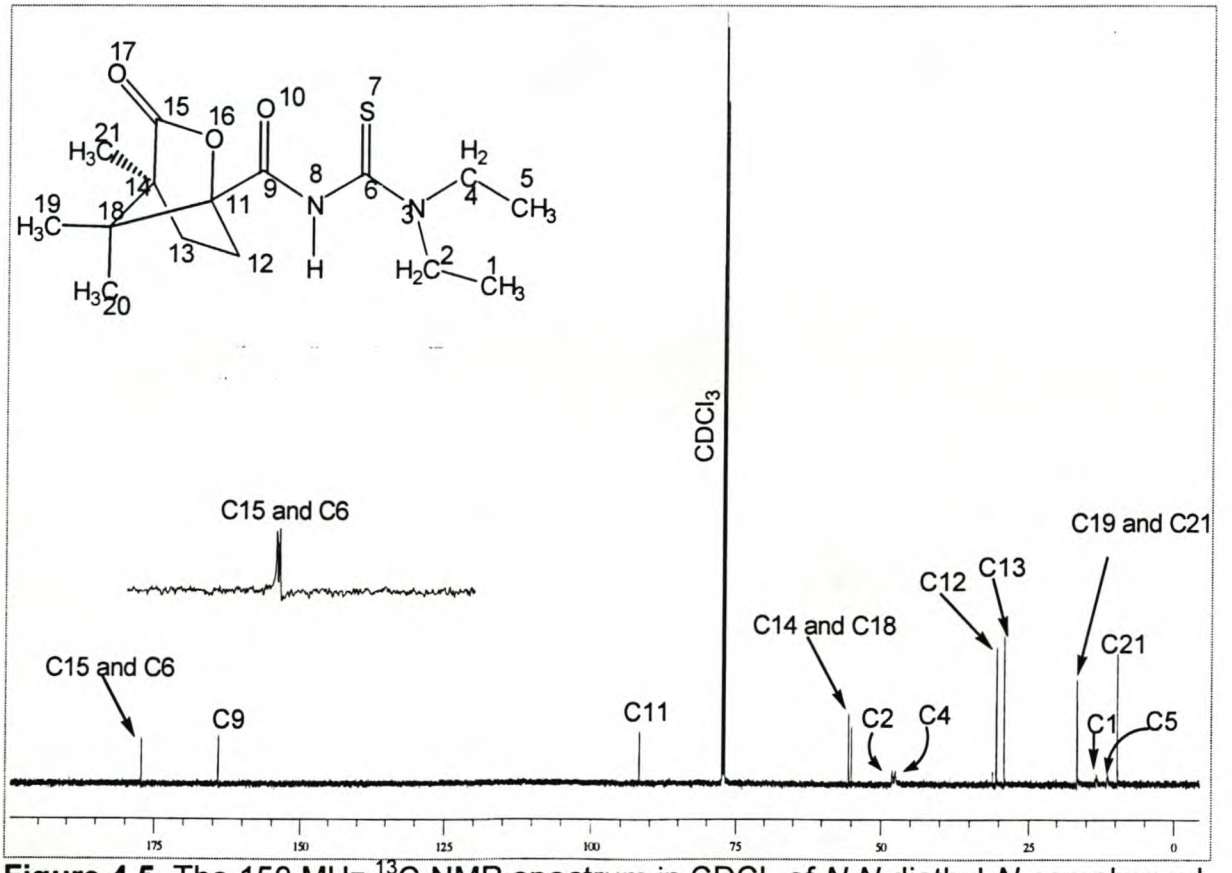

Figure 4.5. The 150 MHz ^{13}C NMR spectrum in $CDCl_3$ of *N,N*-diethyl-*N*-camphanoyl-thiourea (HL^8).

Final confirmation of the correct assignments of the ^{1}H and ^{13}C NMR spectra of HL^8 was obtained by using two-dimensional NMR techniques, these being H-H Correlation Spectroscopy (COSY) and Gradient Heteronuclear (H-C) Single

Quantum Coherence (GHSQC). These spectra are shown in **Figures 4.6 and 4.7** respectively. Thus the chemical shifts, multiplicities and coupling constants of each of the protons in the ligand could be selectively identified with the aid of the 2D spectra. As confirmed by the COSY spectrum, a complete description of the coupling partners (both the germinal and vicinal couplings) of the protons in the ligand is given in **Table 4.2.**

For simplicity the off diagonal peaks of **Figure 4.6** are labelled as A, B, C, D, E, and F. The off diagonal peaks of the COSY spectrum in **Figure 4.6** show the correlations of pairs of nuclei by means of spin coupling.[37] In this case peak A reveals the coupling between protons of carbon 2 (H2) and carbon 1 (H1) in the ligand. Similarly peak B indicates the coupling between protons of carbon 4 (H4) and protons of carbon 5 (H5). In the same fashion peak C indicates the coupling between H(12b) and H(13a) in the camphanic ring of the ligand. Peak D shows coupling between H(12b) and both of H(12a) and H(13b), and *vice versa*. Similarly peak E indicates the coupling between proton H(13a) and both of H(13b) and H(12a) and *vice versa*. Since the chemical shifts of H(12a) and H(13b) were found close to one another, their coupling peak is incorporated in peak F along the diagonal.

The GHSQC spectrum is the result of heteroatom spin coupling between proton and carbon nuclei that are directly bonded to one another in the form of a C-H bond.[37] The spectrum allowed unambiguous assignment of the carbon and proton resonances. Again for simplicity the peaks of the GHSQC spectrum in **Figure 4.7** were labelled I, J, K, L, M, N, O, P, Q, R, S and T. In this case peak I indicates that the poorly resolved protons of H(2) at 3.96 ppm and carbon C(2) at 47.9 ppm are bonded to one another in the HL^8 ligand. Similarly peak J correlates the carbon at 47.5 ppm and the poorly resolved protons at 3.53 ppm. In other words the two atoms are bonded to one another in the ligand. In the same fashion peaks K and L, which correlate to the protons of H(12b) and H(12a) at 2.48 ppm and at 1.97 ppm respectively are directly bonded to the carbon at 30.2 ppm, which is C(12). The same holds true for the other peaks of M, N, O, P, Q, R, S and T, which connect the protons on the vertical axis with their corresponding carbons on the horizontal axis.

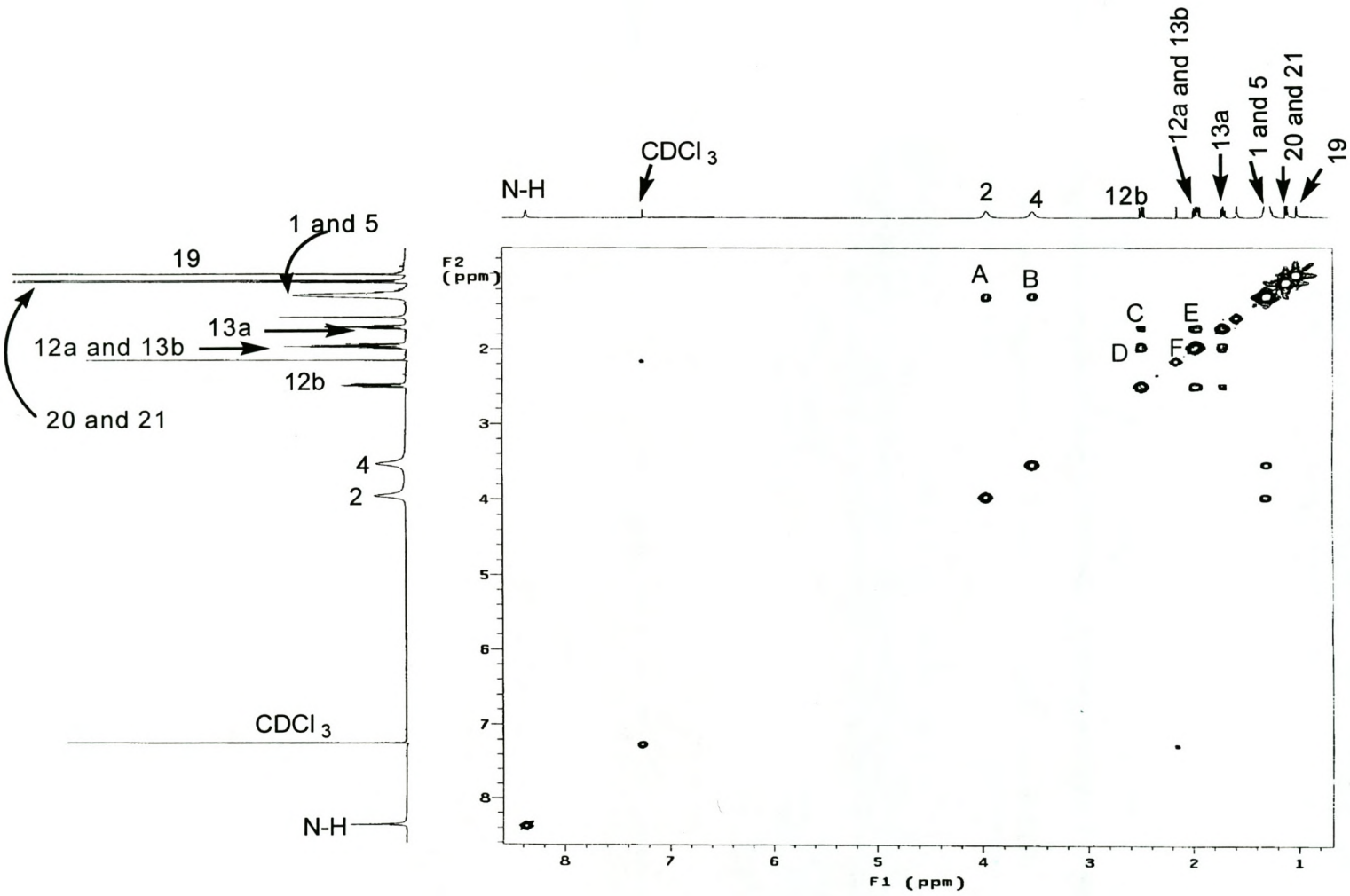

Figure 4.6. The 600 MHz COSY spectrum of *N,N*-diethyl-*N'*-camphanoylthiourea (HL^8).

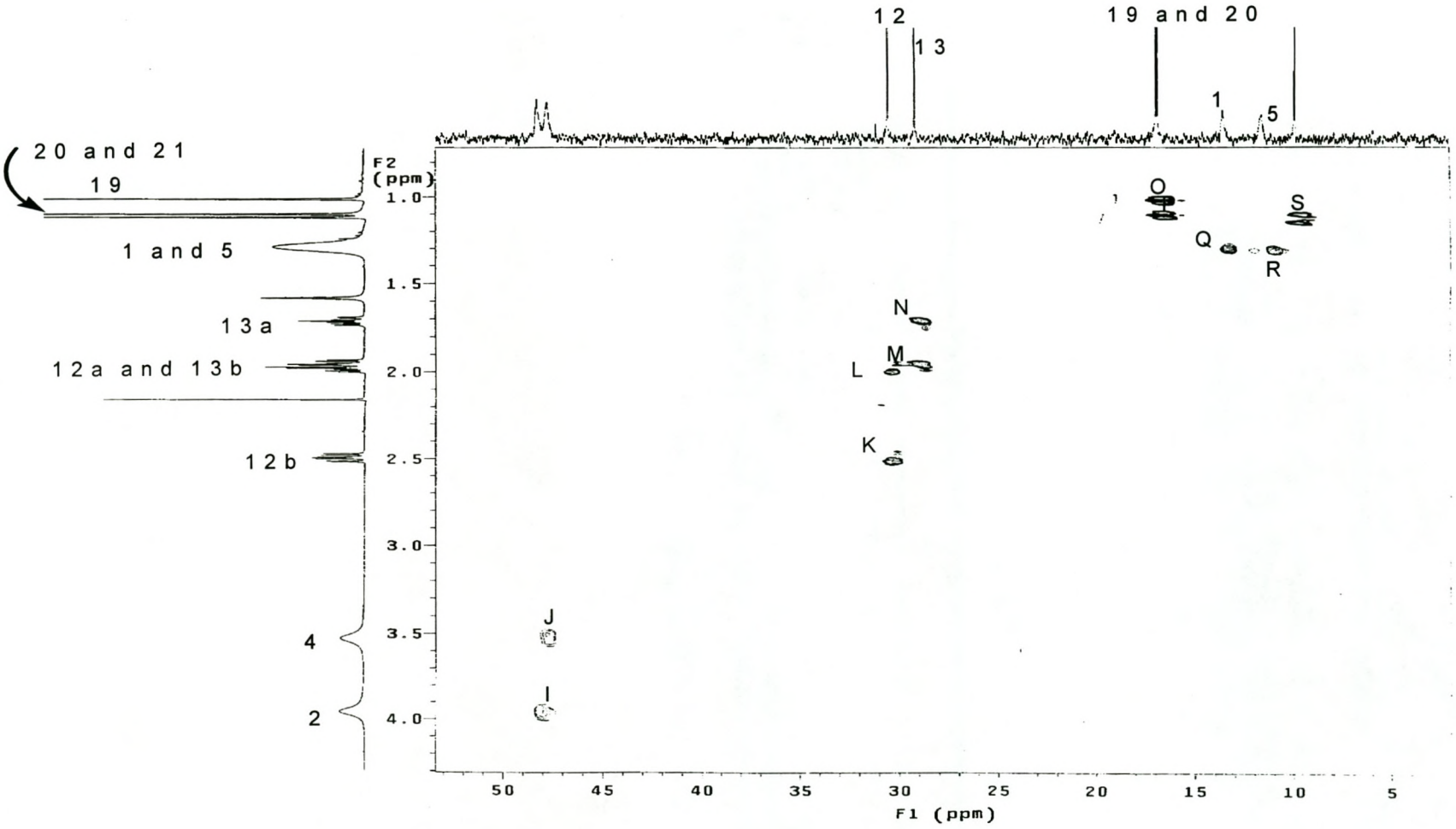

Figure 4.6. The 600 MHz GHSQC spectrum of *N,N*-diethyl-*N*-champhanoylthiourea (HL^8).

The ^{1}H and ^{13}C NMR chemical shifts of HL^{8}, HL^{9}, HL^{10} and HL^{11} are summarised in **Tables 4.3** and **4.4** respectively. The atomic numbering scheme of the ligands are shown in **Figure 4.8**.

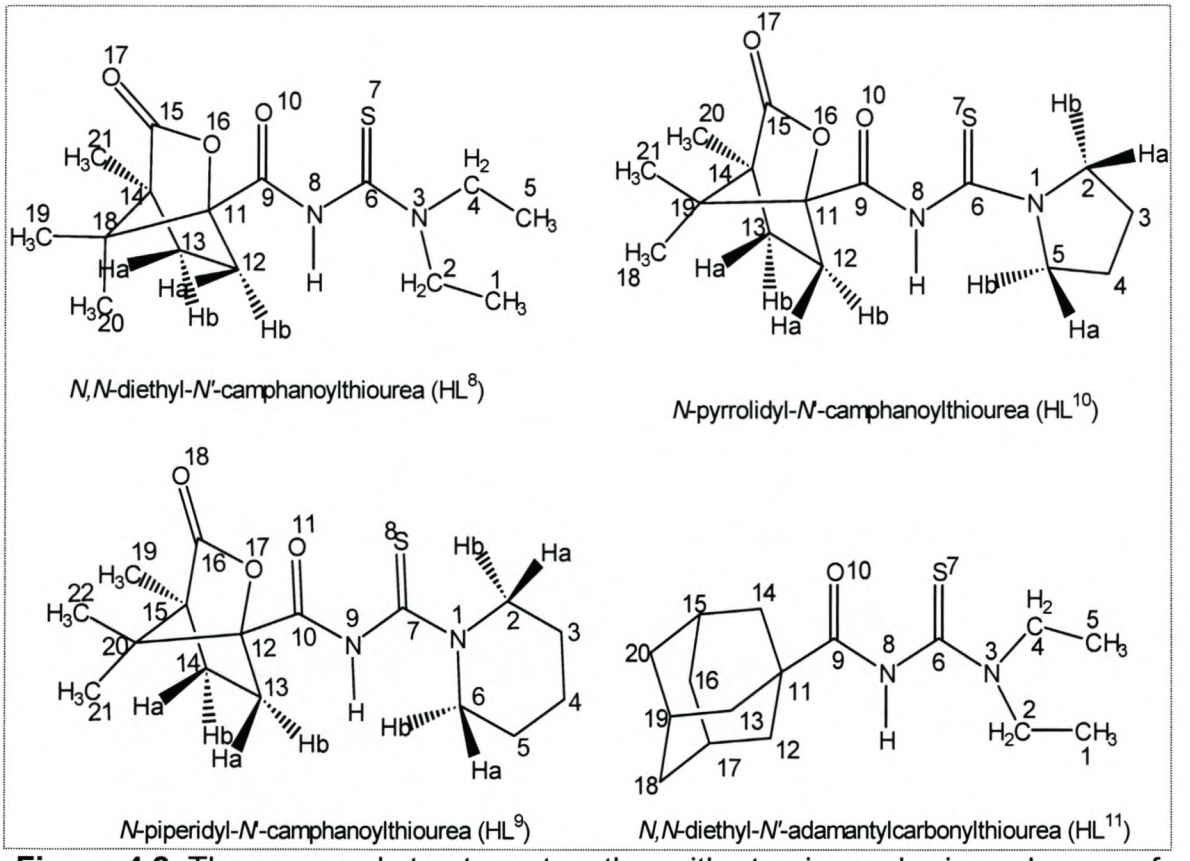

Figure 4.8. The proposed structures together with atomic numbering schemes of HL^{8}, HL^{9}, HL^{10} and HL^{11} ligands.

Table 4.3. 600 MHz ^{1}H NMR chemical shifts of HL^{8}, HL^{9}, HL^{10} and HL^{11} ligands.

Ligand	^{1}H NMR chemical shift (ppm)																	
	N-H	H1	H2	H3	H4	H5	H6	H12	H13	H14	H15	H16	H17	H18	H19	H20	H21	H22
H^{8}	8.37	1.26	3.96	-	3.53	1.26	-	1.97/ 2.48*	1.68/ 1.92*	-	-	-	-	-	1.07	0.98	1.09	-
HL^{9}	8.51	-	3.31/ 3.36*	1.69	1.69	1.69	4.16/ 4.02*	-	2.51/ 1.99*	1.69/ 1.94	-	-	-	-	1.08	-	1.01	1.12 -
HL^{10}	8.52	-	3.62/ 3.64*	3.42	3.41	3.71/ 3.78*	-	1.96/ 2.47*	1.63/ 1.88*	-	-	-	-	1.10	-	0.97	1.09	-
HL^{11}	7.63	1.24-	3.97	-	3.46	1.18	-	1.83	1.83	1.83	2.01	1.65	2.01	1.65	2.01	1.65	-	-

*The two-^{1}H chemical shifts, which are separated by / are assigned to Ha and Hb of the indicated protons.

Table 4.4. 150 MHz ^{13}C NMR chemical shifts of HL^{8}, HL^{9}, HL^{10} and HL^{11} ligands.

Ligand	^{13}C NMR chemical shift (ppm)																				
	C1	C2	C3	C4	C5	C6	C7	C9	C10	C11	C12	C13	C14	C15	C16	C17	C18	C19	C20	C21	C22
H^{8}	13.1	47.9	-	47.4	13.0	177.5	-	1.64.3	-	91.9	30.2	28.8	54.9	177.6	-	-	55.4	16.4	16.5	9.4	-
HL^{9}	-	52.6	26.1	23.8	25.1	53.1	176.3	-	163.3	-	91.7	30.3	28.9	55.0	177.1	-	-	9.6	55.4	16.8	16.6
HL^{10}	-	47.5	24.6	26.7	47.6	177.1	-	165.6	-	93.0	30.4	29.1	54.0	79.0	-	-	16.7	55.4	9.6	16.8	
HL^{11}	11.5	47.5	-	48.0	13.2	179.7		174.1	-	43.22	36.2	36.2	36.2	38.8	27.9	38.8	27.9	38.8	27.9	-	

HL^9 ligand: The ^1H and ^{13}C NMR spectra of this ligand are shown in **Figure A-I and A-II** in appendix A and agree with the proposed structure of the HL^9 ligand shown in **Figure 4.8.** The atomic numbering in the ligand is indicated in **Figure 4.8.**

As a result of the restricted rotation about the C(7)-N(1) bond and presence of electron density from the S atom as well as the π-electrons of the C=S bond, the closest proton H(2) is shielded compared to H(6), the two protons clearly being in different chemical environments. In this case the two broad peaks at 4.16/4.02 ppm are assigned to the two protons on C(6), namely H(6a) and H(6b). Similarly the two broad peaks at 3.51/3.36 ppm are assigned to the two protons on C(2), which are labelled as H(2a) and H(2b). The chemical shifts of H(3), H(4), H(5) and H(14b) overlap with one another at 1.69 ppm. The assignments for the rest of the ^1H and ^{13}C chemical shifts are similar to those for HL^8 discussed earlier and are indicated in **Table 4.3** and **4.4**. As for the HL^8 ligand, the unambiguous assignment of the ^1H and ^{13}C NMR chemical shifts of HL^9 were made on the basis of its two-dimensional (COSY and GHSQC) NMR spectra.

HL^{10} ligand: The ^1H NMR spectrum of HL^{10} is similar to that of HL^8 discussed earlier and agrees with the proposed structure of the ligand shown in **Figure 4.8.** The atomic numbering of the ligand is indicated in **Figure 4.8.**

As a result of the restricted rotation about the N(1)-C(6) bond and the presence of electron density of the nearby S atom as well as the π-electrons of the C=S bond, H(2) protons are shielded compared to the H(5) protons. The two protons on each of C(2) and C(5), namely H(2a), H(2b) and H(5a), H(5b) respectively are in different chemical environments. In this case the poorly resolved peaks at 3.78/3.71 ppm and 2.64/2.42 ppm are assigned to H5a/H5b and H2a/H2b respectively. The rest of the ^1H NMR shifts are indicated in **Table 4.3**. Due to similar reasons as for the protons, the C(2) carbon, which is assumed to be closer to the S atom compared to the C(5) atom is expected to be more shielded than the C(5) atom and hence its ^{13}C NMR peak lies upfield compared to the ^{13}C chemical shift of the C(5) atom. The ^{13}C NMR spectra of the pure HL^{10} ligand is shown in **Figure A-IV** in appendix A.

HL^{11} ligand: The ^{1}H and ^{13}C NMR spectra of this ligand are shown in **Figure 4.33** and **4.34** respectively and agree with the proposed structure of the ligand indicated in **Figure 4.8**.

As for the NMR spectra of the ligands discussed earlier, due to the restricted rotation about the N(3)-C(6) bond, the H(2) and H(4) protons, which are adjacent to N(3), and the two methyl groups H(1) and H(5) are found in different chemical environments. Hence the two broad peaks at 3.97 ppm and 3.46 ppm are assigned to the methylene protons of carbons number 2 and 4 respectively and the chemical shifts of H(1) and H(5) are found at 1.24 and 1.18 ppm respectively. The reason for the assignment of these protons is similar to the reason given for the assignment of the analogous protons of the HL^{8} ligand.

As a result of the free rotation about the C(9)-C(11) bond and complete symmetry of the adamantyl group, the protons of H(12), H(13) and H(14); H(15), H(17) and H(19) as well as H(16), H(18) and H(20) are in the same chemical environment. The ^{1}H NMR peaks at 1.83, 1.65 and 2.01 ppm are assigned to the three group protons of H(12), H(13) and H(14); H(15), H(17) and H(19); and H(16) H(18) and H(20) respectively. For similar reasons the ^{13}C NMR peaks of C(12), C(13) and C(14); C(15), C(17) and C(19) as well as C(16), C(18) and C(20) are in the same chemical environment (see **Figure 4.34**). The ^{1}H and ^{13}C NMR data of HL^{11} are shown in **Table 4.3** and **4.4**. As for the three ligands discussed earlier, the unambiguous assignment of the ^{1}H and ^{13}C NMR spectra of this ligand was supported by 2D NMR experiments of the $\{^{1}H,^{1}H\}$ COSY and $\{^{1}H,^{13}C\}$ GHSQC 2D experiments conducted on the ligand.

4.2 SYNTHESIS AND CHARACTERISATION OF TRANSITIO N METAL (M = Co^{II}, Ni^{II}, Cu^{II}, Zn^{II}, Pt^{II} and Ag^{I}) COMPLEXES OF *N,N*-DIETHYL-*N´*-CAMPHANOYL THIOUREA (HL^8) LIGAND

4.2.1. Preparation of complexes and their general properties

The interest in the HL^8 ligand arises from its versatile complex formation with the transition metal ions. Indeed, the main feature of this ligand is the great variety of coordination modes that it exhibits. Interestingly these coordination modes appear to be as a result of the properties of the camphanoyl moiety.

According to the literature, a metal ion forms as many bonds to ligands as can be fitted around it.[5, 6] Generally bulky ligands favour lower coordination numbers because of steric interaction.[6] Even in cases where square-planar coordination is favoured for electronic reasons, tetrahedral complexes can be formed when steric interactions between ligands are large.[5,6] As a result of the presence of the bulky camphanic group and two ethyl groups in the HL^8 ligand, one can expect this to affect the coordination properties of the ligand. Therefore the next section will discuss the different complexes synthesised by treating the Lewis base of *N,N*-diethyl-*N´*-camphanoylthiourea with the Lewis acids of Co^{2+}, Ni^{2+}, Cu^{2+}, Zn^{2+}, Ag^{+} and Pt^{2+} metal ions.

The complexes were prepared in good yield (91%, 92%, 84%, 62%, 94% and 82% for $H_3O^+\{fac\text{-}[Co(L^8\text{-}S,O)_3]^-\}$, *cis*-$[Ni(L^8\text{-}S,O)_2]$, *trans*-$[Cu(L^8\text{-}S,O)_2]$, *trans/cis*-$[Zn(L^8\text{-}S,O)_2]$, *cis/trans*-$[Pt(L^8\text{-}S,O)_2]$ and $Ag_2[(HL\text{-}S)(L\text{-}\mu\text{-}S,O)]_2$ respectively) according to the procedures discussed in **section 3.3.1**. These complexes were characterised by means of MS, IR spectroscopy, NMR spectroscopy and elemental (C, H, N and S) analysis. The $H_3O^+\{fac\text{-}[Co(L^8\text{-}S,O)_3]^-\}$, *cis*-$[Ni(L^8\text{-}S,O)_2]$, *trans*-$[Cu(L^8\text{-}S,O)_2]$ and $Ag_2[(HL\text{-}S)(L\text{-}\mu\text{-}S,O)]_2$ were also characterised by X-ray diffraction analysis, which is presented in **section 4.2.3**.

All complexes of these metal ions with the HL^8 ligand are air stable in both solid and solution states except the Co(II) complex (see **section 4.2.2.7**). All are readily

soluble in non-polar organic solvents and moderately soluble in polar aprotic solvents and alcohols, but insoluble in water.

4.2.2. Spectroscopic characterisation of transition metal (M = Co^{II}, Ni^{II}, Cu^{II}, Zn^{II}, Pt^{II} and Ag^{I}) complexes of *N,N*-diethyl-*N´*-camphanoylthiourea (HL^8) ligand

4.2.2.1. General overview of the IR and NMR spectroscopic results of the complexes

IR spectra results: The IR spectra of the complexes show characteristic absorption bands in the region of 4000-400 cm^{-1}. The distinctive absorption bands for each complex are summarised in **Table 4.5.** The IR spectra of $H_3O^+\{fac\text{-}[Co(L^8\text{-}S,O)_3]^-\}$, *cis*-$[Ni(L^8\text{-}S,O)_2]$, *trans*-$[Cu(L^8\text{-}S,O)_2]$, *trans/cis*-$[Zn(L^8\text{-}S,O)_2]$ and *cis/trans*-$[Pt(L^8\text{-}S,O)_2]$ all show the deprotonation of the N-H and the shift of the amidic C=O and C=S stretching frequencies from 1707 and 1228 cm^{-1} respectively for the free ligand to lower absorption frequencies in the complexes as indicated in **Table 4.5**. These results indicate that both the sulfur and oxygen atoms of the amidic carbonyl and thiocarbonyl groups are involved in the coordination of the ligands to the metal ions, which means the ligands are coordinated bidentately to the central metal ions *via* both the *S* and *O* donor atoms.

Table 4.5. The distinctive IR stretching frequencies of the free HL^8 ligand and its transition metal complexes.

Compound	absorption frequency (cm^{-1})			
	ν(N-H)	ν(O=C) of the camphanic moiety	ν(O=C)N	ν(C=S)
HL^8	1228	1806	1707	1228
$H_3O^+\{fac\text{-}[Co(L^8\text{-}S,O)_3]^-\}$		1782	1427	817
cis-$[Ni(L^8\text{-}S,O)_2]$		1783	1428	822
trans-$[Cu(L^8\text{-}S,O)_2]$		1784	1429	816
trans/cis-$[Zn(L^8\text{-}S,O)_2]$		1778	1443	813
cis/trans-$[Pt(L^8\text{-}S,O)_2]$		1783	1430	818
$Ag_2[(HL^8\text{-}S)(L^8\text{-}\mu\text{-}S,O)]_2$	1228	1777	1701/1435	797

As indicated in **Table 4.5**, the absorption frequency of the ν(O=C) vibration of the carbonyl group in the camphanoyl moiety, which was at 1808 cm^{-1} in the free HL^8 ligand, is shifted to 1777-1784 cm^{-1} in the complexes, which indicates weakening of the bonds in the complex.

The IR spectrum of $Ag_2[(HL^8\text{-}S)(L^8\text{-}\mu\text{-}S,O)]_2$ however shows two ν(C=O) vibrations for the amidic carbonyl bond [C(O)N] at 1701 and 1435 cm^{-1}. In addition a weak absorption band due to the N-H stretch is also present at 1228 cm^{-1}. These results are discussed in detail in **section 4.2.2.6**.

NMR results: The ^1H and ^{13}C NMR spectra of oxidized *fac*-$[Co^{III}(L^8\text{-}S,O)_3]$, *cis*-$[Ni(L^8\text{-}S,O)_2]$, and *trans* or *cis*-$[Zn(L^8\text{-}S,O)_2]$ consist of a single set of ligand resonance peaks closely resembling those of the free ligand. This indicates the presence of a single isomer for each complex. The ^1H and ^{13}C NMR spectra of the *cis/trans*-$[Pt(L^8\text{-}S,O)_2]$ complex however showed small peaks next to each intense peak of the *cis*-isomer to indicate the presence of a minor *trans*-isomer. The ^1H and ^{13}C NMR chemical shifts of the free HL^8 ligand, *cis*-$[Ni(L^8\text{-}S,O)_3]$, *trans* or *cis*-$[Zn(L^8\text{-}S,O)_3]$, *cis/trans*-$[Pt(L^8\text{-}S,O)_2]$, $Ag_2[(HL^8\text{-}S)(L^8\text{-}\mu\text{-}S,O)]_2$ and *fac*-$[Co^{III}(L^8\text{-}S,O)_3]$, *i.e.* after the $H_3O^+\{$*fac*-$[Co^{II}(L^8\text{-}S,O)_3]^-\}$ is oxidized to *fac*-$[Co^{III}(L^8\text{-}S,O)_3]$ by atmospheric O_2 (discussed in **section 4.2.2.7.B**), are summarised in **Tables 4.6** and **4.7** respectively.

The characterisation of *trans*-$[Cu(L^8\text{-}S,O)_2]$ and freshly prepared (unoxidized) $H_3O^+\{$*fac*-$[Co^{II}(L^8\text{-}S,O)_3]^-\}$ by means of NMR spectroscopy was prevented by the paramagnetic nature of the Cu^{II} (d^9) and Co^{II} (d^7) central metal ions and no NMR data was collected for these complexes.

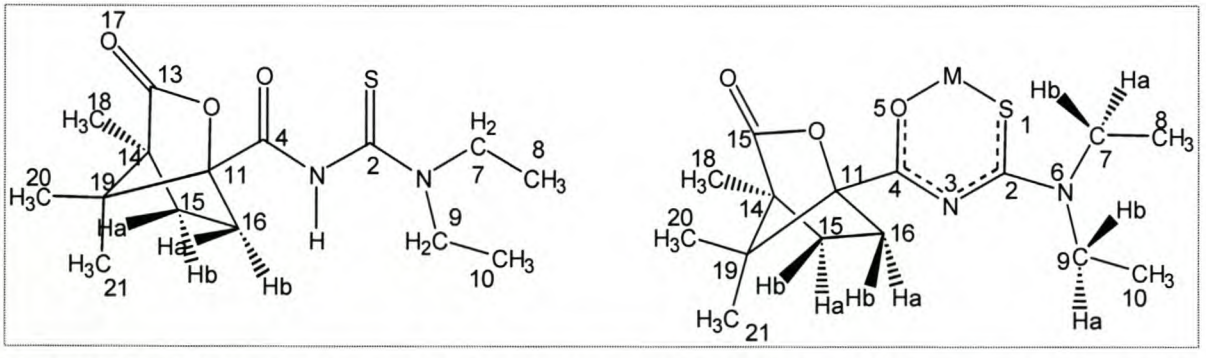

Figure 4.9. The atomic numbering scheme of the free HL^8 ligand and its metal complexes, where M = $Co^{II/III}$, Ni^{II}, Zn^{II}, Pt^{II}, Ag^{I} or Cu^{II}.

Table 4.6. The 600 MHz ^{1}H NMR data for H_3O^+{*fac*-[Co(L^8-*S,O*)$_3$]$^-$}, *cis*-[Ni(L^8-*S,O*)$_2$], *trans* or cis-[Zn(L^8-*S,O*)$_2$], *cis*-[Pt(L^8-*S,O*)$_2$] and $Ag_2[(HL^8\text{-}S)(L^8\text{-}\mu\text{-}S,O)]_2$.

Compound	^{1}H NMR chemical shift (ppm)								
	H7a/Hb	H8	H9a/H9b	H10	H15a/H15b	H16a/H16b	H18	H20	H21
HL^8	3.53	1.26	3.96	1.26	1.68/1.92	1.97/2.48	1.09	1.07	0.98
H_3O^+{*fac*-[Co(L^8-*S,O*)$_3$]$^-$]}	3.58/3.64	1.29, 1.28, 1.15	3.72/3.76	1.13, 1.06	1.60/1.83	1.89/2.40	1.07	1.02	0.92
Cis-[Ni(L^8-*S,O*)$_2$]	3.64/3.58	1.23	3.72/3.76	1.19	1.60/1.85	1.89/2.40	1.07	1.02	0.92
Trans/cis-[Zn(L^8-*S,O*)$_2$]	3.73/3.51	1.14	3.94/3.85	1.26	1.67/1.68	1.94/2.47	1.09	1.09	0.98
Cis-[Pt(L^8-*S,O*)$_2$]	3.64/3.62	1.15	3.78/3.71	1.28	1.63/1.88	1.96/2.47	1.08	1.09	0.94
$Ag_2[(HL^8\text{-}S)(L^8\text{-}\mu\text{-}S,O)]_2$	3.60 for H1 and 8.37 for N-H	1.22	3.94	1.32	1.64/1.89	2.04/2.47	1.22	1.08	1.00

Table 4.7. The 150 MHz ^{13}C NMR chemical shift of H_3O^+{*fac*-[Co(L^8-*S,O*)$_3$]$^-$}, *cis*$^-$-[Ni(L^8-*S,O*)$_2$], *trans* or *cis*-[Zn(L^8-*S,O*)$_2$], *cis*-[Pt(L^8-*S,O*)$_2$] and $Ag_2[(HL^8\text{-}S)(L^8\text{-}\mu\text{-}S,O)]_2$

Compound	^{13}C NMR chemical shift (ppm)											
	C2	C4	C7	C8	C9	C10	C11	C13	C14	C15	C16	C18
HL^8	177.5	164.3	47.5	13.0	47.9	13.1	91.9	177.6	54.9	28.8	30.2	9.4
H_3O^+{*fac*-[Co(L^8-*S,O*)$_3$]$^-$}	176.0	177.7	47.8	15.0	48.0	15.3	96.8	182.6	56.3	31.8	33.2	12.7
Cis-[Ni(L^8-*S,O*)$_2$]	173.5	171.9	45.6	12.2	46.0	12.9	93.67	179.4	54.2	29.3	30.9	9.8
Trans/cis-[Zn(L^8-*S,O*)$_2$]	166.4	172.6	47.5	12.2	47.9	12.8	91.9	177.6	54.9	28.8	30.2	9.4
Cis-[Pt(L^8-*S,O*)$_2$]	169.6	166.4	46.0	11.8	46.7	12.6	94.5	139.7	54.1	29.2	30.8	9.6
$Ag_2[(HL^8\text{-}S)(L^8\text{-}\mu\text{-}S,O)]_2$	176.0	176.7/ 167.4	47.0	12.0	47.2	12.5	93.2	178.7	54.4	29.1	30.5	9.5

The unambiguous assignment of the ^{1}H and ^{13}C NMR spectra of the complexes was based on chemical shift consideration together with information gathered from two dimensional (COSY and GHSQC) NMR experiments conducted for each complex. As a result of the restricted rotation about the C-N′ bond of the C-N′$(CH_2CH_3)_2$ moiety and the lack of two perpendicular symmetry planes in the C-N′ bond of each complex, the N′ atom behaves like a chiral centre and hence the methylene protons adjacent to this atom exhibit diastereotopism. The chemical shift differences, multiplicities and coupling constants of these diastereotopic protons for all the complexes, except $Ag_2[(HL^8\text{-}S)(L^8\text{-}\mu\text{-}S,O)]_2$, are detectable. Each of the ^{1}H NMR peaks of the hydrogen atoms on C(7) and C(9), namely H(7a), H(7b), H(9a) and H(9b), are split into a doublet of quartets, dq (eight peaks each). In this case the H(7) protons, which are closer to the coordination sphere than the H(9) protons are more shielded by the secondary magnetic field of the coordination sphere and so are shifted upfield relative to the H(9) protons. For the same reason the H(8) protons of the complexes are shifted upfield compared to the H(10) protons.

The major difference between the ^{1}H NMR spectra of the complexes and the ^{1}H NMR spectrum of the free HL^8 ligand, besides the absence of the N-H proton in the complexes, is the clearly observed diastereotopism of the methylene protons in the ethyl groups. The presence of diastereotopism in the methylene protons of the free HL^8 ligand does not give measurable multiplicities and coupling constants between the apparently equivalent protons. The ^{1}H NMR spectra of *fac*-$[Co(L^8\text{-}S,O)_3]$, *cis*-$[Ni(L^8\text{-}S,O)_2]$, *cis*-$[Pt(L^8\text{-}S,O)_2]$ and *cis/trans*-$[Zn(L^8\text{-}S,O)_2]$ however clearly show distinct diastereotopic proton chemical shifts with quantifiable multiplicities and coupling constants. This might be due to the repulsion by the secondary anisotropic field of the coordination sphere of the two C-H orbitals of the methylene groups away from the coordination sphere to reduce the H-C-H angle (α). Thereby the amount of interaction between the two C-H bonds increases to give measurable coupling constants for the protons. **Figure 4.10** shows a schematic diagram of the repulsion of the C-H bonds by the electron density in the coordination sphere to decrease the H-C-H angle α, which in turn increases the electronic interaction between the two C-H bonds. This argument is made on the basis of similar cases reported in the literature.[37]

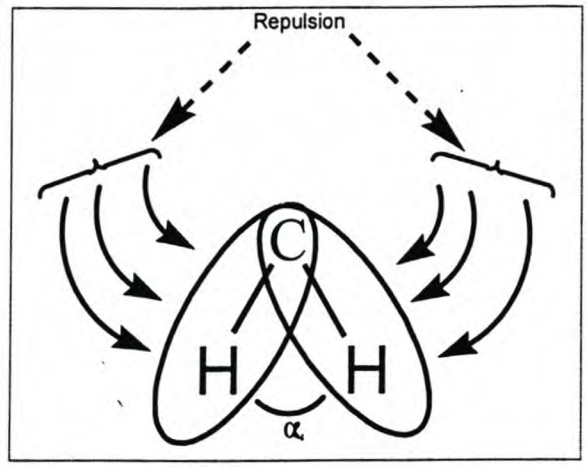

Figure 4.10. The schematic diagram of the repulsion of the two C-H bonds of the CH_2 in the CH_2CH_3 groups by the electron density of the coordination sphere of the complexes. This reduces the H-C-H angle, α, to increase the electronic interaction between the C-H bonds and make the coupling constants of the methylene diastereotopic protons quantifiable.

Generally the ^{13}C NMR chemical shifts of the amidic O=C groups of all the complexes are shifted downfield, whereas the ^{13}C chemical shifts of the C=S group are shifted upfield compared to the ^{13}C chemical shifts of these groups in the free ligand. These results are in agreement with Miller's study[28] (the change of shift of the carbonyl and thiocarbonyl ^{13}C NMR peaks of *N,N*-diethyl-*N'*-acylthiourea ligands when they form transition metal complexes, was briefly discussed in **section 2.2.6**). Normally when the *S* and *O* donor atoms of HL[8] are coordinated to metal ions, the electron density of the donor atoms decreases, as a consequence of this the ^{13}C NMR chemical shift of the O=C and S=C groups of the ligand are expected to shift downfield compared to their corresponding peaks in their free ligand. The amount of the downfield shift is expected to be related to the degree of the electron donation by the donor atoms toward the central metal ions. In this case the ^{13}C chemical shifts of the amidic carbonyl group [C(O)N] are shifted downfield in the complexes relative to the chemical shifts of the same carbons in the free ligands. This could be because of the release of some electron density from the amidic C=O bond toward the metal ion, which makes the carbons of these bonds less shielded than they were in the free ligand. In contrast the ^{13}C chemical shifts of the thiocarbonyl (C=S) group are shifted upfield in the complexes compared to the chemical shifts of the corresponding carbon in the ligand. This may be related to the back electron donation by the central metal toward the π-orbitals of the sulfur donor atom and hence the carbon in the C=S group becomes more shielded than in the free ligand.

4.2.2.2. Spectroscopic characterisation of *cis-bis*(*N,N*-diethyl-*N'*-camphanoyl-thioureato)Ni(II), *cis*-[Ni(L^8-*S,O*)$_2$]

The MS spectrum of this complex showed a peak at *m/z* 681 in the parental ion region of the complex and this is equivalent to the calculated molecular weight of the *cis*-[Ni(L^8-*S,O*)$_2$] complex. The elemental (C, H, N and S) analysis of this complex is also consistent with calculated values for *cis*-[Ni(L^8-*S,O*)$_2$]. The NMR and IR spectra of the complex agree with the structure of the proposed *cis*-[Ni(L^8-*S,O*)$_2$] complex. The deprotonation of the N-H proton, which is evident from both IR and ^{1}H NMR spectra (see **Figure 4.11**), and the weakening of the amidic O=C and S=C bonds seen in the IR spectra with shift in the absorption bands from 1707 and 1228 cm^{-1} for the free ligand respectively to 1428 and 822 cm^{-1} for the complex respectively, indicating a bidentate mode of coordination of the two ligands (with both their *S* and *O* atoms) to the central nickel atom.

Figure 4.11 shows the characteristic differences and similarities between the ^{1}H NMR spectra of the free ligand and the *cis*-[Ni(L^8-*S,O*)$_2$] complex and includes the atomic numbering schemes for both the ligand and the complex. The diastereotopic proton peaks of H(7) and H(9), which are labelled as H(7a), H(7b), H(9a) and H(9b), as well as the peaks of the methyl groups in the complex are expanded for clarity in the proton NMR spectrum of the complex. As discussed earlier, due to the restricted rotation about the C(4)-N(6) bond and lack of two perpendicular symmetry planes about the C(4)-N(6) bond, the N(6) atom behaves like a chiral centre and hence the ^{1}H NMR spectrum of the complex indicates the presence of diastereotopic protons. This diastereotopic effect leads to coupling between apparently equivalent methylene protons of the ethyl groups in the complex. As a result the four doublet of quartets (dq) overlapping at 3.76/3.58 ppm and 3.72/3.64 ppm in the ^{1}H NMR spectrum of the complex are unambiguously assigned to H(9b)/H(9a) and H(7a)/H(7b) respectively. Similarly, due to the restricted rotation about the C(4)-N(6) bond and the presence of paramagnetic anisotropy of the central metal ion, the H(8) and H(10) protons of the methyl groups appear at different chemical shifts. In this case the two triplets (t) at 1.23 and 1.19 ppm are assigned to H(10) and H(8) respectively. This assignment was carried out based on the reasonable assumption that the H(8) is closer to the coordination sphere and hence it is more shielded than H(10).

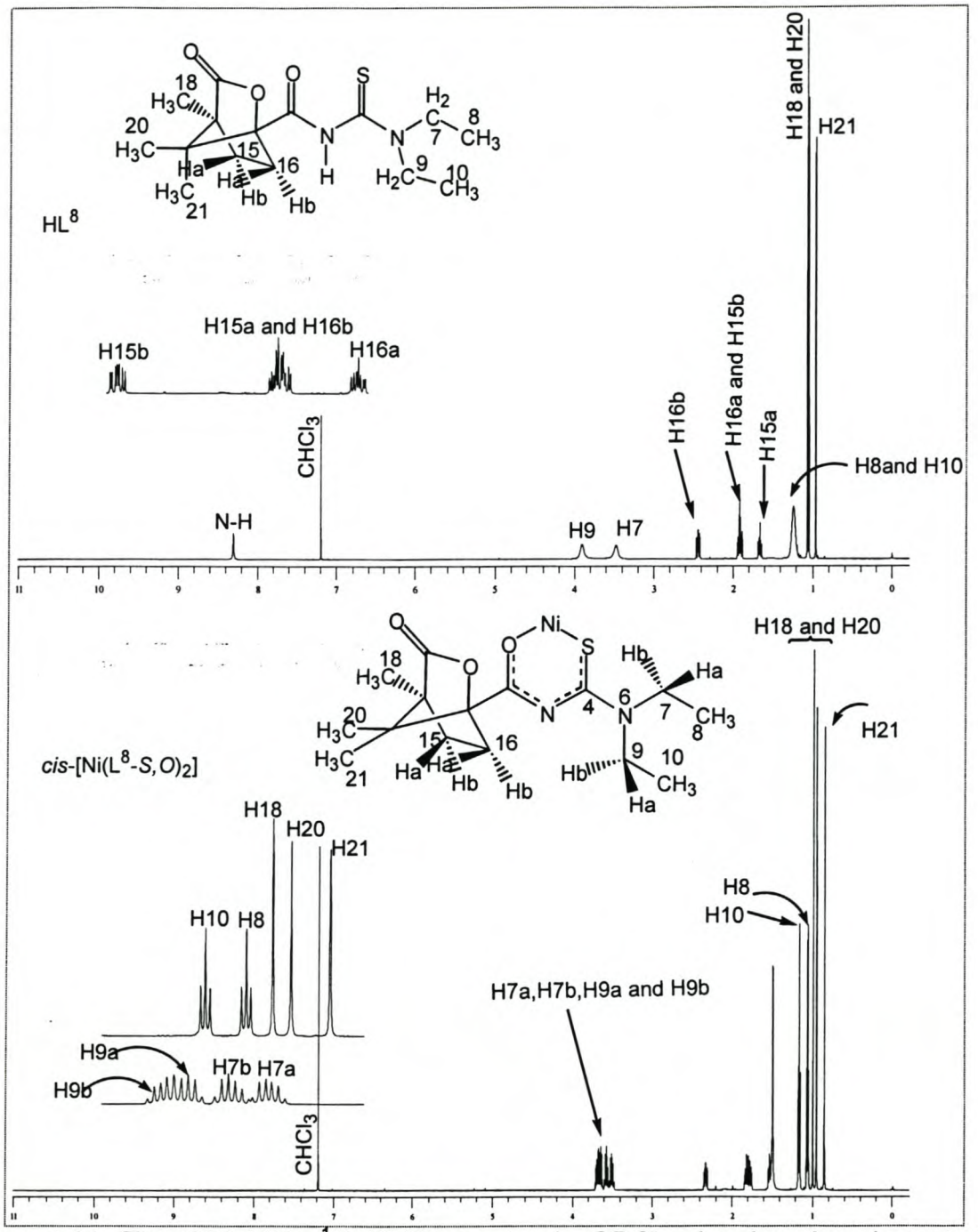

Figure 4.11. The 600 MHz ^{1}H NMR spectra in $CDCl_3$ showing the characteristic differences and similarities between the free ligand (HL^8) and the *cis*-[Ni(L^8-*S,O*)$_2$] complex.

The ^{13}C NMR spectrum of the complex closely resembles the ^{13}C NMR spectrum of the free ligand and this indicates the presence of only one isomer in the complex. **Figure 4.12** shows the characteristic differences and similarities between the ^{13}C NMR spectra of the free ligand and the *cis*-[Ni(L^8-*S,O*)$_2$] complex. The atomic numbering schemes of both the free ligand and the complex are included in **Figure 4.12**.

Again according to the studies by Miller,[28] the ^{13}C NMR peaks at 171.9, 173.4 and 179.4ppm of the *cis*-[Ni(L^8-*S,O*)$_2$] complex are unambiguously assigned to C(4), C(2) and C(13) respectively.

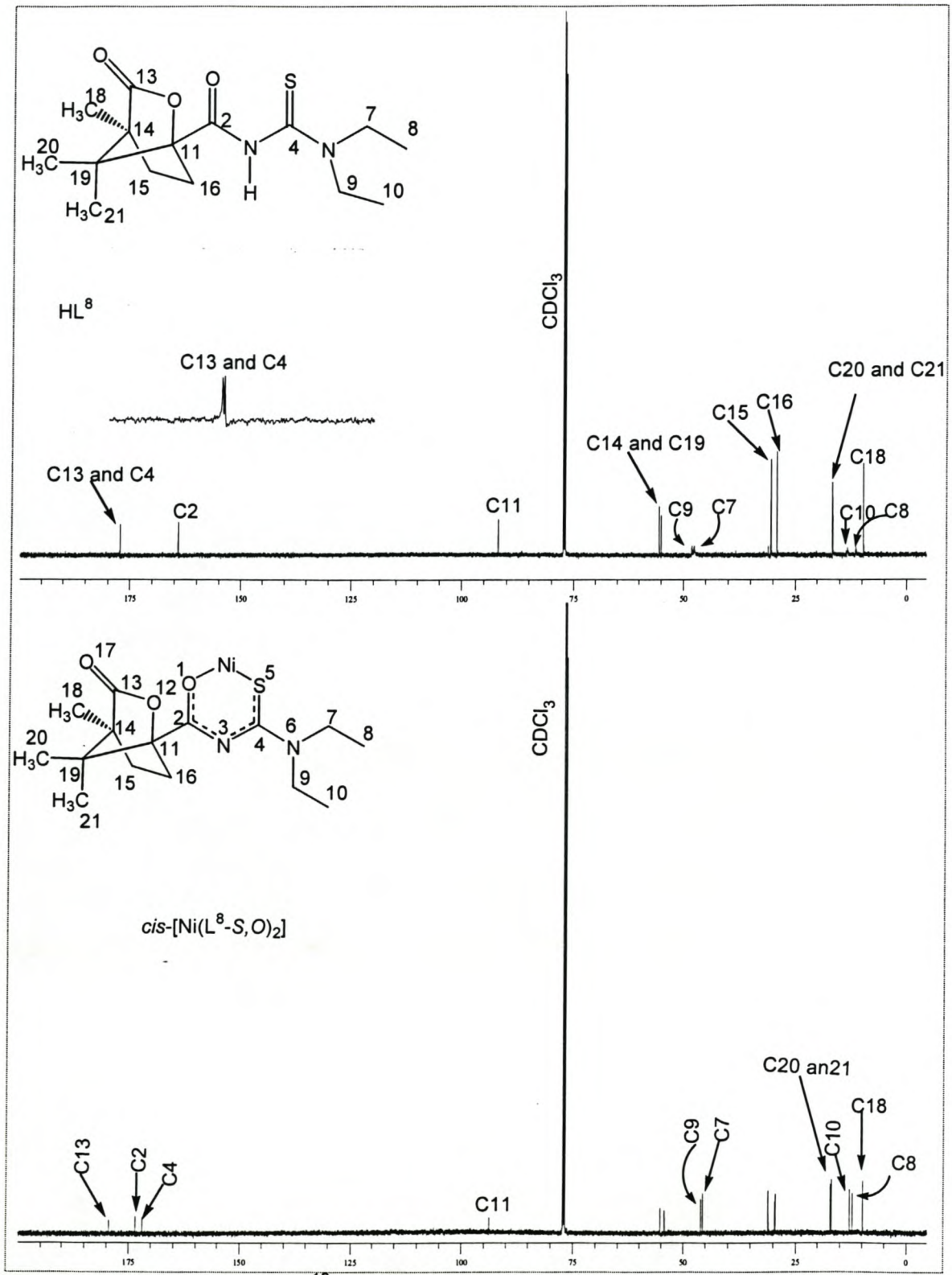

Figure 4.12. The 150 MHz ^{13}C NMR spectra showing the characteristic differences and similarities between the free ligand (HL^8) and the *cis*-[Ni(L^8-*S,O*)$_2$] complex.

The arrangement of the like donor atoms being *cis* to one another to form a *cis*-isomer is confirmed by the X-ray diffraction result of the complex, which will be discussed in **section 4.2.3.2** . This mode of coordination is justified on the basis of greater Ni-S d-π bonding that can be presented in the *cis*-arrangement; each *S* atom can independently interact with nickel d_{xz} and d_{yz} orbitals.[26]

4.2.2.3. Spectroscopic characterisation of *cis/trans-bis*(*N,N*-diethyl-*N´*-camphanoyl thioureato)Pt(II), *cis/trans*-[Pt(L-*S,O*)$_2$]

As for *cis*-[Ni(L^8-*S,O*)$_2$] discussed earlier, the IR and ^{1}H NMR spectra of the complex show the deprotonation of the N-H proton in the complex by the absence of its characteristic signals. In addition to this the IR spectrum of this complex shows the absorption band shift of the amidic ν(C=O) and ν(C=S) bond vibrations from 1707 and 1228 cm^{-1} for the free ligand to 1430 and 818 cm^{-1} for the *cis/trans*-[Pt(L-*S,O*)$_2$] complex. These results indicate the bidentate mode of coordination of the ligands (with their *S,O* donor atoms) to the platinum metal ion.

The mass spectrum showed an intense parental ion peak at *m/z* 819 and this agrees with the expected molecular mass of the predicted *cis/trans-bis*(*N,N*-diethyl-*N´*-camphanoy- lthioureato)Pt(II) complex. The elemental (H, C, N and S) analysis result is also consistent with calculated values for *cis/trans*-[Pt(L^8-*S,O*)$_2$].

Both the ^{1}H and ^{13}C NMR spectra of the complex (**Figures A-VIII** in appendix A and **Figure 4.13** respectively) showed the presence of small peaks next to each of the intense peaks, and this indicates the presence of two isomers in the complex, namely *cis* and *trans*-[Pt(L^8-*S,O*)$_2$] isomers. The ^{13}C NMR spectrum of this complex is shown in **Figure 4.13** and indicates the presence of major and minor isomers in the complex. As for the ^{1}H NMR spectrum of the *cis*-[Ni(L^8-*S,O*)$_2$] complex discussed earlier, the ^{1}H NMR spectrum of the *cis/trans*-[Pt(L^8-*S,O*)$_2$] complex showed that the CH_2 protons of the ethyl groups in the complex are diastereotopic protons.

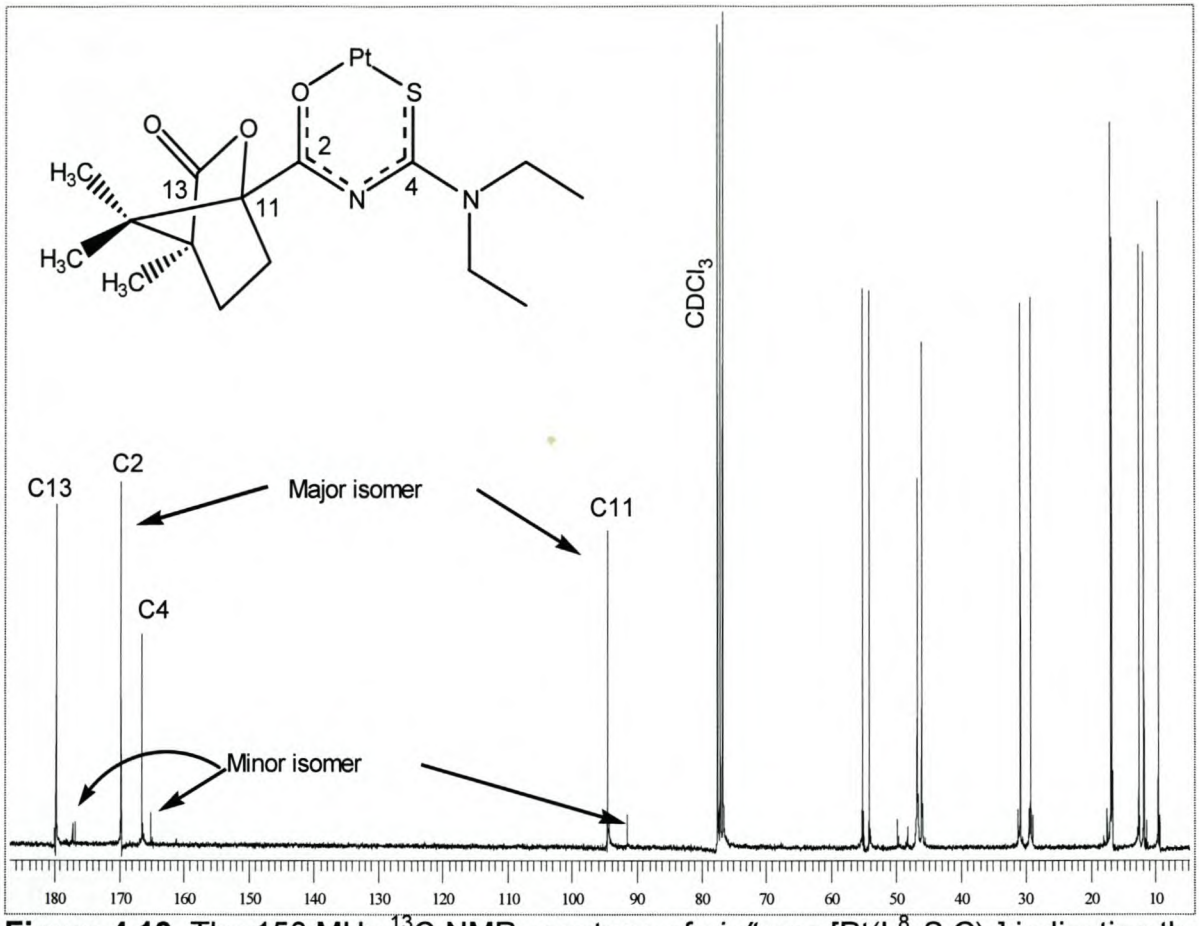

Figure 4.13. The 150 MHz ^{13}C NMR spectrum of *cis/trans*-[Pt(L^8-*S,O*)$_2$] indicating the presence of minor and major isomers of the complex.

The ^{13}C and ^{1}H NMR data of the major isomer, which gives the intense peaks in both the proton and carbon spectra, are summarised in **section 3.3.2.5**. The existence of these isomers in a 97: 3 *cis* to *trans* ratio is confirmed by the ^{195}Pt NMR spectrum of the complex (**Figure 4.14**). This spectrum shows two resonance peaks at –2682 ppm and –2932 ppm and these are assigned to the *cis* and *trans*-[Pt(L^8-*S,O*)$_2$] isomers respectively. This argument is based on the generally observed trend that the ^{195}Pt chemical shifts for *cis*-[Pt(L-*S,O*)$_2$] complexes are further downfield compared to the corresponding *trans*-isomer.[13] From this it is possible to conclude that the intense peaks in the ^{1}H and ^{13}C NMR spectra of the complex are for the *cis*-[Pt(L^8-*S,O*)$_2$ isomer whereas the short peaks are assigned to *trans*-[Pt(L^8-*S,O*)] isomer, this being the minor product.

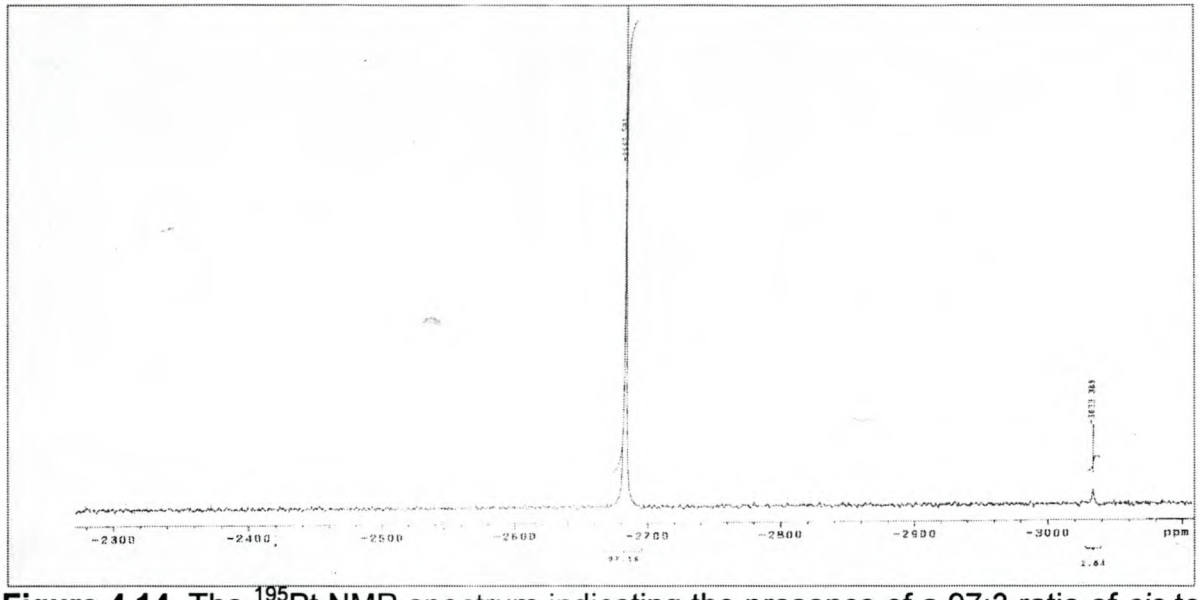

Figure 4.14. The ^{195}Pt NMR spectrum indicating the presence of a 97:3 ratio of *cis* to *trans* isomers in *cis/trans*-[Pt(L-*S,O*)$_2$].

Interestingly after the *cis/trans*-[Pt(L^8-*S,O*)$_2$] complex was recrystallised from an 80:20 (v/v) solution of CH_3CN to $CHCl_3$, which is predominantly a polar solvent, the ^{195}Pt NMR spectrum showed the presence of only the *cis*-isomer, this being indicated by a single, sharp resonance at –2684 ppm (**Figure 4.15**). According to the argument mentioned earlier this is assigned to *cis*-[Pt(L^8-*S,O*)$_2$]. This result indicates that the solvent of crystallisation affects the mode of coordination of the ligands to transition metal ions. From this it can be suggested that the polarity of the solvent of crystallisation is directly related to the polarity of the transition metal complex that can be crystallised from a specific solvent.

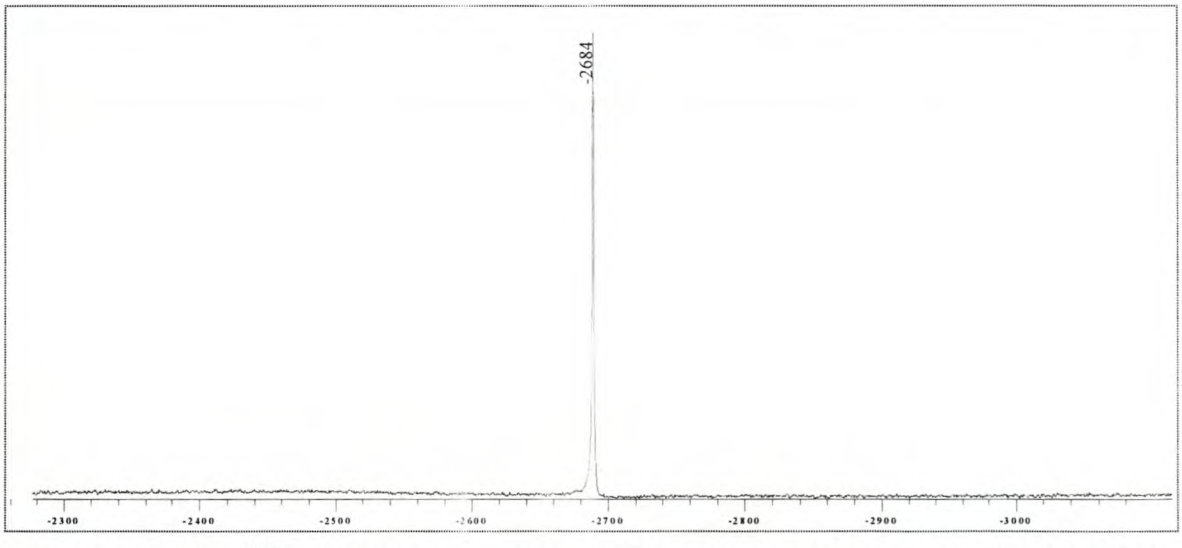

Figure 4.15. The ^{195}Pt NMR spectrum of the Pt-complex after recrystallization from a $CHCl_3$/ CH_3CN mixture indicates the presence of only the *cis*-[Pt(L-*S,O*)]$_2$ isomer.

4.2.2.4. Spectroscopic characterisation of *trans-bis*(*N,N*-diethyl-*N'*-camphanoylthioureato)Cu(II), *trans*-[Cu(L^8-*S,O*)$_2$]

Trans-[Cu(L^8-*S,O*)$_2$] is found to be similar to the Cu(II) complex of *cis-bis*(*N,N*-diethyl-*N'*-benzoylthioureato)Cu(II),[27] with two *N,N*-diethyl-*N'*-camphanoylthiourea ligands being coordinated in a bidentate fashion through their *O* and *S* donor atoms to the Cu(II) ion to form a six-membered chelate ring. This could be seen in the spectroscopic results for the complex. In this case the mass spectrum of the new copper complex showed an intense parent ion peak (M^+) at *m/z* 682 and this is exactly the molecular mass of the expected *trans*-[Cu(L^8-*S,O*)$_2$] complex. The elemental (C, H, N and S) analysis result of this complex is also consistent with calculated values for *trans*-[Cu(L^8-*S,O*)$_2$]. In addition to that the pertinent features of the infrared spectrum of the complex (**Figure A-VII** in appendix A) indicate the deprotonation of the N-H proton in the complex. Moreover the ν(C=O) of the amidic carbonyl [C(O)N] group and ν(C=S) vibration frequencies shifted from 1707 cm^{-1} and 1228 cm^{-1} for the free ligand respectively to 1429 $cm^{-1}$and 816 cm^{-1} of the complex respectively. From previous studies[41] these phenomena indicate that the two ligands are coordinated in a bidentate coordination fashion to the central copper metal ion with both their *S* and *O* donor atoms to give a neutral *trans*-[Cu(L^8-*S,O*)$_2$] complex.

The paramagnetic nature of the Cu(II) d^9 prevented the characterisation of the complex by means of NMR spectroscopy, which would have given information about the *cis/trans* isomer distribution of the complex if indeed present. Nevertheless the TLC result gave an R_f value of 0.54 for the complex in a $CHCl_3$ mobile phase and revealed the presence of only one component in the product, which is *trans*-[Cu(L^8-*S,O*)$_2$]. This result was confirmed by X-ray diffraction analysis of the complex and is discussed in **section 4.2.3.3**.

The preference for the *trans* arrangement of the donor atoms in the *trans*-[Cu(L^8-*S,O*)$_2$] complex is justified on the basis of the steric interaction that can take place between the substituents (camphanic and ethyl groups) of the ligands. The steric interaction can be minimized when the donor atoms of the ligands are arranged in a *trans* manner compared to if there was a *cis* arrangement of the donor atoms in the coordination sphere of the complex. In addition to this the weakening of the IR ν(C=O) vibration of the carbonyl group in the camphanic moiety from 1806 cm^{-1} for

the free ligand to 1784 cm^{-1} in the complex might indicate the release of some electron density from the camphanic group toward the amidic oxygen donor atom. According to the speculation of Koch,[29] discussed in **section 2.3.2**, this phenomenon makes the amidic oxygen donor atom softer and stabilizes the *trans* isomer, which might be the reason for the *trans*-isomer formation of this complex.

4.2.2.5. Spectroscopic characterisation of *trans/cis-bis*(*N,N*-diethyl-*N´*-camphanoyl- thioureato)Zn(II), *trans/cis*-[Zn(L^8-*S,O*)$_2$]

The presence of two ligands and one Zn metal ion in the complex is confirmed from its MS result, which showed an intense parental ion (M^+) peak at *m/z* 688, and elemental (C, H, N and S) analysis result, which is consistent with the calculated value of the empirical formula of *trans/cis*-[Zn(L^8-*S,O*)$_2$].

The IR and NMR results of this complex also agree with the expected mode of coordination of the ligands to the zinc metal ion. In this case, as for the ^{1}H NMR and IR spectra of the Ni^{II} and Pt^{II} complexes discussed earlier, both the ^{1}H NMR and IR spectra of the complex confirmed the deprotonation of the N-H proton in the complex. In addition the IR spectrum of the complex showed the absorption band shifts of the amidic ν(C=O) and ν(C=S) vibrations from 1707 cm^{-1} and 1228 cm^{-1} for the free ligand to 1443 cm^{-1} and 813 cm^{-1} for the complex respectively. From previous studies,[41] this indicates the bidentate mode of coordination of the two ligands to the zinc metal ion through their *S* and *O* donor atoms.

Since the atomic radius of Zn(II) is smaller than the atomic radius of Cu(II), more steric interaction among the ethyl and camphanic groups of the complex is expected when comparing with the steric interaction of the organic groups in the *trans*-[Cu(L^8-*S,O*)$_2$] complex. The ν(C=O) vibration frequency of the carbonyl group in the camphanic moiety is also reduced from 1806 cm^{-1} for the free ligand to 1778 cm^{-1} for the complex. As speculated earlier in the copper complex, this might indicate the release of some electrons toward the amidic oxygen donor atom to make the donor atom softer and more suitable for *trans* complex formation. Thus the mode of coordination of the ligands in the complex is expected to give the *trans*-[Zn(L^8-*S,O*)$_2$] isomer. However this analysis cannot be conclusive as the stereochemistry of the complex needs to be confirmed by means of X-ray diffraction analysis.

The ^{13}C NMR spectrum of the complex is shown in **Figure A-VI** in appendix A and resembles the spectrum of the free ligand. This indicates the presence of only one isomer, which is confirmed by the TLC result, which gives a single R_f value of 0.53 in a $CHCl_3$ mobile phase.

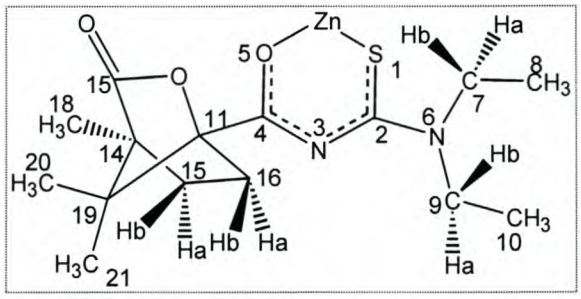

Figure 4.16. The atomic numbering scheme of *trans/cis*-[Zn(L^8-*S,O*)$_2$].

Similar to the ^1H NMR spectra of *cis*-[Ni(L^8-*S,O*)$_2$] and *cis/trans*-[Pt(L^8-*S,O*)$_2$], the ^1H NMR spectrum of this complex showed the presence of diastereotopic methylene protons, namely H(9a)/H(9b) and H(7a)/H(7b) at 3.94/3.85 ppm and 3.73/3.51 ppm respectively. The reason for the presence of the diastereotopic effect in these protons is the same as the reason given for the analogous protons of *fac*-[Co(L^8-*S,O*)$_2$] and *cis*-[Ni(L^8-*S,O*)$_2$] discussed earlier. Due to the presence of the electron density of the sulfur donor atom plus the secondary anisotropic field of the Zn, which shields the closer H(8) more than H(10), and the absence of rotation about the C(2)-N(6) bond, the two triplet peaks at 1.26 and 1.14 ppm are assigned to H(10) and H(8) protons respectively . The chemical shifts of the rest of the protons and carbons are indicated in **Table 4.6** and **4.7** respectively.

4.2.2.6. Spectroscopic characterisation of *tetrakis*(*N,N*-diethyl-*N'*-camphanoyl-thioureato)diargentate(I), $Ag_2[(HL^8\text{-}S)(L^8\text{-}\mu\text{-}S,O)]_2$

Unlike the ^1H NMR and IR spectra of the Ni^{II}, Pt^{II} and Zn^{II} complexes discussed earlier, the ^1H NMR and IR spectra of $Ag_2[(HL^8\text{-}S)(\ L^8\text{-}\mu\text{-}S,O)]_2$ only indicate the partial deprotonation of the N-H proton of the ligand. The IR spectra in **Figure 4.17** compares the two ν(C=O) vibrations of the amidic carbonyl bond [C(O)N] of the complex at 1701 and 1435 cm^{-1} with the absorption frequency of the amidic ν(C=O) vibrations in the IR spectrum of the free HL^8 ligand. This indicates that the ν(C=O) bond vibration frequency of the amidic carbonyl bond in the complex is shifted from

1707 cm^{-1} for the free ligand to 1435 cm^{-1} for the complex. However there is still a peak at 1701 cm^{-1} in the IR spectrum of the complex. The 1701 cm^{-1} and 1435 cm^{-1} absorption frequencies are assigned to the amidic ν(C=O) vibrations for a non-bonded *O* atom and an *O* donor atom bonded to the Ag(I) ion respectively. The ν(C=S) vibration frequency of the complex is also shifted from 1228 cm^{-1} for the free ligand to 797 cm^{-1} for the complex. This means that some of the ligands in the complex are bonded with both oxygen and sulfur donor atoms, whereas the other ligands are bonded to the Ag(I) ion with their sulfur donor atoms only and their oxygen donor atoms are left uncoordinated. This mode of coordination of the ligands around each Ag^{I} was confirmed from X-ray diffraction anlysis of the complex, which is discussed in **section 4.2.3.4**.

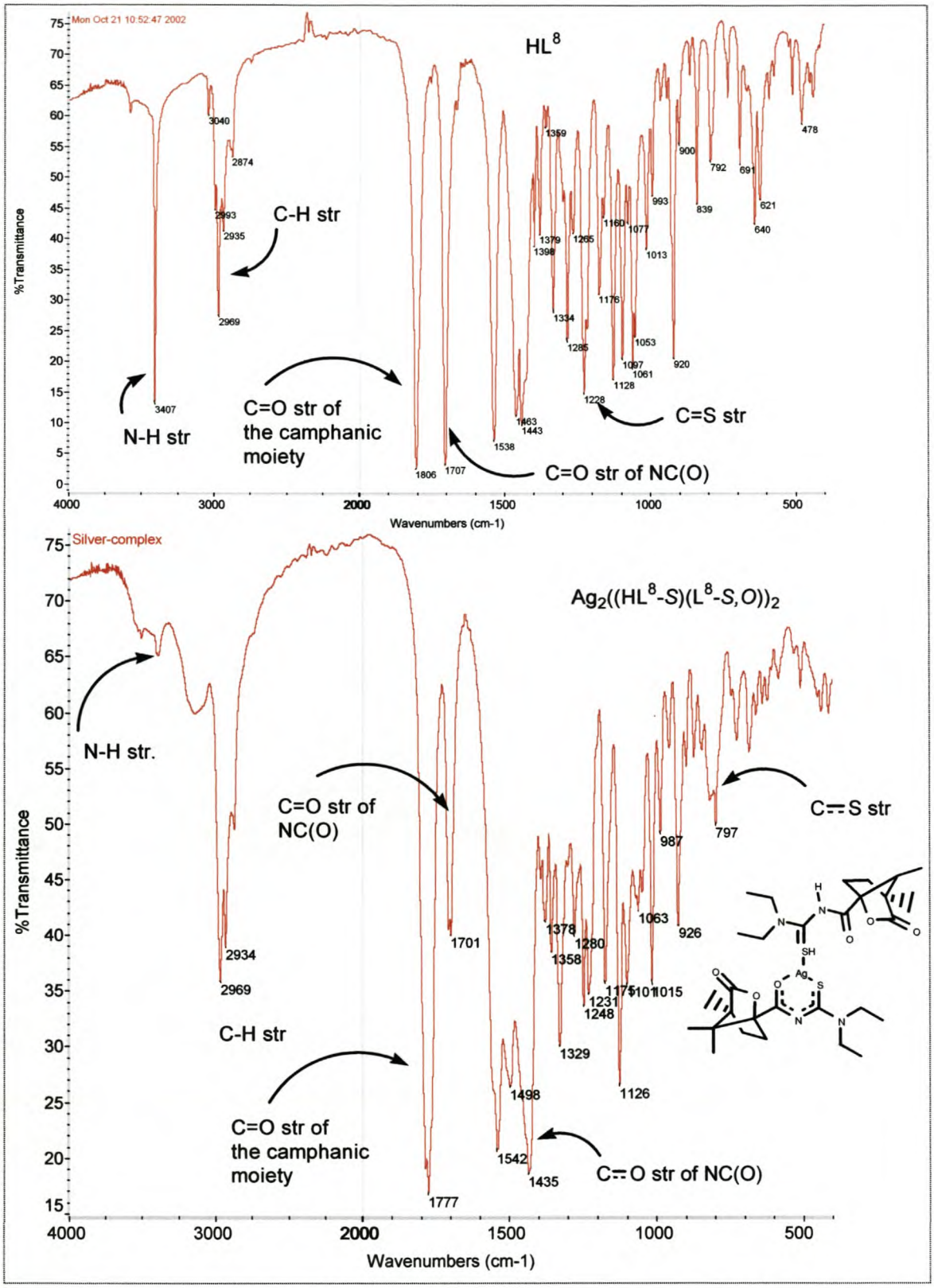

Figure 4.17. IR spectra showing the difference between the free ligand (HL^8) and $Ag_2[(HL^8\text{-}S)(L^8\text{-}\mu\text{-}S,O)]_2$ complex. The $Ag_2[(HL^8\text{-}S)(L^8\text{-}\mu\text{-}S,O)]_2$ complex shows the presence of non-bonded and bonded oxygen donor atoms of the amidic carbonyl bond, which are indicated by the peaks at 1701 and 1435 cm^{-1} respectively. The presence of a very weak ν(N-H) absorption band at around 3407 cm^{-1} indicates partial deprotonation of the ligands in the complex. The C=S stretching frequency shifted from 1228 cm^{-1} for the free ligand to 797 cm^{-1} for the complex.

The two poorly resolved ^{1}H NMR peaks of $Ag_2[(HL^8\text{-}S)(L^8\text{-}\mu\text{-}S,O)]_2$ at 3.94 ppm and 3.58 ppm are assigned to the protons on C(9) and C(7) respectively. However unlike the corresponding ^{1}H NMR peaks of the *fac*-$[Co(L^8\text{-}S,O)_3]$, *cis*-$[Ni(L^8\text{-}S,O)_2]$, $Zn(L^8\text{-}S,O)_2$ and *cis*-$[Pt(L^8\text{-}S,O)_2]$ discussed earlier, the multiplicities and coupling constants of these protons in the silver complex are not detectable. Whereas the ^{1}H NMR peaks of the camphanic group in the complex are well resolved and their chemical shifts, multiplicities as well as their coupling constants are summarised in **section 3.3.2.6**. This unambiguous assignment of the ^{1}H and ^{13}C NMR spectra of this complex was carried out with the assistance of two-dimensional COSY and GHSQC NMR spectra.

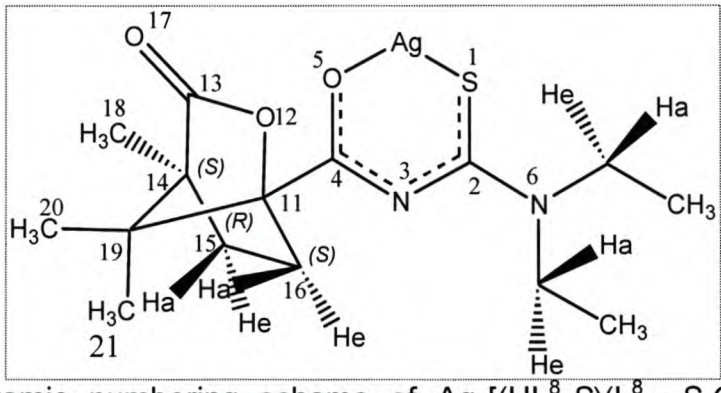

Figure 4.18. Atomic numbering scheme of $Ag_2[(HL^8\text{-}S)(L^8\text{-}\mu\text{-}S,O)]_2$. The atomic numbering of the unidentate ligands $(HL^8\text{-}S)$ are the same as the bidentate ligands $(L^8\text{-}S,O)^-$ in the complex.

The ^{13}C NMR spectrum of the complex is shown in **Figure A-IX** in appendix A and resembles the ^{13}C NMR spectrum of the free ligand, except for the peaks of the amidic carbonyl [C(O)N] moiety. Two peaks are seen in this case indicating the bonded and non-bonded oxygen donor atoms of the C(O)N moiety in the complex. The close resemblance of the ^{13}C NMR spectrum of this complex and the ^{13}C NMR spectrum of the free ligand indicates the presence of one component and this is confirmed from the TLC result, which gives one R_f value of 0.43 with a $CHCl_3$ mobile phase.

Based on Miller's study,[28] the four ^{13}C NMR peaks of the complex at 178.7, 176.7, 167.4 and 176.0 ppm are tentatively assigned to C(13), C(4) of C(4)=O(5) with a bonded *O* donor atom, C(4) of C(4)=O(5) with a non-bonded *O* donor atom, and C(2) respectively. The presence of two peaks for the bonded and non-bonded C(4) carbon agrees with the 1701 and 1435 cm^{-1} absorption frequencies shown in the IR spectrum discussed earlier and the molecular structure of the complex, which is

shown later in **Figure 4.28**. The rest of the ^{13}C chemical shifts of the complex are listed in **section 3.3.2.6**.

4.2.2.7. Characterisation of hydronium *fac*-*tris*(*N,N*-diethyl-*N'*-camphonoyl-thioureato)Co(II), $H_3O^+\{$*fac*-$[Co(L^8$-*S,O*$)_3]^-\}$.

A. Spectroscopic characterisation of $H_3O^+\{$*fac*-$[Co(L^8$-*S,O*$)_3]^-\}$

As indicated in **section 3.3.1.1**, three moles of the ligand reacted with one mole of Co^{II} to form the cobalt complex. The presence of three ligands with one Co atom in the complex is confirmed by means of MS with a value of *m/z* 993 (M^+, 11%). Since the complex formation reaction was started with Co^{II}, the overall complex would be expected to be anionic with three ligands bidentately bonded to it, because each ligand is assumed to be anionic on deprotonation of the N-H. A charged complex of this type of ligand is expected to be soluble in distilled water. However the cobalt complex was recrystallized from water, and this indicates that the overall charge of the complex must be neutral. So, what could make the complex neutral? There are three possible ways to get a neutral Co^{II} complex with three HL type ligands and these are:

a) Presence of a counter ion (X^+) that neutralises the charge of the overall anionic complex (*i.e* when three ligands are bidentately bonded to one Co^{II}).

b) One of the three ligands in the complex is neutral (HL-*S*) and bonded with its *S* atom only to the Co^{II}, whereas the other two ligands are anionic (L-*S,O*)$^-$ bonding with both their *S* and *O* atoms forming a Co^{II}(L-*S,O*)$_2$(HL-*S*) complex.

c). The Co^{II} oxidizes to Co^{III} during the complex formation reaction to form a Co^{III}(L-*S,O*)$_3$ complex.

The freshly prepared crystals of this complex appeared to contain Co(II) complex because the paramagnetic nature of the Co(II) (d^7) prevented the characterisation of the complex by means of ^1H and ^{13}C NMR spectroscopy and hence no NMR information was obtained for the freshly prepared cobalt complex. But after two weeks a further attempt at NMR spectroscopy gave good ^1H and ^{13}C NMR spectra, which is an indication of the oxidation of the Co(II) to Co(III) (d^6, diamagnetic) by atmospheric O_2 in the complex (see **section 4.2.2.7.B**). The ^1H NMR spectrum shows the deprotonation of the N-H of the ligands in the complex by the absence of the N-H peak. From this result, two of the ways of getting a neutral cobalt complex

indicated earlier (b and c) are impossible. The only possible way is "a", which means that there must be a counter ion (X^+) that neutralises the charge of the overall anionic complex (*i.e* when three ligands are bidentately coordinated to one Co^{II}). This hypothesis was confirmed by X-ray diffraction analysis result of the complex, which is discussed in **section 4.2.3.5**.

Though the complex was dried at 110 °C for two hours in a vacuum oven before the IR spectrum was recorded, the spectrum still shows a broad absorption band at 3432 cm^{-1} and this is assigned to ν(O-H) (**Figure 4.19**), which is indicative of the presence of an hydronium ion or water in the complex. The elemental (C, H, N and S) analysis result of the complex is also consistent with the calculated value for H_3O^+{*fac*-[Co(L^8-*S,O*)$_3$]$^-$}. The MS spectrum in turn showed sensible fragmentation consistent with the predicted complex, and the mass of H_2O as a base peak. This clearly seems to indicate that each of the negatively charged *fac*-[Co^{II}(L^8-*S,O*)$_3$]$^-$ ions is neutralised by an uncoordinated hydronium counter ion ($X^+ = H_3O^+$) in the complex.

Since the N-H proton is expected to be deprotonated during the complex formation by the weak base of CH_3CO_2Na (see **reaction scheme 3.2**), the disappearance of the peak of this proton from the IR spectrum of the cobalt complex is expected. As indicated in **section 4.2.2.1**, the ν(O=C) vibration absorption band of the C(O)N moiety is shifted from 1707 cm^{-1} for the free HL^8 ligand to 1427 cm^{-1} for the cobalt complex. Similarly the ν(S=C) vibration absorption frequency of the free ligand is shifted from 1228 cm^{-1} to 817 cm^{-1} in the complex. These spectroscopic results indicate that both the sulfur and oxygen atoms of the amidic carbonyl and thiocarbonyl groups are involved in the coordination of the ligands to the cobalt metal ion. The absorption frequency ν(O=C) of the carbonyl group in the camphanoyl moiety, which was at 1808 cm^{-1} in the free HL^8 ligand, is also shifted to 1782 cm^{-1} in the complex, which indicates weakening of the bonds in the complex. The broad absorption band at 3432 cm^{-1} is assigned to the ν(O-H) vibration of H_3O^+/H_2O. **Figure 4.19** shows the characteristic differences between the IR spectra of the free ligand and the H_3O^+{*fac*-[Co(L^8-*S,O*)$_3$]$^-$} complex.

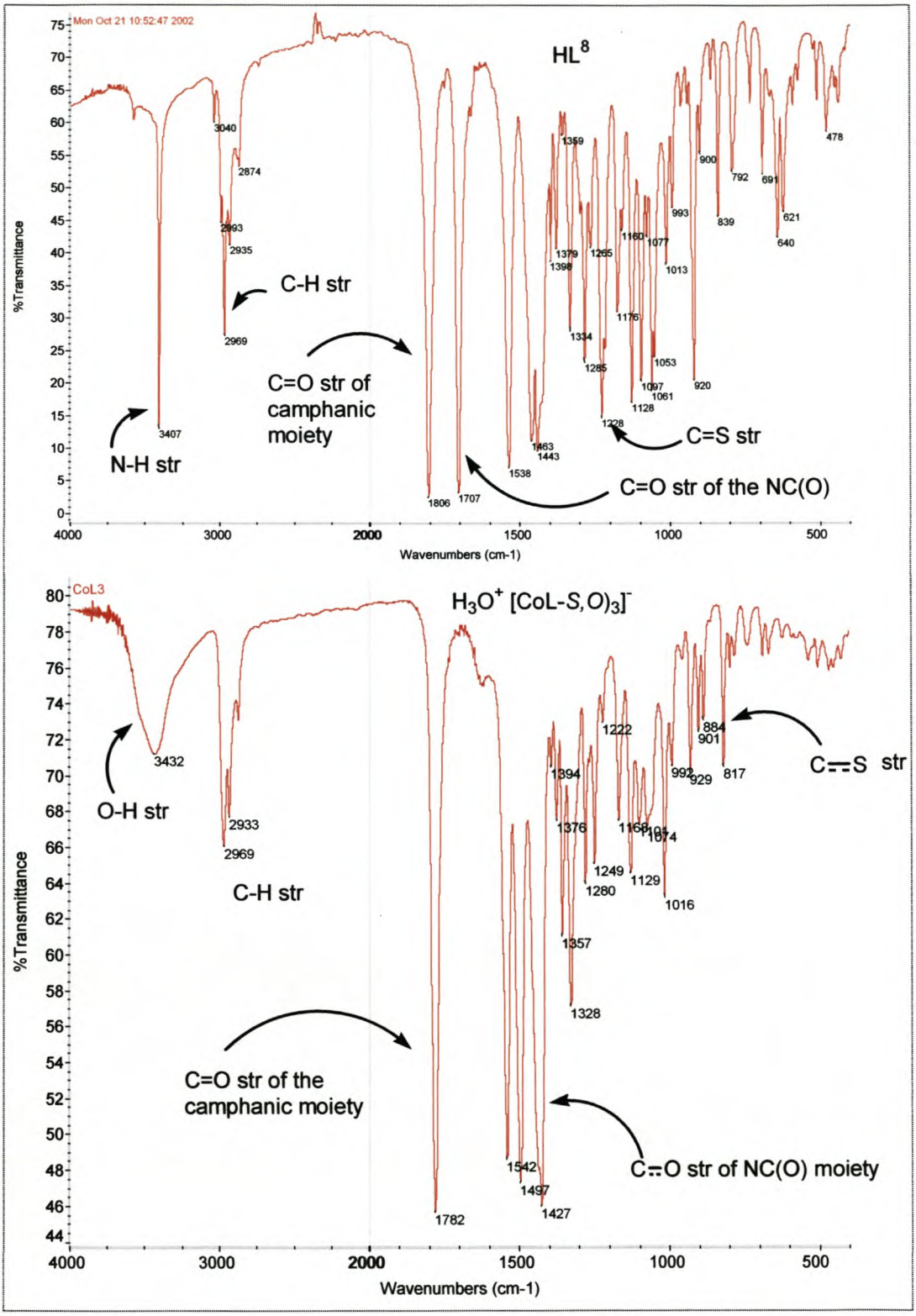

Figure 4.19. The IR spectra of $H_3O^+\{fac\text{-}[Co(L^8\text{-}S,O)_3]^-\}$ and the free ligand (HL^8) showing the absorption band shifts of the amidic ν(C=O) and ν(C=S) from 1707 and 1228 cm^{-1} for the free ligand to 1427 and 817 cm^{-1} for the complex respectively. The IR spectrum of the complex shows a broad absorption band at 3432 cm^{-1} for the ν(O-H) vibration of the hydronium counter ion/H_2O.

^{1}H and ^{13}C NMR spectra of the *fac*-[Co^{III}(L^{8}-*S,O*)$_3$] complex (after the Co^{II} is oxidized to Co^{III} by atmospheric O_2): The ^{1}H NMR spectrum of the *fac*-[Co^{III}(L^{8}-*S,O*)$_3$] complex is shown in **Figure 4.21**. The chemical shifts, multiplicities and coupling constants of the proton spectrum are listed in **section 3.3.2.1**.

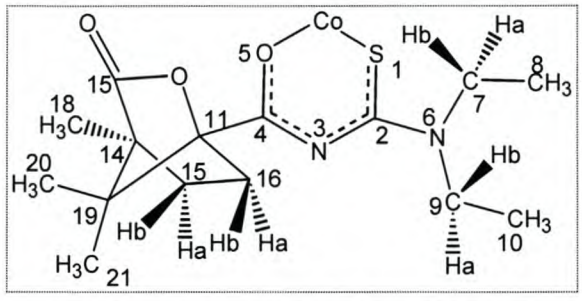

Figure 4.20. Atomic numbering scheme of *fac*-[Co(L^{8}-*S,O*)$_3$].

The unambiguous assignment of the ^{1}H and ^{13}C NMR spectra of the complex were based on chemical shift consideration together with evidence from the two dimensional (COSY and GHSQC) NMR experiments conducted on the oxidized complex. Similar to the Ni^{II}, Pt^{II} and Zn^{II} complexes discussed earlier, as a result of the restricted rotation about the C(2)-N(6) bond and lack of two perpendicular symmetry planes, the N(6) atom behaves like a chiral centre and hence the methylene protons adjacent to this atom exhibit diastereotopism. The chemical shift differences, multiplicities and coupling constants of these diastereotopic protons are detectable. Each of the ^{1}H NMR peaks of the hydrogen atoms on C(7) and C(9), namely H(7a), H(7b), H(9a) and H(9b) are split into a doublet of quartets, dq (eight peaks each). In this case the H(7) protons, which are closer to the coordination sphere compared to the H(9) protons, are more deshielded by the secondary magnetic field of the coordination sphere compared to the H(9) protons and hence the doublet of quartets at 3.76/3.72 ppm and 3.58/3.64 ppm are assigned to the H(9b)/H(9a) and H(7b)/H(7a) protons respectively. The three triplet peaks (t) at 1.29, 1.28 and 1.15 ppm are assigned to the protons of the methyl groups labelled as H(10). Similarly the two triplet peaks at 1.13 and 1.06 ppm are assigned to the H(8) protons. This indicates that the six methyls of the ethyl groups in the three ligands of the complex are in five different chemical environments. The presence of these protons in different chemical environments might be due to the restricted rotation about the C(2)-N(6) bond plus the different conformations (chair, boat and skew boat) that the six-membered chelate ring of the complex can form in the solution state. The ^{1}H NMR data of the camphanic group and the ^{13}C NMR data of the complex however

closely resemble the NMR data of the free ligand and this indicates the presence of only one isomer in the complex.

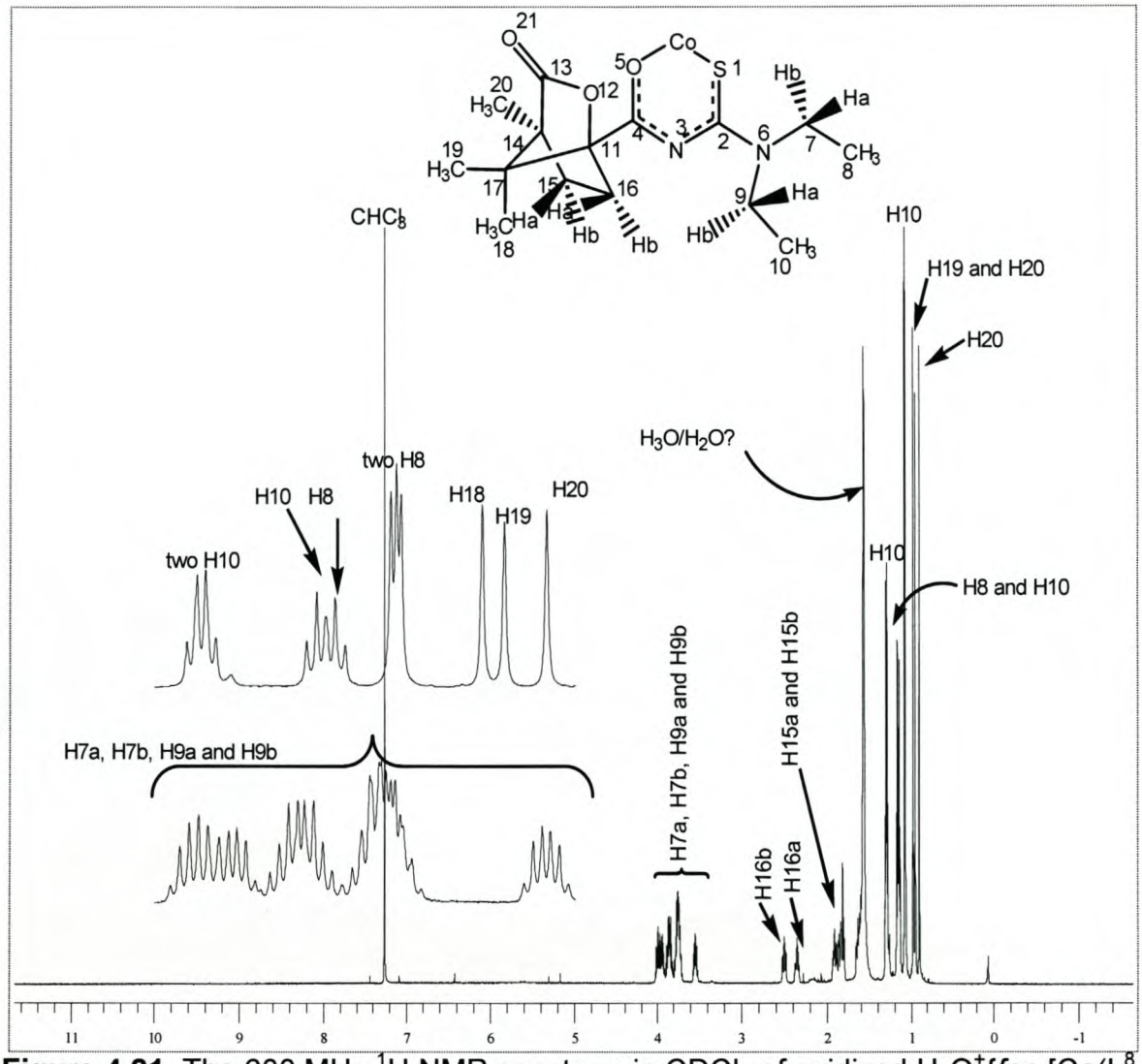

Figure 4.21. The 600 MHz ^{1}H NMR spectrum in $CDCl_3$ of oxidized H_3O^+\{*fac*-[Co(L^8-*S, O*)$_3$]$^-$\} together with the atomic numbering scheme (after the oxidation of Co^{II} to Co^{III} in the complex).

Based on the reasoning presented by Miller,[28] the three ^{13}C NMR spectrum peaks downfield at 176.0, 177.7 and 182.6 ppm are unambiguously assigned to C2, C4 and C13 respectively.

B. Oxidation of Co(II) to Co(III) in H_3O^+ {*fac*-[Co(L^8-*S,O*)$_3$]$^-$} complex

As indicated earlier the characterisation of freshly prepared H_3O^+\{*fac*-[Co(L^8-*S,O*)$_3$]$^-$\} by means of NMR spectroscopy was prevented by the paramagnetic nature of the Co(II) d^7 and no NMR information was obtained. 18 days after the synthesis of the complex, NMR analysis was conducted on the same complex to investigate the

counter ion of the complex, the presence of which was indicated by the MS, IR spectroscopy and X-ray diffraction analysis results. Interestingly the ^{1}H and ^{13}C NMR spectra of the complex, which could not be collected previously because of the paramagnetic nature of the Co(II) in the fresh sample, were now easily obtained with high resolution. This clearly indicates that the dark green $H_3O^+\{fac\text{-}[Co(L^8\text{-}S,O)_3]^-\}$ is air sensitive and thereby the Co(II) d^7 (paramagnetic) is oxidized by atmospheric O_2 to Co(III) (d^6, diamagnetic). The synthetic route for the oxidation of the Co(II) to Co(III) by atmospheric O_2 in the complex is shown in **reaction scheme 4.3**.

$$4(CoL_3)^- H_3O^+ + O_2 \longrightarrow 4Co(L\text{-}S,O)_3 + 6H_2O$$

Reaction scheme 4.3. The oxidation of Co(II) to Co(III) in the $H_3O^+\{fac\text{-}[Co(L^8\text{-}S,O)_3]^-\}$ complex by atmospheric O_2.

During the oxidation reaction the hydronium ion is expected to leave as H_2O. In this case the broad peak at 1.47 ppm of the ^{1}H NMR spectrum of the complex (**Figure 4.21**) is tentatively assigned to the water produced during the oxidation of Co(II) to Co(III) in the complex.

The oxidation of Co(II) to Co(III) by atmospheric O_2 in octahedral cobalt complexes in the presence of ligands is well known. Valence bond theory[5] describes how one electron can easily be lost from an octahedral cobalt complex according to the following principles: The arrangement of electrons in the 3d level of Co(II) is:

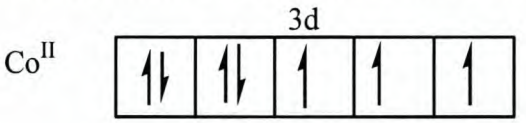

When complex formation occurs *via* octahedral coordination of the cobalt metal ion with ligands, the use of two of the 3d orbitals for d^2sp^3 hybridisation requires the promotion of one 3d electron to the nearest vacant orbital of higher energy, namely 5s.

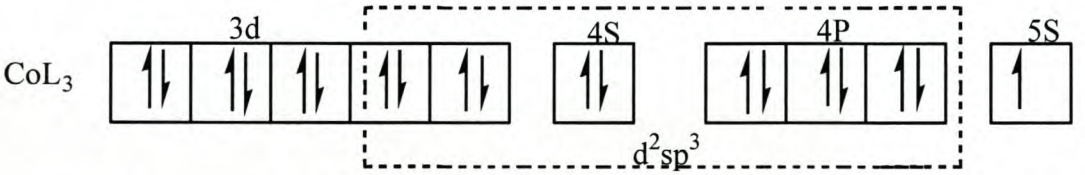

This electron is then easily lost from the higher energy level of the 5s orbital and oxidation to Co(III) can readily occur.[5]

The identity of the Co(III) complex was established not only by its diamagnetic nature, which was indirectly observed by the NMR spectra, but also by UV-Visible spectra of the Co^{II} complex of $H_3O^+\{fac\text{-}[Co(L^8\text{-}S,O)_3]^-\}$. The UV-Visible spectra that followed the oxidation of Co(II) to Co(III) in fresh $H_3O^+\{fac\text{-}[Co(L^8\text{-}S,O)_3]^-\}$ complex by atmospheric O_2 over time are shown in **Figure 4.22**. The test was started from freshly prepared $H_3O^+\{fac\text{-}[Co(L^8\text{-}S,O)_3]^-\}$ precipitate dissolved in dichloromethane. **Figure 4.22** shows the spectra that was collected every 24 hrs for a period of one week. The 1st spectrum indicated by **(a)** in the figure, was taken of freshly prepared $H_3O^+\{fac\text{-}[Co(L^8\text{-}S,O)_3]^-\}$ (unoxidized) and shows two transitions, which are labelled as C and D at λ_{max} = 225 nm and 280 nm respectively. After the first spectrum was taken the solid precipitate was left open to atmospheric O_2. Examination of the successive spectra that were run shows the disappearance of transitions C and D and the appearance of another new peak at λ_{max} = 265 nm with a shoulder at 315 nm. These are labelled as transitions B and A respectively in **Figure 4.22**.

According to previous studies on the electronic structure of Co^{II} complexes,[38] there is a quartet ground state and three spin-allowed electronic transitions in octahedral Co(II) complexes. The visible spectrum of such compounds is dominated by the highest transition of $^4T_{1g}(F) \longrightarrow {}^4T_{1g}(P)$, but the $^4A_{2g}$ level is usually close to the $^4T_{1g}(P)$ level and the transitions to these two levels are close together. The $^4T_{1g}(F) \longrightarrow {}^4A_{2g}$ transition is a two electron transition and is weaker by about a factor of 10^{-2} than the other, while the third allowed transition of $^4T_{1g}(F) \longrightarrow {}^4T_{2g}$ is weak and occurs in the near-infrared region.[38] From previous studies on the electronic structure of Co(III) complexes,[38] it is known that there are two absorption bands in the visible spectra of regular octahedral Co(III) complexes representing transitions to the upper states of $^1T_{1g}$ and $^1T_{2g}$ from the ground state of $^1A_{1g}$, because low spin d^6 complexes possess the orbital singlet ground state $^1A_{1g}$, arising from the strong field configuration $(t_{2g})^6$.

Therefore the two visible transitions, namely C and D of the Co(II) in the unoxidized $H_3O^+\{fac\text{-}[Co(L^8\text{-}S,O)_3]^-\}$ complex shown in **Figure 4.22** are:

$^4T_{1g}(F) \longrightarrow {}^4T_{1g}(P)$ at 280 nm (transition D)

$^4T_{1g}(F) \longrightarrow {}^4A_{2g}$ at 225 nm (transition C)

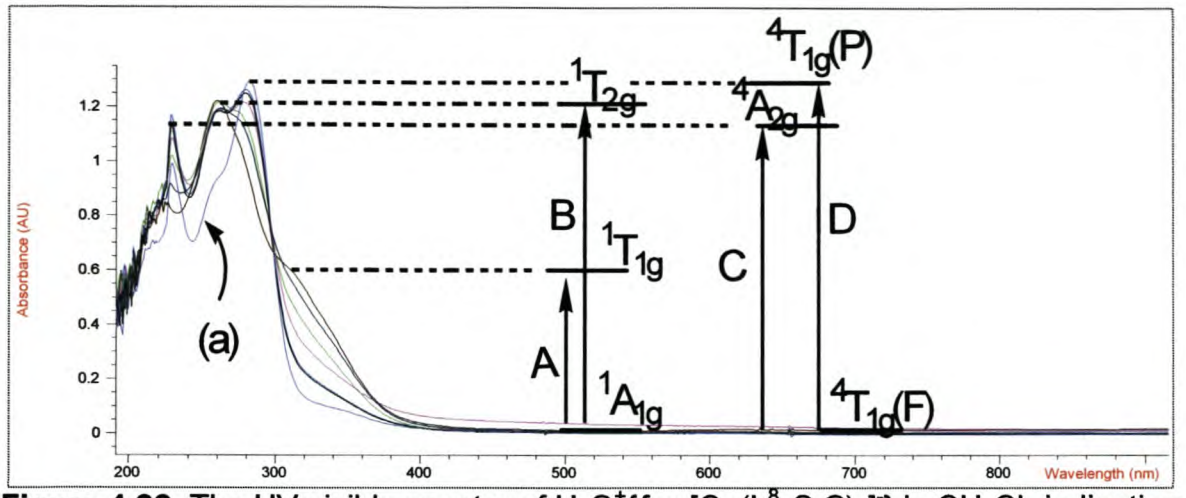

Figure 4.22. The UV-visible spectra of H_3O^+{*fac*-[Co(L^8-*S,O*)$_3$]$^-$} in CH_2Cl_2 indicating the oxidation of Co(II) to Co(III) over time by atmospheric O_2. The disappearance of transitions C and D and appearance of transitions A and B are observed over time.

The third and shortest transition, which is $^4T_{1g}(F) \longrightarrow {}^4T_{2g}$, of Co(II) is not visible and based on the literature[38] this is expected to be in the near-IR region. Similarly the two transitions (A and B) of the Co(III) in the oxidized *fac*-[Co(L^8-*S,O*)$_3$] complex are:

$^1A_{1g} \longrightarrow {}^1T_{2g}$ at 265 nm (transition B)

$^1A_{1g} \longrightarrow {}^1T_{1g}$ at 315 nm (transition A)

4.2.3. Characterisation of *cis*-[Ni(L^8-*S,O*)$_2$], *trans*-[Cu(L^8-*S,O*)$_2$], Ag_2[(HL^8-*S*)(L^8-μ-*S,O*)]$_2$ and H_3O^+{*fac*-[Co(L^8-*S,O*)$_3$]$^-$} by X-ray diffraction analysis

4.2.3.1. General overview of the X-ray diffraction results of the four complexes

As indicated in the spectroscopic results of the complexes in **section 4.2.2**, the HL^8 ligand forms *facial* distorted octahedral H_3O^+{*fac*-[Co(L^8-*S,O*)$_3$]$^-$}, square planar *cis*-[Ni(L^8-*S,O*)$_2$] and *trans*-[Cu(L^8-*S,O*)$_2$], as well as the binuclear Ag^I complex Ag_2[(HL-*S*)(L-μ-*S,O*)]$_2$. The ligand is bidentately coordinated to the Co^{II}, Ni^{II} and Cu^{II} atoms. However the Ag_2[(HL-*S*)(L-μ-*S,O*)]$_2$ complex has monodentate and bidentate modes of coordination of the ligands around each Ag^I metal. The coordination of the HL^8 ligand around the Co^{II}, Ni^{II}, Cu^{II} and Ag^I atoms in these complexes is discussed in detail in the following sections. The crystal data collection and structure refinement parameters for H_3O^+{*fac*-[Co(L^8-*S,O*)$_3$]$^-$}, *cis*-[Ni(L-*S,O*)$_2$], *trans*-[Cu(L-*S,O*)$_2$] and Ag_2[(HL-*S*)(L-μ-*S,O*)]$_2$ are summarised in **Table 4.8**.

Table 4.8. The crystal data collection and structure refinement parameters for $H_3O^+\{fac\text{-}[Co(L^8\text{-}S,O)_3]^-\}$, *cis*-$[Ni(L^8\text{-}S,O)_2]$, *trans*-$[Cu(L^8\text{-}S,O)_2]$ and $Ag_2[(HL^8\text{-}S)(L^8\text{-}\mu\text{-}S,O)]_2$.

	$H_3O^+\{fac\text{-}[(Co(L^8\text{-}S,O)_3)]^-\}$	*cis*-$[Ni(L^8\text{-}S,O)_2]$	*trans*-$[Cu(L^8\text{-}S,O)_2]$	$Ag_2[(HL^8\text{-}S)(L^8\text{-}\mu\text{-}S,O)]_2$
Crystal dimension (mm^3)	0.08 x 0.18 x 0.3	0.20 x 0.20 x 0.10	0.18 x 0.22 0.25	0.15 x 0.15 x 0.13
Empirical formula	$C_{45}H_{69}CoN_6O_9S_3$	$C_{30}H_{46}N_4NiO_6S_2$	$C_{30}H_{46}CuN_4O_6S_2$	$C_{60}H_{94}Ag_2N_8O_{12}S_4$
Measuring temprature (K)	173(2)	203(2)		203(2)
Crystal system	triclinic	monoclinic	Triclinic	Triclinic
Space group	P1	P2(1)	P1	P-1
No. of molecules per unit cell	2	2	2	2
Lattice dimension				
a (Å)	11.1363(2)	8.2528(17)	10.6275(2)	10.236(2)
b (Å)	13.4486(2)	8. 2665(17)	13.1457(2)	15.854(3)
c (Å)	17.8902(4)	24.8800(5)	13.2398(2)	21.359(4)
α (°)	97.14(10)	90	109.02240(10)	91.36(3)
β (°)	91.49(10)	93.50(3)	96.4230(10)	90.40(3)
γ (°)	105.5240(10)	90	105.9890(10)	102.23(3)
Volume of cell ($Å^3$)	2556.66(8)	1694.2(6)	1639.10(5)	3386.2(12)
Z	2	2	2	2
Dc (mg/m^3)	1.294	1.336	1.294	1.433
Radiation, λ (Å)	0.71073	0.71073	0.71073	0.71073
Absorption cooficient (mm^{-1})	0.515	0.741	0.841	0.764
F(000)	1062	724	726	1524
Theta range for data collection	2.28 to 28.32°	2.56 to 27.44°	2.64 to 27.86°	1.60 to 25.63°
Refinement method	Full-matrix least squares on F^2	Full-matrix least-squares on F^2	Full – matrix least-squares on F^2	Full-matrix least-squares on F^2
Limiting indices	-14<=h<=14, -17<=k<=17, -23<=l<=23	-10<=h<=10, -10<=k<=9, -32<=l<=32-	-13<=h<=13, -17<=K<=17, -17<=l<=16-	-12<=h<=12, -19<=k<=19, -25<=l<=25-
Reflections collected / unique	23383/ 23383 [R(int) = 0.0000]	7374 / 7374 [R(int) = 0.0000]	14835 / 14835[R (int) = 0.0000]	22072 / 12038 [R(int) = 0.0432]
Data / restraints / parameters	23383 /3/ 1154	7374 / 1 / 398	14835 / 3 / 771	12038 / 38 / 572
Goodness of fit on F^2	1.023	0.814	0.992	1.146
Final R1	0.0601	0.0370	0.0430	0.1624
wR2	0.1456	0.0885	0.0859	0.4090
Largest diff. peak and hole	1.486 and –0.425 e.$Å^{-3}$	0.349 and -0.277 e.$Å^{-3}$	0.465 and –0.395 e.$Å^{-3}$	2.908 and -1.797 e.$Å^{-3}$

The average bond lengths of C-O, C-S, M-O, M-S, C(2)-N(3), C(4)-N(3) and C(2)-N(6) of the four complexes are summarised in **Table 4.9**, (where M is the metal ion). Generally the C-O and C-S bond lengths of these complexes are longer than normal C=O and C=S double bonds. However the C(2)-N(3), C(4)-N(3) and C(2)-N(6) bond lengths are shorter than a normal C-N bond. This indicates the presence of partial double bonds in the chelate rings of the complexes. These results agree with the analogous bond lengths found in the Co^{III}, Ni^{II} and Cu^{II} complexes of *N,N*-diethyl-*N'*-benzoylthiourea.[23,26,27]

Table 4.9. The average bond lengths for C-O, C-S, M-O, M-S, C(2)-N(3), C(4)-N(3) and C(2)-N(6) bonds of H_3O^+\{*fac*-[Co(L^8-*S,O*)$_3$]$^-$\}, *cis*-[Ni(L-*S,O*)$_2$], *trans*-[Cu(L-*S,O*)$_2$] and Ag_2[(HL-*S*)(L-μ-*S,O*)]$_2$, where M is the metal ion.

Complex	Bond length (Å)						
	C-O	C-S	M-O	M-S	C(2)-N(3)	N(3)-C(4)	C(2)-N(6)
H_3O^+ {*fac*-[Co(L^8-*S,O*)$_3$]$^-$}	1.242	1.731	1.937	2.228	1.319	1.340	1.359
cis-[Ni(L-*S,O*)$_2$]*	1.264	1.717	1.868	2.142	1.355	1.312	1.333
trans-[Cu(L-*S,O*)$_2$]	1.258	1.726	1.913	2.260	1.363	1.304	1.346
Ag_2[(HL-*S*)(L-μ-*S,O*)]$_2$	1.270/ 1.210	1.712	2.57	2.453/ 2.865	1.365/ 1.386	1.280/ 1.380	1.345

*The bond lengths C(2)-N(3), N(3)-C(4) and C(2)-N(6) for the Ni^{II} complex in this table represent the bond lengths C(4)-N(3), N(3)-C(2) and C(4)-N(6) in the molecular structure of the complex respectively (see **Figure 4.23**).

The two C-O bond lengths of 1.270 and 1.210 Å in the silver complex represent the average bond lengths of C-O bonds with a coordinated *O* atom (ligands A and B) and uncoordinated *O* atom (ligands C and D) to the central Ag^I in the complex respectively. Similarly the shorter bond lengths of C(2)-N(3) and N(3)-C(4), which are 1.365 and 1.280 Å respectively, are the bond lengths of the bidentate ligands in the complex, whereas the longer bond lengths of C(2)-N(3) and N(3)-C(4) bonds, which are 1.386 and 1.380 Å respectively, are the bond lengths of the monodentate ligands. The average bond length of the Ag-S bonds in the silver complex is 2.453 Å, except the bond lengths of Ag(I)-S(1A) and Ag(2)-S(1B), which are averaged to 2.865 Å. A detailed explanation about the coordination chemistry of the *cis*-[Ni(L-*S,O*)$_2$], *trans*-

$[Cu(L\text{-}S,O)_2]$, $Ag_2[(HL\text{-}S)(L\text{-}\mu\text{-}S,O)]_2$ and $H_3O^+\{fac\text{-}[Co(L^8\text{-}S,O)_3]^-\}$, is given in **sections 4.2.3.2**, **4.2.3.3**, **4.2.3.4** and **4.2.3.5** respectively.

4.2.3.2. X-ray diffraction results of *cis*-[Ni(L^8-*S,O*)$_2$]

As deduced from the spectroscopic results, both of the ligands in the molecular structure of the *cis*-$[Ni(L\text{-}S,O)_2]$ complex determined by X-ray diffraction are coordinated to the central nickel atom in a bidentate manner with both *S* and *O* donor atoms. In this case the molecular structure of *cis-bis*(*N,N*-diethyl-*N´*-camphanoyl thioureato)Ni(II) shown in **Figure 4.23** is constructed from the discrete Ni(II) ion and two anionic ligands. The crystal packing of the complex is shown in **Figure 4.24**. The crystal data collection and structural refinement parameters of the complex are indicated in **Table 4.8**.

The coordination chemistry of this complex can be compared with the coordination chemistry of *cis-bis*(*N,N*-diethyl-*N´*-benzoylthioureato)nickel(II).[26] Unlike the ethyl groups of *cis-bis*(*N,N*-diethyl-*N´*-benzoylthioureato)Ni(II), the ethyl groups of the *cis*-[Ni(L^8-*S,O*)$_2$] complex are not disordered. The refinement of the crystals converged with a final R-factor of 0.0370, and the largest diffraction peak and hole were 0.349 and –0.277 electrons $Å^{-3}$. The goodness of the fit was 0.814 indicating agreement between the calculated and the observed structures.

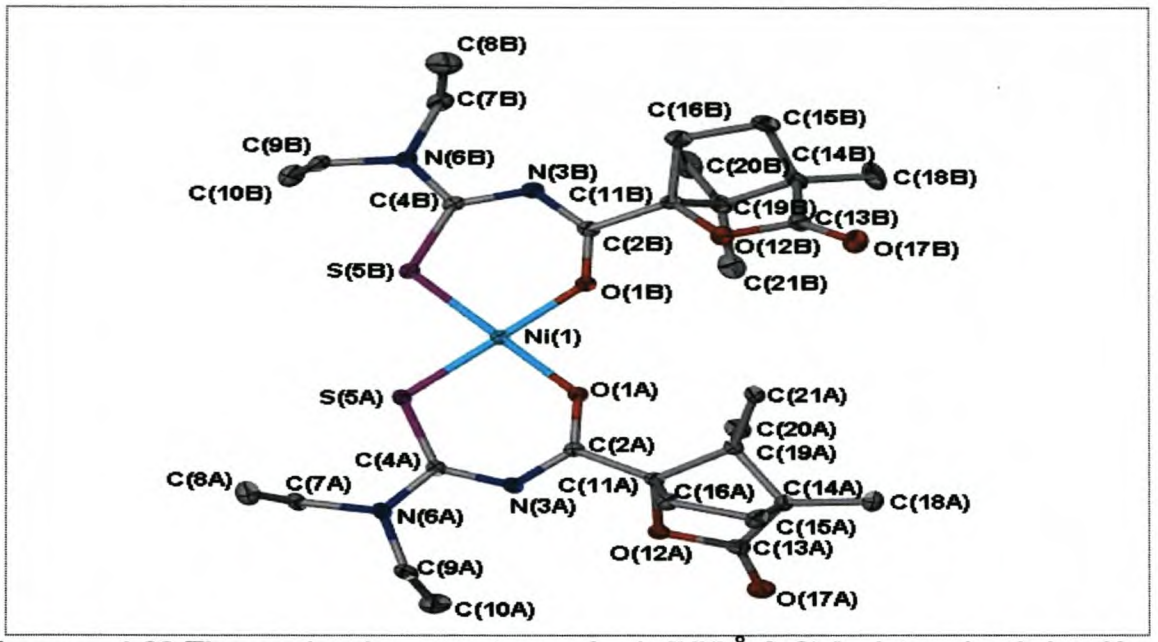

Figures 4.23.The molecular structure of *cis*-[Ni(L^8-*S,O*)$_2$] determined by X-ray diffraction analysis together with its atomic numbering scheme. The selected bond lengths (Å) and angles (°) in the complex are C(2)-N(3) 1.312(4), C(4)-N(6) 1.333(4), C(4)-N(3) 1.355(4), C(7)-N(6), 1.476(4), C-S 1.717(3), C-O 1.264(3), Ni-O 1.868(2), Ni-S 2.142(10), O(1A)-Ni-O(1B) 85.37(9), S(5A)-Ni-S(5B) 85.09(3), O(1B)-Ni-S(5A) 179.79(8), O(1A)-Ni-S(5B) 178.89(9), O(1A)-Ni-S(5A) 94.73(7) and O(1B)-Ni-S(5B) 94.82(6).

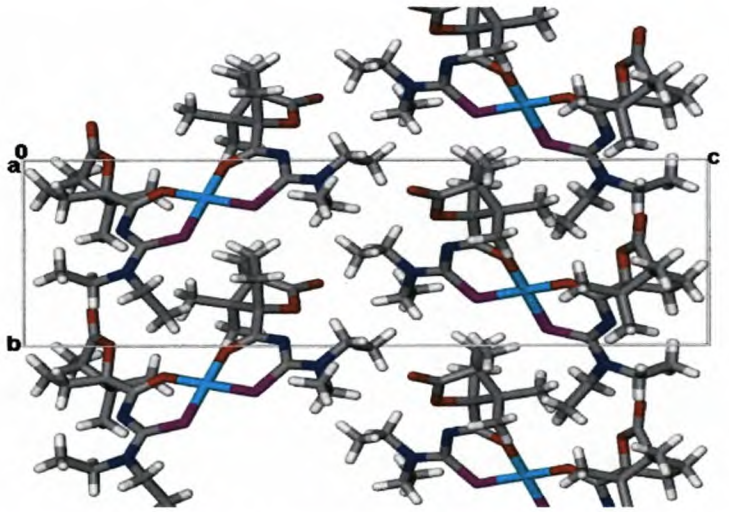

Figure 4.24.The crystal packing diagram for the *cis*-[Ni(L^8-*S'O*)$_2$] complex projected along the a-axis and showing two molecules per unit cell.

The orientation of the sulfur and oxygen atoms in the coordination plane of the complex is *cis,* forming *cis*-[Ni(L^8-*S,O*)]. The preference for this geometry is justified on the basis of greater Ni-*S* d-π bonding that can take place in the *cis* arrangement; each *S* atom can independently interact with a nickel d_{xz} or d_{yz} orbital.[26]

It is evident from the bond distances and angles that the environment about the nickel atom is slightly distorted from ideal square planar geometry. For instance the

bond angles of S(5B)-Ni-O(1B), S(5A)-Ni-O(1A), O(1A)-Ni(1)-O(1B) and S(5A)-Ni(1)-S(5B) are 94.82(6)°, 94.73(7)°, 85.37(9)° and 85.09(30)° respectively, which are slightly deviated from the 90° angle of an ideal square planar structure. The last two of these angles are slightly different from the analogous bond angles in the *cis-bis*(*N,N*-diethyl-*N'*-benzoyl- thioureato)Ni(II) complex,[26] which are averaged to 83° and 87.6° respectively. Whereas the average S-Ni-O bond angle (94.8°) of the *cis*-[Ni(L^8-*S,O*)$_2$] complex is similar to the analogous bond angle (94.7°) of the *cis-bis*(*N,N*-diethyl-*N'*-benzoylthioureato)Ni(II) complex. The angle between the planes of [Ni, S(5A), O(1A)] and [Ni, S(5B), O(1B)] is 179.01°. The average bond distances of Ni-S and Ni-O are 1.868 and 2.143 Å respectively and are similar to the analogous bond lengths found in the literature.[26] Generally the values of the corresponding bond lengths and angles in the complex are the same within error limits and allow averaging of the values for the similar bond lengths and angles. In this case the average bond lengths of C(2)-N(3), C(4)-N(3) and C(4)-N(6) are 1.312(4), 1.355(4) and 1.333(4) Å respectively and these are shorter than a normal C-N single bond, which indicates the presence of delocalised π-electrons in the chelate ring and C(4)-N(6) bond. The shortening of the above three C-N bond distances is in agreement with the corresponding bond distances found in the literature.[26] The C(4)-N(6) bond shortening determined by X-ray diffraction analysis agrees with the restricted rotation of the bond discussed earlier in the ^{1}H and ^{13}C NMR spectra of the ethyl groups of the complex. The average bond lengths of N(6)-C(7) and N(6)-C(9) are 1.476(4) and 1.470(4) Å respectively, which indicates single bond character.

The average Ni-Ni distance between the molecules is 4.10 Å. The Ni(1)-Ni(2) line forms an angle of 75.04° with the [Ni(1), O(1A), O(1B), S(5A) and S(5B)] coordination plane. This is quite similar to the values found in the *cis-bis*(*N,N*-diethyl-*N'*-benzoylthioureato)Ni(II) complex. This intermolecular distance is not short enough to indicate bonding interaction between the central metal atoms. Therefore as a result of the steric hindrance caused by the alkyl groups in the molecules of the complex, the central active part of the *cis*-[Ni(L^8-*S,O*)$_2$] molecule containing Ni, *S* and *O* atoms is shielded preventing the formation of strong intermolecular bonds and hence the forces acting between the different molecules in a unit cell are of a weak van der Waals type.

The atomic coordinates of non-hydrogen atoms, bond lengths, bond angles, torsion angles and final thermal parameters with their estimated standard deviation in parenthesis are listed in **Tables A-1.1, A-1.2**, **A-1.3, A-1.4,** and **A-1.5** respectively in appendix B.

4.2.3.3. X-ray diffraction results of *trans*-[Cu(L^8-*S,O*)$_2$]

The molecular structure of two molecules of the green *trans*-[Cu(L^8-*S,O*)$_2$] complex determined by X-ray diffraction analysis is shown in **Figure 4.25**. The four ligands in the two molecules are labelled as a, b, c and d. The molecular packing of the molecules is shown in **Figure 4.26**. The crystal data collection and structural refinement parameters of the complex are summarised in **Table 4.8**.

Similar to what was indicated by the spectroscopic results in **section 4.2.2.4**, the X-ray diffraction result indicates that two ligands are coordinated to the central copper ion in a bidentate manner with their *S* and *O* donor atoms. The two ethyl groups of the ligands in the complex showed some disorder. The crystal structure was refined to a final R-factor of 0.043 while the largest diffraction peak and hole were 0.465 and –395 electrons $Å^{-3}$. The goodness of fit was 0.992 indicating an excellent agreement between the calculated and the observed structures.

Interestingly the like donor atoms in the coordination plane of the complex are oriented *trans* to each other. Thus unlike the *cis*-[Ni(L^8-*S,O*)$_2$] complex discussed earlier, the treatment of the HL^8 ligand with Cu(II) gave exclusively *trans*-[Cu(L^8-*S,O*)$_2$]. This crystal structure thus reveals that the one isomer observed for this complex, which was identified from a single TLC spot of R_f value 0.54 in a $CHCl_3$ mobile phase, is solely the *trans*-[Cu(L^8-*S,O*)$_2$] isomer. This is in sharp contrast to the orientation of the donor atoms in the molecular structure of *cis*-[Cu(L-*S,O*)$_2$] complex.[27]

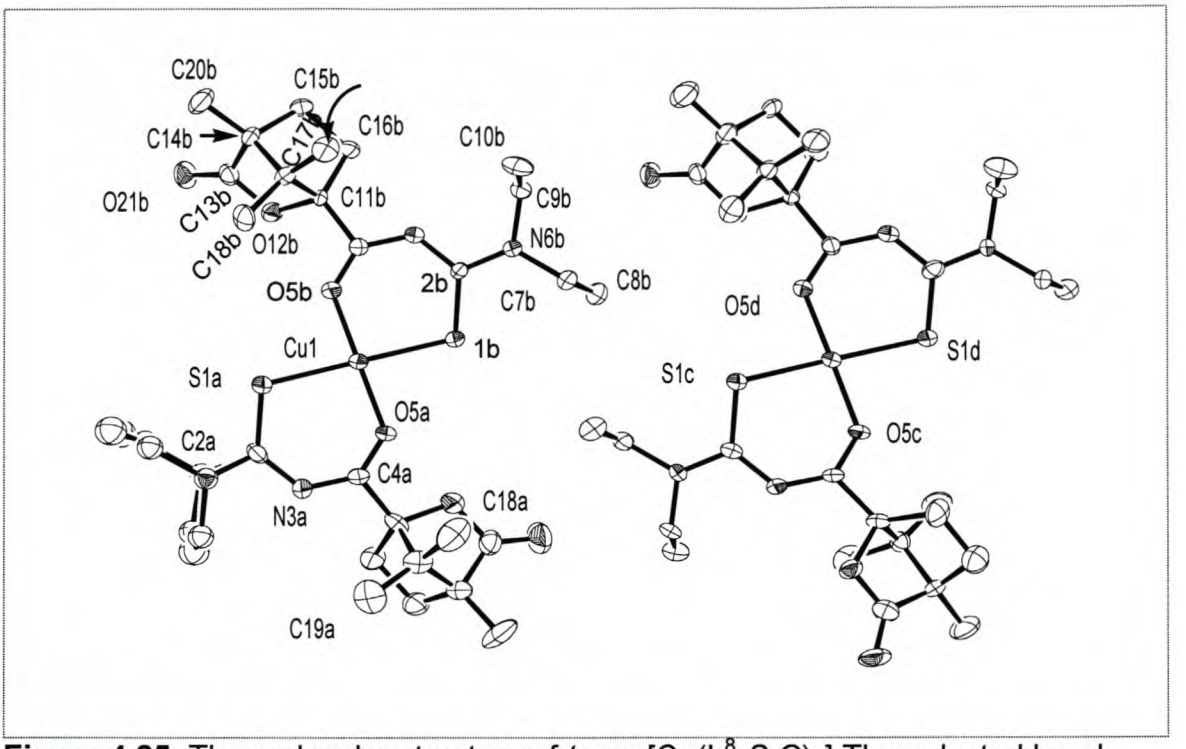

Figure 4.25. The molecular structure of *trans*-[Cu(L^8-*S,O*)$_2$].The selected bond lengths (Å) and angles (°) in the coordination complex are C(2)-N(3) 1.363(5), C(2)-N(6) 1.346(10), C(4)-N(3) 1.304(5), C(9)-N(6) 1.488(10), C-O 1.258(5), C-S 1.726(5), Cu-O 1.913(3), Cu-S 2.260(12), O(5A)-Cu-S(1B) 85.67(9), O(5B)-Cu-S(1A) 87.43(9), S(1B)-Cu-S(1A) 173.77(5), O(5B)-Cu-O(5A) 172.37(16), O(5A)-Cu-S(1A) 93.65(9) and O(5B)-Cu-S(1B) 94.06(9).

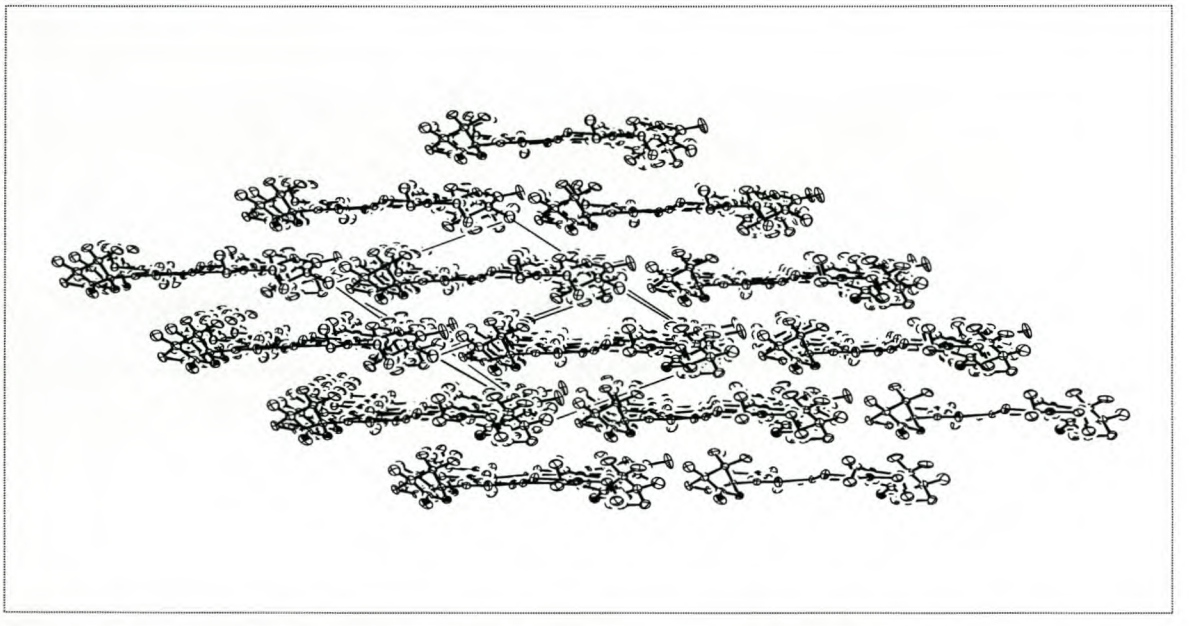

Figure 4.26. The molecular packing diagram of *trans*-[Cu(L^8-*S,O*)$_2$] projected along midway of the a, b and c-axis and showing two molecules per unit cell.

The exclusive formation of the *trans*-complex of this ligand with a transition metal ion is a new phenomenon in the history of the dialkyl substituted thiourea ligands. The largest amount of *trans* isomer that has been seen previously is a maximum of 15%

trans-[Pt(L-*S,O*)$_3$] isomer in combination with 85% *cis*-[Pt(L-*S,O*)$_3$] isomer.[29] As indicated in **section 4.2.2.4**, the preference for the *trans* arrangement of the donor atoms in the *trans*-[Cu(L^8-*S,O*)$_2$] complex is justified on the bases of the steric interaction that can take place between the substituents (camphanic and ethyl groups) of the ligands. This interaction is minimised when the donor atoms of the ligands are arranged in a *trans* manner compared to the *cis* arrangement of the donor atoms in the coordination sphere of the complex. In addition to this the weakening of the ν(C=O) vibration of the carbonyl group in the camphanic moiety from 1806 cm^{-1} for the free ligand to 1784 cm^{-1} in the complex might indicate the release of some electron density from the camphanic group toward the amidic oxygen donor atom. According to the speculation of Koch,[29] discussed in **section 2.3.2**, this phenomenon makes the amidic oxygen donor atom softer and stabilises the *trans* isomer, which might be the case in the *trans* isomer formation of this complex.

The geometry of the complex around the Cu atom is slightly distorted from square planar coordination. In this case the angle between the planes of [Cu(1), S(1A), O(5A] and [Cu, S(1B), O(5B)] is 173.07°, which is quite different from the analogous angle, 31.6°, for the *cis-bis*(*N,N*-diethyl-*N´*-benzoylthioureato)copper(II) complex.[27] The difference between the bond lengths of Cu-S(1A) and Cu-S(1B) is not significant and is averaged to 2.260(12) Å, which is comparable to the average Cu-S bond length found in *cis-bis*(*N,N*-diethyl-*N´*-benzoylthioureato)copper(II).[27] The bond lengths of Cu-O(5A) and Cu-O(5B) are more or less the same, within error limits, and average to 1.913(3) Å, which is similar to the average Cu-O bond length of the *cis-bis*(*N,N*-diethyl-*N´*-benzoylthioureato)copper(II) complex. Generally the values of the corresponding bond lengths and angles in the complex are the same within error limits and allow averaging of the values for the similar bond lengths and angles. The average bond lengths can be considered in good agreement with those reported for the *cis-bis*(*N,N*-diethyl-*N´*-benzoyl thioureato)copper(II).[27]

Similar to the C-N bonds of *cis*-[Ni(L^8-*S,O*)$_2$] complex discussed earlier, the C(2)-N(3), C(2)-N(6) and C(4)-N(3) bond lengths of the *trans*-[Cu(L^8-*S,O*)$_2$] are shorter than a normal C-N bond and this definitely indicates the presence of delocalised π-electrons in the chelate ring and C(2)-N(6) bond. These values agree with the analogous bond lengths reported for *cis-bis*(*N,N*-diethyl-*N´*-benzoylthioureato)

copper(II).[27] The average bond lengths of the C-S and C(4)-O(5) bonds of the *trans*-[Cu(L^8-*S,O*)$_2$] complex are 1.726(5) and 1.258(5) Å respectively and these are remarkably longer than the normal C=S and C=O bonds indicating the coordination of the sulfur and oxygen donor atoms to the copper ion.

The *trans*-[Cu(L^8-*S,O*)$_2$] molecules do not lie above each other in the unit cell of the complex and the Cu-Cu line, which is 4.22 Å long from Cu to Cu, forms an angle of 28° with the [Cu, O(5A), O(5B, S(1A), S(1B)] coordination plane. This intermolecular distance is not short enough to indicate bonding interaction between the central metal atoms. Therefore as a result of the steric hindrance caused by the camphanic and ethyl groups, which shield the central active part of the *trans*-[Cu(L^8-*S,O*)$_2$] molecule comprising of Cu, *S* and *O* atoms, the forces acting between the different molecules in a unit cell are of a weak van der Waals type.

The bond angles between unlike donor atoms of the same ligands, S(A)-Cu-O(A) and S(B)-Cu-O(B), which are 93.65° and 94.06° respectively, are significantly distorted from the ideal angle for a square planar structure. Similarly the bond angles between like donor atoms of different ligands, O(5A)-Cu-O(5B) and S(1A)-Cu-S(1B), are 172.37° and 173.77° respectively, which are remarkably distorted from 180° and hence the mode of coordination of the complex is notably deformed from the ideal square planar coordination toward tetrahedral coordination. Though the coordination plane of the *trans*-[Cu(L^8-*S,O*)$_2$] complex is distorted from ideal square planar coordination, it is more square planar than the wavy coordination plane of the *cis*-*bis*(*N,N*-diethyl-*N´*-benzoylthioureato) copper(II) complex.[27]

Unlike the *cis*-[Ni(L^8-*S,O*)$_2$] complex discussed in **section 4.2.3.2**, the ethyl groups of the *trans*-[Cu(L^8-*S,O*)$_2$] complex are disordered and after refinement a final R factor of 0.043 was obtained for the crystal structure. **Figure 4.27** shows the disordered ethyl groups in the unit cell of *trans*-[Cu(L^8-*S,O*)$_2$]. The atoms in the ethyl groups of the molecules in the unit cell including the adjacent N atom were observed in two positions each. In this case the pair of atoms leballed as C1a and C1b, C2a and C2b, N1a and N1b, C3a and C3b, as well as C4a and C4b in **Figure 4.27** represent one atom in each pair in the molecule of the complex and are shown in two different positions.

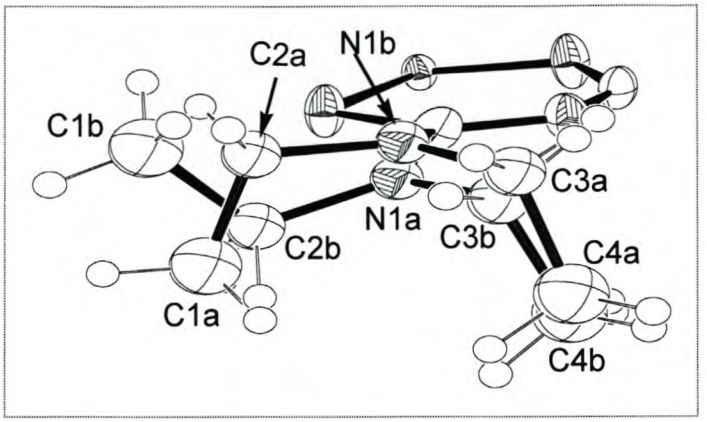

Figure 4.27. The disordered ethyl groups of the *trans*-[Cu(L^8-*S,O*)$_2$] complex showing C1, C2, C3, N and C4 in two different positions, namely C1a and C1b, C2a and C2b, C3a and C3b, N1a and N1b and C4a and C4b respectively.

The atomic coordinates of non-hydrogen atoms, the average bond lengths, angles, torsion angles and final thermal parameters with the estimated standard deviation (e.s.d) in parenthesis are indicated in **Tables A-2.1, A-2.2, A-2.3, A-2.4** and **A-2.5** respectively in appendix B. These crystallographic data are of one molecule of the complex with ligands A and B.

4.2.3.4. X-ray diffraction results of $Ag_2[(HL^8\text{-}S)(L^8\text{-}\mu\text{-}S,O)]_2$

The structure of the $Ag_2[(HL^8\text{-}S)(L^8\text{-}\mu\text{-}S,O)]_2$ complex has been analysed by X-ray crystallography. A view of the dimeric entity is given in **Figure 4.28** together with the atomic numbering scheme. The crystal packing of the complex is shown in **Figure 4.29**. The crystal data collection and structural refinement parameters of the complex are summarised in **Table 4.8**.

The coordination of the HL^8 ligand to silver(I) is different from the coordination of the same ligand to Co(II), Cu(II) and Ni(II). For these latter metal ions the ligand coordinates only in a bidentate manner to yield single mononuclear complexes of Co(II), Cu(II) and Ni(II). The reaction of HL^8 with silver(I) however affords the formation of a binuclear silver(I) complex showing both monodentate and bidentate modes of coordination within the same complex. What is observed in the crystal structure agrees with the observations made from the IR and ^{13}C NMR spectra of the complex discussed in **section 4.2.2.6**.

Each silver atom is bonded to three sulphur atoms (one from the terminal ligands of C or D and two from the bridging ligands of A and B), an oxygen atom and another silver atom (see **Figure 4.28**). In this case the two silver(I) atoms are doubly bridged by two sulfur atoms from the two bidentately coordinated ligands to form a four membered Ag_2S_2 ring. The two terminal ligands exhibit a neutral (HL) form in the coordination and are attached to the central metal silver ions by their sulfur donor atom only, whereas the two bridging ligands exhibit an ionic form (L-*S,O*)$^-$ and hence are bonded to the central silver ion in a bidentate coordination fashion. Each of the sulfur atoms in the two deprotonated ligands is bonded to both silver metal ions and hence act as bridging points for both the silver ions. The two silver(I) atoms and the two bridging sulfur atoms lie strictly in the same plane, forming the Ag_2S_2 core. This mode of coordination results in the S(1B)-Ag(1)-S(1A)-Ag(2) ring forming a parallelogram with opposite sides nearly equal and parallel. The opposite bond lengths in the Ag_2S_2 core are 2.820(4) and 2.907(5) Å for the Ag(1)-S(1A) and Ag(2)-S(1B) bonds respectively and 2.442(4) and 2.455(4) Å for the Ag(2)-S(1A) and Ag(1)-S(1B) bonds respectively. This plane is divided into two scalar triangles by the Ag(1)-Ag(2) bond with length 3.017(2) Å. The opposite obtuse bond angles of S(1B)-Ag(1)-S(1A) and S(1A)-Ag(2)-S(1B) are 112.49(14)° and 110.02(14)° respectively. The two opposite acute angles in the Ag_2S_2 coordination plane are 67.86(11)° and 69.52(11) Å for the Ag(1)-S(1B)-Ag(2) and Ag(2)-S(1A)-Ag(1) bond angles respectively. The S(1B)-Ag(2) and S(1A)-Ag(1) bond lengths are uniquely longer than the other Ag-S bonds present. The differences in the bond distances and angles in the coordination sphere of this complex are probably connected with the steric and electronic profile of the ligands.

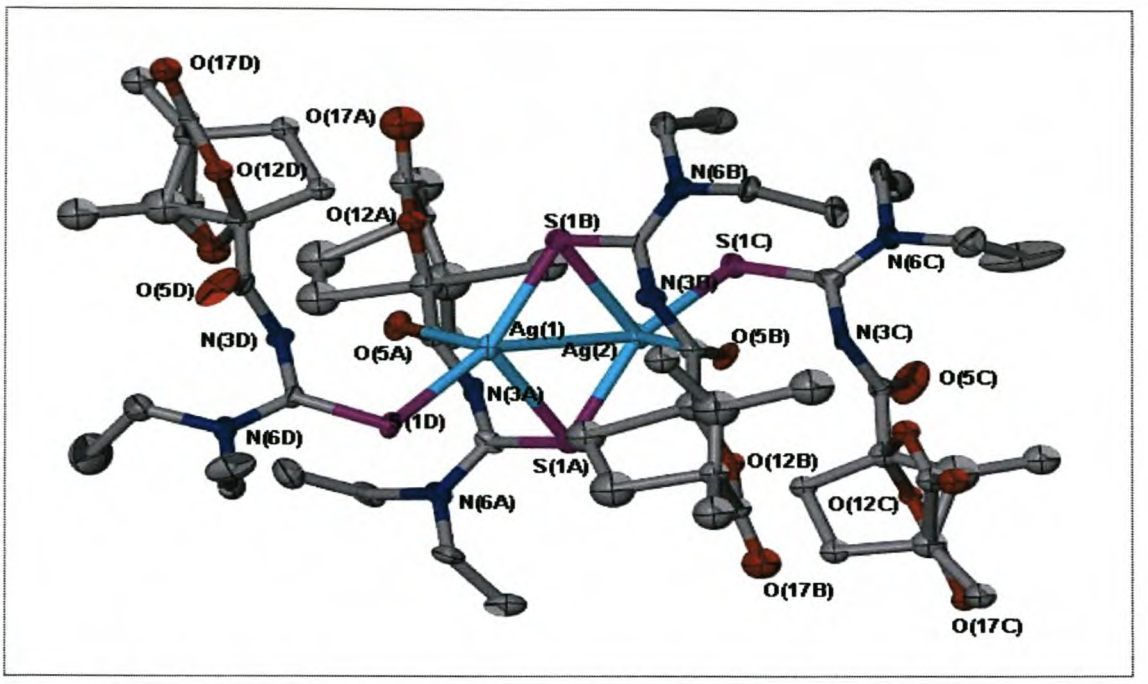

Figure 4.28. The molecular structure of $Ag_2[(HL^8\text{-}S)(L^8\text{-}\mu\text{-}S,O)]_2$ showing two unidentately coordinated (C and D) and two bidentately coordinated HL^8 ligands to two silver(I) atoms. The two Ag(1) atoms are doubly bridged by two sulfur atoms from the bidentate ligands (A and B) to form a four membered Ag_2S_2 ring, which is divided into two scalar triangles by the Ag(1)-Ag(2) bond.

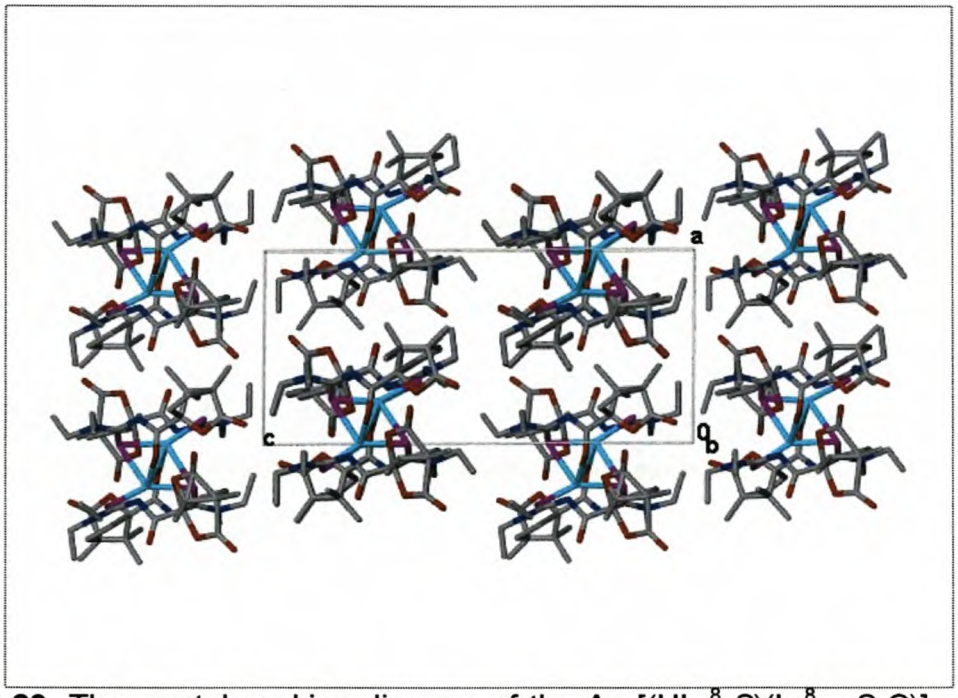

Figure 4.29. The crystal packing diagram of the $Ag_2[(HL_8^8\text{-}S)(L_8^8\text{-}\mu\text{-}S,O)]_2$ projected along the b-axis and showing the presence of two molecules per unit cell.

Since the bond angles around both the silver atoms are completely different from one another, the coordination around each silver(I) atom results in highly deformed square pyramidal environments. The bond lengths of Ag(1)-O(4A) and Ag(2)-O(5B) are more or less equal and averaged to 2.572 Å. The bond lengths of C(4)-N(3),

N(3)-C(2) and C(2)-N(6) in both the unidentate and bidentate ligands in the complex show no appreciable difference and in both ligands (see **Table 4.9**) show the presence of partial double bond character.

The camphanic group of the terminal ligands, which are labelled as C and D in the molecular structure of the complex, suffer from disorder. **Figure 4.30** shows the disordered champhanic group of ligand C in the complex. Such disorder is not observed in the bidentately coordinated ligands, which are labelled as A and B in the molecular structure of the complex. For instance the pairs of O(17C) and O(24C); O(22C) and O(12C) represent one O atom each in the molecule of the complex but they are shown in two different positions.

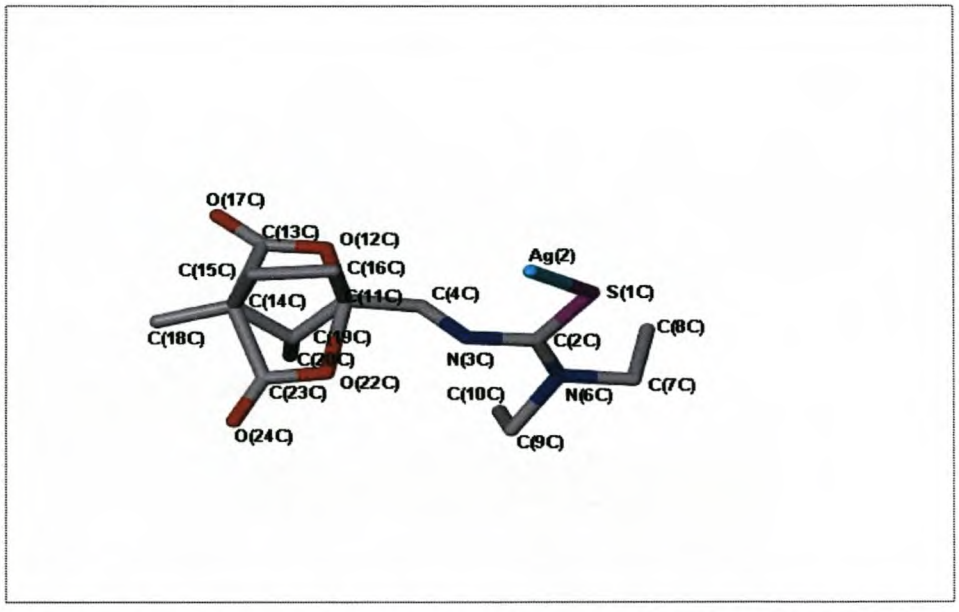

Figure 4.30. The disordered champhanic moiety of the unidentately bonded ligand C in the $Ag_2[(HL_8{}^8\text{-}S)(L_8{}^8\text{-}\mu\text{-}S,O)]_2$ complex showing some atoms in two positions. [O(17C) and O(24C) are of one O atom and similarly O(12C) and O(22C) are of one another O atom shown in two different positions]

The atomic coordinates of non-hydrogen atoms, the average bond lengths, angles, torsion angles and anisotropic displacement parameters with the estimated standard deviation (e.s.d) in parenthesis are indicated in **Tables A-3.1, A-3.2, A-3.3, A-3.4** and **A-3.5** respectively in appendix B.

4.2.3.5. X-ray diffraction results of $H_3O^+\{fac\text{-}[Co(L^8\text{-}S,O)_3]^-\}$

The molecular structure of the $H_3O^+\{fac\text{-}[Co(L^8\text{-}S,O)_3]^-\}$ complex has been determined by heavy atom techniques and all the hydrogen atoms were placed in calculated positions and included in the model during the late stages of the refinement. **Figure 4.31** shows the X-ray diffraction structure of one $H_3O^+\{fac\text{-}[Co(L^8\text{-}S,O)_3]^-\}$ molecule. The hydronium ion is represented by one ellipsoid beside each *fac*-$[Co(L^8\text{-}S,O)_3]^-$ molecule of the complex. The crystal packing of the complex is shown in **Figure 4.32**. The crystal data collection and structural refinement parameters of the complex are summarised in **Table 4.8**.

Similar to the structure of *fac-tris*(*N,N*-diethyl-*N'*-benzoylthioureato)Co(III) determined by X-ray diffraction analysis,[23] the ethyl groups of the *fac-tris*(*N,N*-diethyl-*N'*-camphanoylthiou reato)cobalt(II) complex are highly disordered and the refinement converged with a final R-factor of 0.0601, which is comparable with the R-factor (0.065) of the *fac-tris*(*N,N*-diethyl-*N'*-benzoylthioureato)Co(III) complex.[23] The largest diffraction peak and hole for $H_3O^+\{fac\text{-}[Co(L^8\text{-}S,O)_3]^-\}$ are 1.486 and –0.425 electrons $Å^{-3}$ respectively. The goodness of fit was 1.023 indicating good agreement between the calculated and observed structures.

As predicted from the spectroscopic results, the X-ray diffraction result confirmed that the three HL^8 ligands are coordinated to the Co(II) in a bidentate fashion, in which the Co(II) is bonded to the *S* and *O* donor atoms of each ligand. The geometry about the cobalt atom is distorted octahedral with the O-Co-O and S-Co-S average bond angles being 85.66 and 88.30° respectively. The mode of octahedral coordination of the three ligands around the Co(II) atom results in a facial isomer. This mode of coordination is very similar to that seen in the molecular structure of *fac-tris*(*N,N*-diethyl-*N'*-benzoylthioureato)Co(III) complex determined by X-ray diffraction analysis.[23]

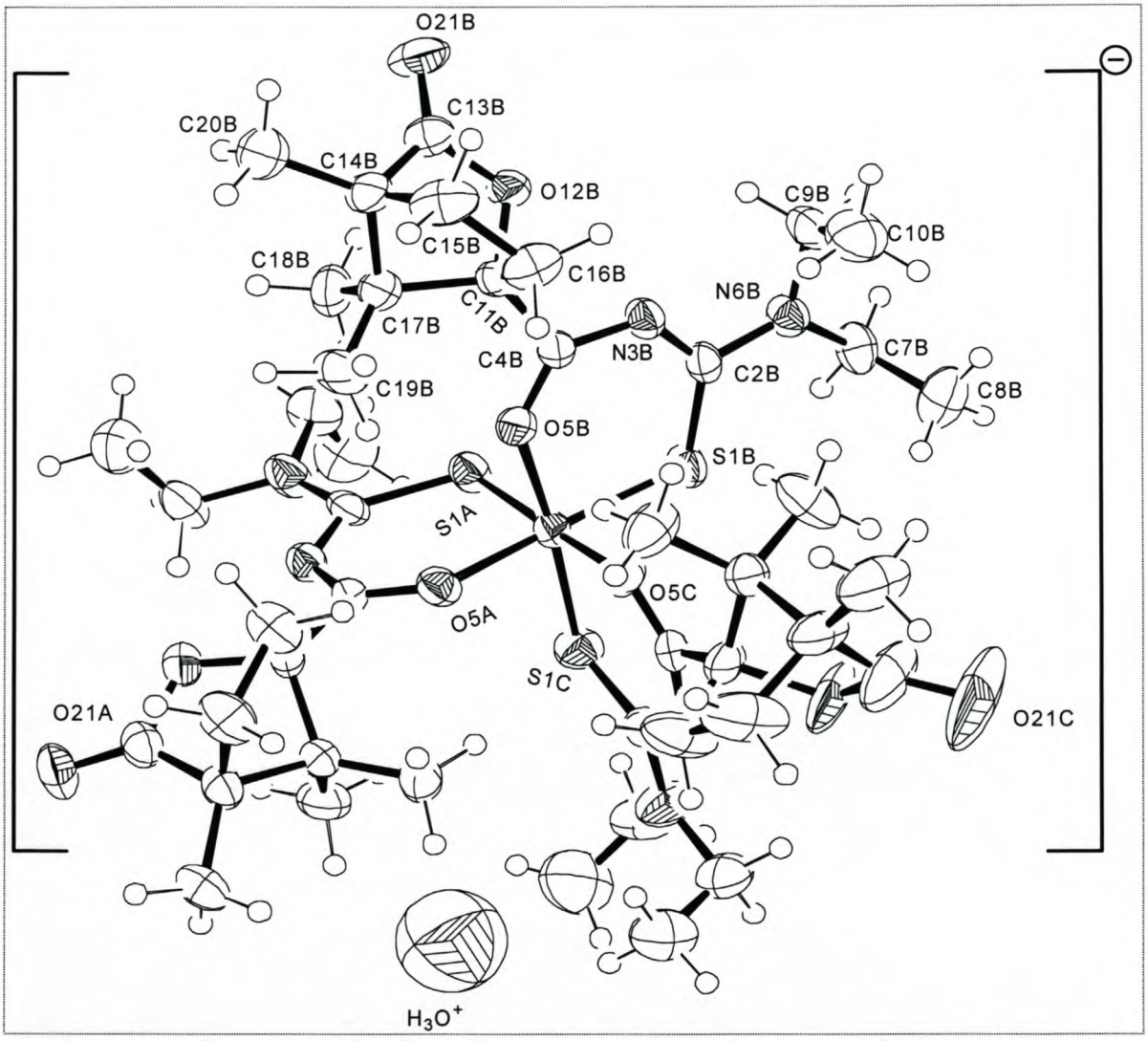

Figure 4.31. Molecular structure of H_3O^+{*fac*-[(Co(L^8-*S,O*)$_3$)]$^-$} together with the atomic numbering scheme showing a hydronium ion next to each molecule of the complex. The selected bond lengths (Å) and angles (°) of the complex are C(2)-N(3) 1.319(6), C(2)-N(6) 1.359(6), C(4)-N(3) 1.340(6), C(9)-N(6) 1.478(7), C(2)-S(1) 1.731(5), C(4)-O(5) 1.242(6), Co(1)-O(5) 1.937(3), Co(1)-S(1) 2.228(3); S(1B)-Co-S(1A) 89.44, S(1C)-Co(1)-S(1A) 87.97, S(1B)-Co(1)-S(1C) 87.48, O(5B)-Co-O(5A) 86.92, O(5C)-Co-O(5A) 85.41 and O(5C)-Co-O(5B) 84.64.

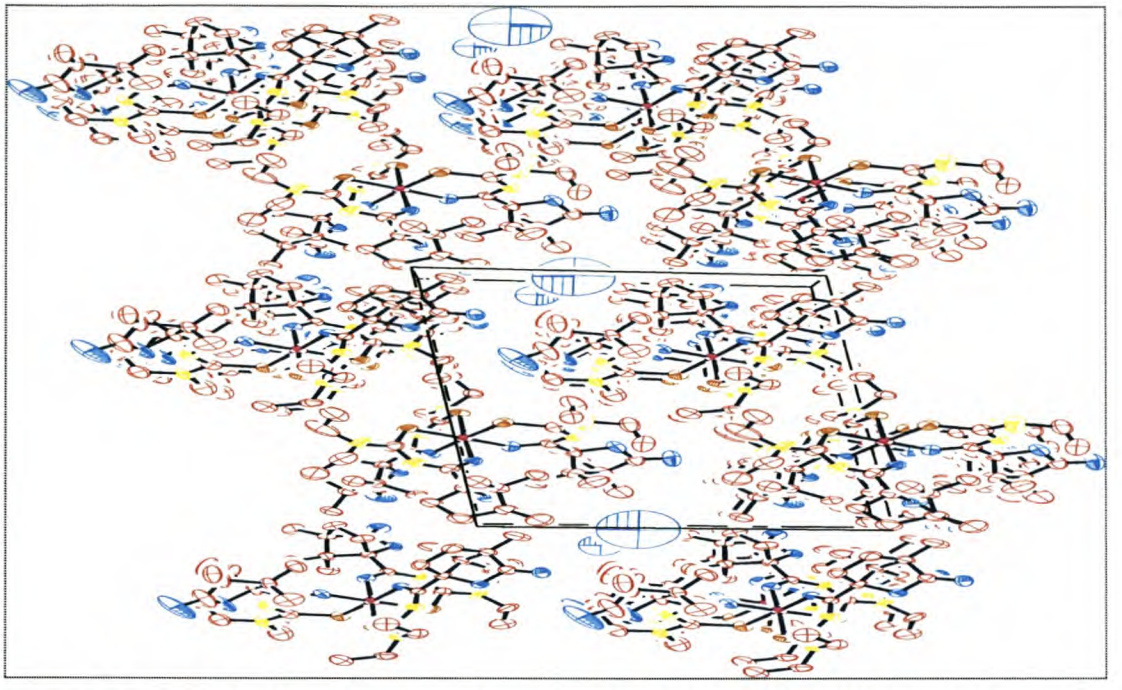

Figure 4.32.The crystal packing diagram of H_3O^+{*fac*-[(Co(L^8-*S,O*)$_3$)]$^-$} projected along the c-axis and showing the presence of two molecules per unit cell.

The average C-O bond distance of the H_3O^+{*fac*-[(Co(L^8-*S,O*)$_3$)]$^-$} complex, which is 1.242(6) Å, is equivalent to the C-O bond length of *fac-tris*(*N,N*-diethyl-*N´*-benzoylthioureato)Co(III). The average C-S bond length, 1.731(5) Å, of the H_3O^+{*fac*-[Co(L^8-*S,O*)$_3$)$^-$] complex is slightly shorter than the average C-S bond length, 1.937(3) Å, of *fac-tris*(*N,N*-diethyl-*N´*-benzoylthioureato)Co(III) and still shows the presence of partial double bond character. However these bonds are significantly longer than normal C=O and C=S bonds indicating weakening of the bonds towards becoming single bonds in the complex. This result agrees with the absorption band shift of these bonds seen in the IR spectrum of the complex when compared to the absorption bands of the corresponding bonds in the free ligand. The average bond lengths of N(3)-C(4), N(3)-C(2) and N(6)-C(2), which are 1.340(6), 1.319(6) and 1.359(6) Å, respectively, show partial double bond character and are similar to the values for the C-N bonds of a related complex.[23] The partial double bond character of these bonds decreases in order of N(3)-C(2) > N(3)-C(4) > N(6)-C(2). The bond lengths of the N(6)-C(7) and N(6)-C(9) bonds, which are 1.452(6) Å and 1.478(7) Å respectively, reflect single bond character. The bond angles between the like donor atoms of different ligands [S(1B)-Co-S(1A), S(1C)-Co-S(1A) and S(1B)-Co-S(1C)] are not significantly different from one another and the average value of these bond angles is 88.30 Å, which varies slightly from the corresponding average S-Co-S bond angle of 86.7(1)° in *fac-tris*(*N,N*-diethyl-*N'*-benzoylthioureato)Co(III). Similarly the

average bond angle of O(5B)-Co(1)-O(5A), O(5C)-Co-O(5A) and O(5C)-Co-O(5B) is 85.66°, which is more or less the same as the average O-Co-O bond angle of 85.40° for *fac-tris*(*N,N*-diethyl-*N´*-benzoylthioureato)Co(III).

The selected bond lengths, bond angles, atomic coordinates of the non-hydrogen atoms and anisotropic displacement parameters with their standard deviation in parenthesis are listed in **Tables A-4.1, A-4.2, A-4.3,** and **A-4.4** respectively in appendix B.

4.3. TRANSITION METAL (M = Ni^{II} and Cu^{II}) COMPLEXES OF LIGAND HL^{11}

The *cis/trans-bis*(*N,N*-diethyl-*N´*-adamantylcarbonylthioureato) Ni(II), *cis/trans*-[Ni(L^{11}-*S,- O*)$_2$], and *trans/cis-bis*(*N,N*-diethyl-*N´*-adamantylcarbonylthioureato)Cu(II), *trans/cis*-[Cu(L^{11}-*S,O*)$_2$], complexes were prepared in high yields of 88 % and 84 % respectively. This was carried out according to the procedures employed to prepare the *cis*-[Ni(L^8-*S,O*)$_2$] and *trans*-[Cu(L^8-*S,O*)$_2$] complexes as discussed in **sections 3.3.1.2** and **3.3.1.3** respectively, from *N,N*-diethyl-*N´*-adamantylcarbonylthiourea and $Ni(CH_3CO_2)_2{\cdot}4H_2O$ and $Cu(NO_3)_2{\cdot}3H_2O$ metal salts. The identity and purity of these complexes are characterised by means of MS, IR spectroscopy, NMR spectroscopy and elemental (C, H, N and S) analysis as indicated in the following section.

4.3.1. Spectroscopic characterisation of *cis/trans*-[Ni(L^{11}-*S,O*)$_2$] and *trans/cis*-[Cu(L^{11}-*S,O*)$_2$]

The parental ion (M^+) region of the MS spectra of the two complexes showed intense peaks at *m/z* 646 and 651, which are the expected molecular masses of *cis/trans*-[Ni(L^{11}-*S,O*)$_2$] and *trans/cis*-[Cu(L^{11}-*S,O*)$_2$] respectively. The C, H, N and S analysis results are within 0.5 % of the calculated values for the expected empirical formulae of the two complexes. The IR spectra of both complexes show deprotonation of the N-H, which is also indicated in the ^{1}H NMR spectrum of the *cis/trans*-[Ni(L^{11}-*S,O*)$_2$] complex (see **Figure 4.33**). Moreover the IR spectra of both complexes showed absorption band shifts for the ν(C=O) and ν(C=S) vibrations from 1644 and 1235 cm^{-1} respectively in the free ligand to lower absorption frequencies in the complexes (see **Table 4.10**). These spectroscopic results indicate that the two HL^{11} ligands are

bidentately coordinated to the central metal ions of Ni^{II} and Cu^{II} with their *O* and *S* donor atoms.

Table 4.10. The amidic O=C and C=S stretching frequencies of *cis/trans*-[Ni(L^{11}-*S,O*)$_2$], *trans/cis*-[Cu(L^{11}-*S,O*)$_2$] and the free HL^{11} ligand.

Compound	absorption frequency (cm^{-1})	
	O=CN	NC=S
HL^{11}	1644	1235
cis/trans-[Ni(L^{11}-*S,O*)$_2$]	1422	804
trans/cis-[Cu(L^{11}-*S,O*)$_2$]	1419	795

NMR spectroscopic results: As for the NMR results for *trans*-[Cu(L^{8}-*S,O*)$_2$] discussed in **section 4.2.2.4**, the characterisation of this complex by means of NMR spectroscopy was prevented by the paramagnetic nature of the Cu(II) (d^9) ion, which would have given the *cis* and *trans* isomer distribution of the complex. However the TLC of the complex gave an R_f value of 0.36 in a $CHCl_3$ mobile phase and indicated the presence of only one component in the complex. The stereochemistry of this component will have to be identified by X-ray diffraction analysis in the future.

The *cis/trans*-[Ni(L^{11}-*S,O*)$_2$] complex was characterised by means of NMR spectroscopy and the ^{1}H NMR spectrum of *cis/trans*-[Ni(L^{11}-*S,O*)$_2$] together with the ^{1}H NMR spectrum of the free ligand is shown in **Figure 4.33**. The atomic numbering schemes of both the free ligand and complex are included in **Figure 4.33**. The peaks of H(7) and H(9) as well as the peaks of the methyl groups in the complex are expanded for clarity. In this case the ^{1}H NMR spectrum of the complex shows two overlapping quartets (q) peaks at 3.62 and 3.62 ppm and these are assigned to the H(9) and H(7) protons. This assignment is based on the reasonable assumption that the H(7) protons are closer to the coordination sphere compared to the H(9) protons and are thus more shielded than the H9 protons by the secondary magnetic field of the coordination sphere. For similar reasons the two triplets at 1.16 and 1.09 ppm are assigned to the protons H(10) and H(8) respectively.

As a result of the free rotation about the C(4)-C(11) bond and the complete symmetry of the adamantyl group, the chemical shifts of the H(12), H(13) and H(14) protons are the same and appear in the ^{1}H NMR spectrum at 1.92 ppm. Similarly H(16), H(18)

and H(20) appear at 1.63 ppm and the chemical shifts of H(15), H(17) and H(19) are coincident at 1.79 ppm.

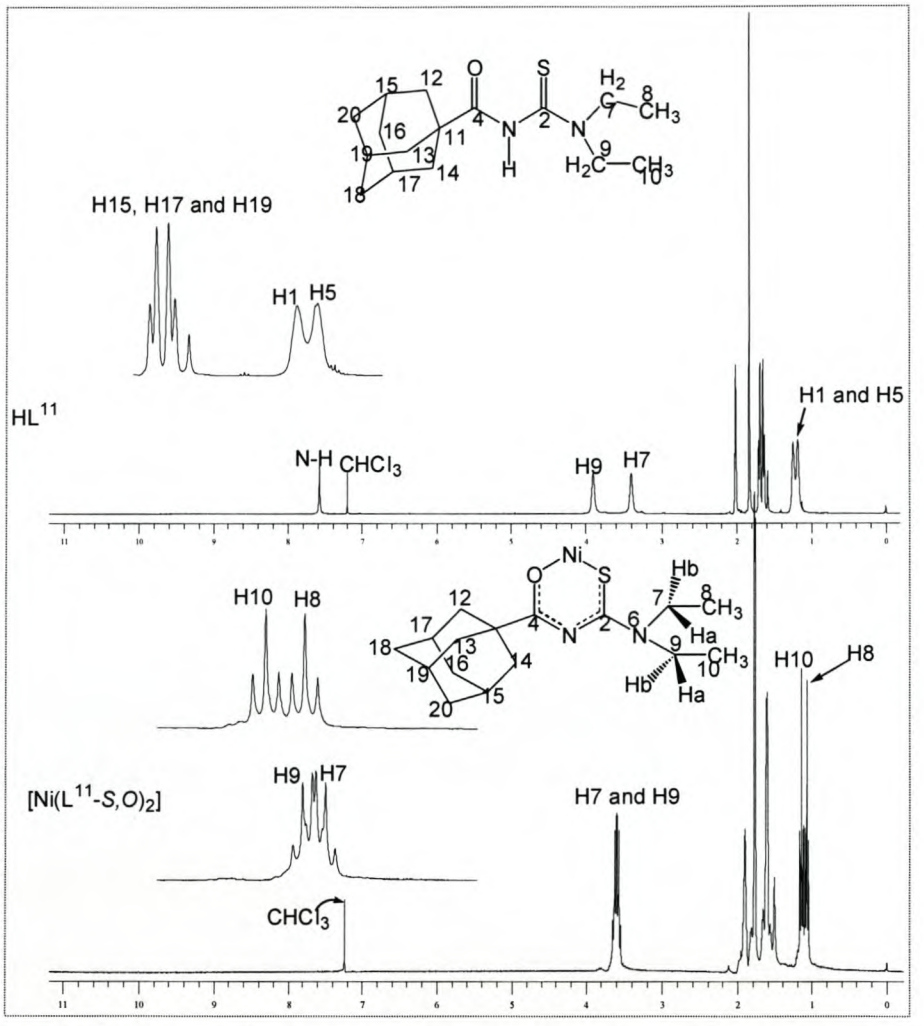

Figure 4.33. The 600 MHz ^{1}H NMR spectra in $CDCl_3$ showing the difference between the free ligand (HL^{11}) and *cis/trans*-[Ni(L^{11}-*S,O*)$_2$] complex.

The ^{13}C NMR spectrum of the complex shows two peaks quite far downfield at 186.5 and 172.6 ppm. These are assigned to the C(4) and C(2) carbons respectively based on the evidence presented by Miller (see **section 2.2.6**).[28] The rest of the ^{13}C NMR data of the complex are listed in **section 3.3.2.7**.

The ^{13}C NMR spectrum of *cis/trans*-[Ni(L^{11}-*S,O*)$_2$] closely resembles the ^{13}C NMR spectrum of the free HL^{11} ligand (see **Figure 4.34**) indicating the presence of one isomer for the complex. It is reported that the d^8 transition metals need greater M-*S* d-π bonding. This can be obtained *via* a *cis* arrangement of the donor atoms of the ligands, so each *S* atom can independently interact with the metal d_{xz} or d_{yz} orbital.[26]

Thus the geometry of this complex is expected to be *cis* as for the *cis*-[Ni(L^8-*S,O*)$_2$] complex discussed in **section 4.2.3.1**.

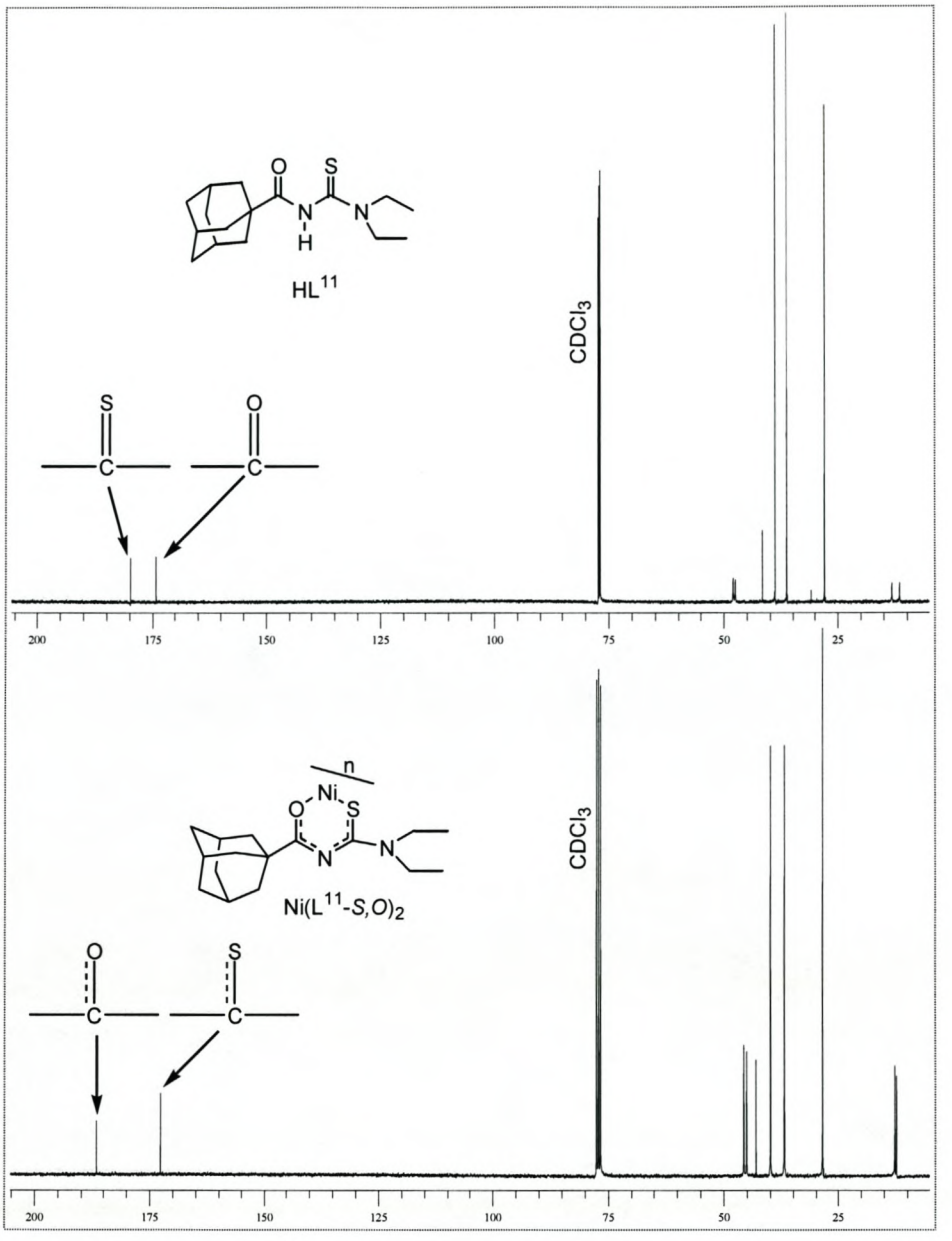

Figure 4.34. The 150 MHz ^{13}C NMR spectra in $CDCl_3$ showing the characteristic difference between the free ligand (HL^{11}) and Ni(L^{11}-*S,O*)$_2$ complex.

CHAPTER FIVE

CONCLUDING REMARKS

5.1.CONCLUSION

N,N-diethyl-*N´*-camphanoylthiourea (HL^8), *N*-piperidyl-*N´*-camphanoylthiourea (HL^9), *N*-pyrrolidyl-*N´*-camphanoylthiourea (HL^{10}) and *N,N*-diethyl-*N´*-adamantylcarbonylthiourea (HL^{11}) have been synthesised and characterised for the first time. The structures of these ligands have a significant effect on their coordination chemistry with transition metal ions.

The HL^8 ligand forms H_3O^+{*fac*-[Co(L^8-*S,O*)$_3$]$^-$}, *cis*-[Ni(L^8-*S,O*)$_2$], *trans*-[Cu(L^8-*S,O*)$_2$] and Ag_2[(HL^8-*S*)(L^8-μ-*S,O*)]$_2$ complexes and the X-ray diffraction results of these complexes indicate that the ligand binds in a bidentate coordination fashion to the Co(II), Ni(II) and Cu(II) metal ions. The mode of coordination of this ligand to Co^{II} results in a distorted facial octahedral coordination sphere whereas the mode of coordination of this ligand to both Ni^{II} and Cu^{II} results in a square planar structure. The *S* and *O* donor atoms of the ligand are arranged *cis* and *trans* to each other in the Ni^{II} and Cu^{II} complexes respectively. The reaction of HL^8 with silver(I) however results in the formation of a binuclear silver(I) complex showing both monodentate and bidentate coordination modes within the same molecule of the complex. In this case the two silver(I) atoms are doubly bridged by two sulfur atoms from two bidentately coordinated ligands to form a four membered Ag_2S_2 ring, which is bisected into two scalar triangles by the Ag(1)-Ag(2) bond. The coordination of the ligand around each Ag^I forms a distorted square pyramidal coordination sphere and indicates the presence of two unidentate and two bidentate ligands coordinated to two Ag^I atoms in one molecule of the complex.

The formation of exclusively *trans*-[Cu(L^8-*S,O*)$_2$] with HL^8 ligand is a new phenomenon in the history of these types of thiourea ligands. Previously, the highest amount of *trans* isomer (*i.e. trans*-[Pt(L^7-*S,O*)$_2$] observed was 15% in a *cis-trans* mixture prepared with *N,N*-dibutyl-*N´*-naphthoylthiourea (HL^7).[29]

Interestingly, the deep green H_3O^+{*fac*-[Co(L-*S,O*)$_3$]$^-$} complex is air sensitive. The Co^{II} H_3O^+{*fac*-[Co(L-*S,O*)$_3$]$^-$} complex readily oxidizes to Co^{III} in the complex. The oxidation of Co^{II} to Co^{III} in the complex by atmospheric O_2 is confirmed by NMR and UV-Vis spectroscopy.

As indicated earlier the structure of the HL^8 ligand showed a significant effect on its coordination chemistry as well as the percentage yield of its transition metal ion complexes. The percentage yields for the metal-complexes $H_3O^+\{fac\text{-}[Co(L^8\text{-}S,O)_3]^-\}$, *cis*-$[Ni(L^8\text{-}S,O)_2]$, *trans*-$[Cu(L^8\text{-}S,O)_2]$ and *trans/cis*-$[Zn(L^8\text{-}S,O)_2]$ complexes, which are 91%, 92%, 84% and 62% respectively, decrease from left to right in the periodic table for these metals ions. Similarly their melting points, which are 228 °C, 222 °C, 175 °C , and 125 °C for the Co(II), Ni(II), Cu(II) and Zn(II) complexes of this ligand respectively, decrease from left to right in the periodic table for these metal ions. These clearly indicate that the stability of the complexes decreases in order of *fac*-$[Co(L^8\text{-}S,O)_3]$ > *cis*-$[Ni(L^8\text{-}S,O)_2]$ > *trans*-$[Cu(L^8\text{-}S,O)_2]$ > *trans/cis*-$[Zn(L^8\text{-}S,O)_2]$. The bulky camphanic group plus the two-ethyl groups of the ligand are expected to affect these properties predominantly. It is well known from previous studies[5,40] that the radii of metal ions of the same charge decrease from left to right along the period in the periodic table due to the increase in their nuclear charge. Thus the steric interaction that can be offered by the camphanic and ethyl groups of the complexes and bite angle strain are expected to increase in order of *fac*-$[Co(L^8\text{-}S,O)_3]$ < *cis*-$[Ni(L^8\text{-}S,O)_2]$ < *trans*-$[Cu(L^8\text{-}S,O)_2]$ < *trans/cis*-$Zn(L^8\text{-}S,O)_2$. As a result the Zn(II) ion complex, which has the smallest radius metal ion in the series, is expected to be the least stable and therefore the percentage yield of the *trans/cis*-$[Zn(L^8\text{-}S,O)_2]$ complex was the lowest obtained in this project.

The bidentate mode of coordination of the HL^8 and HL^{11} ligands to the metal ions discussed earlier can be recognised from their spectroscopic studies. The deprotonation of the N-H proton, which is indicated by the absence of the charactestic signal in both the IR and ^1H NMR spectra of the complex, and the absorption band shifts of the amidic ν(C=O) and ν(C=S) vibrations toward lower frequencies in the complexes with respect to the analogous bond vibrations of the free ligand are good indications of the bidentate mode of coordination of the ligands (with both *S* and *O* atoms) to the central metal ions. This agrees with the X-ray diffraction results, which show the elongation of the C=S and amidic C=O bonds in the chelate ring of the complexes compared to their corresponding normal double bonds. The shift of the amidic C=O and C=S stretching frequencies from higher absorption bands in the free ligand to lower absorption bands in the complexes (see **Table 5.1**) is in agreement with the analogous results in the literature.[41]

Table 5.1. The shift of the amidic C=O and C=S stretching frequencies from higher frequencies in the free ligand to lower frequencies in the complex forms.

Compound	Absorption frequency (cm^{-1})	
	O=CN	NC=S
HL^8	1707	1228
$H_3O^+\{fac\text{-}[Co(L^8\text{-}S,O)_3]^-\}$	1427	817
cis-$[Ni(L^8\text{-}S,O)_2]$	1428	822
trans-$[Cu(L^8\text{-}S,O)_2]$	1429	816
trans/cis-$[Zn(L^8\text{-}S,O)_2]$	1443	813
cis-$[Pt(L^8\text{-}S,O)_2]$	1430	818
$Ag_2[(HL^8\text{-}S)(L^8\text{-}\mu\text{-}S,O)]_2$	1701/1435	797
HL^{11}	1644	1235
cis/trans-$[Ni(L^{11}\text{-}S,O)_2]$	1422	804
trans/cis-$[Cu(L^{11}\text{-}S,O)_2]$	1419	795

The absorption bands of the ν(C=O) vibrations of the carbonyl group in the camphanic moieties of all the metal complexes made with the HL^8 ligand are reduced by an average of 24.83 cm^{-1} from the absorption band for the same bond vibration of the free ligand (1806 cm^{-1}) and this is an indication of the release of some π-electron density toward the atoms in the chelating rings.

Normally when the *S* and *O* donor atoms of HL^8 and HL^{11} ligands are coordinated to metal ions the electron density of the donor atoms decreases, as a consequence the ^{13}C NMR chemical shifts of the amidic O=C and S=C groups of the ligand are expected to be shifted downfield compared to their corresponding peaks in the free ligand. The amount of downfield shift is expected to be related to the degree of the electron donation by the donor atoms towards the central metal ion. **Table 5.2** shows a comparison of the ^{13}C chemical shifts of the thiocarbonyl (C=S) and amidic carbonyl groups in the free HL^8 and HL^{11} ligands and in their complexes. The ^{13}C chemical shifts of the amidic carbonyl group [C(O)N] are shifted downfield in the complexes relative to the chemical shifts of the same carbons in the free ligands. This is because of the release of some electron density from the amidic C=O bond toward the metal ion, which makes the carbons of these bonds less shielded than they were in their free ligand. Whereas the ^{13}C chemical shifts of the thiocarbonyl

(C=S) group are shifted upfield in the complexes compared to the chemical shifts of the corresponding carbon in the ligands. This may be related to the back electron donation by the central metal towards the π-orbitals of the sulfur donor atoms and hence the carbons in the thiocarbonyl group become more shielded than they were in the free ligand. The unambiguous assignment of these ^{13}C NMR peaks of the amidic carbonyl and thiocarbonyl groups in the complexes are made based on Miller's study, which is discussed in **section 2.2.6**.[28]

Table 5.2. The ^{13}C NMR chemical shifts of the thiocarbonyl and amidic carbonyl groups of the free HL^8 and HL^{11} ligands and their transition metal complexes.

Compound	^{13}C NMR chemical shift (ppm)	
	NC=S group	C(O)N group
HL^8	177.5	164.3
H_3O^+\{*fac*-[Co(L^8-*S,O*)$_3$]$^-$\}	176.0	177.7
cis-[Ni(L^8-*S,O*)$_2$]	171.9	173.5
trans/cis-[Zn(L^8-*S,O*)$_2$]	166.4	172.6
cis-[Pt(L^8-*S,O*)$_2$]	166.4	169.6
Ag_2[(HL^8-*S*)(L^8-μ-*S,O*)]$_2$	176.0	176.7/167.4
HL^{11}	179.7	174.1
cis/trans-[Ni(L^{11}-*S,O*)$_2$]	172.6	186.5

The ^1H and ^{13}C NMR spectra of all the complexes discussed in chapter three, except those of the platinum complex before recrystallisation from $CH_3CN/CHCl_3$ solution mixture and those complexes with paramagnetic central metal ions, consist of a single set of ligand resonance peaks closely resembling those of the uncoordinated ligand. This clearly indicates the presence of a single isomer for each complex. The platinum complex however showed small peaks next to each intense peak of the *cis*-isomer to indicate the presence of minor *trans*-isomer in combination with the dominant *cis*-isomer. Interestingly, after the *cis/trans*-[Pt(L^8-*S,O*)$_2$] was recrystallised from an 80:20 (v/v) CH_3CN to $CHCl_3$ solution, which is a predominantly polar solvent, the ^{195}Pt NMR spectrum showed the presence of only the *cis*-isomer, which is more polar than the *trans*-isomer. This clearly indicates that the solvent of crystallisation affects the mode of coordination of the ligands to transition metal ions. From this it can be concluded that the polarity of the solvent of crystallisation is directly related to

the polarity of the transition metal complex that can be crystallised from that specific solvent.

The treatment of Ni(II) with the HL^8 ligand formed only one isomer {*cis*-[Ni(L^8-*S,O*)]}, which was identified from its ^1H and ^{13}C NMR spectra. However the treatment of Pt(II) with the same ligand using the same solvents and reaction conditions gave a mixture of 97 % *cis* and 3 % *trans*-[Pt(L^8-*S,O*)$_2$]. These results indicate that the effect of steric interaction between ligands in the d^8 group metal complexes is immaterial. The preference for *cis*-isomer formation in this group of metals is probably related to the greater M-*S* d-π bonding that can be obtained in the *cis* arrangement of the donor atoms of the ligands in which each *S* atom can independently interact with the metal (M) d_{xz} or d_{yz} orbital.[26]

5.2. REMARKS

►From the experimental results of the *cis*-[Ni(L^8-*S,O*)$_2$] and *cis*-[Pt(L^8-*S,O*)$_2$] complexes, it is concluded that steric hindrance by the camphanic and ethyl groups has little or no effect on the formation of the *trans*-isomer of the d^8 metal complexes with the HL type ligands. However the preference for this geometry is justified on the basis of greater M-*S* d-π bonding that can be obtained in the *cis* arrangement of the donor atoms of the ligands, so each *S* atom can independently interact with the metal d_{xz} or d_{yz} orbital.[26] This argument is interesting and convincing, but to provide an even more concrete and convincing basis for this reasoning the subject still needs to be investigated further.

►As seen in the *cis*-[Pt(L^8-*S,O*)$_2$] complex, the $CHCl_3/CH_3CN$ 20:80 (V/V) solvent influenced the coordination chemistry of the recrystallised *cis*-[Pt(L^8-*S,O*)$_2$] complex. The polarity of the complex that formed was directly related to the polarity of the recrystallisation solvent. To complete this study on recrystallisation, more solvents need to be investigated.

►Though the colour change during and after the oxidation was not visible, it is known from the UV-Vis study that the oxidation of Co(II) to Co(III) in the H_3O^+{*fac*-[Co(L^8-*S,O*)$_3$]$^-$} complex by the atmospheric O_2 is fast. This phenomenon should be fully studied and explored to the extent of creating a free O_2 sensor device using this complex.

►The modification of chitosan with camphanoylisothiocyanate is left incomplete in this research simply because of solvent problems. Therefore future work is required to design an appropriate solvent for the chitosan study to be successful.

REFERENCES

1. G. Skjak-BRÆK, T. Anthonsen and P. Sandford, Chitin and Chitosan, 1988, Elsevier science publishers Ltd, NEW YORK, p. 3-79.
2. K. C. Sole, P. M. Cole, J. S. Preston and D. J. Robinson, Proceedings of the international solvent extraction conference, 2002, Vol 2, Chris Van Rensburg publishers (pty) Ltd, South Africa, p. 453-457.
3. H. Sashiwa, Y. Shigemasa, *Carbohydrate polymer*, 2002, **47**, 191.
4. S. Nishimura, O. Kohge, K. Kurita, C. Vittavatvong and H. Kuzuhara, *Chem. Lett.*, 1990, 243.
5. J. E. Huheey, Inorganic chemistry, principles of structure and reactivity, 1983, 3rd ed, Harper and Row publishers, New York, p. 312-315, 387-428.
6. J. E. Huheey, E. A. Keiter and R. L. Keiter, Inorganic chemistry, principles of structure and reactivity, 1993, 4th edi, Harper Collins college publisher, New York, p. 344-355.
7. K. R. Koch, *Coordination chemistry reviews*, 2001, **216-217**, 473.
8. K. R. Koch, C. Sacht, S. Bourne, *Inorg. Chem. Acta.*, 1995, **232**, 109.
9. M. Schuster, *Fresenius. Z. Anal. Chem.*, 1992, **342**, 791.
10. P. Vest, M. Schuster, K. -H. König, *Fresenius Z. Anal. Chem.*, 1991, **341**, 566.
11. P. Vests, M. Schuster, K. -H. König, *Fresenius Z. Ana. Chem.*, 1991, **339**, 142.
12. K. R. Koch, C. Sacht, T. Grimmbacher, S. Bourne, *S. Afr. J. Chem.*, 1995, **48**, 71.
13. S. Bourne and K. R. Koch, *J. Chem. Soc., Dalton Trans.*, 1993, 2071.
14. E. Neucki, *Ber.*, 1873, **6**, 598.
15. I. B. Douglas, F. B. Dains, *J. Am. Chem. Soc.,* 1934, **56**, 719.
16. T. Tokii, S, Nakahara, N. Hashimoto, M. Koikawa, M. Nakashima, H. Matsushima, *Bull. Chem. Soc. Jpn.*, 1995, **68**, 2533.
17. Schuster M, Kugler B., Köning K-H, *Fresenius J. Anal. Chem.*, 1990, **338**, 717.
18. K. R. Koch, Tarron Grimmbacher and Cheryl Sacht, *Polyhedr*, 1998, **17**, 267.

19. J. March, advanced organic chemistry, 1992, 4th edi, John Wiley and Sons, United States and Canada, p. 429.

20. J. Sieler, R. Richter, E. Hoyer, *Z. Anorg. Chem.*, 1990, **580,** 167.

21. K. R. Koch, A. Coetzee, Y. Wang, *J. Chem. Soc., Dalton Trans.*, 1999, 1013.

22. R. Flores-Centurion, R. Richter, J. Angulo-Comejo, L. Beyer, *Bot. Soc. Quin. Peru.*, 1999, **65**, 211.

23. W. Bensch, M. Schuster, *Z. Kristallogr.*, 1995, **210**, 68.

24. W. Bensch, M. Schuster, *Z. Anorg. Allg. Chem.*, 1992, **615**, 93.

25. K. R. Koch, S. A. Bourne, A. Coetzee, J. Miller, *J. Chem. Soc., Dalton Trans.*, 1999, 3157.

26. P. Knuuttila, H. knuuttila, H. Hennig and L. Beyer, *Acta. Chem. Scand.*, 1982, **36**, 541.

27. R. Richter, L. Beyer, J. Kaiser, *Z. Anorg. Allg. Chem.*, 1980, **461**, 67.

28. J. Miller, PhD thesis, 2000, University of Cape Town.

29. K. R Koch, J. du Toit, M. R. Caira and C. Sacht, *J. Chem. Soc., Dalton Trans.*, 1994, 785.

30. A. Irving, K. R. Koch and M. Matoetoe, *Inorg. Chem. Act.,* 1993, **206**, 193.

31. M. Schuster, M. Sador, *Fresenius Z. Anal. Chem.*, 1996, **356**, 326.

32. J. R. Dilworth, J. S. Lewis, J. R. Miller, Yifan Zheng, *Polyhedron*, 1993, **12**, 221.

33. Z. Otwinowski and W. Minor, *Methods Enzymol.*, 1996, **276**, 307

34. G. M. Sheldrick, SHELX-97, University of Göttingen.

35. J. Barbour, X-SEED (http://www.lbarbour.com/xseed/) University of Missouri-Columbia, 1999.

36. M. M. Habtu, M.Sc thesis, 2003, University of Stellenbosch.

37. D. L. Pavia, G. M. Lampmaan and G.. Kriz, 1997, Introduction to Spectroscopy, Sauders college publishing, p. 76,52-53, 188, 420-429,.

38. F. A. Cotton and G. Wilkinson, Advanced Inorganic Chemistry, 1988, 5th edi, John Wiley and Son, New York, p. 729-740.

39. R. Hesse and L. Nilson, *Acta. Chem. Scand.*, 1969, **23**, 825.

40. I. S. Butler and J. F. Harrod, Inorganic chemistry: Principle and applications, 1989, Benjamin/cummings publishing company, USA, p. 45.

41. R. A. Bailey, K. L. Rothaupt and R. K. Kullnig, *Inorg. Chem. Acta.*, 1988, **147**, 233.

42. A. R. Oki, P. R. Bommarreddy, H. Zhang and N. Hosmane, *Inorg. Chem. Acta.,* 1995, **231**, 103-107.

43. C. Sacht, M. S. Datt, S. Otto and A. Roodt, *J. Chem. Soc., Dalton Trans.*, 2000, 727.

44. D. A. Redfield and J. H. Nelson, *Inorg. Chem.*, 1973, **12**, 15.

45. De-Jiche, Gang Li, Xiao-Lan yao, Yu-Zhu, Da-Peng Zhou, *J. Chem. Soc., Dalton Trans.,* 1999, 1683.

46. Engh and Huber, *Acta. cryst.,* 1999, **A47**, 392.

47. F. Dietze, S. Schmidt, E. Hoyer and L. Beyer, *Z. Anorg. Allg.Chem.*, 1991, **595**, 35.

48. F. Scandola, O. Traverso, V. Balzani, G. L. Zucchini and V. Carassiti, *Inorg. Chem. Acta.*, 1967, **1**, 76.

49. G. Fitzt, L. Beyer, J. Sieler, R. Richter, J. kaiser, E. Hoyer, *Z. Anorg. Allg. Chem.*, 1997, **433**, 237.

50. G. Kemp, A. Roodt, W. Purcell, K. R Koch, *J. Chem. Soc. Dalton trans*, 1997, 4481.

51. G. Kemp, W. Purcell, K. R. Koch, *Rhedium express*, 1996, 17.

52. J. Hartung und L. Beyer, *Z. Anorg. Chem.*, 1993, **619**: 1295.

53. J. Sieler, R. Richter, E. Hoyer, L. Beyer, O. Lindqvist, L. Andersen, Z. *Anorg. Allg. Chem.*, 1990, **580**, 167.

54. J. Vicente, J. A. Abad, M. Chicote, M. Abrisqueta, J. Lorca, and M. Carmen Ramirez de Arellano, *Organometallics*, 1998, **17**, 1564.

APPENDIX A: SELECTED SPECTRA

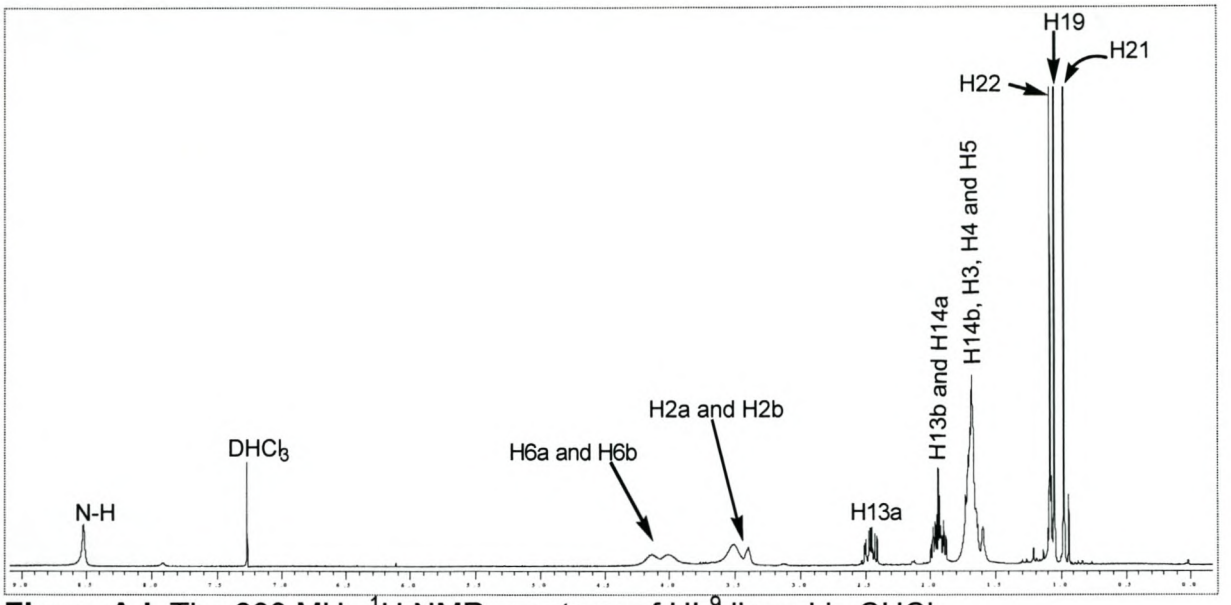

Figure A-I. The 600 MHz ^{1}H NMR spectrum of HL^{9} ligand in $CHCl_3$.

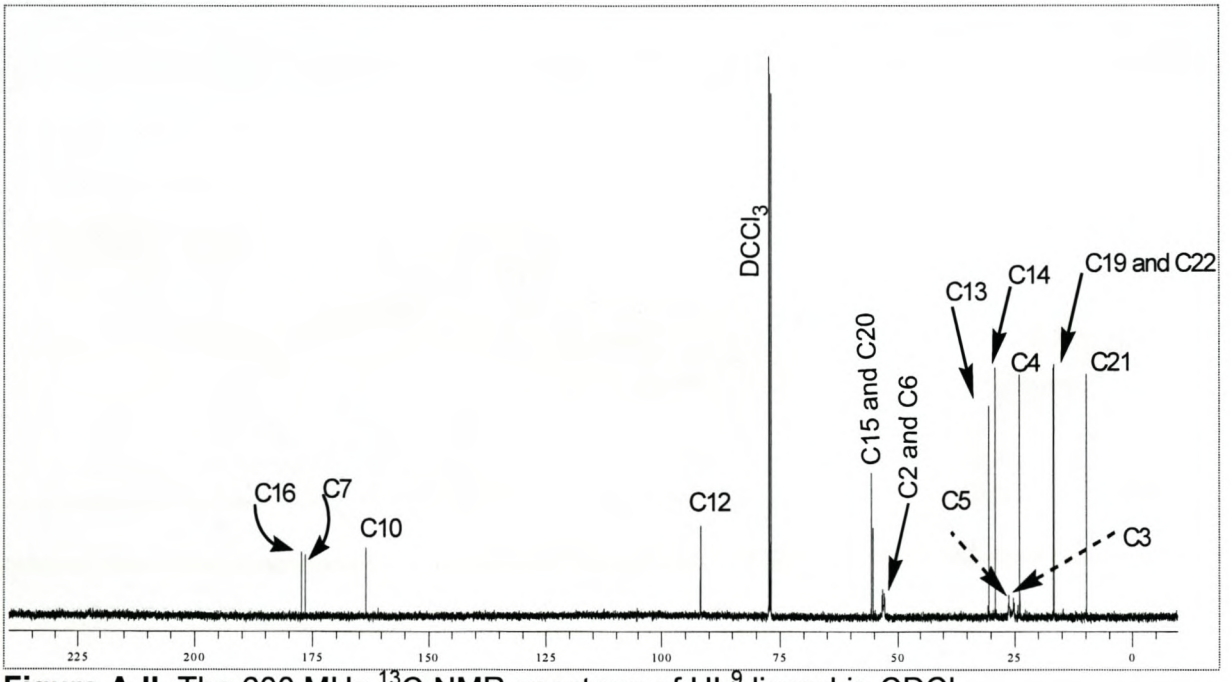

Figure A-II. The 600 MHz ^{13}C NMR spectrum of HL^{9} ligand in $CDCl_3$.

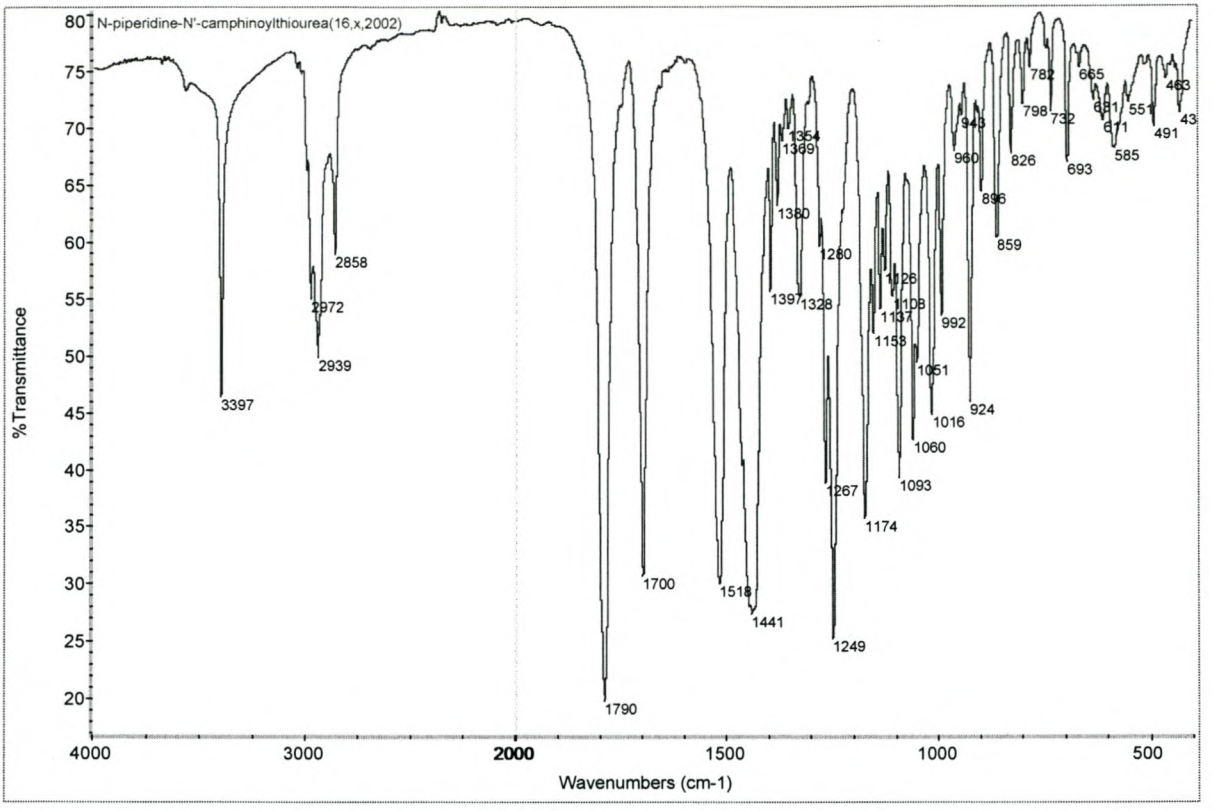

Figure A-III. The IR spectrum of HL^9 ligand recorded as KBr.

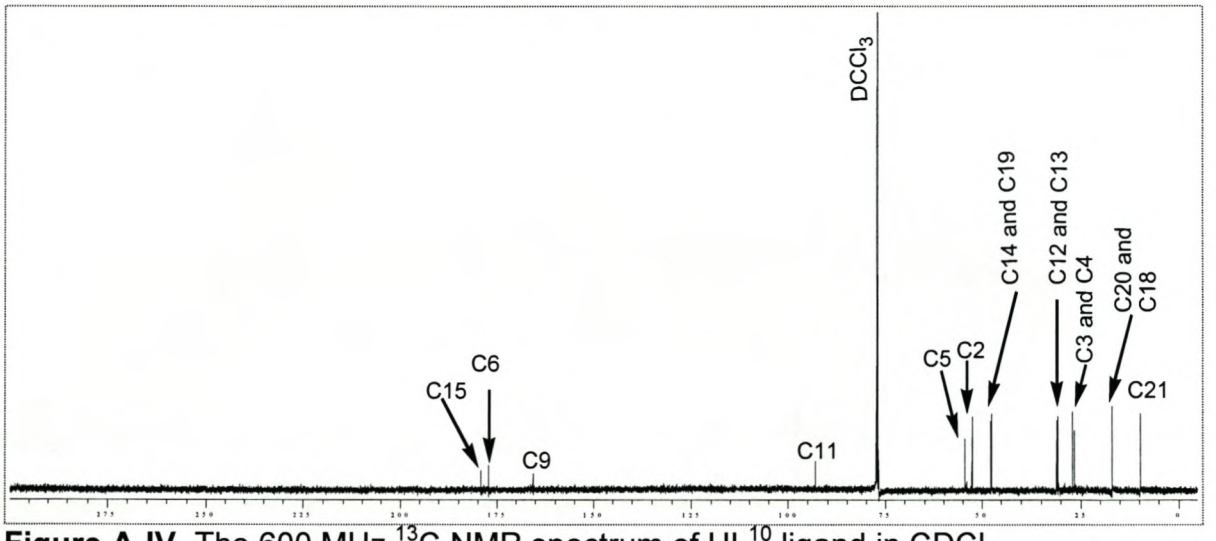

Figure A-IV. The 600 MHz ^{13}C NMR spectrum of HL^{10} ligand in $CDCl_3$.

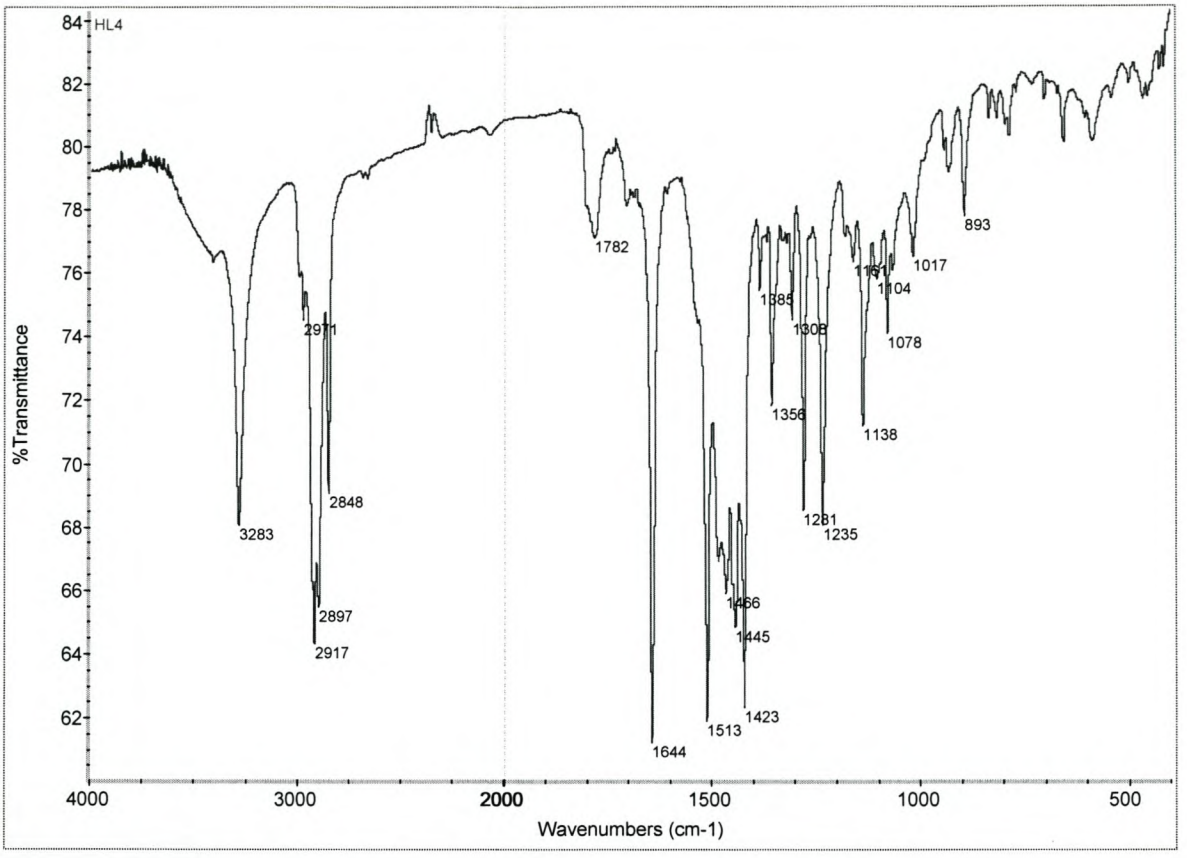

Figure A-V. The IR spectrum of HL^{11} ligand recorded as KBr.

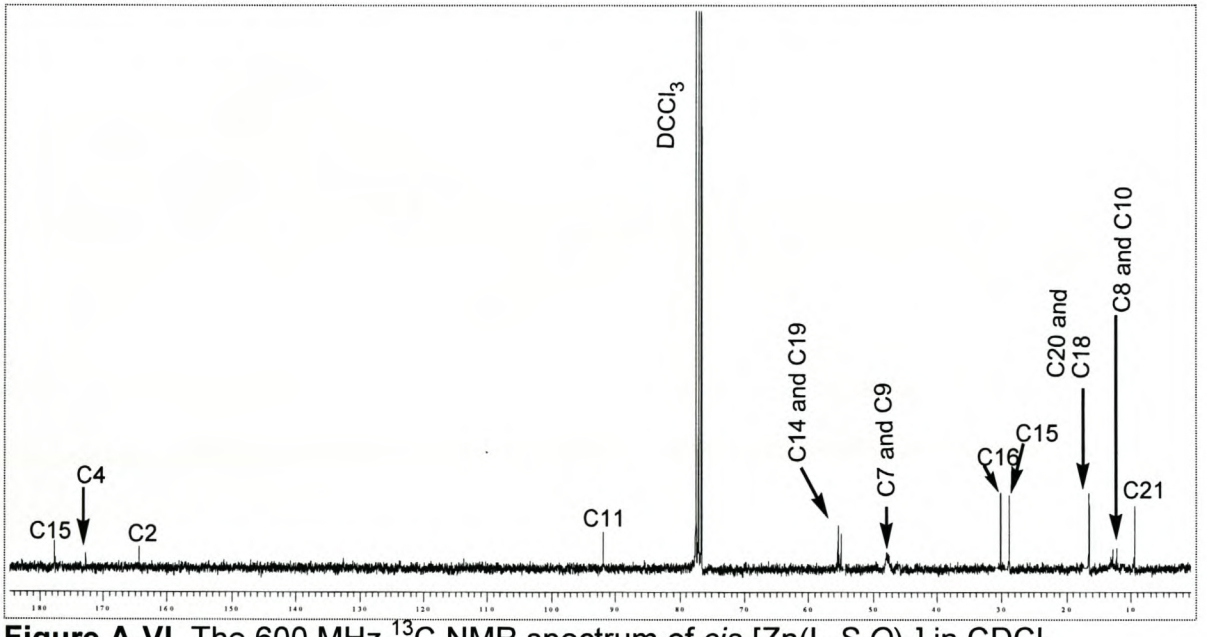

Figure A-VI. The 600 MHz ^{13}C NMR spectrum of *cis*-[Zn(L-*S*,*O*)$_2$] in $CDCl_3$.

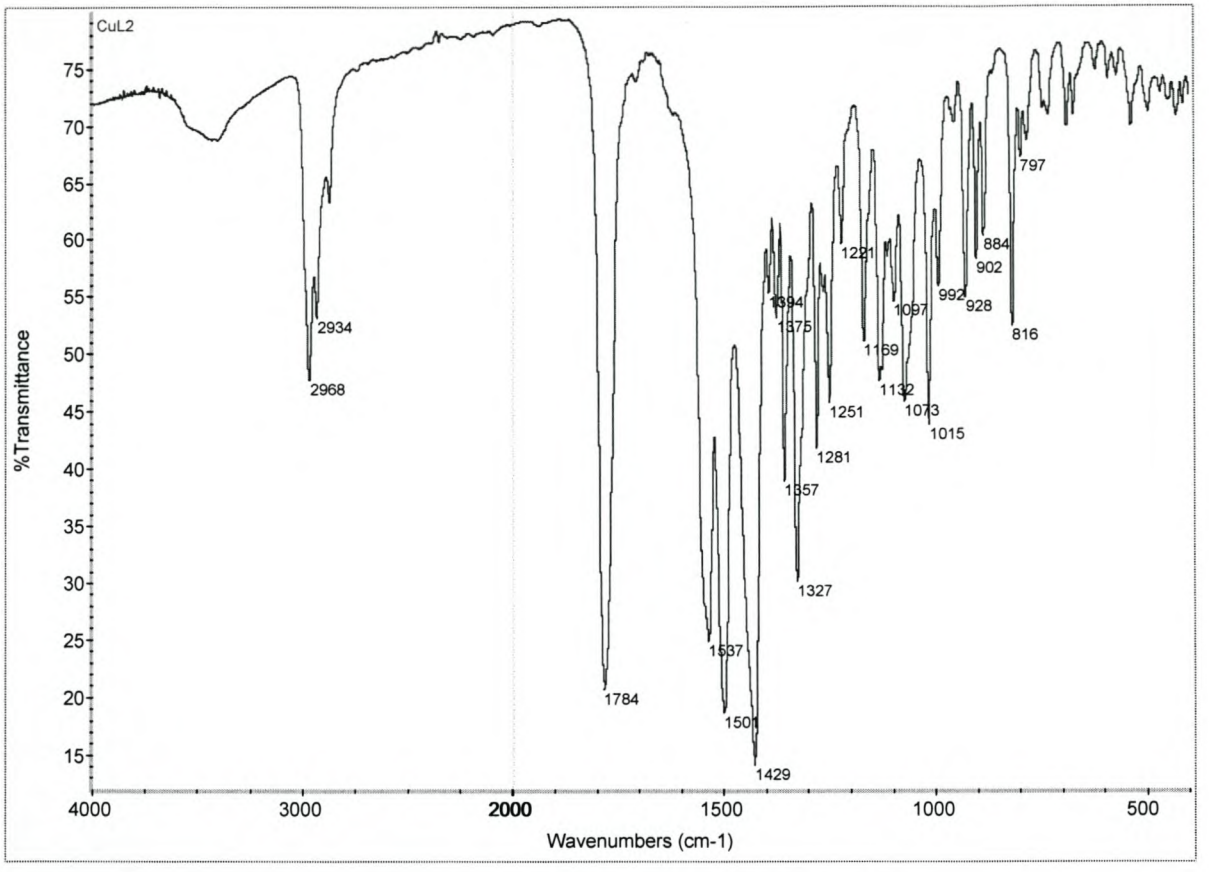

Figure A-VII. The IR spectrum of *trans*-[Cu(L^8-*S*,*O*)$_2$] complex recorded as KBr.

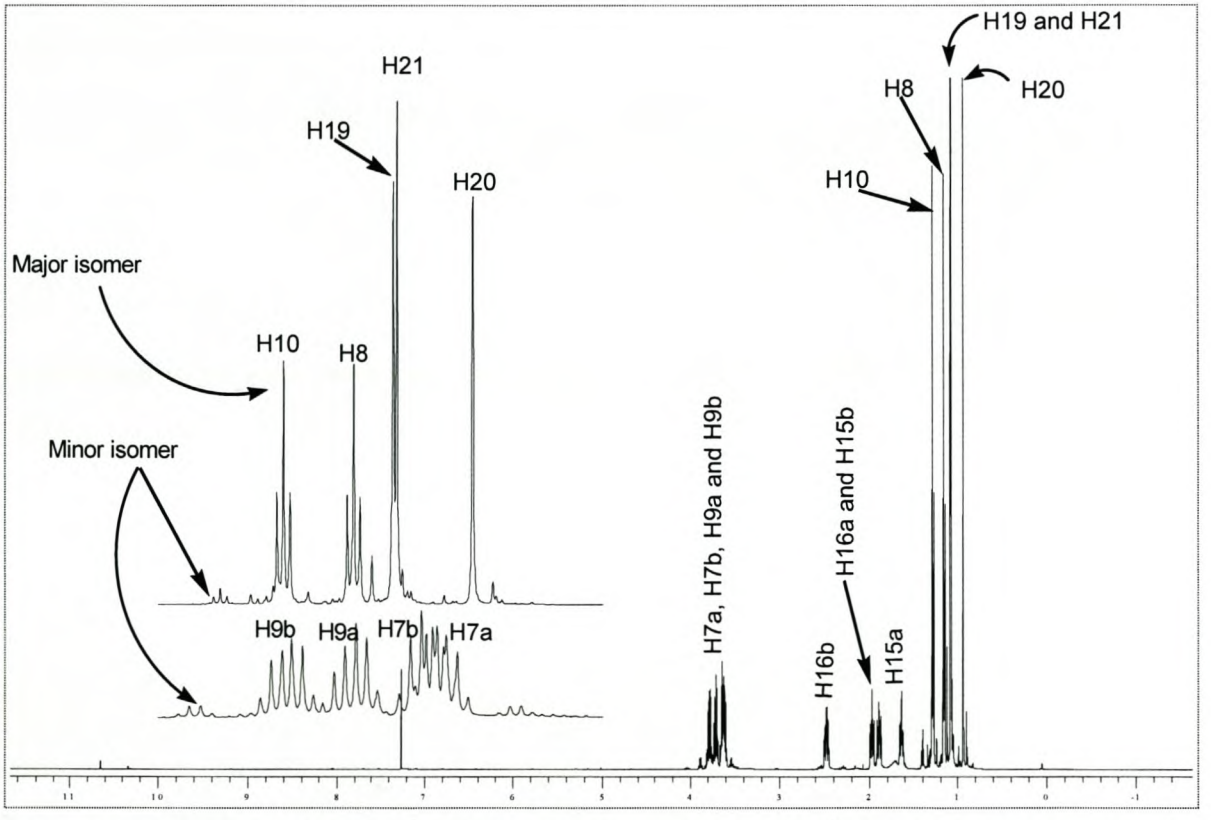

Figure A-VIII. The 600 MHz ^{1}H NMR spectrum of *cis*-[Pt(L^8-*S*,*O*)$_2$] in $CDCl_3$; showing the presence of minor and major isomers in the complex.

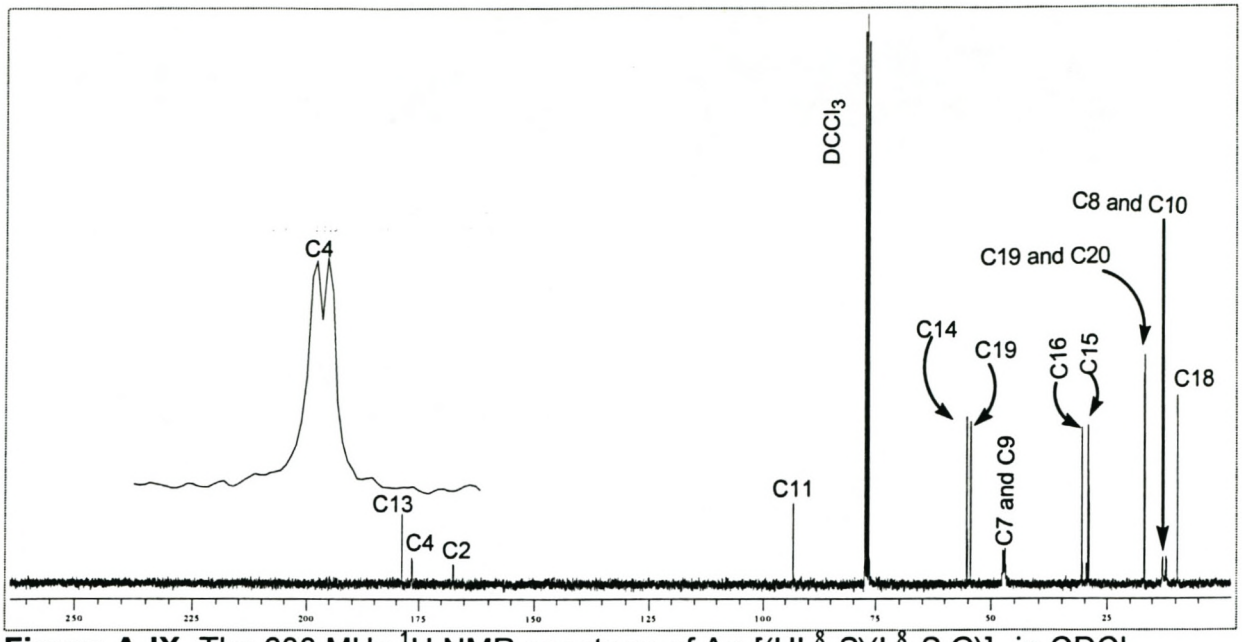

Figure A-IX. The 600 MHz ^{1}H NMR spectrum of $Ag_2[(HL^8\text{-}S)(L^8\text{-}S,O)]_2$ in $CDCl_3$.

APPENDIX B: TABLES OF CRYSTALLOGRAPHIC DATA OF H_3O^+ {*fac*-(Co(L-*S,O*)$_3$]$^-$}, *cis*-[Ni(L-*S.O*)$_2$], *trans*-[Cu(L-*S,O*)$_2$] AND $Ag_2(HL^8\text{-}S)(L^8\text{-}\mu\text{-}S,O)_2$ COMPLEXES OF HL^8 LIGAND.

1. *Cis-bis*(*N,N*-diethyl-*N´*-camphanoylthioureato)Nickel(II), *cis*-[Ni(L-*S.O*)$_2$]

Table A-1.1. Atomic coordinates (x 10^4) and equivalent isotropic displacement parameters (Å^2 x 10^3) of *cis*-[Ni(L^8-*S,O*)$_2$] complex. U(eq) is defined as one third of the trace of the orthogonalized Uij tensor.

Atoms	x	Y	z	U(eq)
Ni(1)	236(1)	7046(1)	7329(1)	30(1
O(1A)	1260(3)	5269(3)	7046(1)	40(1)
C(2A)	1017(4)	4495(4)	6609(1	32(1)
N(3A)	16(3)	4718(3)	6196(1)	37(1)
C(4A)	1043(4)	5990(4)	6152(1)	36(1)
S(5A)	1306(1)	7482(1)	6622(1)	52(1)
N(6A)	1946(3)	6067(3)	5690(1)	43(1)
C(7A)	3063(4)	7409(4)	5549(1)	44(1)
C(8A)	4790(4)	7043(6)	5679(2)	61(1)
C(9A)	1845(5)	4797(5)	5278(1)	61(1)
C(10A)	489(6)	5073(7)	4921(2)	83(2)
C(11A)	2074(4)	3012(4)	6562(1)	32(1)
O(12A)	2763(2)	3021(3)	6028(1)	38(1)
C(13A)	4014(4)	1946(5)	6066(1)	43(1)
C(14A)	4116(4)	1260(4)	6628(1)	42(1)
C(15A)	2584(4)	191(4)	6628(2)	49(1)
C(16A)	1169(4)	1407(4)	6588(1)	39(1)
O(17A)	4802(3)	1648(4)	5689(1)	62(1)
C(18A)	5707(5)	444(5)	6794(2)	64(1)
C(19A)	3620(4)	2786(4)	6938(1)	36(1)
C(20A)	4828(4)	4166(5)	6912(2)	52(1)
C(21A)	3304(4)	2453(4)	7531(1)	48(1)
O(1B)	1585(2)	6661(2)	7953(1)	37(1)
C(2B)	1795(3)	7432(3)	8389(1)	33(1)
N(3B)	1164(3)	8794(3)	8553(1)	37(1)
C(4B)	10(4)	9643(4)	8259(1)	33(1)
S(5B)	917(1)	9131(1)	7649(1)	36(1)
N(6B)	436(3)	11026(3)	8482(1)	42(1)
C(7B)	423(5)	11643(5)	8980(2)	57(1)
C(8B)	404(6)	11081(7)	9455(2)	86(2)
C(9B)	1743(3)	12065(5)	8252(1)	42(1)
C(10B)	1122(5)	13399(5)	7915(2)	56(1)
C(11B)	3063(4)	6757(4)	8790(1)	36(1)
O(12B)	3126(3)	4990(2)	8736(1)	38(1)
C(13B)	4607(4)	4532(4)	8963(1)	42(1)
C(14B)	5481(4)	6041(4)	9157(1)	52(1)
C(15B)	4546(6)	6564(6)	9640(2)	80(2)
C(16B)	2858(5)	7047(6)	9387(1)	65(1)
O(17B)	5003(3)	3139(3)	8999(1)	57(1)
C(18B)	7319(5)	5827(5)	9252(2)	88(2)
C(19B)	4854(4)	7241(4)	8707(1)	43(1)
C(20B)	5209(6)	9022(5)	8826(2)	75(1
C(21B)	5391(4)	6800(5)	8151(2)	54(1)

Table A–1.2. Selected bond lengths of *cis*-[Ni(L^8-*S,O*)$_2$.

Bond	Length(Å)	Bond	Length(Å)
Ni(1)-O(1A)	1.855(2)	C(19A)-C(20A)	1.519(5)
Ni(1)-O(1B)	1.881(2)	C(19A)-C(21A)	1.538(4)
Ni(1)-S(5A)	2.139(10)	O(1B)-C(2B)	1.261(3)
Ni(1)-S(5B)	2.145(9)	C(2B)-N(3B)	1.317(4)
O(1A)-C(2A)	1.267(4)	C(2B)-C(11B)	1.509(4)
C(2A)-N(3A)	1.307(4)	N(3B)-C(4B)	1.359(4)
C(2A)-C(11A)	1.514(4)	C(4B)-N(6B)	1.333(4)
N(3A)-C(4A)	1.351(4)	C(4B)-S(5B)	1.711(3)
C(4A)-N(6A)	1.333(4)	N(6B)-C(7B)	1.480(4)
C(4A)-S(5A)	1.722(3)	N(6B)-C(9B)	1.467(4)
N(6A)-C(7A)	1.471(4)	C(7B)-C(8B)	1.476(6)
N(6A)-C(9A)	1.473(4)	C(9B)-C(10B)	1.495(6)
C(7A)-C(8A)	1.511(5)	C(11B)-O(12B)	1.468(4)
C(9A)-C(10A)	1.488(6)	C(11B)-C(16B)	1.524(4)
C(11A)-O(12A)	1.476(4)	C(11B)-C(19B)	1.557(5)
C(11A)-C(16A)	1.527(4)	O(12B)-C(13B)	1.368(4)

Table A–1.3. Selected bond angles of *cis*-[Ni(L^8-*S,O*)$_2$] complex.

Bond angle	Degree	Bond angle	Degree
O(1A)-Ni(1)-O(1B)	85.4(9)	C(2A)-C(11A)-C(19A)	120.6(2)
O(1A)-Ni(1)-S(5A)	94.7(7)	C(2B) -C(11B)-C(16B)	118.2(3)
O(1B)-Ni(1)-S(5A)	179.8(8)	C(21A)-C(19A)-C(11A)	114.8(3)
O(1A)-Ni(1)-S(5B)	178.9(9)	C(20A)-C(19A)-C(14A)	113.4(3)
O(1B)-Ni(1)-S(5B)	94.8(6)	C(21A)-C(19A)-C(14A)	113.5(3)
S(5A)-Ni(1)-S(5B)	85.1(3)	C(11A)-C(19A)-C(14A)	91.7(2)
C(2A)-O(1A)-Ni(1)	132.4(19)	C(2B)-O(1B)-Ni(1)	131.8(18)
O(1A)-C(2A)-N(3A)	131.7(3)	O(1B)-C(2B)-N(3B)	131.6(3)
O(1A)-C(2A)-C(11A)	114.4(2)	O(1B)-C(2B)-C(11B)	115.8(2)
N(3A)-C(2A)-C(11A)	113.9(2)	N(3B)-C(2B)-C(11B)	112.5(3)
C(2A)-N(3A)-C(4A)	123.3(3)	C(2B)-N(3B)-C(4B)	123.5(3)
N(6A)-C(4A)-N(3A)	115.0(3)	N(6B)-C(4B)-N(3B)	114.9(3)
N(6A)-C(4A)-S(5A)	117.7(2)	N(6B)-C(4B)-S(5B)	117.5(2)
N(3A)-C(4A)-S(5A)	127.3(2)	N(3B)-C(4B)-S(5B)	127.6(2)
C(4A)-S(5A)-Ni(1)	110.2(10)	C(4B)-S(5B)-Ni(1)	110.1(11)
C(4A)-N(6A)-C(7A)	123.4(3)	C(4B)-N(6B)-C(7B)	120.9(3)
C(4A)-N(6A)-C(9A)	120.9(3)	C(4B)-N(6B)-C(9B)	123.7(3)
C(7A)-N(6A)-C(9A)	115.7(2)	C(7B)-N(6B)-C(9B)	115.4(3)
N(6A)-C(7A)-C(8A)	112.6(3)	N(6B)-C(7B)-C(8B)	109.9(4)
N(6A)-C(9A)-C(10A)	112.4(4)	N(6B)-C(9B)-C(10B)	112.4(3)
O (12A)-C(11A)-C(2A)	108.7(2)	O(12B)-C(11B)-C(2B)	109.5(2)
C(2A)-C(11A)-C(16A)	114.5(2)	C(2B)-C(11B)-C(19B)	104.6(3)

Table A–1.4. Torsion angles of *cis*-[Ni(L^8-*S,O*)$_2$].

Angle	Degree	Angle	Degree
O(1B)-Ni(1)-O(1A)-C(2A)	173.7(3)	O(1A)-Ni(1)-O(1B)-C(2B)	174.9(3)
S(5A)-Ni(1)-O(1A)-C(2A)	6.1(3)	S(5A)-Ni(1)-O(1B)-C(2B)	68.0(21)
S(5B)-Ni(1)-O(1A)-C(2A)	87.0(4)	S(5B)-Ni(1)-O(1B)-C(2B)	4.0(3)
Ni(1)-O(1A)-C(2A)-N(3A)	2.5(6)	Ni(1)-O(1B)-C(2B)-N(3B)	1.6(5)
Ni(1)-O(1A)-C(2A)-C(11A)	75.2(2)	Ni(1)-O(1B)-C(2B)-C(11B)	177.4(2)
O(1A)-C(2A)-N(3A)-C(4A)	4.0(6)	O(1B)-C(2B)-N(3B)-C(4B)	3.3(5)
C(11A)-C(2A)-N(3A)-C(4A)	78.3(3)	C(11B)-C(2B)-N(3B)-C(4B)	179.3(3)
C(2A)-N(3A)-C(4A)-N(6A)	176.4(3)	C(2B)-N(3B)-C(4B)-N(6B)	177.4(3)
C(2A)-N(3A)-C(4A)-S(5A)	3.9(5)	C(2B)-N(3B)-C(4B)-S(5B)	2.9(5)
N(6A)-C(4A)-S(5A)-Ni(1)	178.6(2)	N(6B)-C(4B)-S(5B)-Ni(1)	172.2(2)
N(3A)-C(4A)-S(5A)-Ni(1)	1.0(3)	N(3B)-C(4B)-S(5B)-Ni(1)	8.1(3)
O(1A)-Ni(1)-S(5A)-C(4A)	4.4(15)	O(1A)-Ni(1)-S(5B)-C(4B)	93(4)
O(1B)-Ni(1)-S(5A)-C(4A)	12.0(21)	O(1B)-Ni(1)-S(5B)-C(4B)	7.0(14)
S(5B)-Ni(1)-S(5A)-C(4A)	176.7(14)	S(5A)-Ni(1)-S(5B)-C(4B)	173.2(12)
N(3A)-C(4A)-N(6A)-C(7A)	176.1(3)	N(3B)-C(4B)-N(6B)-C(7B)	6.7(5)
S(5A)-C(4A)-N(6A)-C(7A)	4.2(5)	S(5B)-C(4B)-N(6B)-C(7B)	173.6(3)
N(3A)-C(4A)-N(6A)-C(9A)	2.5(5)	N(3B)-C(4B)-N(6B)-C(9B)	175.4(3)
S(5A)-C(4A)-N(6A)-C(9A)	177.2(3)	S(5B)-C(4B)-N(6B)-C(9B)	4.3(4)
C(4A)-N(6A)-C(7A)-C(8A)	95.9(4)	C(4B)-N(6B)-C(7B)-C(8B)	92.9(4)
C(9A)-N(6A)-C(7A)-C(8A)	85.4(4)	C(9B)-N(6B)-C(7B)-C(8B)	89.0(4)
C(4A)-N(6A)-C(9A)-C(10A)	84.5(4)	C(4B)-N(6B)-C(9B)-C(10B)	95.7(4)
C(7A)-N(6A)-C(9A)-C(10A)	94.1(4)	C(7B)-N(6B)-C(9B)-C(10B)	82.3(4)
O(1A)-C(2A)-C(11A)-O(12A)	133.0(3)	O(1B)-C(2B)-C(11B)-O(12B)	31.4(4)
N(3A)-C(2A)-C(11A)-O(12A)	48.9(3)	N(3B)-C(2B)-C(11B)-O(12B)	152.0(2)
O(1A)-C(2A)-C(11A)-C(16A)	109.9(3)	O(1B)-C(2B)-C(11B)-C(16B)	151.0(3)
N(3A)-C(2A)-C(11A)-C(16A)	68.2(4)	N(3B)-C(2B)-C(11B)-C(16B)	32.3(4)
O(1A)-C(2A)-C(11A)-C(19A)	16.7(4)	O(1B)-C(2B)-C(11B)-C(19B)	83.2(3)
N(3A)-C(2A)-C(11A)-C(19A)	165.1(3)	N(3B)-C(2B)-C(11B)-C(19B)	93.4(3)
C(2A)-C(11A)-O(12A)-C(13A)	163.8(3)	C(2B)-C(11B)-O(12B)-C(13B)	159.6(2)
C(2A)-C(11A)-C(16A)-C(15A)	170.8(3)	C(2B)-C(11B)-C(16B)-C(15B)	166.8(3)
C(2A)-C(11A)-C(19A)-C(20A)	57.2(4)	C(2B)-C(11B)-C(19B)-C(21B)	56.4(4)
C(2A)-C(11A)-C(19A)-C(21A)	69.4(4)	C(2B)-C(11B)-C(19B)-C(20B)	69.8(4)
C(2A)-C(11A)-C(19A)-C(14A)	173.7(3)	C(2B)-C(11B)-C(19B)-C(14B)	172.4(3)

Table A–1.5. Anisotropic displacement parameters ($Å^2$ x 10^3) of *cis*-[Ni(L^8-*S,O*)$_2$]. The anisotropic displacement factor exponent takes the form: -2 π^2 [$h^2a^{*2}U11$ + ...+ 2hka*b*U12]

	U11	U22	U33	U23	U13	U12
Ni(1)	34(1)	29(1)	26(1)	5(1)	6(1)	9(1)
O(1A)	48(1)	39(1)	32(1)	10(1)	11(1)	20(1)
C(2A)	38(2)	32(2)	27(2)	6(1	12(1)	13(1)
N(3A)	44(2)	37(2)	30(1)	7(1)	10(1)	11(1)
C(4A)	40(2)	36(2)	31(2)	17(1)	24(1)	33(1)
S(5A)	63(1)	49(1)	39(1)	6(1)	15(1)	22(1)
N(6A)	52(2)	44(2)	33(1)	2(1)	12(1)	19(2)
C(7A)	55(2)	44(2)	30(2)	3(2)	9(2)	21(2)
C(8A)	56(2)	71(2)	56(2)	21(2)	31(2)	30(2)
C(9A)	80(3)	58(2)	41(2)	11(2)	2(2)	48(3)
C(10A)	108(4)	103(4)	38(2)	4(1)	5(1)	10(1)
C(11A)	41(2)	31(2)	22(1)	4(1)	2(1)	16(1)
O(12A)	43(1)	49(1)	21(1)	11(2)	4(1)	13(2)
C(13A)	43(2)	57(2)	29(2)	5(1)	5(1)	25(2)
C(14A)	46(2)	48(2)	31(2)	6(2)	1(2)	17(2)
C(15A)	63(2)	37(2)	48(2)	6(1)	2(1)	8(1)
C(16A)	44(2)	35(2)	38(2)	14(1)	4(1)	27(2)
O(17A)	54(1)	97(2)	35(1)	11(2)	11(2)	43(2)
C(18A)	65(3)	76(3)	51(2)	5(1)	6(1)	13(1)
C(19A)	39(2)	42(2)	26(2)	9(2)	10(2)	8(2)
C(20A)	45(2)	65(2)	44(2)	3(1)	8(1)	28(2)
C(21A)	55(2)	59(2)	27(2)	8(1)	8(1)	14(1)
O(1B)	45(1)	35(1)	29(1)	1(1)	0(1)	3(1)
C(2B)	38(2)	34(2)	26(2)	5(1)	3(1)	10(1)
N(3B)	46(2)	34(2)	30(1)	6(1)	2(1)	6(1)
C(4B)	35(2)	33(2)	31(2)	9(1)	6(1)	14(1)
S(5B)	40(1)	36(1)	33(1)	13(1)	9(1)	17(1)
N(6B)	49(2)	38(2)	39(2)	20(2)	8(2)	18(2)
C(7B)	61(2)	53(2)	55(2)	18(3)	2(2)	19(3)
C(8B)	87(3)	112(4)	58(3)	16(2)	3(1)	15(2)
C(9B)	41(2)	41(2)	43(2)	4(2)	4(2)	15(2)
C(10B)	61(2)	45(2)	61(2)	2(1)	2(1)	12(1)
C(11B)	52(2)	31(2)	24(1)	4(1)	1(1)	5(1
O(12B)	47(1)	29(1)	37(1)	5(1)	5(2)	142)
C(13B)	59(2)	38(2)	29()	11(2)	28(2)	18(2)
C(14B)	63(2)	46(2)	42(2)	13(2)	28(2)	49(3)
C(15B)	131(4)	72(3)	33(2)	1(2)	2(2)	42()
C(16B)	99(3)	73(2)	22(2)	7(1)	5(1)	19(1)
O(17B)	75(2)	37(1)	58()	24(3)	70(3	20(2)
C(18B)	82(3)	60(3)	111(4)	7(2)	19(1)	3(2)
C(19B)	44(2)	35(2)	47(2)	9(2)	44(3)	6(2)
C(20B)	77(3)	39(2)	103(4)	16(2)	2(2)	2(2)

2. *Trans-bis*(*N,N*-diethyl-*N´*-camphanoylthioureato)Cu(II) *trans*-[Cu(L-*S,O*)$_2$]

Table A-2.1. Atomic coordination (x 10^4) and equivalent isotropic displacement parameters (Å^2 x 10^3) of *trans*-[Cu(L^8-*S,O*)$_2$]. The U(eq) is defined as one third of the trace of the orthogonalized Uij tensor.

Atoms	X	Y	Z	U(eq)
C(2A)	7809(4)	2642(4)	11857(3)	29(1)
C(2B)	4481(4)	5885(3)	11176(3)	20(1)
C(4A)	7859(4)	3191(4)	10323(3)	27(1)
C(4B)	3900(4)	4875(3)	12352(3)	21(1)
C(7A)	7573(8)	1531(7)	13107(6)	36(2)
C(7B)	4939(5)	7177(4)	10156(3)	31(1)
C(8A)	8405(7)	2247(6)	14256(6)	52(2)
C(8B)	4147(5)	6543(4)	8982(3)	42(1)
C(9A)	9414(16)	1630(13)	11872(11)	20(4)
C(9B)	3357(4)	7337(3)	11417(3)	27(1)
C(10A)	8374(11)	188(9)	10895(8)	53(4)
C(10B)	4094(4)	8373(4)	12415(3)	40(1)
C(11A)	8324(4)	2914(3)	9235(3)	31(1)
C(11B)	2999(4)	4790(3)	13156(3)	19(1)
C(13A)	8265(5)	3370(4)	7743(3)	41(1)
C(13B)	2169(4)	3658(4)	14090(3)	30(1)
C(14A)	9550(5)	3130(4)	8016(4)	36(1)
C(14B)	2408(4)	4917(4)	14745(3)	28(1)
C(15A)	9002(4)	1805(4)	7719(3)	40(1)
C(15B)	1299(4)	5176(4)	14101(3)	30(1)
C(16A)	8181(5)	1677(3)	8584(3)	33(1)
C(16B)	1715(4)	5096(4)	13015(3)	26(1)
C(17A)	9768(4)	3592(4)	9274(3)	36(1)
C(17B)	3688(4)	5479(3)	14394(3)	24(1)
C(18A)	10074(5)	4882(4)	9750(4)	57(2)
C(18B)	4909(4)	5184(4)	14776(3)	36(1)
C(19A)	10820(5)	3304(4)	9844(4)	53(2)
C(19B)	4067(5)	6757(3)	14720(3)	37(1)
C(20A)	10568(5)	3489(5)	7426(4)	67(2)
C(20B)	2447(5)	5195(4)	15959(3)	47(1)
Cu(1)	6016(1)	4159(1)	11439(1)	24(1)
N(3A)	8210(4)	2653(3)	10917(3)	31(1)
N(3B)	3798(3)	5631(3)	11928(2)	23(1)
N(6A)	8140(7)	1888(6)	12239(4)	24(2)
N(6B)	4264(3)	6735(3)	10921(2)	16(3)
O(5A)	7186(3)	3858(3)	10466(2)	38(1)
O(5B)	4668(3)	4284(3)	12266(2)	34(1)
O(12A)	7535(3)	3233(3)	8478(2)	38(1)
O(12B)	2551(3)	3603(2)	13111(2)	28(1)
O(21A)	7864(4)	3620(3)	6989(3)	65(1)
O(21B)	1741(3)	2836(3)	14295(2)	44(1)
S(1A)	6750(1)	3295(1)	12490(1)	34(1)
S(1B)	5477(1)	5191(1)	10499(1)	28(1)

Table A-2.2. Average selected bond lengths of *trans*-[Cu(L^8-*S,O*)$_2$].

Bond	Bond length (Å)	Bond	Bond length(Å)
C(2)-N(6	1.346(10)	C(11)-C(17)	1.534(6)
C(2)-N(3)	1.363(5)	C(13)-O(12)	1.217(5)
C(2)-S(1)	1.726(5)	C(13)-O(12)	1.337(5)
C(4)-O(5)	1.258(5)	C(13)-C(14)	1.515(6)
C(4)-N(3)	1.304(5)	C(14)-C(20)	1.466(6)
C(4)-C(1)	1.538(6)	C(14)-C(17)	1.540(5)
C(7)-N(6)	1.501(9)	C(14)-C(15)	1.573(6)
C(4)-C((8)	1.513(10)	C(15)-C(16)	1.539(6)
C(9)-N(6)	1.488(10)	C(17)-C(19)	1.481(6)
C(9)-C(10)	1.542(2)	C(17)-C(18)	1.526(6)
C(11)-O(12)	1.471(4)	Cu(1)-O(5)	1.913(3)
C(11)-C(16)	1.528(5)	Cu(1)-S(1)	2.260(11)

Table A-2.3. Selected bond angles of *trans*-[Cu(L^8-*S,O*)$_2$] complex.

Angle	Degree	Angle	Degree
N(6A)-C(2A)-N(6A)	23.4(5)	C(11A)-C(16A)-C(15A)	101.9(3)
N(6A)-C(2A)-N(3A)	111.2(5)	C(19A)-C(17A)-C(18A)	109.0(4)
N(6A)-C(2A)-S(1A)	119.0(5)	C(19A)-C(17A)-C(11A)	114.8(4)
N(3A)-C(2A)-S(1A)	128.3(3)	C(18A)-C(17A)-C(11A)	113.3(4)
O(5A)-C(4A)-N(3A)	131.7(4)	C(19A)-C(17A)-C(14A)	114.6(4)
O(5A)-C(4A)-C(11A)	115.4(3)	C(18A)-C(17A)-C(14A)	111.7(4)
N(3A)-C(4A)-C(11A)	112.9(4)	C(11A)-C(17A)-C(14A)	92.7(3)
N(6A)-C(7A)-C(8A)	113.7(7)	O(5A)-Cu(1)-S(1B)	85.7(9)
C(10A)-C(9A)-N(6A)	112.0(7)	O(5B)-Cu(1)-O(5A)	172.4(16)
O.(12A)-C(11A)-C(16A)	104.5(3)	O(5A)-Cu(1)-S(1A)	93.7(9)
O(12A)-C(11A)-C(17A)	102.1(3)	O(5B)-(Cu(1)-S(1B)	94.1(9)
C(16A)-C(11A)-C(17A)	104.2(3)	O(5B)-Cu(1)-S(1A)	87.4(9)
O(12A)-C(11A)-C(4A)	108.9(3)	S(1B)-Cu(1)-S(1A)	173.8(5)
C(16A)-C(11A)-C(4A)	118.9(3)	C(4A)-N(3A)-C(2A)	125.3(4)
C(17A)-C(11A)-C(4A)	116.8(3)	C(2A)-N(6A)-C(9A)	121.1(5)
O(21A)-C(13A)-O(12A)	121.6(4)	C(2A)-N(6A)-C(7A)	124.5(5)
O(21A)-C(13A)-C(14A)	108.6(3)	C(9A)-N(6A)-C(7A)	114.4(5)
O(12A)-C(13A)-C(14A)	108.6(3)	C(2A)-N(6A)-C(9A)	119.6(8)
C(20A)-C(14A)-C(13A)	114.0(4)	C(2A)-N(6A)-C(7A)	120.6(9)
C(20A)-C(14A)-C(17A)	123.8(4)	C(9A)-N(6A)-C(7A)	117.1(9)
C(13A)-C(14A)-C(17A)	98.7(3)	C(4A)O(5A)-Cu(1)	131.6(3)
C(20A)-C(14A)-C(15A)	113.9(4)	C(13A)-O(12A)-C(11A)	105.9(3)
C(13A)-C(14A)-C(15A)	101.3(4)	C(2A)-S(1A)-Cu(1A)	107.9(14)
C(17A)-C(14A)-C(15A)	103.6(3)	C(2B)-S(1B)-Cu(1)	107.2(13)
C(16A)-C(15A)-C(14A)	101.3(4)	C((4B)-O(5B)-Cu(1)	131.6(3)

Table A-2.4. Selected torsion angles of *trans*-[Cu(L^8-*S,O*)$_2$].

Angle	Degree	Angle	Degree
O(5A)-C(4A)-C(11A)-O(12A)	16.6(5)	N(6A)-C(2A)-N(6A)-C(9A)	84.3(16)
N(3A)-C(4A)-C(11A)-O(12A)	161.5(3)	N(3A)-C(2A)-N(6A)-C(9A)	18.1(13)
O(5A)-C(4A)-C(11A)-C(16A)	135.7(4)	S(1A)-C92A)-N(6A)-C(9A)	175.1(9)
N(3A)-C(4A)-C(11A)-C(16A)	42.4(5)	N(6A)-C(2A)-N(6A)-C(7A)	76.3(16)
O(5A)-C(4A)-C(11A)-C(17A)	98.4(4)	N(3A)-C(2A)-N(6A)-C(7A)	178.7(9)
N(3A)-C(4A)-C(11A)-C(17A)	83.5(5)	S(1A)-C(2A)-N(6A)-C(7A)	14.5(14)
O(5B)-C(4B)-C(11B)-O(12B)	36.9(4)	C(10A)-C(9A)-N(6A)-C(2A)	70.4(16)
N(3B)-C(4B)-C(11B)-C(12B)	147.9(3)	C(10A)-C(9A)-N(6A)-C(7A)	90.9(15)
O(5B)-C(4B)-C(11B)-C(16B)	157.7(4)	C(8A)-C97A)-N(6A)-C(2A)	79.3(14)
N(3B)-C(4B)-C(11B)-C(16B)	27.1(5)	C(8A)-C(7A)-N(6A)-C(9A)	81.8(15)
O(5B)-C(4B)-C(11B)-C(17B)	77.5(4)	N(3B)-C(2B)-N(6B)-C(7B)	177.7(3)
N(3B)-C(4B)-C(11B)-C(17B)	97.8(4)	S(1B)-C(2B)-N(6B)-C(7B)	5.7(5)
C(4A)-C(11A)-C(16A)-C(15A)	168.9(3)	N(3B)-C(2B)-N(6B)-C(9B)	0.2(5)
C(4B)-C(11B)-C(16B-C(15B)	167.2(3)	S(1B)-C(2B)-N(6B)-C(9B)	176.4(3)
C(16A)-C(11A)-C(17A)-C(19A)	62.2(4)	C(8B)-C(7B)-N(6B)-C(2B)	89.5(4)
C(4A)-C(11A)-C(17A)-C(18A)	55.5(5)	C(8B)-C(7B)-N(6B)-C(9B)	92.4(4)
C(4A)-C(11A)-C(17A)-C(14A)	170.6(3)	C(10B)-C(9B)-N(6B)-C(2B)	92.7(4)
C(4B)-C(11B)-C(17B)-C(19B)	70.5(5)	C(10B)-C(9B)-N(6B)-C(7B)	85.4(4)
C(4B)-C(11B)-C(17B)-C(18B)	55.895)	N(3A)-C(4A)-O(5A)-Cu(1)	16.0(8)
O(5A)-C(4A)-N(3A)-C(2A)	5.1(8)	C(11A)-C(4A)-O(5A)-Cu(1)	161.6(3)
C(11A)-C(4A)-N(3A)-C(2A)	172.5(4)	O(5B)-Cu(1)-O(5A)-C(4A)	83.1(11)
N(6A)-C(2A)-N(3A-C(4A)	164.3(7)	S(1B)-Cu(1)-O(5A)-C(4A)	171.4(4)
N(6A)-C(2A)-N(3A)-C(4A)	170.5(5)	S(1A)-Cu(1)-O(5A)-C(4A)	14.8(4)
S(1A)-C(2A)-N(3A)-C(4A)	1.0(7)	N(3B)-C(4B)-O(5B)-Cu(1)	2.6(7)
O(5B)-C(4B)-N(3B)-C(2B)	6.2(7)	C(11B)-C(4B)-O(5B)-Cu(1)	176.7(2)
C(11B)-C(4B)-N(3B)-C(2B)	179.5(3)	O(5A)-Cu(1)-O(5B)-C(4B)	96.5(11)
N(6B)-C(2B)-N(3B)-C(4B)	176.1(4)	S(1B)-Cu(1)-O(5B)-C(4B)	8.8(4)
S(1B)-C(2B)-N(3B)-C(4B)	7.6(6)	S91A)-Cu(1)-O(5B)-C(4B)	165.2(4)
N(6A)-C(2A)-N(6A)-C(9A)	76.1(14)	N(6A)-C(2A)-S(1A)-Cu(1)	166.6(7)
N(3A)-C(2A)-N(6A)-C(9A)	11.4(8)	N(3A)-C(2A)-S(1A)-Cu(1)	2.4(5)
S(1A)-C(2A)-N(6A)-C(9A)	177.8(5)	O(5B)-Cu(1)-S(1A)-C(2A)	165.2(19)
N(6A)-C(2A)-N96A)-C(7A)	106.2(16)	S(1B)-Cu(1)-S(1A)-C(2A)	90.8(5)
N(3A)-C(2A)-N(6A)-C(7A)	166.4(6)	N(6B)-C(2B)-S(1B)-Cu(1)	165.9(3)
S(1A)-C(2A)-N(6A)-C(7A)	4.5(8)	N(3B)-C(2B)-S(1B)-Cu(1)	18.0(4)
C(10A)-C(9A)-N(6A)-C(2A)	93.9(8)	O(5B)-Cu(1)-S(1B)-C(2B)	14.9(17)
C(10)-C(9A)-N(6A)-C(7A)	84.1(8)	O(5A)-Cu(1)-S(1B)-C(2B)	172.6(18)
C(8A)-C(7A)-N(6A)-C(2A)	92.0(8)	S(1A)-Cu(1)-S(1B)-C(2B)	88.6(5)
C(8A)-C(7A)-N(6A)-C(9A)	90.1(8)		

Table A-2.5. Anisotropic displacement parameters (Å^2 x 10^3) of *trans*-[Cu(L^8-*S,O*)$_2$]. The anisotropic displacement factor exponent takes the form: $-2\pi^2$[h2a*^{2}U_{11} + ... + 2hka*b*U_{12}].

Atoms	U11	U22	U33	U23	U13	U12
C(2A)	37(3)	30(3)	26(2)	11(2)	6(2)	20(2)
C(2B)	23(2)	21(2)	20(2)	10(2)	9(2)	8(2)
C(4A)	33(3)	31(3)	26(2)	12(2)	14(2)	18(2)
C(4B)	23(2)	24(2)	20(2)	9(2)	7(2)	11(2)
C(7B)	40(3)	33(3)	34(2)	20(2)	20(2)	19(2)
C(8B)	63(3)	54(3)	28(2)	24(2)	22(2)	35(3)
C(9B)	26(2)	30(3)	32(2)	15(2)	10(2)	14(2)
C(10B)	44(3)	34(3)	41(2)	3(2)	12(2)	23(2)
C(11A)	25(2)	31(2)	39(2)	13(2)	1(1)	16(2)
C(11B)	20(2)	24(2)	23(2)	17(2)	10(2)	10(2)
C(13A)	64(3)	38(3)	31(2)	16(2)	17(2)	25(2)
C(13B)	27(2)	36(3)	37(2)	22(2)	7(2)	15(2)
C(14A)	34(3)	40(3)	43(3)	18(2)	17(2)	18(2)
C(14B)	31(2)	43(3)	25(2)	22(2)	15(2)	18(2)
C(15A)	45(3)	46(3)	30(2)	11(2)	11(2)	21(2)
C(15B)	21(2)	43(3)	40(2)	24(2)	18(2)	16(2)
C(16A)	46(3)	21(2)	28(2)	4(2)	11(2)	9(2)
C(16B)	22(2)	36(3)	26(2)	13(2)	7(2)	14(2)
C(17A)	29(3)	32(3)	40(2)	7(2)	6(2)	6(2)
C(17B)	24(2)	28(2)	20(2)	9(2)	8(2)	7(2)
C(18A)	69(4)	32(3)	49(3)	7(2)	18(3)	-6(3)
C(18B)	25(2)	50(3)	37(2)	25(2)	1(2)	12(2)
C(19A)	40(3)	51(3)	46(3)	12(3)	-14(2)	0(3)
C(19B)	40(3)	31(3)	33(2)	9(2)	6(2)	7(2)
C(20A)	62(4)	100(5)	43(3)	31(3)	33(3)	21(4)

C(20B)	48(3)	73(4)	32(2)	29(2)	19(2)	24(3)
Cu(1)	30(1)	25(1)	25(1)	12(1)	14(1)	17(1)
N(3A)	40(2)	35(2)	31(2)	21(2)	16(2)	23(2)
N(3B)	27(2)	24(2)	23(2)	10(2)	10(2)	14(2)
N(6B)	26(2)	24(2)	23(2)	10(1)	9(1)	12(2)
O(5A)	52(2)	51(2)	41(2)	29(2)	31(2)	41(2)
O(5B)	41(2)	45(2)	44(2)	31(2)	28(2)	30(2)
O(12A)	38(2)	51(2)	36(2)	22(1)	12(1)	24(2)
O(12B)	28(2)	26(2)	33(2)	14(1)	13(1)	8(1)
S(1A)	50(1)	45(1)	29(1)	22(1)	21(1)	35(1)
S(1B)	42(1)	32(1)	27(1)	18(1)	21(1)	25(1)

3. *Tetrakis*(*N,N*-diethyl-*N'*-camphanoylthioureato)diargentate(I), $Ag_2(HL^8\text{-}S)(L^8\text{-}\mu\text{-}S,O))_2$ complex.

Table A–3.1. Atomic coordinates (x 10^4) and equivalent isotropic displacement parameters ($Å^2$ x 10^3) of $Ag_2(HL^8\text{-}S)(L^8\text{-}\mu\text{-}S,O))_2$ complex. U(eq) is defined as one third of the trace of the orthogonalized Uij tensor.

Atoms	X	Y	Z	U(eq)
Ag(1)	7834(1)	3734(1)	2690(1	43(1)
Ag(2)	10055(1)	5170(1)	2266(1)	45(1)
S(1A)	10005(4)	4759(3)	3362(2)	39(1)
C(2A)	10772(14)	3916(12)	3398(7)	41(4)
N(3A)	11341(12)	3596(8)	2882(6)	34(3)
C(4A)	10665(16)	3055(10)	2468(7)	37(3)
O(5A)	9416(12)	2698(8)	2483(7)	55(3)
N(6A)	10927(15)	3533(9)	3938(6)	45(3)
C(7A)	10410(20)	3815(14)	4542(8	55(5)
C(8A)	11450(20)	4507(17)	4887(10)	72(6)
C(9A)	11600(20)	2799(14)	3982(10)	64(6)
C(10A)	10630(30)	1959(16)	3937(12)	83(7)
C(11A)	11440(20)	2823(15)	1919(10)	66(5)
O(12A)	10598(11)	2523(8)	1396(5)	45(3)
C(13A)	11420(20)	2324(13)	967(9)	55(5)
C(14A)	12796(17)	2544(11)	1184(8)	44(4)
C(15A)	12550(40)	1630(20)	1729(17)	126(12)
C(16A)	11810(30)	1740(20)	2158(15)	102(9)
O(17A)	11030(20)	2133(14)	439(10)	102(6)
C(18A)	13950(40)	2410(20)	810(16)	115(10)
C(19A)	12750(40)	2970(30)	1781(18)	128(12)
C(20A)	12440(30)	3980(20)	1530(14)	94(8)
C(21A)	13930(20)	3121(13)	2242(9)	55(5)
S(1B)	7749(4)	4156(3)	1594(2)	44(1)
C(2B)	6881(16)	4999(8)	1582(8)	36(4)
N(3B)	6439(12)	5297(9)	2122(6)	41(3)
C(4B)	7189(17)	5845(11)	2523(8)	42(4)
O(5B)	8414(10)	6166(7)	2471(6)	44(3)
N(6B)	6602(14)	5280(9)	1047(7)	46(3)
C(7B)	6950(20)	4943(12)	437(10)	57(5)
C(8B)	8400(20)	5416(18)	232(11)	78(7)
C(9B)	5910(20)	6016(11)	1023(10)	55(5)
C(10B)	6900(30)	6932(13)	1075(11)	75(7)
C(11B)	6380(20)	6030(16)	3115(11)	75(6)
O(12B)	7374(11)	6532(7)	3555(5)	42(3)
C(13B)	6576(17)	6739(11)	4024(8)	44(4)
C(14B)	5122(18)	6453(12)	3810(9)	51(4)
C(15B)	5130(30)	5470(20)	4077(15)	108(10)
C(16B)	5760(30	7119(12)	3563(12)	86(7)
O(17B)	4120(30)	6570(20)	4485(8)	82(5)
C(18B)	5120(30)	6300(20)	4254(14)	95(8)
C(19B)	5620(30)	7190(20)	3198(16)	114(10)
C(20B)	3930(20)	5645(15)	2857(16)	111(10)
C(21B)	11331(5)	5918(3)	2869(10)	67(6)
S(1C)	11032(18)	6950(12)	1400(2)	49(1)
C(2C)	10693(13)	7239(7)	1444(8)	45(4)
N(3C)	11630(18)	7752(11)	2013(6)	33(3)
C(4C)	11150(20)	7432(10)	2392(8	99(6)
N(6C)	11550(30)	7167(13)	965(7)	65(5)
C(7C)	13080(40)	7310(18)	337(10)	80(8)
C(8C)	10510(20)	8281(15)	340(12)	102(10)
C(9C)	11590(30)	8800(40)	970(12)	72(6)
C(10C)	11210(20)	7981(14)	988(17)	190(30)

APPENDIX B

C(11C)	12700(20)	8322(14)	3048(9)	59(5)
O(12C)	12670(20)	8755(16)	3311(10)	29(6)
C(13C)	10760(20)	8682(15)	3786(11)	11(5)
C(14C)	10409(18)	7754(12)	3874(11)	69(6)
C(15C)	10738(17)	7251(11)	4074(8)	49(4)
C(16C)	13360(20)	9139(16)	3476(7)	42(4)
O(17C)	10440(20)	9349(13)	4207(11)	38(6)
C(18C)	10790(40)	8760(20)	4333(9)	55(5)
C(19C)	11540(30)	9580(17)	3171(16)	112(10)
C(20C)	9560(20)	8174(14)	2903(12)	79(7)
O(22C)	9260(30)	8580(20)	2911(9)	45(5)
C(23C)	8240(20)	8827(15)	3367(16)	53(8)
O(24C)	6801(6)	2969(3)	3424(11)	56(6)
S(1D)	6672(16)	1914(9)	3611(2)	55(1)
C(2D)	7077(12)	1603(9)	3461(7)	35(3)
N(3D)	6114(19)	1117(10)	2886(6)	36(3)
C(4D)	4952(13)	891(11)	2484(8)	46(4)
O(5D)	6219(15)	1318(9)	2617(9)	87(6)
N(6D)	5590(30	1564(13)	3873(7)	47(3)
C(7D)	4160(30)	1540(20)	4450(9)	67(6)
C(8D)	6160(20)	382(13	4366(13)	95(9
C(9D)	6930(50)	10(20)	3772(9)	55(5)
C(10D)	6643(18)	889(12)	4220(20)	157(18)
C(11D)	5150(30)	574(19)	1855(8)	49(4)
O(12D)	5360(30)	120(20)	1504(13	45(8)
C(13D)	7210(20)	116(14)	1022(14)	23(7)
C(14D)	7585(18)	1049(12)	1052(10)	61(5)
C(15D)	7242(17)	1601(11)	856(8)	49(4)
C(16D)	4540(30)	230(20	1416(8)	46(4)
O(17D)	7420(20)	557(1)	642(14)	53(8)
C(18D)	7070(30)	60(20)	577(10)	66(6)
C(19D)	6100(30)	754(19)	1768(16)	110(10)
C(20D)	8200(20)	648(16)	2009(13)	89(8)
O(22D)	8520(40)	250(20)	2055(11)	63(7)
C(23D)	9480(20)	94(16)	1607(16)	61(9)

Table A–3.2. Selected bond length of $Ag_2(HL^8\text{-}S)(L^8\text{-}\mu\text{-}S,O))_2$ complex.

Bond	Length(Å)	Bond	Length(Å)
Ag(1)-S(1B)	2.46(4)	S(1C)-C(2C)	1.73(18)
Ag(1)-S(1D)	2.46(5)	C(2C)-N(6C)	1.28(2)
Ag(1)-O(5A)	2.57(13)	C(2C)-N(3C)	1.36(2)
Ag(1)-S(1A)	2.82(4)	N(3C)-C(4C)	1.37(2)
Ag(1)-Ag(2)	3.02(2)	C(4C)-O(5C)	1.21(2)
Ag(2)-S(1A)	2.44(4)	C(4C)-C(11C)	1.53(3)
Ag(2)-S(1C)	2.45(4)	N(6C)-C(7C)	1.48(3)
Ag(2)-O(5B)	2.57(11)	N(6C)-C(9C)	1.62(3)
Ag(2)-S(1B)	2.91(5)	C(7C)-C(8C)	1.54(4)
S(1A)-C(2A)	1.69(17)	C(9C)-C(10C)	1.23(4)
C(2A)-N(6A)	1.34(2)	C(11C)-C(19C)	1.42(4)
C(2A)-N(3A)	1.38(2)	C(11C)-C(16C)	1.49(3)
N(3A)-C(4A)	1.30(2)	C(11C)-O(12C)	1.60(3)
C(4A)-O(5A)	1.28(2)	C(11C)-O(22C)	1.81(3)
C(4A)-C(11A)	1.50(3)	O(12C)-C(13C)	1.22(3)
N(6A)-C(9A)	1.48(2)	C(13C)-O(17C)	1.21(3)
N(6A)-C(7A)	1.49(2)	C(13C)-C(14C)	1.94(3)
C(7A)-C(8A)	1.53(3)	C(14C)-C(19C)	1.51(4)
C(9A)-C(10A)	1.48(3)	C(14C)-C(15C)	1.51(3)
C(11A)-C(19A)	1.35(4)	C(14C)-C(18C)	1.51(3)
C(11A)-O(12A)	1.42(2)	C(14C)-C(23C)	1.85(4)
C(11A)-C(16A)	1.92(4)	C(15C)-C(16C)	1.57(2)
O(12A)-C(13A)	1.32(2)	C(19C)-C(20C)	1.49(4)
C(13A)-O(17A)	1.20(3)	O(22C)-C(23C)	1.23(4)
C(13A)-C(14A)	1.45(3)	C(23C)-O(24C)	1.19(4)
C(14A)-C(19A)	1.43(4)	S(1D)-C(2D)	1.673(15)
C(14A)-C(18A)	1.48(4)	C(2D)-N(6D)	1.32(2)
C(14A)-C(15A)	1.86(4)	C(2D)-N(3D)	1.411(19)
C(15A)-C(16A)	1.23(4)	N(3D)-C(4D)	1.39(2)
C(19A)-C(21A)	1.52(4)	C(4D)-O(5D)	1.21(2)
C(19A)-C(20A)	1.79(4)	C(4D)-C(11D)	1.51(3)
S(1B)-C(2B)	1.753(14)	N(6D)-C(7D)	1.48(2)
C(2B)-N(6B)	1.29(2)	N(6D)-C(9D)	1.48(2)
C(2B)-N(3B)	1.35(2)	C(7D)-C(8D)	1.47(3)
N(3B)-C(4B)	1.32(2)	C(9D)-C(10D)	1.45(4)
C(4B)-O(5B)	1.26(2)	C(11D)-C(19D)	1.48(4)
C(4B)-C(11B)	1.57(3)	C(11D)-C(16D)	1.51(2)
N(6B)-C(7B)	1.47(2)	C(11D)-O(12D)	1.67(3)
N(6B)-C(9B)	1.49(2)	C(11D)-O(22D)	1.77(3)
C(7B)-C(8B)	1.58(3)	O(12D)-C(13D)	1.29(4)
C(9B)-C(10B)	1.58(3)	C(13D)-O(17D)	1.20(4)

Table A–3.3. Selected bond angles of $Ag_2(HL^8\text{-}S)(L^8\text{-}\mu\text{-}S,O))_2$ complex.

Bond angle	Degree	Bond angle	Degree
S(1B)-Ag(1)-S(1D)	151.5(18)	C(2B)-N(6B)-C(7B)	124.7(15)
S(1B)-Ag(1)-O(5A)	94.8(3)	C(2B)-N(6B)-C(9B)	119.5(15)
S(1D)-Ag(1)-O(5A)	94.5(3)	C(7B)-N(6B)-C(9B)	115.8(15)
S(1B)-Ag(1)-S(1A)	112.5(14)	N(6B)-C(7B)-C(8B)	111.3(16)
S(1D)-Ag(1)-S(1A)	95.1(16)	N(6B)-C(9B)-C(10B)	113.5(17)
O(5A)-Ag(1)-S(1A)	85.4(3)	C(19B)-C(11B)-O(12B)	109.0(2)
S(1B)-Ag(1)-Ag(2)	63.2(12)	C(19B)-C(11B)-C(4B)	134.0(2)
S(1D)-Ag(1)-Ag(2)	144.2(14)	O(12B)-C(11B)-C(4B)	105.5(17)
O(5A)-Ag(1)-Ag(2)	87.3(3)	C(19B)-C(11B)-C(16B)	91.0(2)
S(1A)-Ag(1)-Ag(2)	49.3(9)	O(12B)-C(11B)-C(16B)	101.5(16)
S(1A)-Ag(2)-S(1C)	148.3(18)	C(4B)-C(11B)-C(16B)	111.6(18)
S(1A)-Ag(2)-O(5B)	91.7(3)	C(2C)-S(1C)-Ag(2)	104.4(6)
S(1C)-Ag(2)-O(5B)	100.1(3)	N(6C)-C(2C)-N(3C)	121.2(16)
S(1A)-Ag(2)-S(1B)	110.0(14)	N(6C)-C(2C)-S(1C)	121.5(13)
S(1C)-Ag(2)-S(1B)	100.8(16)	N(3C)-C(2C)-S(1C)	117.3(12)
O(5B)-Ag(2)-S(1B)	81.7(3)	C(2C)-N(3C)-C(4C)	120.8(14)
S(1A)-Ag(2)-Ag(1)	61.14(11)	O(5C)-C(4C)-N(3C)	122.1(18)
S(1C)-Ag(2)-Ag(1)	148.4(14)	O(5C)-C(4C)-C(11C)	119.9(18)
O(5B)-Ag(2)-Ag(1)	85.7(2)	N(3C)-C(4C)-C(11C)	118.0(16)
S(1B)-Ag(2)-Ag(1)	48.9(9)	C(2C)-N(6C)-C(7C)	124.1(16)
C(2A)-S(1A)-Ag(2)	106.4(6)	C(2C)-N(6C)-C(9C)	119.9(16)
C(2A)-S(1A)-Ag(1)	90.9(6)	C(7C)-N(6C)-C(9C)	114.2(16)
Ag(2)-S(1A)-Ag(1)	69.5(11)	N(6C)-C(7C)-C(8C)	107.0(2)
N(6A)-C(2A)-N(3A)	115.0(15)	C(10C)-C(9C)-N(6C)	95.0(3)
N(6A)-C(2A)-S(1A)	122.0(13)	C(19C)-C(11C)-C(16C)	118.0(2)
N(3A)-C(2A)-S(1A)	122.9(12)	C(19C)-C(11C)-C(4C)	121.0(2)
C(4A)-N(3A)-C(2A)	123.7(13)	C(16C)-C(11C)-C(4C)	117.1(16)
O(5A)-C(4A)-N(3A)	127.0(15)	C(19C)-C(11C)-O(12C)	96.0(2)
O(5A)-C(4A)-C(11A)	117.0(15)	C(4C)-C(11C)-O(22C)	102.4(14)
N(3A)-C(4A)-C(11A)	116.1(15)	O(12C)-C(11C)-O(22C)	149.1(17)
C(4A)-O(5A)-Ag(1)	115.4(10)	C(13C)-O(12C)-C(11C)	109.0(2)
C(2A)-N(6A)-C(9A)	123.1(15)	C(2D)-S(1D)-Ag(1)	106.9(6)
C(2A)-N(6A)-C(7A)	122.0(15)	N(6D)-C(2D)-N(3D)	115.3(13)
C(9A)-N(6A)-C(7A)	114.9(14)	N(6D)-C(2D)-S(1D)	122.8(12)
N(6A)-C(7A)-C(8A)	111.8(16)	N(3D)-C(2D)-S(1D)	121.8(11)
N(6A)-C(9A)-C(10A)	111.6(19)	C(4D)-N(3D)-C(2D)	119.0(14)
C(19A)-C(11A)-C(4A)	134.0(2)	O(5D)-C(4D)-N(3D)	123.6(18)
O(12A)-C(11A)-C(4A)	111.7(17)	O(5D)-C(4D)-C(11D)	122.0(16)
C(2B)-S(1B)-Ag(1)	106.8(6)	N(3D)-C(4D)-C(11D)	114.5(16)
C(2B)-S(1B)-Ag(2)	94.4(5)	C(2D)-N(6D)-C(7D)	119.3(14)
Ag(1)-S(1B)-Ag(2)	67.9(11)	C(2D)-N(6D)-C(9D)	124.5(14)
N(6B)-C(2B)-N(3B)	121.3(14)	C(7D)-N(6D)-C(9D)	115.9(14)
N(6B)-C(2B)-S(1B)	118.4(13)	N(6D)-C(7D)-C(8D)	112.9(19)
N(3B)-C(2B)-S(1B)	120.2(12)	C(10D)-C(9D)-N(6D)	115.0(2)
C(4B)-N(3B)-C(2B)	124.8(14)	C(19D)-C(11D)-C(4D)	119.6(19)
O(5B)-C(4B)-N(3B)	126.1(15)	C(19D)-C(11D)-C(16D)	116.4(19)
O(5B)-C(4B)-C(11B)	122.1(16)	C(4D)-C(11D)-C(16D)	119.7(15)
N(3B)-C(4B)-C(11B)	111.8(15)	C(19D)-C(11D)-O(12D)	96.0(2)
C(4B)-O(5B)-Ag(2)	119.6(10)	C(4D)-C(11D)-O(12D)	96.0(15)

Table A–3.4. Selected torsion angles of $Ag_2(HL^8\text{-}S)(L^8\text{-}\mu\text{-}S,O))_2$ complex.

Torsion angle	Degree	Torsion angle	Degree
S(1B)-Ag(1)-Ag(2)-S(1A)	177.0(16)	S(1C)-Ag(2)-O(5B)-C(4B)	132.1(12)
S(1D)-Ag(1)-Ag(2)-S(1A)	7.8(2)	S(1B)-Ag(2)-O(5B)-C(4B)	32.5(12)
O(5A)-Ag(1)-Ag(2)-S(1A)	86.3(3)	Ag(1)-Ag(2)-O(5B)-C(4B)	16.6(12)
S(1B)-Ag(1)-Ag(2)-S(1C)	19.7(2)	N(3B)-C(2B)-N(6B)-C(7B)	175.1(15)
S(1D)-Ag(1)-Ag(2)-S(1C)	171.1(3)	S(1B)-C(2B)-N(6B)-C(7B)	0.0(2)
O(5A)-Ag(1)-Ag(2)-S(1C)	77.0(4)	N(3B)-C(2B)-N(6B)-C(9B)	7.0(2)
S(1A)-Ag(1)-Ag(2)-S(1C)	163.2(3)	S(1B)-C(2B)-N(6B)-C(9B)	177.7(12)
S(1B)-Ag(1)-Ag(2)-O(5B)	82.7(3)	C(2B)-N(6B)-C(7B)-C(8B)	87.0(2)
S(1D)-Ag(1)-Ag(2)-O(5B)	86.5(3)	C(9B)-N(6B)-C(7B)-C(8B)	90.6(19)
O(5A)-Ag(1)-Ag(2)-O(5B)	179.4(4)	C(2B)-N(6B)-C(9B)-C(10B)	85.0(2)
S(1A)-Ag(1)-Ag(2)-O(5B)	94.3(3)	C(7B)-N(6B)-C(9B)-C(10B)	93.0(2)
S(1D)-Ag(1)-Ag(2)-S(1B)	169.2(3)	O(5B)-C(4B)-C(11B)-C(19B)	130.0(3)
O(5A)-Ag(1)-Ag(2)-S(1B)	96.7(3)	N(3B)-C(4B)-C(11B)-C(19B)	52.0(3)
S(1A)-Ag(1)-Ag(2)-S(1B)	77.0(16)	O(5B)-C(4B)-C(11B)-O(12B)	6.0(2)
S(1C)-Ag(2)-S(1A)-C(2A)	78.6(7)	N(3B)-C(4B)-C(11B)-O(12B)	171.5(15)
O(5B)-Ag(2)-S(1A)-C(2A)	168.9(6)	O(5B)-C(4B)-C(11B)-C(16B)	115.0(2)
S(1B)-Ag(2)-S(1A)-C(2A)	87.1(6)	N(3B)-C(4B)-C(11B)-C(16B)	62.0(2)
Ag(1)-Ag(2)-S(1A)-C(2A)	84.7(6)	C(4B)-C(11B)-O(12B)-C(13B)	174.1(15)

S(1C)-Ag(2)-S(1A)-Ag(1)	163.3(2)	C(4B)-C(11B)-C(16B)-C(15B)	178.0(2)
O(5B)-Ag(2)-S(1A)-Ag(1)	84.2(2)	C(4B)-C(11B)-C(19B)-C(14B)	171.0(2)
S(1B)-Ag(2)-S(1A)-Ag(1)	2.4(13)	C(4B)-C(11B)-C(19B)-C(21B)	59.0(4)
S(1B)-Ag(1)-S(1A)-C(2A)	110.0(5)	C(4B)-C(11B)-C(19B)-C(20B)	61.0(4)
S(1D)-Ag(1)-S(1A)-C(2A)	77.4(5)	S(1A)-Ag(2)-S(1C)-C(2C)	91.0.1(7)
O(5A)-Ag(1)-S(1A)-C(2A)	16.7(6)	O(5B)-Ag(2)-S(1C)-C(2C)	102.5(7)
Ag(2)-Ag(1)-S(1A)-C(2A)	107.1(5)	S(1B)-Ag(2)-S(1C)-C(2C)	117.6(7)
S(1B)-Ag(1)-S(1A)-Ag(2)	2.9(15)	Ag(1)-Ag(2)-S(1C)-C(2C)	156.4(17)
S(1D)-Ag(1)-S(1A)-Ag(2)	75.4(14)	Ag(2)-S(1C)-C(2C)-N(6C)	25.0(15)
O(5A)-Ag(1)-S(1A)-Ag(2)	90.4(3)	Ag(2)-S(1C)-C(2C)-N(3C)	81.0(2)
Ag(2)-S(1A)-C(2A)-N(6A)	179.5(13)	N(6C)-C(2C)-N(3C)-C(4C)	97.9(16)
Ag(1)-S(1A)-C(2A)-N(6A)	111.5(14)	S(1C)-C(2C)-N(3C)-C(4C)	4.0(3)
Ag(2)-S(1A)-C(2A)-N(3A)	2.7(15)	C(2C)-N(3C)-C(4C)-O(5C)	174..2(15)
Ag(1)-S(1A)-C(2A)-N(3A)	71.6(13)	C(2C)-N(3C)-C(4C)-C(11C)	179.0(2)
N(6A)-C(2A)-N(3A)-C(4A)	100.5(18)	N(3C)-C(2C)-N(6C)-C(7C)	0.0(3)
S(1A)-C(2A)-N(3A)-C(4A)	82.4(19)	S(1C)-C(2C)-N(6C)-C(7C)	17.0(3)
C(2A)-N(3A)-C(4A)-O(5A)	4.0(3)	N(3C)-C(2C)-N(6C)-C(9C)	164.1(15)
C(2A)-N(3A)-C(4A)-C(11A)	176.3(15)	S(1C)-C(2C)-N(6C)-C(9C)	82.0(3)
N(3A)-C(4A)-O(5A)-Ag(1)	50.0(2)	C(2C)-N(6C)-C(7C)-C(8C)	111.0(3)
C(11A)-C(4A)-O(5A)-Ag(1)	130.6(14)	C(9C)-N(6C)-C(7C)-C(8C)	84.0(3)
S(1B)-Ag(1)-O(5A)-C(4A)	83.2(11)	C(2C)-N(6C)-C(9C)-C(10C)	86.0(3)
S(1D)-Ag(1)-O(5A)-C(4A)	123.8(11)	C(7C)-N(6C)-C(9C)-C(10C)	95.0(3)
S(1A)-Ag(1)-O(5A)-C(4A)	29.0(11)	O(5C)-C(4C)-C(11C)-C(19C)	118.0(2)
Ag(2)-Ag(1)-O(5A)-C(4A)	20.4(11)	N(3C)-C(4C)-C(11C)-C(19C)	61.0(2)
N(3A)-C(2A)-N(6A)-C(9A)	3(2)	O(5C)-C(4C)-C(11C)-C(16C)	13.0(2)
S(1A)-C(2A)-N(6A)-C(9A)	179.6(15)	N(3C)-C(4C)-C(11C)-C(16C)	165.2(15)
N(3A)-C(2A)-N(6A)-C(7A)	178.2(15)	O(5C)-C(4C)-C(11C)-O(12C)	141.0(18)
S(1A)-C(2A)-N(6A)-C(7A)	1.0(2)	N(3C)-C(4C)-C(11C)-O(12C)	40.3(19)
C(2A)-N(6A)-C(7A)-C(8A)	9.01(2)	O(5C)-C(4C)-C(11C)-O(22C)	41.0(3)
C(9A)-N(6A)-C(7A)-C(8A)	90.0(2)	N(3C)-C(4C)-C(11C)-O(22C)	79.0(2)
C(2A)-N(6A)-C(9A)-C(10A)	94.0(2)	C(4C)-C(11C)-O(12C)-C(13C)	175.0(4)
C(7A)-N(6A)-C(9A)-C(10A)	86.0(2)	C(4C)-C(11C)-C(16C)-C(15C)	73.4(14)
O(5A)-C(4A)-C(11A)-C(19A)	-170(3)	C(4C)-C(11C)-C(19C)-C(20C)	126.0(3)
N(3A)-C(4A)-C(11A)-C(19A)	10(4)	C(4C)-C(11C)-C(19C)-C(14C)	106.0(2)
O(5A)-C(4A)-C(11A)-O(12A)	23.0(2)	C(4C)-C(11C)-O(22C)-C(23C)	178.0(3)
N(3A)-C(4A)-C(11A)-O(12A)	157.2(15)	S(1B)-Ag(1)-S(1D)-C(2D)	122.9(6)
O(5A)-C(4A)-C(11A)-C(16A)	81.0(2)	O(5A)-Ag(1)-S(1D)-C(2D)	128.8(6)
N(3A)-C(4A)-C(11A)-C(16A)	98.7(18)	S(1A)-Ag(1)-S(1D)-C(2D)	176.4(13)
C(4A)-C(11A)-O(12A)-C(13A)	178.1(16)	Ag(2)-Ag(1)-S(1D)-C(2D)	1.9(15)
C(4A)-C(11A)-C(16A)-C(15A)	173.0(3)	Ag(1)-S(1D)-C(2D)-N(6D)	68.0(2)
C(4A)-C(11A)-C(19A)-C(14A)	179.0(2)	Ag(1)-S(1D)-C(2D)-N(3D)	113.2(15)
C(4A)-C(11A)-C(19A)-C(21A)	26.0(6)	N(6D)-C(2D)-N(3D)-C(4D)	6.0(3)
C(4A)-C(11A)-C(19A)-C(20A)	84.0(3)	S(1D)-C(2D)-N(3D)-C(4D)	174.5(14)
S(1D)-Ag(1)-S(1B)-C(2B)	78.8(6)	C(2D)-N(3D)-C(4D)-O(5D)	171.1(17)
O(5A)-Ag(1)-S(1B)-C(2B)	172.5(6)	C(2D)-N(3D)-C(4D)-C(11D)	11.0(2)
S(1A)-Ag(1)-S(1B)-C(2B)	85.5(5)	N(3D)-C(2D)-N(6D)-C(7D)	2.0(2)
Ag(2)-Ag(1)-S(1B)-C(2B)	87.9(5)	S(1D)-C(2D)-N(6D)-C(7D)	176.4(14)
S(1D)-Ag(1)-S(1B)-Ag(2)	166.7(3)	N(3D)-C(2D)-N(6D)-C(9D)	86.0(2)
O(5A)-Ag(1)-S(1B)-Ag(2)	84.6(3)	S(1D)-C(2D)-N(6D)-C(9D)	88.0(2)
S(1A)-Ag(1)-S(1B)-Ag(2)	2.5(13)	C(2D)-N(6D)-C(7D)-C(8D)	120.0(3)
S(1A)-Ag(2)-S(1B)-C(2B)	103.5(6)	C(9D)-N(6D)-C(7D)-C(8D)	67.0(3)
S(1C)-Ag(2)-S(1B)-C(2B)	84.1(6)	C(2D)-N(6D)-C(9D)-C(10D)	87.0(3)
O(5B)-Ag(2)-S(1B)-C(2B)	14.7(6)	C(7D)-N(6D)-C(9D)-C(10D)	93.0(2)
Ag(1)-Ag(2)-S(1B)-C(2B)	106.3(6)	O(5D)-C(4D)-C(11D)-C(19D)	117.0(2)
S(1A)-Ag(2)-S(1B)-Ag(1)	2.78(15)	N(3D)-C(4D)-C(11D)-C(19D)	63.0(2)
S(1C)-Ag(2)-S(1B)-Ag(1)	169.6(13)	O(5D)-C(4D)-C(11D)-C(16D)	14.0(2)
O(5B)-Ag(2)-S(1B)-Ag(1)	91.6(3)	N(3D)-C(4D)-C(11D)-C(16D)	166.0(16)
Ag(1)-S(1B)-C(2B)-N(6B)	173.9(11)	O(5D)-C(4D)-C(11D)-O(12D)	140.2(19)
Ag(2)-S(1B)-C(2B)-N(6B)	117.9(12)	N(3D)-C(4D)-C(11D)-O(12D)	39.7(18)
Ag(1)-S(1B)-C(2B)-N(3B)	1.4(13)	O(5D)-C(4D)-C(11D)-O(22D)	41.0(3)
Ag(2)-S(1B)-C(2B)-N(3B)	66.7(12)	N(3D)-C(4D)-C(11D)-O(22D)	162.0(2)
N(6B)-C(2B)-N(3B)-C(4B)	104.7(19)	C(4D)-C(11D)-O(12D)-C(13D)	35.0(4)
S(1B)-C(2B)-N(3B)-C(4B)	80.1(19)	C(4D)-C(11D)-C(16D)-C(15D)	73.8(15)
C(2B)-N(3B)-C(4B)-O(5B)	1.0(3)	C(4D)-C(11D)-C(19D)-O(22D)	176.1(19)
C(2B)-N(3B)-C(4B)-C(11B)	177.7(16)	C(4D)-C(11D)-C(19D)-C(23D)	140.0(3)
N(3B)-C(4B)-O(5B)-Ag(2)	52.0(2)	C(4D)-C(11D)-C(19D)-C(14D)	69.0(2)
C(11B)-C(4B)-O(5B)-Ag(2)	124.7(16)	C(4D)-C(11D)-C(19D)-C(20D)	54.0(3)
S(1A)-Ag(2)-O(5B)-C(4B)	77.5(12)		

Table A–3.5. Anisotropic displacement parameters ($Å^2$ x 10^3) for $Ag_2(HL^8\text{-}S)(L^8\text{-}\mu\text{-}S,O))_2$ complex. The anisotropic displacement factor exponent takes the form: $-2\pi^2$ [$h^2a^{*2}U11$ + ... + 2hka*b*U12]

Atoms	U11	U22	U33	U23	U13	U12
Ag(1)	41(1)	29(1)	60(1)	7(1)	5(1)	8(1)
Ag(2)	49(1)	35(1)	52(1)	14(1)	11(1)	13(1)
S(1A)	41(2)	37(2)	41(2)	3(2)	2(2)	12(2)
C(2A)	20(7)	62(11)	42(9)	15(8)	11(6)	10(7)
N(3A)	32(7)	20(6)	52(8)	0(5)	7(6)	10(5)
O(5A)	40(7)	40(7)	81(9)	1(6)	3(6)	1(5)
N(6A)	52(9)	45(8)	41(8)	9(6)	2(6)	15(7)
C(7A)	68(12)	68(13)	29(9)	9(8)	7(8)	12(10)
C(8A)	71(14)	99(18)	47(11)	10(11)	2(10)	24(13)
C(9A)	80(15)	71(14)	51(11)	21(10)	13(10)	35(12)
C(10A)	99(19)	70(16)	80(16)	27(13)	3(14)	15(14)
S(1B)	50(2)	39(2)	47(2)	1(2)	3(2)	19(2)
C(2B)	42(9)	0(6)	64(11)	1(6)	12(7)	5(6)
N(3B)	27(7)	54(9)	40(7)	3(6)	2(5)	7(6)
O(5B)	28(6)	30(6)	69(8)	11(5)	3(5)	-6(5)
N(6B)	42(8)	41(8)	51(9)	3(7)	7(6	3(6)
C(7B)	59(12)	40(11)	69(13)	8(9)	7(9)	5(9)
C(8B)	80(16)	100(20)	61(13)	5(12)	8(11)	45(15)
C(9B)	77(14)	25(9)	69(12)	4(8)	16(10)	20(9)
C(10B)	107(19)	36(11)	85(16)	15(10)	6(13)	22(12)
S(1C)	67(3)	37(2)	47(2)	9(2)	22(2)	21(2)
C(2C)	47(10)	57(11)	37(9)	2(8)	13(7)	21(8)
N(3C)	40(7)	10(6)	50(8)	1(5)	1(6)	9(5)
C(4C)	49(11)	37(9)	45(9)	3(7)	6(8)	15(8)
O(5C)	45(9)	72(12)	170(19)	20(11)	10(10)	3(8)
N(6C)	123(16)	32(8)	43(9)	9(7)	26(9)	22(9)
C(7C)	150(30)	26(10)	65(14)	14(9)	35(14)	15(12)
C(8C)	170(30)	77(18)	71(17)	4(13)	41(18)	50(20)
C(9C)	60(14)	66(15)	82(16)	1(11)	24(11)	5(11)
C(10C)	55(18)	79(11)	155(16)	55(11)	11(8)	14(7)
N(6D)	57(9)	30(8)	53(9)	5(6)	10(7)	6(7)
C(7D)	115(19)	42(11)	47(11)	2(8)	32(11)	18(11)
C(8D)	75(17)	130(20)	82(18)	37(16)	13(13)	22(16)
C(9D)	59(12)	52(12)	59(12)	6(9)	14(9)	23(10)
C(10D)	230(50)	100(30)	170(40)	0(20)	60(30)	80(30)

4. *Fac-tris*(*N,N*-diethyl-*N'*-camphanoylthioureato)Cabalt(III), H_3O^+ {*fac*-(Co(L-*S,O*)$_3$]$^-$}

Table A–4.1. The average selected bond lengths of H_3O^+{*fac*-[Co(L-*S,O*)$_3$]$^-$} complex.

Bonds	length(Å)	Bonds	Length(Å)
C(2)-N(3)	1.319(6)	C(4)-O(5)	1.242(6)
C(2)-N(6)	1.359(6)	C(11)-C(16)	1.523(6)
C(2)-S(1)	1.731(5)	C(13)-O(21)	1.213(6)
C(4)-O(5)	1.242(4)	C(13)-C(14)	1.500(7)
C(4)-N(3)	1.340(6)	C(14)-C(20)	1.515(7)
C(4)-C(11)	1.524(6)	C(14)-C(15)	1.555(8)
C(7)-N(6)	1.452(6)	C(14)-C(17)	1.568(7)
C(7)-C(8)	1.499(8)	C(15)-C(16)	1.561(7)
C(9)-N(6)	1.478(7)	C(17)-C(19)	1.504(8)
C(9)-(10)	1.508(9)	C(17)-C(18)	1.533(8)
C(11)-O(12)	1.462(5)	Co(1)-O(5)	1.937(3)
C(2)-s(1)	1.886(9)	Co(1)-S(1)	2.228(13)

Table A–4.2. Selected bond angles of H_3O^+{*fac*-[Co(L-*S,O*)$_3$]$^-$}.

Bond angle	Degree	Bond angle	Degree
N(3A)-C(2A)-N(6A)	113.8(4)	O(5B)-Co(1)-O(5A)	86.9(14)
N(3A)-C(2A)-S(1A)	129.1(3)	O(5C)-Co(1)-S(1B)	91.2(11)
N(6A)-C(2A)-S(1A)	117.1(4)	O(5A)-Co(1)-S(1C)	94.9(10)
N(6B)-C(2B)-N(3B)	114.0(5)	O(5A)-Co(1)-S(1B)	175.3(10)
N(6B)-C(2B)-S(1B)	118.4(4)	O(5C)-Co(1)-S(1C)	95.5(11)
N(3B)-C(2B)-S(1B)	127.6(4)	O(5B)-Co(1)-S(1C)	177.5(11)
N(6C)-C(2C)-N(3C)	114.9(4)	O(5A)-Co(1)-S(1C)	90.8(11)
N(6C)-C(2C)-S(1C)	116.8(4)	S(1B)-Co(1)-S(1C)	87.5(5)
N(3C)-C(2C)-S(1C)	128.3(4)	O(5C)-Co(1)-S(1A)	176.6(11)
O(5A)-C(4A)-N(3A)	130.9(4)	O(5B)-Co(1)-S(1A)	91.2(11)
O(5A)-C(4A)-C(11)	114.6(4)	O(5A)-Co(1)-S(1A)	94.9(10)
N(3A)-C(4A)-C(11A)	114.3(4)	S(1B)-Co(1)-S(1A)	89.5(5)
O(5B)-C(4B)-N(3B)	130.8(5)	S(1C)-Co(1)-S(1A)	88.0(5)
O(5B)-C(4B)-C(11B)	114.3(4)	C(2A)-N(3A)-C(4A)	125.7(4)
N(3B)-C(4B)-C(11B)	114.3(4)	C(4B)-N(3B)-C(2B)	126.9(5)
O(5C)-C(4C)-N(3C)	132.0(4)	C(2C)-N(3C)-C(4C)	125.7(4)
O(5C)-C(4C)-C(11C)	110.1(4)	C(2A)-N(6A)-C(7A)	122.8(4)
N(3C)-C(4C)-C(11C)	117.9(4)	C(2A)-N(6A)-C(9A)	120.2(4)
N(6A)-C(7A)-C(8A)	114.9(5)	C(7A)-N(6A)-C(9A)	117.0(4)
N(6B)-C(7B)-C(8B)	107.9(8)	C(2B)-N(6B)-N(9B)	121.9(5)
N(6C)-C(7C)-C(8C)	11.3(6)	C(2B)-N(6B)-N(7B)	122.6(5)
N((6A)-C(9A)-C(10A)	112.3(5)	C(7B)-N(6B)-N(9B)	114.9(5)
N(6B)-C(9B)-C(10B)	113.2(5)	C(2C)-N(6C)-C(7C)	125.3(5)
N(6C)-C(9C)-C(10C)	109.9(5)	C(2C)-N(6C)-C(9C)	121.9(4)
C(4A)-C(11A)-C(17A)	118.1(4)	C(7C)-N(6C)-C(9C)	112.8(4)
C(4B)-C(11B)-C(17B)	120.5(4)	C(4A)-O(5A)-Co(1)	130.6(3)
C(4C)-C(11C)-C(17C)	116.2(4)	C(4B)-O(5B)-Co(1)	131.0(3)
C(4A)-C(11A)-O(12A)	108.2(3)	C(4C)-O(5C)-Co(1)	130.5(3)
C(4B)-C(11B)-O(12B)	108.1(4)	C(2A)-S(1A)-Co(1)	107.6(16)
C(4C)-C(11C)-O(12C)	109.7(3)	C(2B)-S(1B)-Co(1)	108.8(18)
O(5C)-Co(1)-O(5B)	85.4(14)	C(2C)-S(1C)-Co(1)	107.7(18)
O(5C)-Co(1)-O(5A)	84.6(14)		

Table A-4.3. Atomic coordinates (x 10^4) and equivalent isotropic displacement parameters of ($Å^2$ x 10^3) of H_3O^+{*fac*-[Co(L-*S,O*)$_3$]$^-$}. U(eq) is defined as one third of the trace of the orthogonalized Uij tensor.

Atoms	X	Y	Z	U(eq)
C(2A)	91(4)	7348(4)	598093)	33(1)
C(2B)	4426(4)	4554(4)	6167(3)	43(1)
C(2C)	3905(4)	8582(4)	7113(3)	37(1)
C(4A)	2(4)	8040(3)	7253(2)	31(1)
C(4B)	2596(4)	4641(4)	6913(3)	38(1)
C(4C)	4081(4)	7321(3)	7934(3)	30(1)
C(7A)]	534(5)	6859(4)	4661(3)	47(1)
C(7B)	6335(6)	4149(6)	5301(5)	87(2)
C(7C)	3734(6)	10149(5)	6494(3)	60(2)
C(8A)	605(7)	5758(5)	4480(4)	75(2)
C(8B)	7494(8)	4011(7)	5639(7)	116(3)
C(8C)	4530(9)	9894(7)	5823(4)	90(2)
C(9A)	2267(5)	7807(4)	5617(3)	47(1)
C(9B)	5671(6)	2722(5)	5866(4)	63(2)
C(9C)	5077(5)	9833(5)	7549(4)	57(2)
C(10A)	2869(6)	7116(6)	6008(4)	68(2)
C(10B)	6200(6)	2402(5)	6583(4)	71(2)
C(10C)	4345(7)	10515(5)	8255(4)	75(2)
C(11A)	814(4)	8768(3)	7903(2)	33(1)
C(11B)	1923(4)	3962(4)	7243(3)	47(1)
C(11C)	4664(4)	6924(4)	8644(3)	33(1)
C(13A)	2035(4)	10413(4)	8186(3)	41(1)
C(13B)	966(6)	2707(5)	6854(5)	95(3)
C(13C)	6247(4)	6996(4)	9387(2)	41(1)
C(14A)	1468(5)	10011(4)	8879(3)	43(1)
C(14B)	421(5)	3294(4)	7641(4)	67(2)
C(14C)	5940(5)	5960(4)	9362(3)	43(1)
C(15A)	2160(5)	9182(5)	9020(3)	56(2)
C(15B)	1491(6)	2939(5)	8163(6)	89(3)
C15C)	4656(5)	6262(5)	9810(3)	54(1)
C(16A)	1660(5)	8297(4)	8345(3)	48(1)
C(16B)	2526(5)	3420(5)	7885(5)	76(2)
C(16C)	3769(5)	6903(5)	9301(3)	49(1)
C(17A)	168(5)	9332(4)	8511(3)	42(1)
C(17B)	540(4)	4384(3)	7511(3)	42(1)
C(17C)	5570(4)	5843(4)	8536(3)	41(1)
C(18A)	606(5)	9977(5)	8179(4)	61(2)
C(18B)	251(5)	4840(6)	6878(4)	74(2)
C(18C)	6628(5)	5753(4)	7944(3)	56(1)
C(19A)	600(6)	8656(6)	9031(3)	73(2)
C(19B)	281(5)	5180(4)	8210(3)	60(2)
C(19C)	5018(6)	4838(4)	8326(3)	61(2)
C(20A)	1533(6)	10849(5)	9541(1)	72(2)
C(20B)	808(5)	3140(5)	7889(5)	86(2)
C(20C)	6946(6)	5117(5)	9636(4)	67(2)
Co(1)	2517(1)	6785(1)	6767(1)	33(1)]
N(3A)	607(4)	7874(3)	6633(2)	36(1)
N(3B)	3661(4)	4137(3)	6525(2)	42(1)
N(3C)	4351(4)	8122(3)	7714(2)	36(1)
N(6A)	916(4)	7330(3)	5436(2)	38(1)
N(6B)	5437(4)	3865(4)	5833(3)	59(1)
N(6C)	4208(4)	9455(3)	7043(3)	48(1)
O(5A)	1092(3)	7640(3)	7406(2)	35(1)
O(5B)	2061(3)	5599(2)	7056(2)	38(1)
O(5C)	3379(3)	6769(3)	7673(2)	38(1)
O(12A)	1651(3)	9632(2)	7592(2)	36(1)
O(12B)	1907(4)	3090(4)	6653(3)	91(2)
O(12C)	5434 (3)	7585(2)	8954(2)	41(1)
O(21A)	2756(3)	11240(3)	8104(2)	57(1)
O(21B)	703(7)	2011(6)	6501(5)	176(4)
O(21C)	7043(3)	7310(3)	9714(2)	56(1)
S(1A)	1465(1)	6727(1)	5727(1)	41(1)
S(1B)	4245(1)	5854(1)	6102(1)	45(1)
S(1C)	2956(1)	8193(1)	6443(1)	38(1)

Table A–4.4. Anisotropic displacement parameters ($Å^2$ x 10^3) of H_3O^+{*fac*-[Co(L-*S,O*)$_3$]$^-$}. The anisotropic displacement factor exponent takes the form: $-2\pi^2[h2a^{*2}U_{11} \ldots + 2hka^*b^*U_{12}]$.

Atoms	U11	U22	U33	U23	U13	U12
C(2A)	38(3)	32(2)	34(3)	7(2)	11(2)	17(2)
C(2B)	30(2)	47(3)	47(3)	4(2)	0(2)	7(2)
C(2C)	24(2)	38(3)	50(3)	10(2)	10(2)	7(2)
C(4A)	36(2)	29(2)	30(2)	4(2)	5(2)	12(2)
C(4B)	34(2)	36(3)	43(2)	4(2)	12(2)	12(2)
C(4C)	27(2)	31(2)	31(2)	2(2)	6(2)	7(2)
C(7A)	55(3)	63(3)	29(2)	6(2)	10(2)	25(2)
C(7B)	60(4)	68(4)	116(6)	0(4)	1(4)	7(3)
C(7C)	78(4)	62(4)	47(3)	30(3)	19(3)	19(3)
C(8A)	102(5)	65(4)	56(3)	9(3)	3(3)	29(4)
C(8B)	80(5)	95(6)	192(11)	40(7)	29(6)	46(5)
C(8C)	125(7)	89(6)	61(4)	12(4)	2(4)	35(5)
C(9A)	42(3)	52(3)	49(3)	9(2)	15(2)	13(2)
C(9B)	49(3)	50(3)	79(4)	6(3)	5(3)	5(2)
C(9C)	55(3)	51(3)	81(4)	35(3)	38(3)	29(3)
C(10A)	47(3)	77(4)	82(4)	14(3)	3(3)	20(3)
C(10B)	61(4)	66(4)	83(5)	17(3)	1(3)	11(3)
C(10C)	86(5)	50(4)	94(5)	7(4)	29(4)	25(3)
C(11A)	32(2)	34(2)	32(2)	8(2)	5(2)	5(2)
C(11B)	35(3)	27(2)	78(3)	8(2)	5(2)	15(2)
C(11C)	37(2)	32(2)	31(2)	4(2)	11(2)	15(2)
C(13A)	39(2)	40(3)	41(2)	4(2)	4(2)	5(2)
C(13B)	69(4)	57(4)	160(8)	35(4)	36(5)	43(3)
C(13C)	39(2)	50(3)	34(2)	1(2)	5(2)	13(2)
C(14A)	48(3)	42(3)	32(2)	3(2)	4(2)	2(2)
C(14B)	38(3)	32(3)	13296)	4(3)	4(3)	16(2)
C(14C)	46(3)	4593)	39(2)	6(2)	16(2)	15(2)
C(15A)	58(3)	57(3)	43(3)	12(2)	15(2)	1(3)
C(15B)	50(3)	63(4)	168(8)	64(5)	1(4)	16(3)
C(15C)	54(3)	67(4)	45(3)	2193)	792)	18(3)
C(16A)	55(3)	36(3)	53(3)	12(2)	8(2)	11(2)
C(16B)	40(3)	67(4)	136(6)	58(4)	19(3)	18(3)
C(16C)	44(3)	68(3)	38(3)	10(2)	3(2)	19(2)
C(17A)	41(3)	42(3)	35(2)	4(2)	4(2)	2(2)
C(17B)	33(2)	32(2)	62(3)	1(2)	7(2)	13(2)
C(17C)	45(3)	36(3)	40(2)	5(2)	18(2)	5(2)
C(18A)	42(3)	64(4)	73(4)	23(3)	5(3)	20(3)
C(18B)	33(3)	105(5)	88(4)	20(4)	19(3)	20(3)
C(18C)	44(3)	60(3)	51(3)	2(2)	6(2)	7(2)
C(19A)	61(4)	89(5)	44(3)	8(3)	21(3)	18(3)
C(19B)	61(3)	49(3)	70(4)	8(2)	38(3)	24(3)
C(19C)	79(4)	38(3)	70(4)	43(4)	64(5)	19(3)
C(20A)	72(4)	75(4)	49(3)	21(3)	12(3)	3(3)
C(20B)	49(3)	40(3)	171(8)	9(4)	26(4)	21(3)
C(20C)	72(4)	61(4)	65(4)	15(3)	42(3)	9(3)
N(3A)	34(2)	42(2)	33(2)	6(2)	9(2)	10(2)
N(3B)	28(2)	37(2)	56(2)	6(2)	2(2)	8(2)
N(3C)	39(2)	33(2)	40(2)	10(2)	13(2)	15(2)
Co(1)	29(1)	35(1)	34(1)	2(1)	4(1)	10(1)
N(6A)	39(2)	44(2)	32(2)	5(2)	8(2)	11(2)
N(6B)	47(3)	50(3)	71(3)	0(2)	25(2)	6(2)
N(6C)	49(2)	46(3)	57(3)	24(2)	23(2)	18(2)
O(5A)	37(2)	34(2)	30(2)	0(1)	4(1)	5(1)
O(5B)	38(2)	31(2)	43(2)	-8(1)	2(1)	13(1)
O(5C)	32(2)	40(2)	43(2)	8(2)	6(2)	12(2)
O(12A)	38(2)	34(2)	30(1)	4(1)	5(1)	2(1)
O(12B)	67(3)	65(3)	137(4)	60(3)	40(3)	48(2)
O(12C)]	43(2)	38(2)	43(2)	1(1)	11(1)	14(1)
O(21A)	60(2)	39(2)	58(2)	4(2)	2(2)	7(2)
O(21B)	134(5)	130(5)	260(9)	123(6)	77(6)	106(5)
O(21C)	58(2)	64(2)	55(2)	5(2)	21(2)	30(2)
S(1A)	35(1)	55(1)	31(1)	5(1)	3(1)	12(1)
S(1B)	33(1)	46(1)	53(1)	4(1)	5(1)	10(1)
S(1C)	99(1)	41(1)	39(1)	11(1)	10(1)	14(1)